Computational Biomechanics/Biotribological Modelling of Natural and Artificial Hip Joints

Junyan Li

Submitted in accordance with the requirements for the degree of
Doctor of Philosophy

The University of Leeds
School of Mechanical Engineering

July, 2013

The candidate confirms that the work submitted is his own, except where work which has formed part of jointly-authored publications has been included. The contribution of the candidate and the other authors to this work has been explicitly indicated below. The candidate confirms that appropriate credit has been given within the thesis where reference has been made to the work of others.

1. **Chapter 5** of this thesis is based on a jointly-authored paper:

LI, J., STEWART, T. D., JIN, Z., WILCOX, R. K. & FISHER, J. The influence of size, clearance, cartilage properties, thickness and hemiarthroplasty on the contact mechanics of the hip joint with biphasic layers. Journal of Biomechanics. 2013. 46, 1641-1647.

The work was done by the candidate and supervised by the co-authors.

2. **Chapter 6** of this thesis is based on a jointly-authored manuscript which is under review:

LI, J., JIN, Z., FISHER, J & WILCOX, R. K. Biphasic investigation of contact mechanics in natural human hips during activities.

The work was done by the candidate and supervised by the co-authors.

3. **Chapter 9** of this thesis is based on a jointly-authored manuscript which is under review:

LI, J., Wang, Q., JIN, Z., Williams, S., FISHER, J & WILCOX, R. K. Experimental validation of a new biphasic model of the contact mechanics of the porcine hip.

The computational work was done by the candidate and supervised by the co-authors. The experiment was conducted by Wang, Q.

4. **Chapter 3** of this thesis is partly based on a jointly-authored manuscript which is under review:

LI, J., Redmond, A., JIN, Z., FISHER, J., Stone, H. S., STEWART, T. D. Hip kinematics and contact forces in asymptomatic total hip replacement patients differ from normal healthy individuals.

The candidate carried out the computational work and statistical analysis. Redmond, A. and Stone, H. S. contributed to the gait measurement. The project was supervised by the co-authors

5. **Chapter 3** of this thesis is partly based on a jointly-authored manuscript which is under review:

LI, J., McWilliams, A. B., JIN, Z., FISHER, J., Stone, H. S., Redmond, A. & STEWART, T. D. Influence of leg length inequality on hip reaction forces.

The candidate carried out the computational work and statistical analysis. Redmond, A. and Stone, H. S. contributed to the gait measurement. The project was supervised by the co-authors

Acknowledgements

I have been very fortunate to complete my thesis in less than three years owing to the help and support of others.

I am honoured to be supervised by Prof. Fisher, Prof. Jin, Prof. Wilcox and Dr. Stewart, and grateful for their guidance, ideas and support that led me to become a professional researcher directly from an innocent graduate. Dr. Redmond deserves special mention for his time spent on my work and manuscripts.

I appreciate Prof. Ateshian from Columbia University, Prof. Weiss from University of Utah and Prof. Rasmussen from Aalborg University for the in-depth discussions and resources they generously provided that were very important to my research.

I thank Debra, Cheryl, Jane, Carol, Dureid, Ted and Graham for their timely assistances whenever I bother them. I would also thank the 442c guys for their help during my 1st year PhD. I would never forget the time I spent with the IMBE FC guys. I also appreciate the intelligent discussions I had with my IMBE colleagues.

I am thankful to my housemates for their tolerance on my laziness, the mutual encouragement and the enjoyable time we spent together.

I am grateful to the scholarship from university of Leeds, as well as the funding from EPSRC and WELMEC for sponsoring my research.

Lastly, I am the luckiest person in the world for being the child of my mom and dad. I am always grateful to my grandparents, who are no longer with us, for their love and efforts.

Abstract

The excellent hip function and potential degeneration are closely linked with the unique structure of the joint cartilage that is principally composed of a solid phase and a fluid phase. Once damaged, the joint may need to be replaced by prosthesis in order to restore function in hip kinematics and kinetics. However, to what extent this can be achieved has yet to be quantified. On the other hand, the role of fluid pressurisation which plays in hip function has been poorly understood. The aim of this thesis was to address these issues.

To evaluate the gait abnormality, particularly in terms of hip contact forces, a musculoskeletal model of lower extremity was constructed in a rigid-body dynamics frame, and the hip kinematics and kinetics were determined and cross-compared for a group of asymptomatic total hip replacement (THR) patients, THR patients with symptoms of symptomatic leg length inequality (LLI) and normal healthy people. Significant abnormal patterns in gait kinetics were observed for the asymptomatic THR patients, and this abnormality was greater for the LLI patients.

To understand contact mechanics and the associated fluid pressurisation within the hip cartilage, a three dimensional finite element (FE) hip model with biphasic cartilage layers were developed. The protocol was compared to other solvers. A set of sensitivity studies were undertaken to evaluate the influence of model parameters, and then the model was evaluated under a range of loads with different activities. In all the cases, the fluid supported over 90% of the load for a prolonged period, potentially providing excellent hip function and lubrication. The musculoskeletal model and FE joint were combined to investigate the performance of the non-operated joint of the THR / LLI patients during gait which was found to function in a mechanically abnormal but not adverse environment. Lastly, the methodology of the biphasic hip modelling was validated using an experimental porcine hip of hemiarthroplasty. Good agreement was achieved between the FE predictions and the experimental measurement of the contact area.

Table of Contents

List of Tables

List of Figures

Abbreviations

BW	Body weight
RBD	Rigid-body dynamics
FE	Finite element
THR	Total hip replacement
EMG	Electromyography
LLI	Leg length inequality
DE	Discrete element
BMI	Body mass index
CI	Confidence intervals

Chapter 1
Introduction and Literature Review

1.1 Introduction

The human hip joint has a ball and socket configuration connecting the femur to the pelvis, with articular cartilage covering the bones of the acetabulum and femoral head at the contact surfaces. The hip joint is one of the most heavily loaded joints in human body. In daily activities, the joint may support loads ranging from 250% BW during normal walking (Bergmann et al., 2001) to 900% BW when stumbling occurs (Bergmann et al., 1993). Although transmitting such large loads, the human hip joint can move in a nearly frictionless way, owing to the extremely low coefficient of friction of the contact surfaces ranging from 0.001 to 0.02 (Jin et al., 1997, Mow and Lai, 1980) and the unique structure of the articulate cartilage (Mow et al., 1980, Mow and Lai, 1980, Mow et al., 1984, Ateshian and Mow, 2005). Although the natural hip joint can function normally during the lifespan of a person, it may be damaged due to mechanical factors such as wear, and abnormal loading conditions which are usually believed to be among the main reasons for osteoarthritis. Osteoarthritis is the most common joint disorders affecting millions of people in the UK (Felson, 1988, Peach et al., 2005). Once affected by osteoarthritis, the natural hip joint may need to be replaced by an artificial one.

Human hip joints have been studied extensively due to the high incidence of diseases. One important aspect in the investigation of the natural hip joint during motion is the biomechanics, which are directly related to the kinematic and kinetic behaviour. The application of biomechanics to natural hip joints mainly concerns the mechanism of the musculoskeletal system and the resulting joint forces and motions. Through the investigation of biomechanics, the kinetic performance of the hip joint can be obtained through the body kinematics. To better understand the function of healthy

hip joints and the pathology of hip joint diseases, it is necessary to investigate the local mechanical environment. In addition to biomechanical studies, a large number of investigations have focused on the tribology of the natural hip joint to understand the friction, wear and lubrication. One of the important considerations in tribology is contact mechanics, which deals with how load is transferred between two contacting surfaces.

Most of the experimental studies of contact forces and contact mechanics of natural hip joints have been carried out either through implanting transducers on endo-prosthesis *in vivo* (Hodge et al., 1986, Bergmann et al., 2001) or through placing transducers or pressure-sensitive film on cadaveric hip joints (Brown and Shaw, 1983, Afoke et al., 1987, Anderson et al., 2008). However, these techniques are invasive, costly, non-repeatable, and unsuitable to undertake extensive parametric evaluations. To help overcome this problem, analytical approaches and computational modelling techniques such as RBD and FE have been adopted.

RBD is usually adopted in the investigation of biomechanics of natural hip joints because it is computationally efficient in dealing with the musculoskeletal system and able to provide body kinetics on a subject-specific level (Anderson and Pandy, 2001, Pandy, 2001, Erdemir et al., 2007). On the other hand, a number of studies on the contact mechanics and tribology of natural hip joints have been conducted using the FE method (Anderson et al., 2008, Anderson et al., 2010, Harris et al., 2012, Henak et al., 2011, Ferguson et al., 2000a, Ferguson et al., 2000b). However, most studies on contact mechanics of the natural joint adopted previous experimental joint forces that were derived from patients with artificial joints as model inputs, and furthermore, few studies have successfully predicted the time dependent behaviour of the natural hip cartilage in a three dimensional model under physiological loads, even though the time dependent behaviour of the cartilage plays an essential role in hip function.

Consequently, it is important to take into account both biomechanical and the time dependent tribological factors in the investigation of natural hip joints. This thesis focuses on combining computational biomechanics and biotribological modelling of natural hip joints to predict the contact

mechanics. This chapter reviews in general the anatomy, biomechanics modelling, tribology and contact mechanics for natural hip joints.

1.2 Hip joint

The hip joint is a ball-and-socket joint which can rotate in all directions and belongs to the most moveable type of synovial joints. Unlike the shoulder which is another ball-and-socket joint, the hip provides not only mobility but also provides support for the body. Due to its deep socket, the acetabulum, strong joint capsule and surrounding ligaments and muscles, the hip joint is the strongest weight-bearing joint of the body.

1.2.1 Bones

The hip joint is formed where the roughly spherical head of the femur fits into the cup-like acetabulum serving as the connection between pelvis and femur as shown in **Figure 1.1** and **Figure 1.2**.

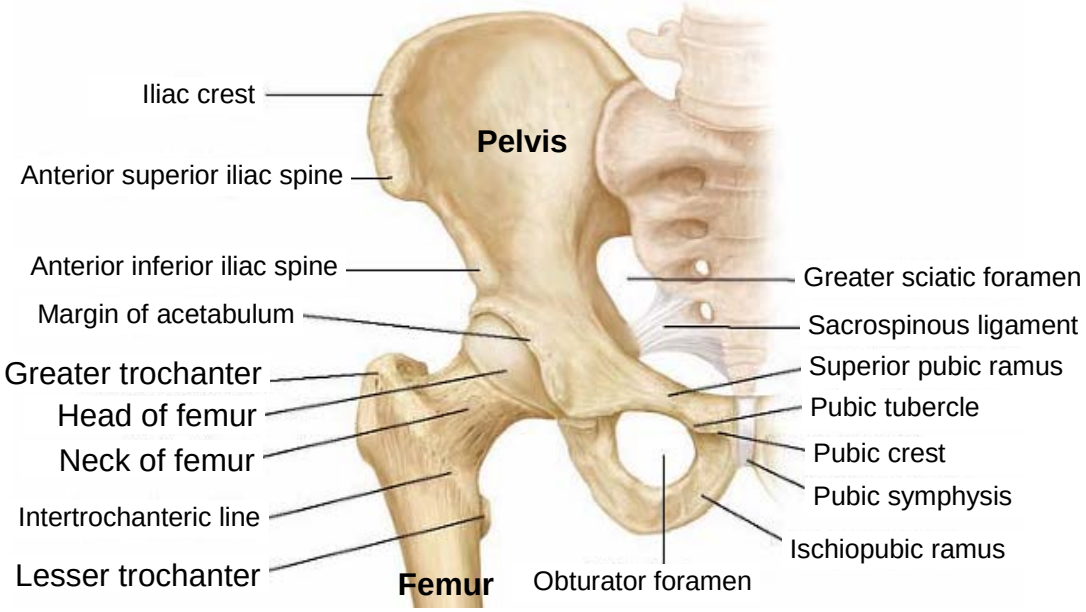

Figure 1.1 Anterior view of skeleton of the hip (Tank et al., 2009).

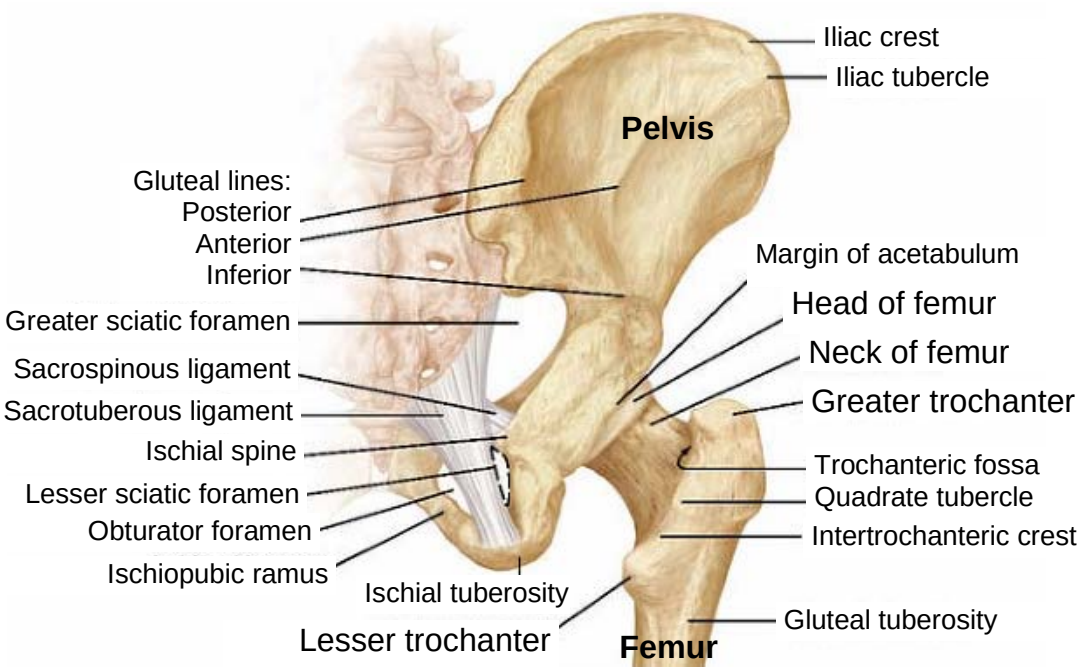

Figure 1.2 Posterior view of skeleton of the hip (Tank et al., 2009).

The femur is the longest bone in the body, divided into three parts: the upper femur beginning from femoral head and neck to the lower limit of the lesser trochanter; the shaft beginning from the lesser trochanter to the distal portion; and the distal portion forming the lower end of the femur which articulates with the knee joint. The greater trochanter and lesser trochanter are two protrusions projecting from the upper and lower part of the base of the femoral neck respectively, serving as the attachment points of strong muscles (Valliappan et al., 1977). The femoral neck lies between the femoral head and the greater and lesser trochanter, connecting the femoral head with femoral shaft.

The angle between the femoral neck axis and shaft axis, namely the neck-shaft angle, is approximately 130 ± 7 degrees (mean ± standard deviation) (Reikeras et al., 1982). The femoral neck connects to the femoral head, which is the highest part of the femur and forms roughly two thirds of a sphere. The diameter of the femoral head ranges from 40 to 60 mm according to the size of the individual (Hoaglund and Low, 1980).

Articulating with the femoral head, the acetabulum is a cup-shaped cavity where the three components of the pelvis (ilium, ischium, and pubis) meet

(**Figure 1.3**). The ilium is the superior bone of the pelvis. The ischium forms the inferior and posterior part of the pelvis. The pubis is the inferior and anterior part of the pelvis. These three bones constitute the pelvis which, together with the sacrum, transfer the weight of the upper body to the hip joint (Phillips et al., 2007).

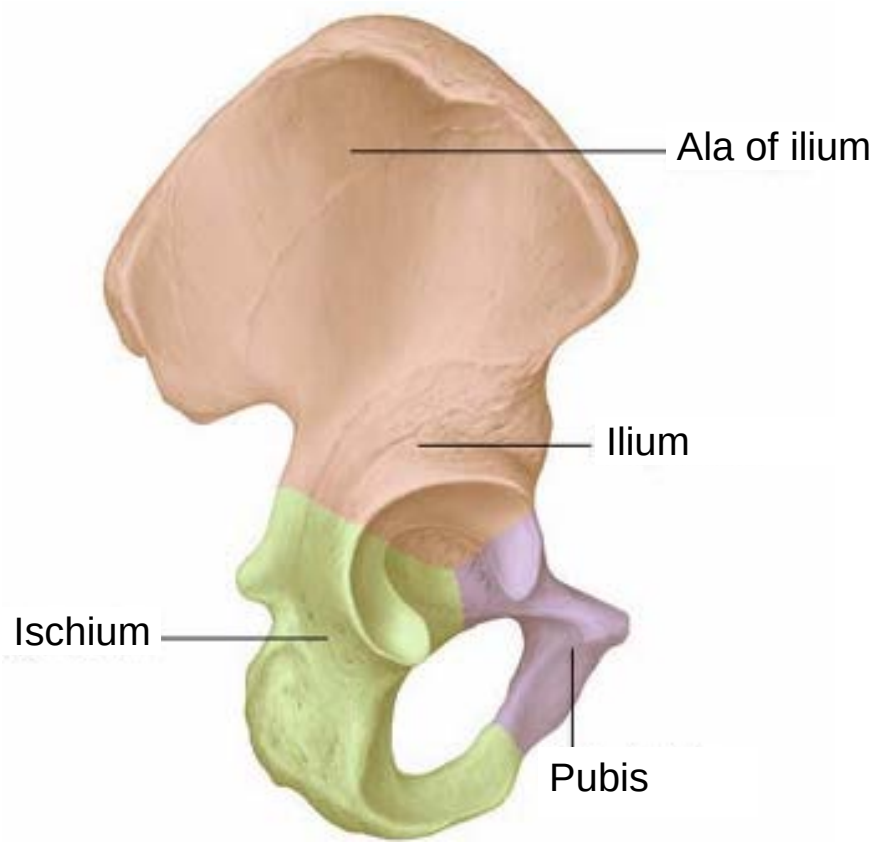

Figure 1.3 Lateral view of the right half of the pelvis illustrating the regions that form the acetabulum (Tank et al., 2009).

1.2.2 Capsule, ligaments and muscles

Around the interior surface of the hip joint lies a thin membrane called the synovial membrane which produces synovial fluid that lubricates the articular cartilage (**Figure 1.4**). Outside this membrane is the hip joint capsule enclosing the entire hip joint. This capsule is a dense fibrous tissue attached to the bone. It stabilizes the joint through movement limitation and, at the same time, facilitates the large range movement of the hip joint (Ralphs and Benjamin, 1994). The thickened part of the capsule forms the capsule

ligaments which help provide hip stability (Hewitt et al., 2001, Ito et al., 2009). The major ligaments are shown in **Figure 1.5**.

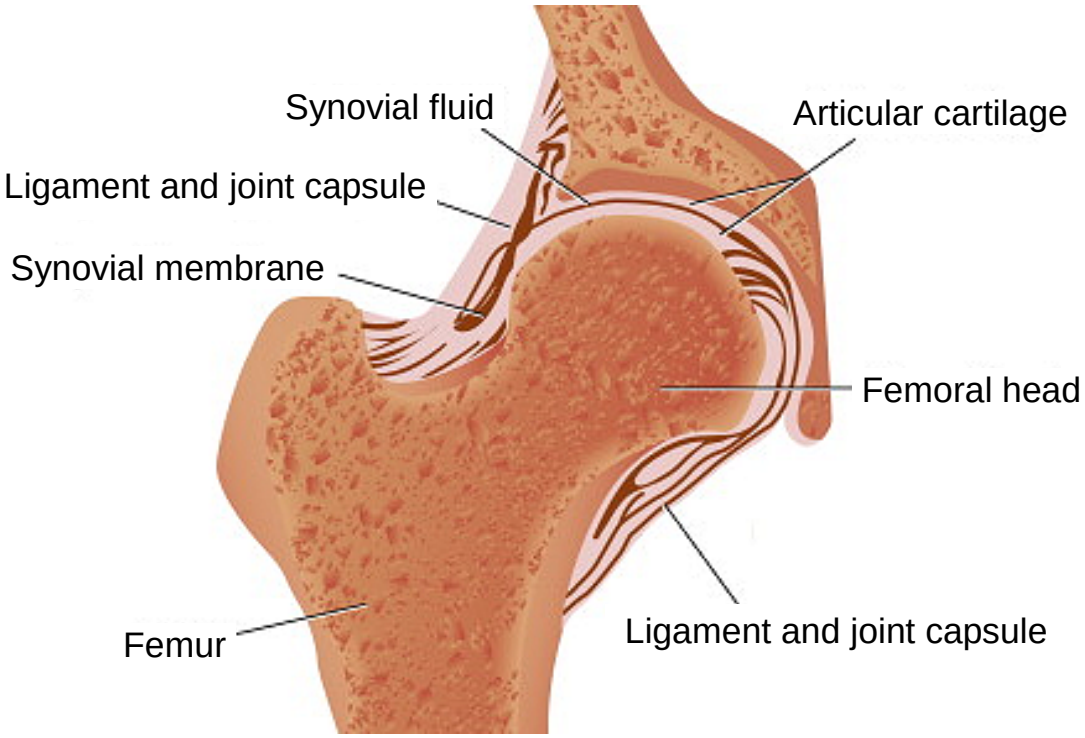

Figure 1.4 Coronal section through hip joint (Baura, 2012)

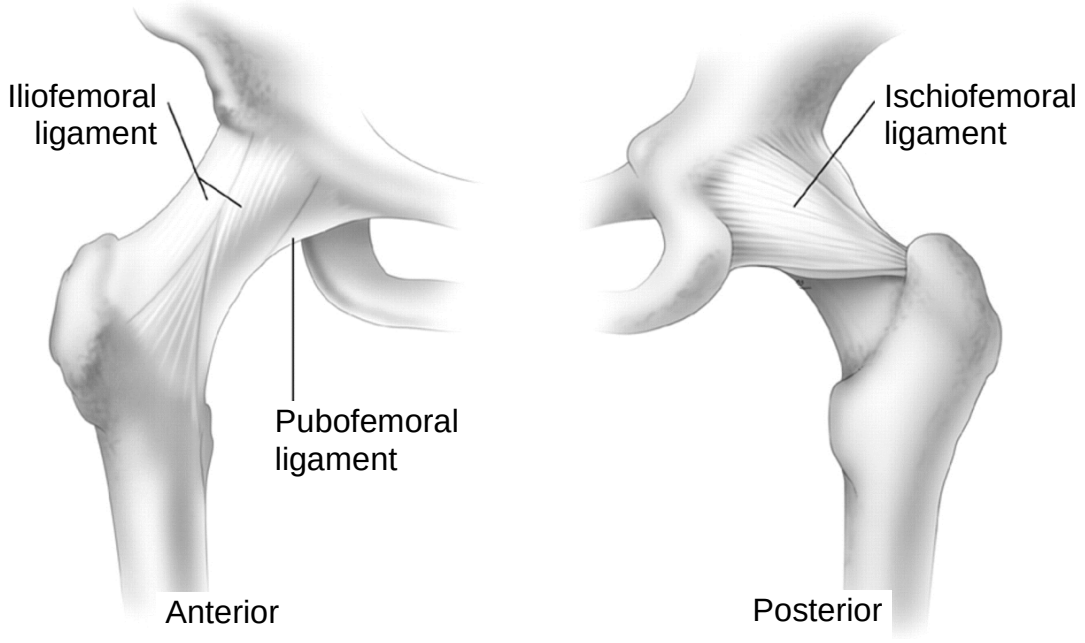

Figure 1.5 Major ligaments of the hip joint (Kelly et al., 2003)

The hip joint muscles line outside the hip joint ligaments driving the motion of the bones as well as assisting the ligaments in providing stability. There are over 20 muscles around the hip joint, and the major muscles are shown in **Figure 1.6**.

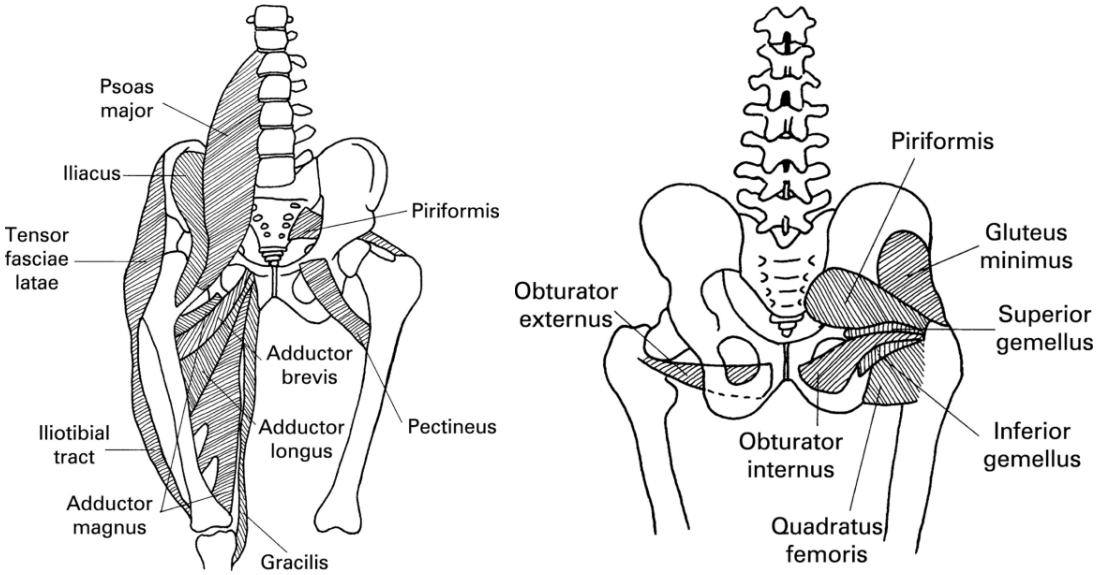

Figure 1.6 Anterior (left) and posterior (right) view of the pelvis, hip joint, and upper femur displaying the major muscles (Manning et al., 2008)

1.2.3 Cartilage and labrum

The hip joint cartilage is classified as articular cartilage. It covers the surface of the femoral head and the inside of the acetabulum, bearing the load and functioning as lubrication for the hip joint. Around the outer edge of the acetabulum is a meniscus rim of fibrocartilage called the labrum (**Figure 1.7**). This is attached to the osseous margin of the acetabulum and deepens the acetabular socket, thus extending the coverage of femoral head (Ferguson et al., 2000a, Ferguson et al., 2000b).

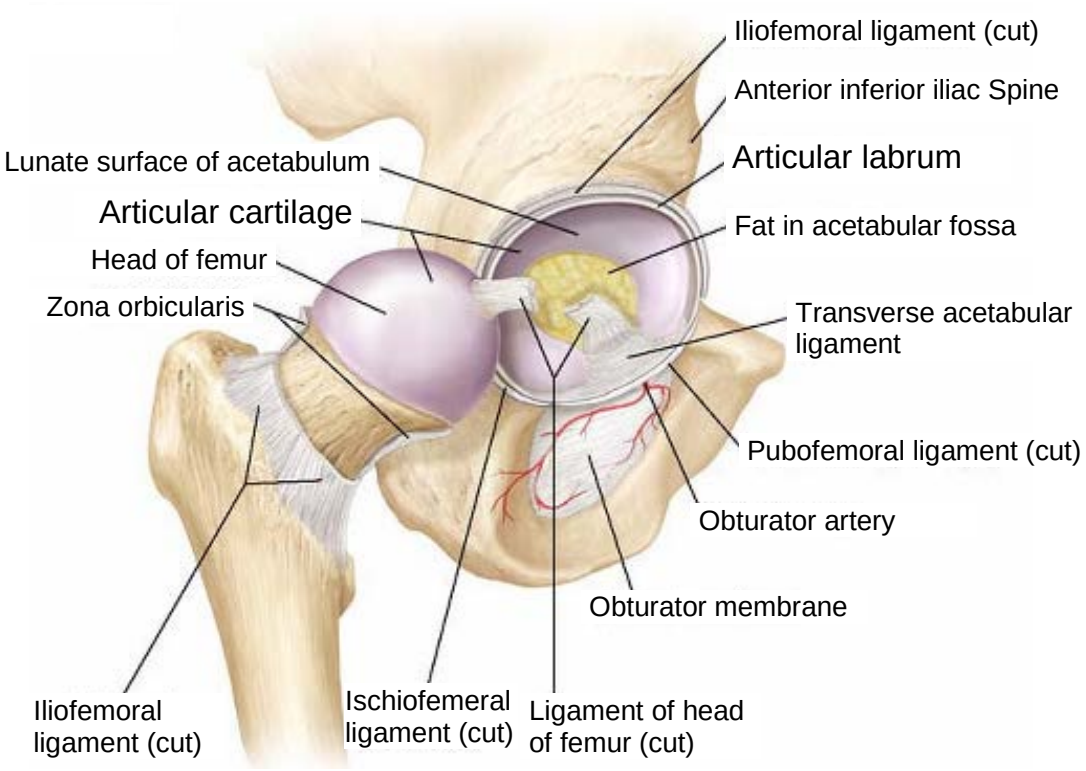

Figure 1.7 The structure of the hip joint (Tank et al., 2009).

The thickness of articular cartilage of human hip joint is not uniform across the whole joint area but its variations between different regions of the acetabulum and the femoral head are generally not significant (Shepherd and Seedhom, 1999). The thickness of the cartilage of the femoral head and acetabulum reported by different literatures varies but mainly ranges from 1 to 3 mm (Athanasiou et al., 1994, Adam et al., 1998, Naish et al., 2006, Shepherd and Seedhom, 1999). The thickness of articular cartilage is related to gender, age and joint health, and also varies between individuals. Cartilage thinning was found in patients with osteoarthritis and in elderly women (Hudelmaier et al., 2001, Karvonen et al., 1994, Fenlin and Frieman, 1998, Hunter et al., 2008). Also, males were reported to have higher thickness of cartilage than females (Jones, Glisson et al. 2000).

The cartilage structure and continuum modelling will be mentioned in **section 1.6**.

1.3 Hip kinematics

The hip joint is a ball-and-socket joint and has a large range of motion, second only to shoulder. Regarding the hip joint, kinematics describes the motion of bodies and systems without consideration of the related force. To describe the kinematics of the hip joint, three mutually perpendicular planes are generally adopted: the sagittal plane, the frontal plane and the transverse plane (**Figure 1.8**). The sagittal plane is the vertical plane which divides the body into the left and right sections. Perpendicular to the sagittal plane and the ground is the frontal plane which separates the anterior and posterior parts. The transverse plane is the horizontal plane bisecting the body into the superior and inferior halves. The motion of the hip joint has three degrees of freedom depicted as three pairs of principle directions: flexion and extension (moving the thigh forward and backward respectively within the sagittal plane), adduction and abduction (moving the thigh inward and outward respectively within the frontal plane), and internal rotation and external rotation (along the axis perpendicular to the transverse plane, causing the knee to turn inward and outward respectively).

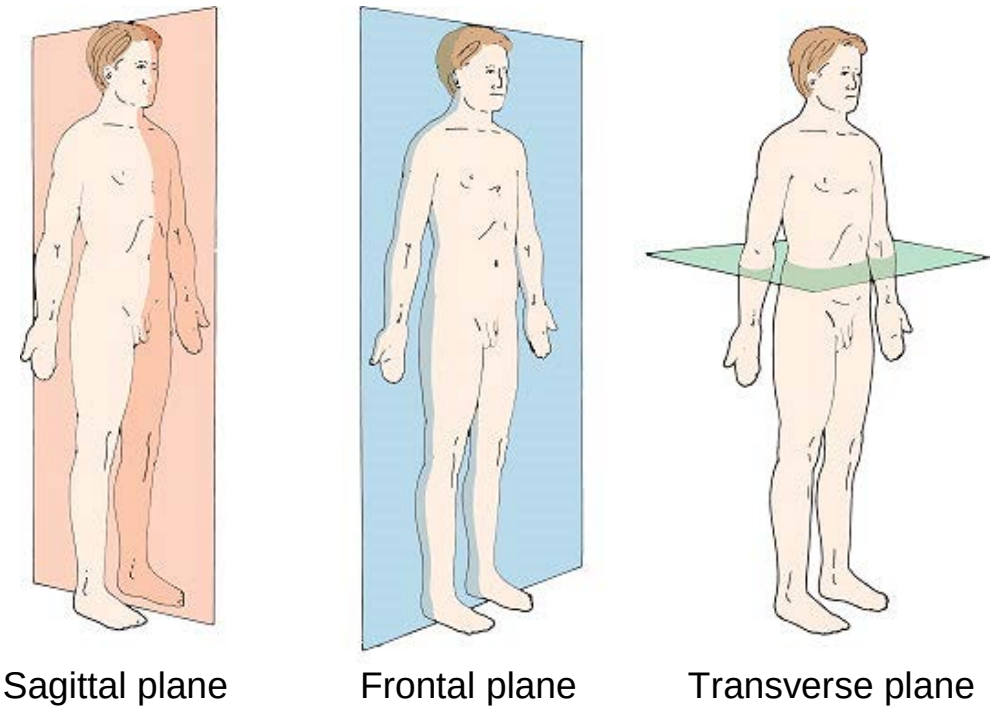

Figure 1.8 Sagittal, frontal, and transverse planes (Selinger, 2007).

The most common form of human activity is walking, the manner of which is called gait. The gait cycle is a single sequence of motion beginning and ending at heel strike of the same foot. Each gait cycle is divided into two phases: the stance phase and the swing phase. The stance phase describes the entire time interval when foot is on the ground and contributes to about 60% of the gait cycle. The swing phase is the term which depicts the time interval when foot is lifted from the ground, and constitutes around 40% of the gait cycle. The hip joint moves in all of its three degrees of freedom during a gait cycle. The kinematic information during gait is shown in **Figure 1.9**.

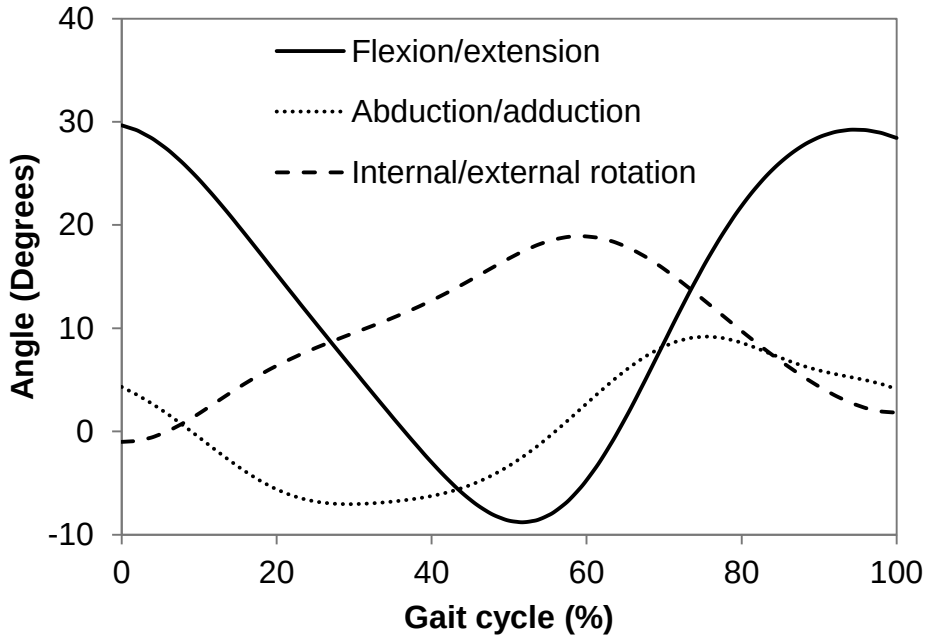

Figure 1.9 Range of motion as a function of gait cycle during normal walking (Bergmann et al., 2001).

Gait pattern measurements have been generally carried out non-invasively through attaching markers to the skin in relation to bony landmarks (Crowninshield et al., 1978). The motion of the skin makers can be then captured by photographic cameras, and the movement of joints in relation to time recorded. However, the skin movement and the location of skin makers could both affect the accuracy of this method (Baker, 2006). More recent attempts have been made to measure bones and joints directly in gait

patterns through MRI (Asakawa et al., 2003, Rebmann and Sheehan, 2003, Barrance et al., 2005) or fluoroscopy (Stagni et al., 2005).

1.4 Hip kinetics

Hip joint kinetics refers to the forces and moments generated in the joint during motion. It is closely related to the BW, motion and muscle forces and is assumed to play a significant role in the degeneration of the hip joint (Paul, 1967). During normal walking, the hip joint contact force typically involves two peaks which occur at heel-strike and toe-off (**Figure 1.10**). Studies on hip joint kinetics have been carried out using both experimental approaches and analytical/computational methods.

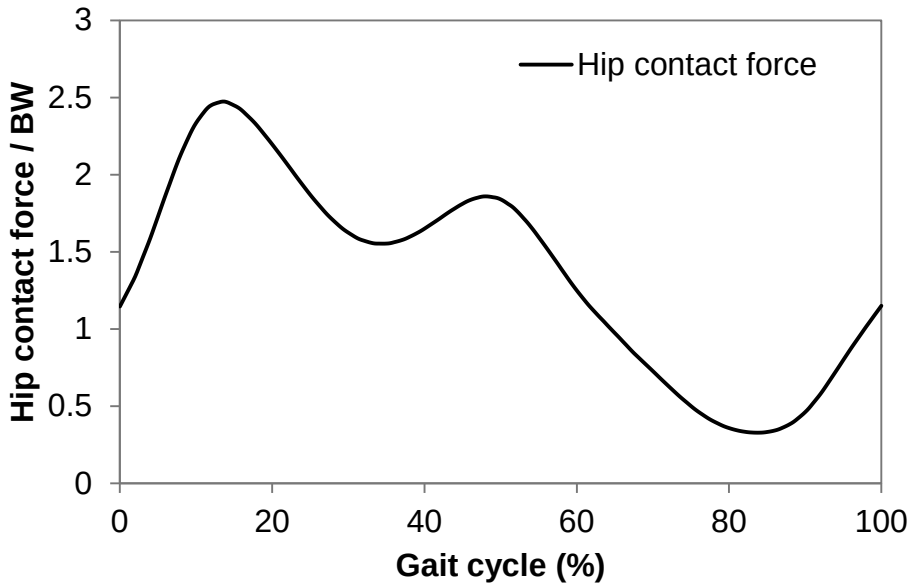

Figure 1.10 Magnitude of hip joint force normalized by BW as a function of gait cycle during normal walking (Bergmann et al., 2001). The maximum hip joint force occurred at approximately 14% of the cycle.

Analytical studies can predict joint kinetics non-invasively. Paul (1967) calculated the maximum contact force at the hip joint during walking to be 3 to 5 times BW through experimental measurements of body kinematics and ground reaction (ground-to-foot) force. However, since the musculoskeletal

analytical model is a redundant system in which the unknowns outnumber their equations, unique solutions cannot be achieved and optimization is required. More recently, computational simulation has become popular in the determination of joint forces and muscle forces using musculoskeletal models based on anthropometry (Anderson and Pandy, 2001, Pandy, 2001, Erdemir et al., 2007)

Table 1-1 Peak hip contact forces normalized by BW of 11 activities (Bergmann et al., 1993, Bergmann et al., 2001). The peak loads data of the first nine activities were averaged data from three patients (Bergmann et al., 2001). The data of the last two activities were based on individual measurements (Bergmann et al., 1993).

Activity	Peak contact force /BW
Slow walking	2.42
Normal walking	2.38
Fast walking	2.50
Up stairs	2.51
Down stairs	2.60
Standing up	1.90
Standing down	1.56
Standing on 2-1-2 legs	2.31
Knee bend	1.43
Jogging	5.84
Stumbling	8.70

In the case of experimental studies, *in vivo* measurements have been usually carried out with instrumented prostheses to obtain contact forces (Rydell, 1966, Bergmann et al., 2001, Kotzar et al., 1991). In these studies, hip joints of patients with joint diseases were replaced by instrumented prostheses embedded with transducers to measure joint force. Measurements were conducted during a variety of daily activities. **Table 1-1** lists peak forces of during daily activities measured by Bergmann et al. (1993, 2001). However, such invasive techniques cannot be applied to measure the kinetics for healthy joints.

1.5 Hip kinetics: musculoskeletal modelling

Muscle forces and joint forces can be determined computationally using a musculoskeletal model which is derived from anthropometry. Such models are usually based on RBD for computational efficiency (Erdemir et al., 2007, Pandy, 2001, Paul, 1967, Crowninshield et al., 1978).

1.5.1 Rigid-body dynamics musculoskeletal modelling

The RBD model for the hip kinetics calculation usually involves the lower extremity of human body including the pelvis, thigh, shank, and foot of both legs (Erdemir et al., 2007, Wehner et al., 2009). Also for computational efficiency, the joints are assumed to be in simple forms. For example, the hip joints, knee joints and ankle joints were usually modelled respectively as spherical joints with three rotational degrees of freedom, hinge joints with one rotational degree of freedom, and cardan joints with two rotational degrees of freedom (Wehner et al., 2009). These bones and joints, together with the surrounding muscles, form the musculoskeletal model. The muscle forces and the resulting contact forces of the hip joint can be calculated based on the kinematics of the lower limb and the ground reaction force which can be measured non-invasively.

Early attempts to simulate dynamic movement of the lower extremity were usually based on two dimensional musculoskeletal models; for example,

sagittal-plane models (Cole et al., 1996, Piazza and Delp, 1996). With the development of musculoskeletal analysis software such as OpenSim (Delp et al., 2007), SIMM (Musculographics, USA), LIFEMOD (LifeModeler, Inc., USA), and AnyBody (AnyBody Technology, Denmark), three dimensional musculoskeletal models with detailed anatomical muscle data can be established (Delp and Loan, 1995, Al Nazer et al., 2008, Damsgaard et al., 2006).

Based on Newton's second law, the basic relationship between the force applied and motion of the body segments in a musculoskeletal model can be expressed in the matrix form (**Equation ((1.1)**) (Pandy, 2001)

$$M\left(\underline{q}\right)\underline{\ddot{q}} + C\left(\underline{q}\right)\underline{\dot{q}}^2 + \underline{G}\left(\underline{q}\right) + R\left(\underline{q}\right)F^{MT} + E\left(\underline{q},\underline{\dot{q}}\right) = \underline{0} \qquad \textbf{(1.1)}$$

Where $\underline{q}$ is the vector of the coordinates for the segments. $M\left(\underline{q}\right)$ is the system mass matrix. $C\left(\underline{q}\right)\underline{\dot{q}}^2$ is a vector of centrifugal and Coriolis forces and torques. $\underline{G}\left(\underline{q}\right)$ is a vector of gravity forces and torques. $R\left(\underline{q}\right)$ is the matrix of muscle moment arms. F^{MT} is the vector of muscle forces. $R\left(\underline{q}\right)F^{MT}$ is the vector of muscle torques. $E\left(\underline{q},\underline{\dot{q}}\right)$ is the external forces and torques.

1.5.2 Muscle modelling and recruitment type

In musculoskeletal modelling, the simplest type of muscle model is an ideal force generator similar to a simple spring. Besides, the mechanical behaviour of muscles is often described by the famous Hill-type model (**Figure 1.11**) which accounts for the interaction of the force, length and velocity of the muscle, as well as the passive stiffness of the muscle and the elasticity of the tendon (Zajac, 1989, Winters and Stark, 1985).

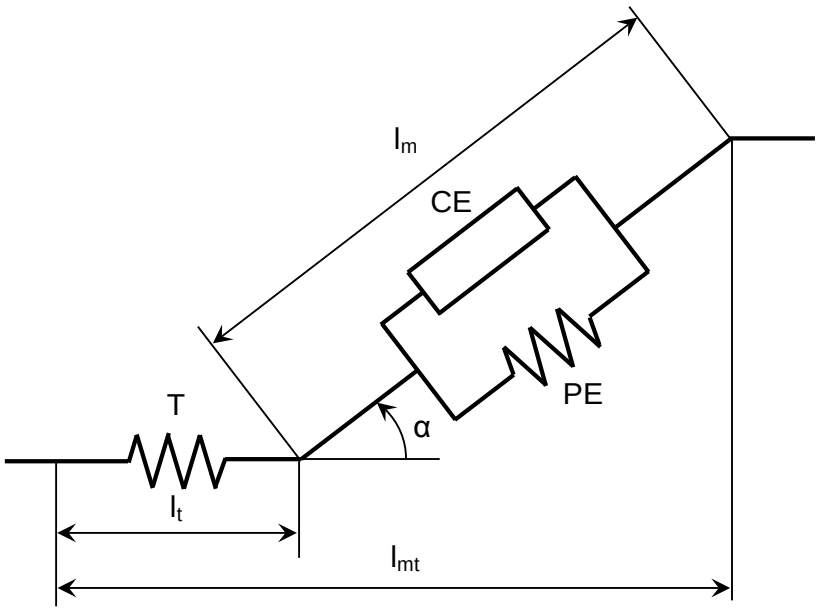

Figure 1.11 Schematic representation of the Hill musculotendon actuation (Zajac, 1989). The force-length-velocity property of muscles was modelled by a Hill-type contractile element (CE). The muscle's passive stiffness was represented by a passive element (PE). The stiffness of the tendon (T) was also incorporated.

To evaluate the influence of force-length-velocity properties of muscle on the predicted muscle forces, Anderson and Pandy (2001) conducted inverse dynamics simulation in two sets where muscles were modelled respectively as ideal force generators and materials with force-length-velocity properties. For normal walking which involves relatively low speed and a small range of motion, there was little discrepancy between the results calculated from muscles with force-length-velocity properties and those based on muscles modelled as ideal force generators.

In a musculoskeletal model, the number of muscles and ligaments crossing the hip joint is greater than the degrees of freedom for the motion of the hip joint. Therefore the hip joint forms a redundant system, which means that the muscle and ligaments forces cannot be determined uniquely (Fernandez and Pandy, 2006). Early attempts to solve this problem reduced the number of muscles and ligaments to equal the number of degrees of freedom by simplifying the muscles and ligaments into groups (Paul, 1967). More recent attempts have focused on optimization theories which are usually based on the following form:

Minimize the function

$G(F^{MT})$

Subject to

$$R\left(\underline{q}\right)F^{MT} = T_{MT} \quad \textbf{(1.2)}$$

$$0 \leq F^{MT} \leq F_{max} \quad \textbf{(1.3)}$$

Where T_{MT} is the joint torques generated by external forces and inertia forces. F_{max} is the maximum force a muscle can produce.

The minimization of cost function $G(F^{MT})$ is based on the assumptions for underlying neuronal control system. For example, in the linear muscle recruitment which minimizes the sum of muscle forces or muscle stresses, all the joint muscles are assumed to co-operate to generate the least forces required. Besides linear muscle recruitment, there are many other factors that can be minimised such as the sum of muscle forces squared (Collins, 1995, Glitsch and Baumann, 1997), muscle stresses squared (Glitsch and Baumann, 1997), muscle stresses cubed (Brand et al., 1986, Glitsch and Baumann, 1997, Pedersen et al., 1997), higher (>3) power of muscle stresses (Crowninshield and Brand, 1981), maximum single muscle stress (Rasmussen et al., 2001) as well as composite recruitment criteria which involve several single term recruitment types (Praagman et al., 2006).

It remains debated within the literature as to which muscle recruitment criteria is the most accurate. Crowninshield and Brand (1981) found that minimizing sum of muscle stresses cubed predicted the closest result to experimental EMG patterns (this will be mentioned in the next section). However, Glitsch and Baumann (1997) argued that squared muscle stresses minimization produced the best consistency with EMG patterns. Regardless of the parameters used, it should be noted that musculoskeletal modelling tends to predict higher muscle forces and joint contact forces, potentially because of the lack of realistic wrapping of muscle paths around the joint or

due to the absence of soft tissue (e.g. muscle volume), both of which make moment arms smaller than the real value. By far, however, numerical techniques serve as the only approach to predict contact forces for healthy joints.

1.5.3 Inverse solution and forward solution

Once the musculoskeletal model has been formulated, the muscle forces and joint force can be determined by either inverse or forward dynamics.

Inverse dynamics is usually referred to as static optimization in that it carries out a different optimization procedure at each moment of the movement when joint torques can be determined to optimize muscle forces (Pandy, 2001). Although inverse dynamics is computationally efficient, it is thought to have two main drawbacks. First, inverse dynamics requires accurate recording of body kinematics which is not easy to achieve (Patriarco et al., 1981). Second, the dynamic process cannot be properly characterized because of the time independent nature of inverse dynamics (Pandy, 2001).

Forward dynamics, on the other side, avoids these problems by using an initial set of muscle activations as inputs to obtain the corresponding body motions. Then the muscle activations are optimized to best reproduce the experimentally measured kinematics. Consequently, forward dynamics is usually referred to as a dynamics optimization approach. However, this process of multiple integrations makes the forward dynamics optimization much more computationally involved, as compared with inverse dynamics (Erdemir et al., 2007).

Although these two optimization methods adopt different approaches, the results of muscle forces and joint contact forces predicted by the two methods were found to be similar (Anderson and Pandy, 2001, Pandy, 2001). A comparison of inverse and forward dynamics was conducted by Anderson and Pandy (2001). For the purpose of using the same set of body motions and joint torques, the joint moments calculated by the forward dynamics were adopted as the input for the inverse dynamics. Highly similar results were found between forward and inverse dynamics in predicting

muscle forces and joint contact forces. However, this method of comparison only demonstrated that the static approach and the dynamic approach numerically predicted similar results; the model sensitivity to measurement errors in kinematic inputs was not evaluated, because the inputs of the inverse dynamics approach were not taken from kinematics data directly.

Generally speaking, both inverse dynamics and forward dynamics have two drawbacks. First, the right form of cost function which can represent the true mechanism of human muscles is unknown (Buchanan and Shreeve, 1996). Second, the optimization theories may not suit for patients who suffer from neurological impairments which make their muscle patterns different from those of normal people, or for patients with pain who may tend to avoid mechanical stress on the painful tissue (Erdemir et al., 2007). These problems in optimization methods can be overcome by an experimental approach called EMG which measures whether muscles are active or not through the electrical potential generated by activated muscle cells under the skin. Instead of solely optimizing muscle forces through cost functions, the muscle forces measured by EMG can be used as inputs to both forward dynamics (Koo and Mak, 2005, Piazza and Delp, 1996) and inverse dynamics (Amarantini and Martin, 2004, Lloyd and Besier, 2003). Nevertheless, EMG is not capable of measuring forces of deep muscles. Direct *in vivo* measurement of muscle forces can be carried out during a surgery in which a tendon is attached with a force transducer (Dennerlein et al., 1998, Schuind et al., 1992). However, such approaches are too invasive to be applied to clinical applications and may alter the muscle collaboration pattern.

1.6 Cartilage structure and continuum modelling

1.6.1 Structure

In biomechanical terms, articular cartilage is considered to be composed of two principal phases: a solid phase which includes chondrocytes, collagen fibrils, proteoglycans and other glycoproteins, and a water-like fluid phase made up of water and electrolytes (Mow et al., 1984, Mow and Lai, 1980).

Other authors have considered the charge as an additional phase (Lai et al., 1991).

The fluid phase or interstitial fluid weighs about 60% to 85% of the cartilage (Mow et al., 1992). Collagen forms the largest portion of the organic solid phase weighing about half of the dry weight. The second major component of the matrix are proteoglycans which account for 20% - 30% of the dry weight (Mow and Guo, 2002). At the ultrastructure level, collagen has a high degree of depth dependence, forming four major zones or layers: a superficial tangential zone where collagen fibrils are densely packed and oriented parallel to the surface; a middle zone composed of randomly and sparsely arranged collagen fibrils; a deep zone in which collagen fibrils form larger bundles, cross the tidemark and insert perpendicularly into the final calcified zone which anchors the cartilage to the bony structure (**Figure 1.12**) (Mow et al., 1984, Mow et al., 1992).

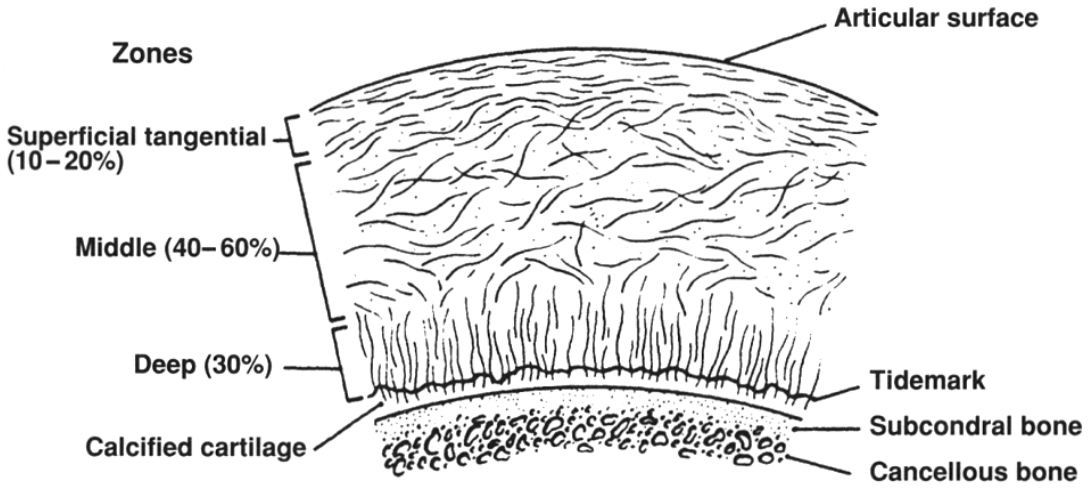

Figure 1.12 The arrangement of collagen network of articular cartilage forms four major zones. (Mow et al., 1992)

In addition to collagen, the fluid and proteoglycan content of articular cartilage show different densities with depth as well, with fluid content decreasing and proteoglycan percentage increasing from the articular surface to deeper regions (Mow et al., 1984).

The labrum is also believed to be composed of a fluid phase and a solid phase formed by collagen fibre bundles. However, the material and constitutive property of the labrum has been poorly reported (Ferguson et al., 2000b, Ferguson et al., 2000a).

The collagen fibrils are strong in tension but weak in compression. However, the articular cartilage as a whole is not too weak to sustain a compression, because the collagen fibrils are intertwined to form a fibrous network in which the huge proteoglycans are trapped, forming a porous architecture which the fluid can flow through. The relative fluid flow through the porous structure generates a frictional drag which accounts for the time dependent viscoelastic response of the tissue. Apart from the solid-fluid interaction, the mechanical response of the tissue is also linked with the charge in the cartilage. The proteoglycans in the cartilage contain a high concentration of negatively charged groups, together with the high concentration of the electrolytes in the fluid, endowing the tissue a potential to swell and gain or lose water depending on the external ionic or mechanical environment (Mow et al., 1984).

The excellent load bearing function of the cartilage is believed to be contributed to by the interstitial fluid. Generally, the interstitial fluid supports most of the load transmitted to the articulate cartilage for a long period due to the frictional drag, leaving only a small portion of load to the solid structure (Ateshian et al., 1994), and sustaining a nearly frictionless mechanical environment for the hip joint (McCann et al., 2009, Forster and Fisher, 1996). On the other hand, the labrum has been shown to help in impeding the fluid exudation (or cartilage consolidation) process, due to its lower permeability as compared with the articular cartilage (Ferguson et al., 2000b, Ferguson et al., 2000a, Ferguson et al., 2003, Haemer et al., 2012).

1.6.2 Cartilage continuum modelling

Articular cartilage is a viscoelastic, non-linear, inhomogeneous, anisotropic and multiphasic biomaterial (Li et al., 2000, Mow et al., 1984). As the main contributors to load carrying are collagen fibrils and proteoglycans, the mechanical properties of articular cartilage are non-uniform with depth (Mow

and Guo, 2002, Roth and Mow, 1980). For example, the compressive aggregate modulus increases markedly with depth from the superficial to the deep layers of articular cartilage (Wang et al., 2001, Roth and Mow, 1980), while the permeability decreases with depth (Mow et al., 1984, Mow and Guo, 2002).

Single phase assumptions which regard the cartilage as elastic or viscoelastic were widely adopted in early determinations of cartilage properties (Sokoloff, 1966, Kempson et al., 1971, Hayes and Mockros, 1971, Parsons and Black, 1977) as well as in recent models of whole articular joints (Anderson et al., 2008, Henak et al., 2011, Harris et al., 2012). However, these single phase assumptions are not able to account for interstitial fluid of articular cartilage and the effect of different phases (i.e. fluid phase and solid phase) on the mechanical behaviour of the tissue.

As the fluid flow plays a vital role in the time dependent mechanical behaviour of articular cartilage, it is necessary to distinguish the interstitial fluid as a distinct phase and consider articular cartilage as at least a biphasic material (Mow et al., 1984). Biphasic theory assumes that articular cartilage is composed of a porous solid matrix phase and a fluid phase, both of which are intrinsically incompressible. The aggregate as a whole is compressible because fluid is able to flow through the micro-pores of the solid matrix. During compression, the hydrostatic pressure developed in the interstitial fluid initially plays the leading role in supporting the load. Then the cartilage begins to deform as the load squeezes away the interstitial fluid. Ultimately, the fluid flow ceases and the interstitial fluid pressure drops towards zero. At this stage, the solid cartilage matrix holds the entire load (Eckstein et al., 1999). Owing to the low permeability of articular cartilage, the process of fluid flow and fluid exudation is greatly resisted thus a high fluid pressure is maintained during a prolonged period of time (Ateshian et al., 1994, Mow et al., 1980).

In biphasic theory, the stress of the mixture T is contributed by both the fluid pressure p and the stress caused by the deformation of the solid matrix T^s. So the stress of the two phases can be coupled as:

$$T = -pI + T^s \qquad \textbf{(1.4)}$$

On the other hand, the displacement of the two phases can be coupled by the conservation of mass which requires that:

$$div\ (v^s + w) = 0 \quad \textbf{(1.5)}$$

Where v^s is the velocity of the solid matrix and w is the fluid flux relative to the solid matrix.

Because the fluid flux is related to both the gradient of fluid pressure as well as the porous structure of the tissue, the fluid pressure and fluid flux can be linked by:

$$w = -K \cdot \mathrm{grad}\ p \quad \textbf{(1.6)}$$

Where K is defined as the permeability of the cartilage representing the capacity of the porous solid matrix to allow fluid to flow through it.

The simplest form of biphasic theory is linear biphasic theory which assumes a linearly elastic solid phase, infinitesimal strains, constant permeability and an inviscid fluid phase (Mow et al., 1980). To better represent the mechanical behaviour of articular cartilage, this theory was extended to allow nonlinearities including strain-dependent permeability (Lai and Mow, 1980, Holmes, 1985, Accardi et al., 2011), tension-compression nonlinear solid phase (Soltz and Ateshian, 2000), solid matrix viscoelasticity (Mak, 1986), and spatial fibril orientations (Schwartz et al., 1994). The values of the parameters in these biphasic theories were usually derived by optimization approaches based on the observed force-displacement relationship of cartilage samples when loaded (Athanasiou et al., 1994, Soltz and Ateshian, 2000, Pawaskar et al., 2011). Material properties of normal human cartilage vary among different joint, location on joint and specimen. For example, elastic modulus and permeability for human hip cartilage range from 0.6 MPa to 1.8 MPa and 0.00036 to 0.00143 mm^4/Ns respectively (Athanasiou et al., 1994). Generally, human articular cartilage has an elastic modulus ranging from 0.5 MPa to 1.8 MPa, Poisson's ratio ranging from 0 to

0.1, and permeability ranging from 0.00036 to 0.0017 mm^4/Ns (Ateshian and Hung, 2006, Athanasiou et al., 1994, Mononen et al., 2012). It should be noted that the tissue properties derived from various assumptions may be different even for the same test on the same specimen (Cohen et al., 1993).

Although biphasic theory can properly represent the viscoelastic behaviour and the interstitial fluid of articular cartilage, it does not account for the interaction between the fixed charged groups in the proteoglycans and the ions in the interstitial fluid. Hence, triphasic theory (Lai et al., 1991) with an individual phase for ions and quadriphasic theory with separate anionic and cationic phases was proposed (Huyghe and Janssen, 1997). These theories are able to account for the swelling effect of the cartilage as well as the response of the tissue to the external ionic environment. However, the biphasic theory already counts in the contribution of the charge to the mechanical response of the tissue. If there is little variation in the external ionic environment (e.g. *in vivo* circumstance) and the contribution of the charge is not of interest, biphasic theory is appropriate to accurately represent the fluid-solid interaction.

1.7 Hip osteoarthritis and arthroplasty

1.7.1 Osteoarthritis

Osteoarthritis, which is the most prevalent disease leading to disability in an aging population, affects joint cartilage and subchondral bone, causing pain and joint dysfunction. It mainly involves progressive loss of articular cartilage, subchondral bone thickening, sclerosis and new bone formation (Peat et al., 2001, Felson, 1988). The exact etiology of osteoarthritis is as yet poorly understood, but the possible risk factors are age, overuse, obesity, trauma, malformation or deformity, muscle weakness or misalignment, joint laxity, congenital and other diseases (Vignon et al., 2006, Dagenais et al., 2009). Also, mechanical factors are generally regarded as one of the major reasons for the onset of osteoarthritis (Radin et al., 1972, Sharma et al., 2003, Davis, 1988). Diagnosis of osteoarthritis is widely carried out by x-ray because the occurrence of osteoarthritis and the loss of

cartilage leads to joint space narrowing which is detectable on radiographs (Felson, 1988, Nevitt et al., 1995, Dougados et al., 1996, Kellgren et al., 1963).

Besides structural changes, osteoarthritis-affected joint are often accompanied by increased water content and permeability of the cartilage (Brocklehurst et al., 1984, Alexopoulos et al., 2005, Armstrong and Mow, 1982, Martin and Buckwalter, 2002, Martin and Buckwalter, 2001) and reduced cartilage aggregate modulus (Akizuki et al., 1986, Armstrong and Mow, 1982, Lane et al., 1979).

1.7.2 Hemiarthroplasty and total hip replacement

Patients with hip trauma or hip disease such as osteoarthritis usually suffer from great pain which affects their locomotion patterns. To relieve their pain and to restore a normal locomotion, THR or hemiarthroplasty is required.

Hip hemiarthroplasty, in which only one of the articulating surfaces is replaced with artificial material, is manly used for femoral neck fractures (Gebhard et al., 1992, van der Meulen et al., 2002) or osteoarthritis treatment if only one of the two articular cartilage surfaces has deteriorated (Devas and Hinves, 1983).

In THR, both the femoral head and the acetabulum are replaced with prosthesis. The modern THR was proposed by John Charnley (Charnley, 1964, Charnley, 1972) who used a metallic femoral head against an ultra-high molecular polyethylene. Since then, many types of hip replacements have been developed. Based on the adoption and combination of different materials for the acetabulum (cup) and the femoral head (ball), THR can be categorized into many types such as a polyethylene cup bearing against a metal ball, a metal ball and cup, and a ceramic ball and cup (Fisher, 2011).

1.7.3 The influence of hip arthroplasty on gait

Usually, the kinematics and kinetics of THR patients do not return to those of healthy people even years after THR surgery. For example, THR patients

(one year after surgery) were found to have reduced hip contact forces and adduction moments when ascending and descending stairs (Foucher et al., 2008, Foucher et al., 2007).

In the case of gait analysis, a reduced ground reaction force was detected for the THR patients, particularly for the affected limb (McCrory et al., 2001, Long et al., 1993). Besides, THR patients walk with a lower speed, a decreased hip mobility (Perron et al., 2000, Madsen et al., 2004) and different muscle activity patterns (Long et al., 1993). Moreover, hip arthroplasty affects not only the kinematics of the operated limb but also the non-operated limb (Beaulieu et al., 2010). The mobility of both the operated and the non-operated limb of THR patients was reduced as compared to their healthy counterparts (Beaulieu et al., 2010). The alterations in kinematics and kinetics of hip locomotion patterns may be a result of patients' adaptations preoperatively or postoperatively to stimuli such as pain, instability or muscle weakness (Sicard-Rosenbaum et al., 2002).

1.7.4 Leg length inequality

Although THR has become one of the most successful orthopaedic interventions (Nilsdotter et al., 2003), patients commonly have a difference in their leg lengths after THR (McWilliams et al., 2011). If LLI is evident, THR patients will be symptomatic and may complain of "mechanical problems, pain and neurological deficit" (McWilliams et al., 2011). In the case of severe symptoms, a revision arthroplasty may be expected.

LLI following THR may be due to several different reasons. For example, the limb can be lengthened if the femoral stem protrudes or the cup is placed too low. Sometimes the surgeon may increase limb length deliberately to offset the instability caused by component mal-positioning (McWilliams et al., 2011). The mechanical symptoms of LLI include instability, dislocation and limp, thus potentially altering the mobility patterns, loads and wear of the hip (McWilliams et al., 2011, Bhave et al., 1999). LLI patients following THR were found to exhibit a decreased range of hip motion (Budenberg et al., 2012). However, the influence of LLI on hip kinetics during gait has not been quantified yet.

1.8 Biphasic lubrication

The hip joint is nearly frictionless during motion, because the coefficient of friction of cartilage is extremely low, ranging from 0.001 to 0.02 (Jin et al., 1997, Mow and Lai, 1980). This mainly owns to the high fluid support ratio in the cartilage.

As the total load transferred between the articulating surfaces (W) is shared by both the fluid phase (W_f) and solid phase (W_s) (**Equation (1.7)**), the friction coefficient between articulating cartilage surfaces is principally determined by the solid-fluid phase interactions.

$$W = W_f + W_s \quad \textbf{(1.7)}$$

As the friction contributed by the fluid phase is minimal compared with the solid phase, the friction force can be expressed as (Forster and Fisher, 1996):

$$F_T = \mu_S \times W_s \quad \textbf{(1.8)}$$

Where F_T is the total friction force; μ_s is the effective coefficient of friction attributed to the solid phase. If dividing the above equation by the total load, the total coefficient of friction for the aggregate (μ_T) can be derived as:

$$\mu_T = \mu_s \times \frac{W_s}{W} \quad \textbf{(1.9)}$$

From the above equation, it can be inferred that μ_s equals to the “equilibrium coefficient of friction” which describes the situation of equilibrium stage when the solid phase supports the entire load.

Generally, the fluid phase supports more than 90% of the load for the hip joint (Forster and Fisher, 1996, Forster and Fisher, 1999, Ateshian, 2009, Pawaskar et al., 2010, Haemer et al., 2012), leaving a low level of stress to

the solid phase and thus maintaining a low friction coefficient for the cartilage. As the cartilage becomes consolidated, less load is shared by the fluid phase, leaving more portion of load to the solid matrix, raising solid-solid contact and thus increasing coefficient of friction. This phenomenon has been demonstrated experimentally by many researchers (Forster and Fisher, 1996, Forster and Fisher, 1999, Krishnan et al., 2004).

1.9 Hip contact mechanics

Contact mechanics of hip joint is generally concerned with the contact pressure, contact area, stresses and deformation which arise as the result of two bodies brought into contact. It plays a vital role in the pathological mechanism for osteoarthritis which is the most common hip joint disorder. It is well identified that local stress distribution plays a much more important role than global joint loading on osteoarthritis pathology and provides information for preoperative planning and postoperative rehabilitation of the hip (Genda et al., 2001, Yoshida et al., 2006). Studies on contact mechanics of hip joint have been carried out from either experimental or analytical/computational approaches.

1.9.1 Experimental studies

Contact pressure of the hip joint can be measured in several approaches. Brown and Shaw (1983) measured contact stress of human hip joint by insetting an array of compliant miniature transducers in the femoral head cartilage of cadaveric hip joints. However, these discrete locations of transducers cannot infer the pressure distribution over the whole of the cartilage surface. To overcome this limitation, pressure-sensitive film was employed to determine contact pressure of natural hip joint (Afoke et al., 1987). This method is debated because the thickness (0.2 mm) and stiffness of such film may introduce measurement artefacts, considering the high congruence of the hip joint. Besides, these methods can only be applied to cadaveric human hip joints, due to their highly invasive nature. *In vivo*

measurements of contact mechanics of human hip joints can only be conducted on patients requiring femoral head or acetabulum replacement so that transducers can be embedded on the instrumented prosthesis (Krebs et al., 1991, Hodge et al., 1989, Hodge et al., 1986, Rushfeldt et al., 1981). Peak pressure of hip joints predicted by various experimental studies is listed in **Table 1-2**. Generally, the predictions using transducers embedded inside the cartilage are lower than those adopting pressure-sensitive film. This may be either because that the transducers might not be positioned at the cartilage region that bears the highest pressure, or due to the thickness of the film which affects the hip congruence.

Fluid pressurization measurement was conducted by Ferguson et al. (2003) in a study on the influence of the labrum on the fluid pressurization in hip joints. One transducer was inserted into the hip joints to measure the fluid film pressurization, and the cartilage consolidation rate was recorded by the displacement of the testing machine. However, direct measurement of fluid pressure distribution inside the cartilage of the natural hip joint is currently difficult and has only been achieved for very simple configurations which deviate from the real situation inside the hip joint due to unrealistic boundary conditions, level of confinement, etc. (Soltz and Ateshian, 1998, Park et al., 2003).

Table 1-2 Peak contact pressure of hip predicted by experimental studies

Reference	Peak pressure (MPa)	Load (N)	Activities	Measurement method
(Hodge et al., 1986)	7.00	--	Ascending stairs	Pressure-sensitive transducers on endoprostheses
	7.14	--	Rising from chair	
	6.72	--	Single-leg stance during a gait	
(Hodge et al., 1989)	4.0	--	Walking	Pressure-sensitive transducers on endoprostheses
	4.5	--	Ascending stairs	
	9.7	--	Rising from chair	
(Brown and Shaw, 1983)	8.80	2700	Walking	Transducers inserted in the cartilage of cadaveric hip joints
(Afoke et al., 1987)	4.9 - 10.2	2000 - 2500	Static load from walking, 27^0 flexion of femur	Pressure-sensitive film on cadaveric hip joints
	1.3 – 2.15	750 - 1500	0^0 neutral	
	6.0 – 10.4	2100 - 2900	18^0 extension	
(von Eisenhart et al., 1999)	7.7 ± 1.95 (mean ± standard deviation)	345% × BW	Walking	Pressure-sensitive film on cadaveric hip joints
(Anderson et al., 2008)	> 10	< 2000	Walking	Pressure-sensitive film on cadaveric hip joints

1.9.2 Analytical studies

Analytical/theoretical attempts on calculation of contact mechanics for the hip joint are easy to begin with, because the contact parameters can be derived directly from one or several equations (Eberhardt et al., 1990, Ipavec et al., 1999, Brinckmann et al., 1981). A comparison of results for different analytical studies on hip joints is listed in **Table 1-3**. Although these studies provide an initial understanding of the hip function, a great degree of assumptions were made including boundary conditions, material properties, model geometries, etc., and therefore, the accuracy of these studies were greatly limited. Besides, the analytical approach for the biphasic cartilage theory has not yet been applied to a hip joint model and has only been utilized for confined/unconfined models or indentation models (Ateshian et al., 1994, Ateshian and Wang, 1995, Ateshian et al., 1998, Soltz and Ateshian, 2000). To achieve more accurate predictions for the hip contact mechanics, other approaches (e.g. FE) are preferred.

Table 1-3 Analytical predictions on peak contact pressure of natural hip joints

Reference	Peak hip contact pressure (MPa)	Load (N)	Activities
(Brinckmann et al., 1981)	3.72	2494	Walking
(Ipavec et al., 1999)	3.00	2000	Walking
(Daniel et al., 2008)	1.79	836	Walking
	2.04	836	Ascending stairs
	2.08	847	Descending stairs

1.9.3 Computational studies

As an non-invasive approach, computational modelling can be applied to investigate the influence of model parameters, such as material properties (Wei et al., 2005) and geometry simplifications (Anderson et al., 2010). Besides, computational modelling is able to provide a wide range of model mechanics information including the distribution of stress, strain and fluid pressurization. These parameters are not experimentally measurable. Consequently, computational approaches enable a more systematic investigation on joints mechanics, as compared with experiments.

The FE method has been widely used for predicting contact mechanics of the hip joint. Early attempts estimated contact stresses of hip joint using greatly simplified two dimensional FE models (Brown and DiGioia, 1984, Ferguson et al., 2000b, Wei et al., 2005). As the development of FE commercial software in recent years, more complicated models have been attempted to better understand hip function, such as three dimensional models (Bachtar et al., 2006), models with subject-specific geometry (Anderson et al., 2008) and biphasic hip models (Pawaskar et al., 2010, Pawaskar, 2010).

Subject-specific FE models of the hip joint make allowance for the variation of hip geometry and material properties among patients (Anderson et al., 2008, Harris et al., 2012, Henak et al., 2011). Solid models were generally created from CT / MRI scanned images. Although the construction of such models requires manual segmentation and smoothing from the original images, they are believed to provide more realistic joint geometric parameters (Anderson et al., 2010). As compared with models with ideal geometry (i.e. spherical hip joint and uniform thickness), Anderson et al. (2010) argued that subject-specific geometric parameters have a great influence on the contact mechanics of the hip joint. So far, subject-specific hip joint modelling has only been applied to cartilage models with simplified constitutive relationship (e.g. hyperelastic).

Joint modelling with biphasic cartilage layers has been mostly conducted using two dimensional models (Ferguson et al., 2000b, Ferguson et al., 2000a, Haemer et al., 2012). These studies have the potential to provide

brief parametric information such as the influence of labrum on cartilage consolidation. However, these two dimensional models contain little details on the geometric parameters of the model, and therefore, three dimensional modelling is needed to provide more accurate information. Several studies have incorporated biphasic cartilage into three dimensional models of hip hemiarthroplasty, where the femoral head of the natural hip joint is replaced by a rigid prosthesis (Pawaskar et al., 2010, Pawaskar et al., 2011). However, the application of such methodology to the natural hip joint modelling which involves biphasic cartilage-on-cartilage contact has not been successful, due to convergence issues. For other joint such as knee, biphasic whole joint modelling has also been attempted three dimensionally (Gu and Li, 2011, Mononen et al., 2012, Halonen et al., 2013, Mattei et al., 2013). However, in the case of biphasic cartilage-on-cartilage contact, none of these studies applied a high physiological load for a prolonged period to reflect the time dependent behaviour of the joint cartilage. So far, it seems that no studies have successfully applied biphasic cartilage to three dimensional whole joint modelling that involves biphasic cartilage-on-cartilage contact under physiological loads.

An alternative method to calculate contact mechanics for the hip joint is DE analysis (Genda et al., 2001, Yoshida et al., 2006, Abraham et al., 2013). Within this method, the hip joint cartilage was divided into smooth fine mesh elements attached with compressive springs and shear springs to simulate compressive and shearing resistance in response to joint forces. In this way, stresses on the articular cartilage were proportional to the deformation of the springs after relative displacement occurs between the contact surfaces. Although DE analysis shows good computational efficiency, its simplified theory is not applicable to many complex situations such as biphasic modelling for the cartilage.

The peak contact pressures within models of the natural hip joint calculated by various authors using FE and DE approaches are listed in **Table 1-4**. Contact areas were not listed because they were not reported in all of these studies and they are believed to be not as directly linked with joint damage. Large variations exist within the literatures, potentially due to different geometric assumptions, boundary conditions, material properties, etc.

Table 1-4 Computational predictions for peak contact pressure of natural hip joints during daily activities

Reference	Peak contact pressure (MPa)	Load (N)	Activity	Solving method
(Yoshida et al., 2006)	2.87	--	Slow walking	DE
	3.26	--	Normal walking	
	3.28	--	Fast walking	
	5.71	--	Ascending stairs	
	3.77	--	Descending stairs	
	8.97	--	Rising from chair	
	9.36	--	Sitting on chair	
	3.65	--	Knee bending	
(Anderson et al., 2008)	10.78	1988	Normal walking	FE
	11.61	2127	Ascending stairs	
	12.73	2203	Descending stairs	
(Bachtar et al., 2006)	5.50	1988	Walking	FE
	5.34	1587	Rising from chair	
	4.99	1212	Knee bending	
(Pawaskar et al., 2010)	2.97	2050	Slow walking	FE
	2.78	1988	Normal walking	
	2.99	2118	Fast walking	
	2.98	1587	Rising from chair	
	2.57	1322	Sitting down	
	4.63	2203	Descending stairs	
	3.00	2127	Ascending stairs	
	2.42	1212	Knee bending	
	4.40	2125	Standing on 2-1-2 leg	

To evaluate the accuracy of model predictions, both verification and validation are needed. Model verification, which is to check whether the equations are solved correctly, can be conducted by mesh convergence studies as well as by comparing different solvers on the same model. On the other hand, model validation is to check whether model simplifications, material properties or boundary conditions are reasonably set up, by comparing the computed results with the experimentally measured data. Depending on the parameters to validate, simplifications can still be made for other parameters. For example, Anderson et al. (2008) validated the material properties and geometric parameters of a hip model using assumed boundary conditions that may not precisely capture the *in vivo* situation. Generally, validation for hip joints is challenging, because current measurement devices may introduce measurement artefacts to the hip joint which is highly conforming, and similar boundary conditions are difficult to achieve between experiments and computational simulations. Besides, validation against *in vivo* circumstances is impossible for the healthy hip joint due to the invasive measurement techniques.

1.10 Summary

In summary, the investigation of biomechanics and biotribology of the hip joint is necessary to evaluate the mechanical factors that are related to hip function and degeneration as well as potential interventions, and provide pre-operative planning and post-operative rehabilitation strategies. Due to the invasive nature and potential inaccuracy of experimental measurements for the hip joint that is highly conforming, numerical approaches are generally preferred particularly in the investigation of hip kinetics which refers to biomechanics and contact mechanics which is an important parameter in biotribology. RBD musculoskeletal modelling has been widely adopted to predict joint kinetics due to its computational efficiency. On the other hand, FE method serves as an effective technique to calculate joint contact mechanics and is able to provide a wide range of predictions through the incorporation of advanced materials.

Although the interstitial fluid plays an important role in the load bearing and lubrication in the articular cartilage, no studies have successfully incorporated biphasic cartilage layers to the whole joint modelling under physiological loads. Besides, the performance of hip kinetics and contact mechanics of THR patients with LLI is unknown. Solving these problems provides an important step forward in the understanding of hip performance. Additionally, the combination of biomechanics and biotribology opens the opportunities to investigate the hip performance more systematically and comprehensively.

This thesis focuses on establishing a musculoskeletal model to analyse and characterise the hip kinetics for different cohorts of people, developing a hip joint with biphasic cartilage layers to enable the investigation of its contact mechanics and associated fluid pressurisation and combining these two domains to quantify the differences in the contact mechanics and associated fluid pressurisation that arise from the variation in hip kinetics among different cohorts of people.

1.11 Aims and objectives

1.11.1 Aims

The aim of this thesis is to develop a musculoskeletal model, quantify the hip kinetics for healthy people, asymptomatic THR patients and symptomatic LLI patients, develop a generic three dimensional FE human hip model with biphasic cartilage layers to investigate contact mechanics and the associated fluid pressurisation of the joint, validate the methodology using a porcine hip joint of hemiarthroplasty, apply the model to investigate the effect of different model parameters and daily activities, and combine the musculoskeletal model and the joint model to investigate whether unilateral THR or LLI patients have abnormal contact mechanics on their non-operated healthy hip.

1.11.2 Objectives

1) To develop a RBD musculoskeletal model of human lower extremity to predict hip contact forces from the experimentally measured gait kinematics.
2) To vary the model parameters to justify the simplifications in the measured files of gait kinematics and the model.
3) To apply the developed musculoskeletal model to quantify the hip kinetics for healthy people, asymptomatic THR patients and symptomatic LLI patients.
4) To verify the constitutive relationship of biphasic modelling through comparing the predictions in two different FE solvers.
5) To develop a generic FE model of human hip with biphasic cartilage layers.
6) To vary the model parameters in order to analyse their influences on the model predictions over a prolonged loading period.
7) To apply physiological dynamic loads with spatial and temporal variations to the model in order to investigate the hip contact mechanics and the associated fluid pressurisation during daily activities.
8) To apply the predictions of the musculoskeletal model to the FE model in order to analyse the influence of THR / LLI on the contact mechanics of the non-operated hips.
9) To obtain CT scans of porcine acetabulum to create a subject-specific three dimensional solid model.
10) To develop a FE model of a hemiarthroplasty with biphasic cartilage layers from the scanned solid model.
11) To compare the simulated results to the experimentally measured data to validate the methodology of modelling the hip joint as biphasic.

Chapter 2
Musculoskeletal Modelling: Methodology Development

2.1 Introduction

As a computationally efficient and non-invasive approach, RBD modelling of the musculoskeletal system has been widely applied to the determination of muscle forces and joint forces, largely due to the existing commercial software (e.g. SIMM (Musculographics, USA), LIFEMOD (LifeModeler, Inc., USA), and AnyBody (AnyBody Technology, Denmark)) which provide anatomical information on the human musculoskeletal model such as bone geometry, muscle strength and muscle attachment points. In this study, the inverse dynamics software AnyBody (version 5.0; AnyBody Technology, Denmark) was used to determine joint forces because it enables a wide range of muscle optimization techniques and allows the users to have a great control on the model parameters through its code-operated function.

Within the musculoskeletal approach, the joint contact forces can be predicted from the body kinematics which can be collected non-invasively and easily. For this reason, it can be applied to cohort studies involving large numbers of subjects. However, measurement efficiency is usually preferred particularly for cohort studies, and thus simplifications may be assumed. For example, most of the gait files used in this and the next chapters contain the ground reaction force information for only one limb. On the other hand, there are several means to increase the computational efficiency, including the assumption of muscle modes of simple form, the symmetric scaling of segments, etc. Consequently, it is necessary to verify the adoption of such simplifications and assumptions by analysing their influences on the model predictions.

This chapter covers a brief description of methodology regarding the construction of a musculoskeletal model, and the evaluation of several assumptions in the experimental measurement and computational

modelling. The outcomes from these preliminary tests were used to inform the methodologies employed in the main studies, which are presented in **Chapter 3**.

2.2 Methods

2.2.1 Model construction

A musculoskeletal model was developed based on the LowerGaitExtremity model in AnyBody (version 5.0, AnyBody Technology, Aalborg, Denmark) and is shown in **Figure 2.1**. The musculoskeletal model of the lower extremity in AnyBody has been previously validated in the literature (Forster, 2004, Manders et al., 2008) and comprises a human lower extremity model which includes 340 muscles and 11 rigid bodies representing talus, foot, shank, patella and thigh for both legs and the pelvis. The generic muscle and joint parameters of the lower extremity model in the AnyBody Repository are based on an anthropometric dataset provided by the University of Twente (Horsman and Dirk, 2007). The model was scaled based on marker positions to represent individual variations in the length of the bones.

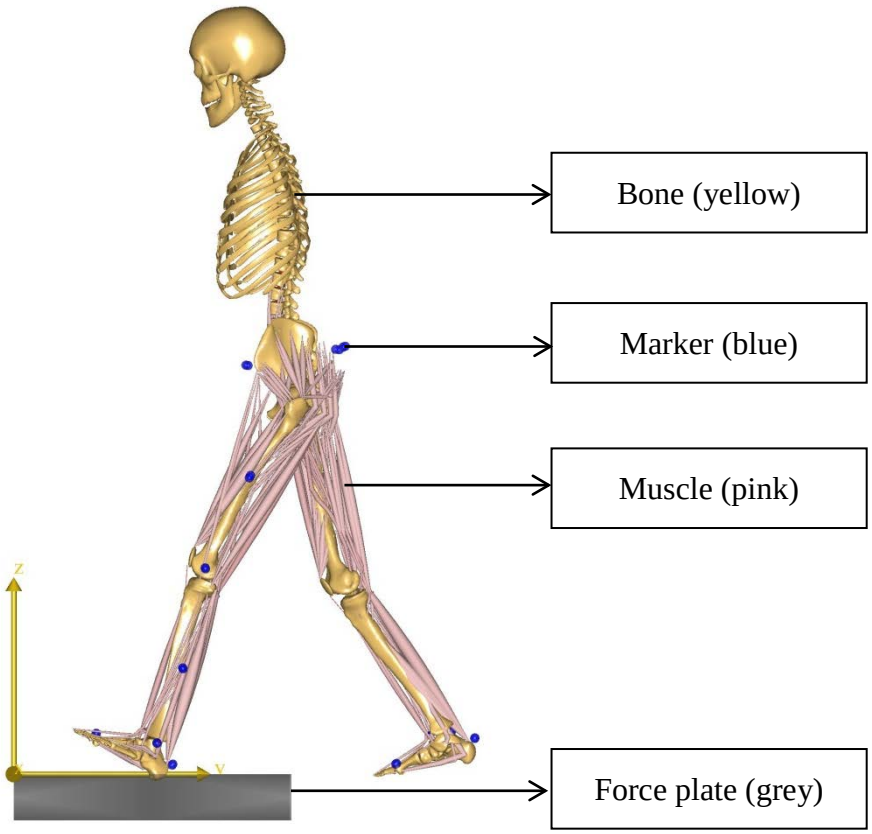

Figure 2.1 The musculoskeletal model developed was composed of bones and muscles. The blue points denote the markers which were used as the initial drivers for the model. The ground reaction force was transferred to the model through the force plate.

The human upper extremity is proposed to have little effect on the investigation of hip joint contact force, as the inverse dynamics are based on a “bottom-up” approach starting with the force plate data for ground reactions. Consequently, the arm segments were excluded for computational efficiency. However, the trunk segments were preserved for attaching the psoas major muscles, which may contribute to the hip joint kinetics. The trunk segments were constrained to the pelvis forming only one rigid body, because their kinematic information is unavailable in the measured gait kinematics.

Within the musculoskeletal model, the hip was simplified as a spherical joint which has three rotational degrees of freedom: flexion/extension, abduction/adduction and internal/external rotation. The knee, patellofemoral

and ankle joints were modelled as hinge joints for flexion/extension, and the subtalar joint was modelled as a hinge joint for inversion/eversion.

The boundary conditions of the model were based on the data in the experimentally measured gait files (in C3D format) which contain the information on the trajectories of markers attached to the lower extremity, ground reaction force and size and position of force plates. The measured gait data for one of the unilateral THR patients with LLI from previous tests (Budenberg et al., 2012) was adopted for all the sensitivities studies in the following sections.

2.2.2 Influence of different scaling approaches

Based on the marker trajectories, the lengths of the segments were scaled and kinematics optimised, reflecting parameters for each participant. In order to investigate the influence of different scaling approaches, both symmetric and asymmetric leg length scaling were performed and the results compared.

2.2.3 Influence of ground reaction force assumptions

The ground reaction force was then applied to the foot segment of the scaled model to perform inverse dynamics for the musculoskeletal model which was driven by the optimized kinematics (joint angles) in the kinematics optimization step. It should be noted that if the foot steps on the edge of the force plate, the ground reaction force may be substantially underestimated. To exclude such circumstances, force plates were included as an environment so that the interaction between the foot and force plate becomes visible. For most of the available gait files, the ground reaction force was measured only for one foot. In order to identify whether there is a difference in the hip contact force of one leg if the ground reaction force of the other foot was kept or removed, the gait file simulated in this chapter contained information on the ground reaction forces for both limbs.

2.2.4 Influence of simple muscle forms

To investigate the influence of the sophisticated Hill type muscle model on the results, muscles were treated as simple models (or ideal force generators) and Hill type respectively and the results were compared.

2.2.5 Influence of different muscle recruitment types

To evaluate the influence of different muscle optimization types on the hip kinetics, several recruitment types were evaluated by the polynomial and max/min optimization functions. The polynomial function is as follows:

$$G = \sum_{i=1}^{n} (\frac{f_i}{N_i})^p \quad \textbf{(2.1)}$$

Where G is the optimization function; i muscle number; n number of muscles; N_i strength of muscle i; f_i force of muscle i; p power of polynomial. The solution to the polynomial optimization problem with increasing p converges to the solution obtained by the min/max function (Rasmussen et al., 2001), given by:

$$G = \max\left(\frac{f_i}{N_i}\right), \quad i = 1, \dots, n \quad \textbf{(2.2)}$$

In this chapter, the polynomial function with $p = 1, \dots, 5$, and the min/max function were evaluated and compared.

2.3 Results

2.3.1 Influence of different scaling approaches

For the symmetric and asymmetric scaling approach, the optimized length of model segments are listed in **Table 2-1** and the resultant hip contact forces are shown in **Figure 2.2**. A slight difference (<5%) in segment length was

detected through the asymmetric scaling approach. The predicted hip contact forces are similar between the two scaling approaches. It should be noted that the gait file simulated is from a THR patient with LLI. For normal healthy people, the degrees of LLI should be smaller and the predictions by different scaling approaches are supposed to be more similar. Consequently, in terms of calculating hip kinetics, both scaling approaches are suitable for normal healthy people. However, the subject analysed may have a lower degree of LLI as compared with other THR or LLI patients. As a result, in the following chapter, the hip kinetics of the normal healthy people was calculated by the symmetric scaling approach which is more computationally efficient, whilst the asymmetric method was adopted for the asymptomatic THR patients and symptomatic LLI patients.

Table 2-1 Optimized length of segments by symmetric and asymmetric scaling approaches for a THR patient with symptoms of LLI. Slight differences were detected in segment length between the two scaling methods.

Segment length (mm)		Thigh length (mm)	Shank length (mm)	Foot length (mm)
Symmetric scaling		39.6	38.7	23.0
Asymmetric scaling	Left	40.1	39.4	22.8
	Right	39.2	38.1	23.1

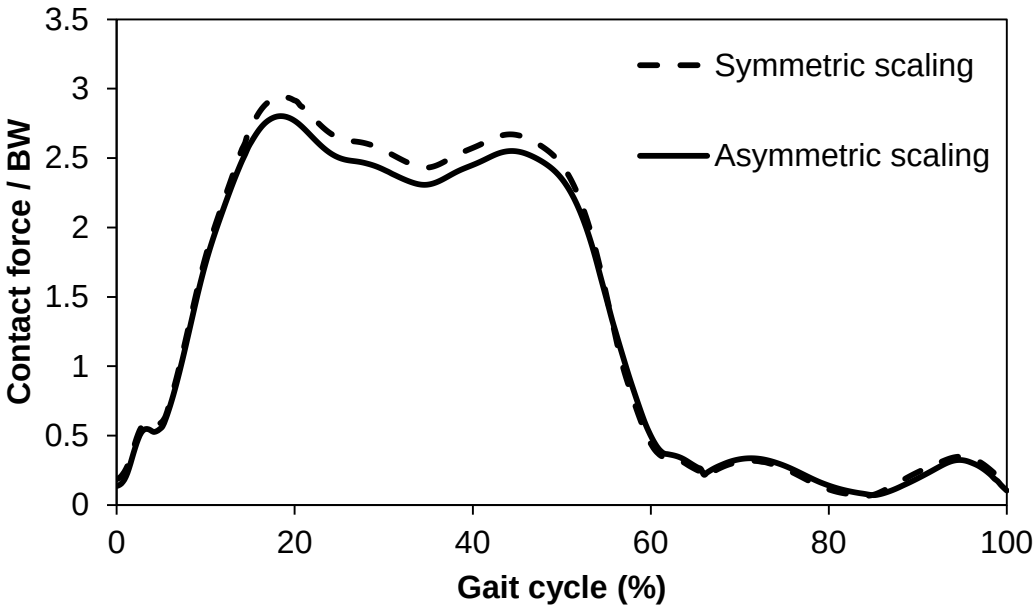

Figure 2.2 Results of BW normalized hip contact force using symmetric and asymmetric length scaling. The hip contact forces were similar between the two scaling approaches.

2.3.2 Influence of ground reaction force assumptions

As shown in **Figure 2.3**, it was found that the exclusion of ground reaction force for one limb does not affect the predicted kinetics for the other limb, suggesting that it is appropriate to use the gait files which contain ground reaction force for only one limb.

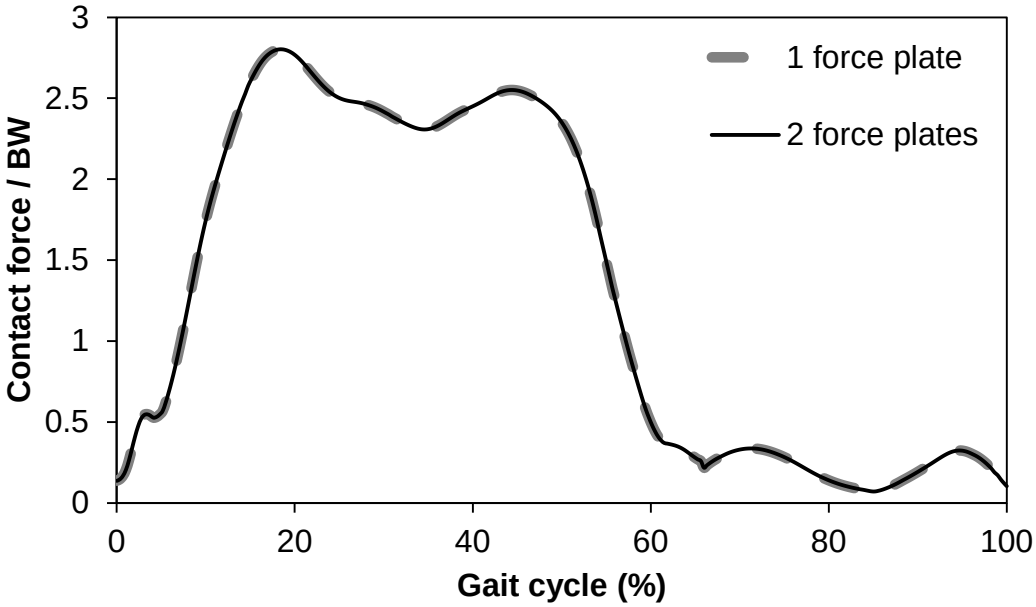

Figure 2.3 Results of BW normalized hip contact force of the model on one or two force plates. Both situations predicted identical results (the two traces nearly overlapped).

2.3.3 Influence of simple muscle forms

Regarding the forms of muscle modelling, the simple muscle model predicted slightly lower hip contact force than the 3-elements Hill type muscle (**Figure 2.4**). This is partly in agreement with a previous study (Anderson and Pandy, 2001) in which it was numerically found that force-length-velocity relationships of the Hill type muscle had little influence on the prediction of muscle forces and contact forces of hip joints during gait. Besides, the model with 3-elements muscles is substantially more computationally involved. As a result, the simple muscle model was adopted in the following chapter.

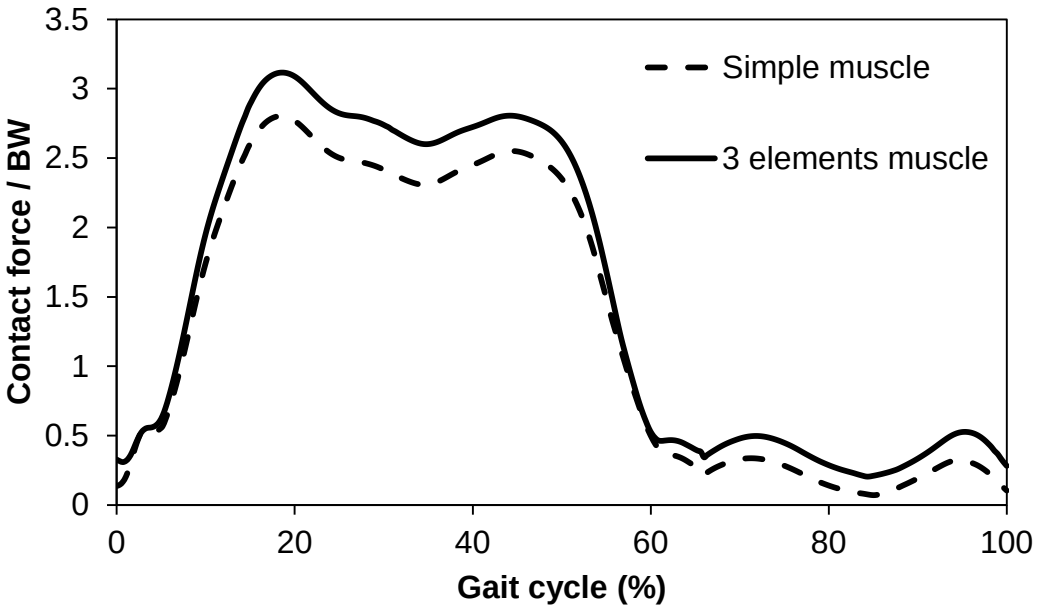

Figure 2.4 Results of BW normalized hip contact force using simple muscle models and the 3-elements Hill type model. The model with 3-elements muscles predicted about 10% higher joint force than the model with simple muscles.

2.3.4 Influence of different muscle recruitment types

As shown in **Figure 2.5**, it was found that there was a great variation in the results for hip models with different optimization functions of the muscle recruitment. Generally, a higher power of the polynomial function generated a higher hip contact force, and similar results were found for powers from 2 to 5. For the human lower extremity, previous studies have shown that power = 2 (Glitsch and Baumann, 1997, Heintz and Gutierrez-Farewik, 2007) or power = 3 (Crowninshield and Brand, 1981) predicted similar results to measured muscle forces. For the above reasons, the quadratic muscle recruitment type (power = 2) was adopted in the following chapter for the model applications.

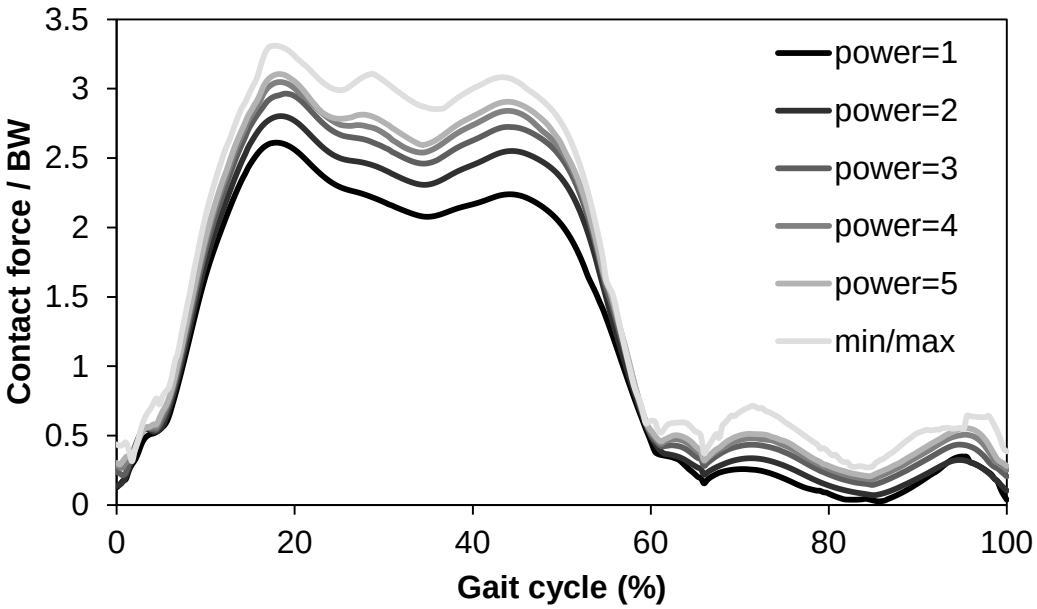

Figure 2.5 Results of BW normalized hip contact force for different optimization functions. The min/max and power = 1 recruitment types predicted the highest and lowest contact force respectively. Similar results were found for the other types (power = 2 to 5).

2.4 Conclusion

The RBD musculoskeletal model was able to predict joint contact forces from the experimentally measured gait files with great computational efficiency (less than 30 min to simulate one gait file). Based on the results found from the sensitivity studies undertaken in this chapter, the following methodology was adopted for the studies presented in **Chapter 3**:

1) The ground reaction force for only one foot was used.
2) The simple muscle model was adopted.
3) The quadratic muscle recruitment type was employed.
4) The symmetric scaling was used for the normal healthy people, whist the asymmetric scaling was adopted for the THR or LLI patient.

Chapter 3
Musculoskeletal Modelling: Application to Different Patient Cohorts

3.1 Introduction

As mentioned in **Chapter 1**, LLI, which refers to a discrepancy in leg lengths, is a common symptom for patients following THR and is believed to affect the rehabilitation performance of THR patients (McWilliams et al., 2011, Budenberg et al., 2012). Investigations into the levels of restoration to normal of activity patterns of THR patients with or without symptoms of LLI will help provide better patient care, pre-operative planning and rehabilitation strategies. Such evaluations have been poorly reported however, particularly in terms of hip contact force, a factor which is directly linked with joint damage (Wearing et al., 2006, Arokoski et al., 2000).

On the other hand, highly standardised joint kinetics have been adopted by previous models and pre-clinical tests, using generic inputs without accounting for the potential gait variations for different cohort. For example, the kinetic data of several THR patients measured by Bergmann et al. (2001) have been widely used in numerical modelling for the natural hip joint (Yoshida et al., 2006, Anderson et al., 2008, Harris et al., 2012), whilst experimental and numerical simulations for artificial hip joints tend to be loaded with the ISO standard hip kinetics (ISO-14242-1, 2002) that were derived from healthy people (Barbour et al., 1999, Williams et al., 2006, Liu et al., 2008). The validity of such standardised adoptions with mismatched cohort has yet to be evaluated.

Physiological hip contact forces can be only measured *in vivo*. However, such measurements are too invasive to be applied to healthy joints or cohort studies involving large numbers of subjects. Therefore, numerical methods serve as a valuable alternative approach. As demonstrated in **Chapter 2**, RBD musculoskeletal modelling enables efficient predictions of joint contact

forces. The aim of this study was to quantify the differences in hip kinematics and kinetics for asymptomatic unilateral THR patients, symptomatic unilateral LLI patients, as well as their normal healthy counterparts during gait using the methods determined in **Chapter 2**. Additionally, the predicted hip kinetics were compared to the ISO standard and previous measured data (Bergmann et al., 2001), in order to help provide guidelines for more realistic inputs of future modelling and testing.

3.2 Methods

The methods determined to be most appropriate from the initial studies in **Chapter 2** were adopted here.

3.2.1 Subjects

Following ethical approval, the gait kinematics and ground reaction forces for different patient groups were measured in Leeds Chapel Allerton Hospital by Dr. Anthony Redmond and Mr. Martin Stone as part of an associated study.

The cohorts studied were normal healthy individuals (‘Normal’), asymptomatic THR patients who exhibited no other co-morbidities (‘THR’), and THR patients with LLI that were symptomatic enough to require consideration for revision surgery (‘LLI’). The asymptomatic THR patients and symptomatic LLI patients were recruited at a minimum of 1 year post-operatively at the time which they were largely recovered following surgery. The marker set was positioned by a single researcher, and joint kinematics were recorded using a clinical gait analysis system comprising of an eight camera passive marker system (Vicon MX ,T40 cameras,150hz, Oxford Metrics, UK) sampling at 180 fps and 2 megapixel resolution. The ground reaction force was measured by twin force plates (Bertec, Colombus, OH, USA) at 1000 Hz. Technical error for the cameras within a working volume of 10 x 11 x 2.5 m was calculated as less than 0.2 mm for this experimental setup. Post-processing was undertaken in Vicon Nexus software (Oxford Metrics, Oxford, UK) and exported as C3D format for joint force modelling.

All of the subjects walked at a normal speed during the measurement. The demographic and anthropometric profiles of the three cohorts are shown in **Table 3-1**.

Table 3-1 Demographic and anthropometric profile of cohorts, compared to literature (mean ± 95% CI). The THR and LLI cohorts and the THR patients of Bergmann had similar age and BMI, compared with which, the healthy individuals were generally younger and had smaller BMI.

Cohorts	Number of subjects	Gender male /female	Age (yrs)	Height (m)	Weight (kg)	BMI (kg/m^2)
Normal	38	19 / 19	44.97 (40.92 to 49.03)	1.701 (1.673 to 1.729)	71.96 (68.02 to 75.90)	24.72 (23.84 to 25.61)
THR	15	4 / 11	64.27 (58.59 to 69.95)	1.705 (1.655 to 1.755)	89.69 (79.73 to 99.66)	30.74 (27.72 to 33.77)
LLI	23	5 / 18	58.70 (54.51 to 62.88)	1.615 (1.583 to 1.646)	72.71 (67.78 to 77.63)	27.86 (26.26 to 29.45
Bergmann (Bergmann et al., 2001)	4	3/1	62.17 (50.70 to 73.63)	1.710 (1.665 to 1.755)	85.26 (73.63 to 96.88)	29.05 (26.45 to 31.65)

3.2.2 Biomechanical analysis

The construction of the musculoskeletal model was descried in **Chapter 2**. Hip contact forces were determined after simulations. For a systematic evaluation of hip kinematics and kinetics, data relating to ground reaction force and hip motion obtained from the C3D files were also listed in this chapter. To offset the effect of BW, the predicted hip contact forces were normalized by BW.

3.2.3 Statistical analysis

Data are presented as mean values, along with the associated 95% CI for each cohort to present the variation within each cohort. The overall means (95% CI) for different cohorts and the results for the operated and non-operated limbs of the THR / LLI patients were compared separately. The means of each cohort were obtained by averaging the mean result of the two limbs for each subject. Because some of the gait data were not normally distributed, non-parametric statistical tests were adopted. All analyses were performed using SPSS v 18.0 (SPSS Inc., Chicago, IL). A Mann-Whitney test was used to determine whether there were differences in kinematics and kinetics between cohorts, and the comparison between operated and non-operated limbs was conducted through a Wilcoxon test. In the Mann-Whitney and Wilcoxon tests, p value was calculated which denotes the result due to chance (e.g. $p \leq 0.05$ means that there is less than 5% probability that the result is due to chance). Spearman correlations were calculated to explore the relationship between the hip contact force and the model inputs, and to investigate which input parameters were most closely related to the hip kinetics. In Spearman correlation, both p and coefficient of correlation R which describes how monotonic the relationship between two variables were determined. Additionally, correlations between the hip contact force and the anthropometric parameters (age, height, weight and BMI) were evaluated. Analyses were conducted to study the correlation for the three discrete data points represented by the middle trough (F_2) and two peaks (F_1 and F_3) of the hip contact force time curves (**Figure 3.1**) for each of the healthy cohort and the asymptomatic THR patients. A significance level $p \leq 0.05$ was regarded as significant throughout.

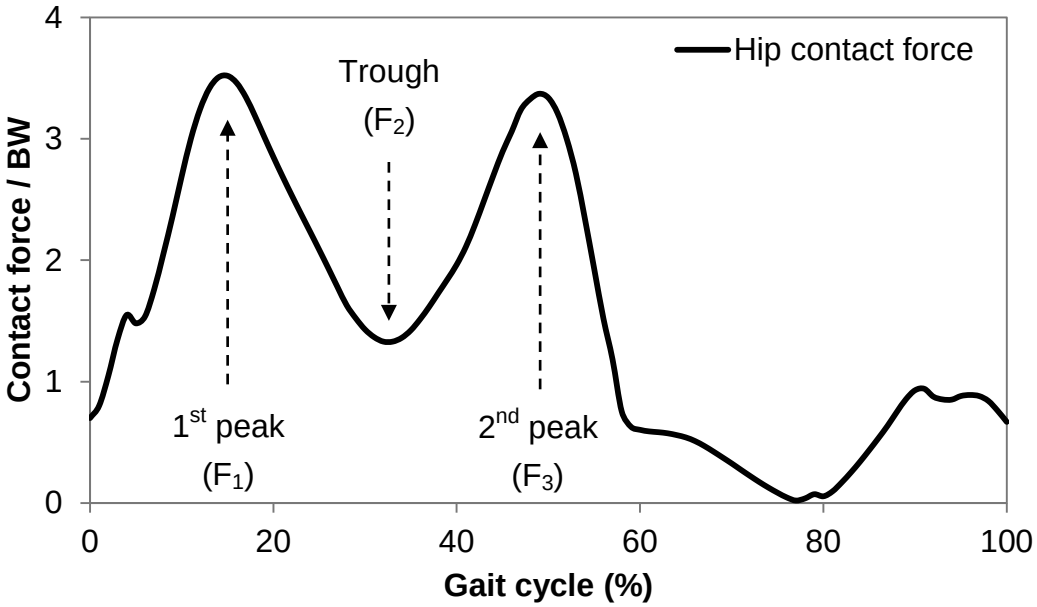

Figure 3.1 Hip contact force for one of the normal healthy people illustrating the middle trough and two peaks.

3.2.4 Comparison with previous studies

The predicted hip contact force for the operated side of the THR / LLI patients were compared with previous *in vivo* measured data (Bergmann et al., 2001) which provided comparative contact force derived from instrumented prostheses implanted in four THR patients on their operated limb. In addition, the difference between ISO data (ISO-14242-1, 2002) and the results of each cohort was evaluated. For clarification, due to the potential differences in coordinate systems used by different studies, all comparisons of joint reaction forces were represented by the magnitude of vectors.

3.3 Results

3.3.1 Velocity, cadence and stride length

The velocity, cadence (measured in steps/min) and stride length for the THR and LLI cohort was significantly reduced, as compared to the healthy individuals (**Table 3-2**). In addition, the velocity and stride length of the LLI

cohort was significantly lower than the asymptomatic THR cohort, although the cadence of these two cohorts was comparable. A similar stride length was observed for the operated and non-operated limbs of the THR and LLI cohort.

Table 3-2 Mean (95% CI) of gait velocity, cadence and stride length in the normal healthy cohort, THR and LLI cohorts for the operated (-O) and non-operated (-NO) side. The normal healthy cohort had significantly higher gait velocity, cadence and stride length than the THR / LLI patients. The THR cohort exhibited greater velocity and stride length than the LLI cohort. Similar stride length was found between the operated and non-operated hips of the THR / LLI patients.

	Velocity (m/s)	Cadence (steps/min)	Stride length (m)
Normal	1.44 (1.39 to 1.50)	121 (119 to 124)	1.43 (1.39 to 1.47)
THR-O	1.09 (1.01 to 1.18)	108 (104 to 112)	1.22 (1.13 to 1.32)
THR-NO			1.23 (1.13 to 1.32)
LLI-O	0.93 (0.83 to 1.03)	109 (104 to 114)	1.02 (0.94 to 1.10)
LLI-NO			1.02 (0.94 to 1.10)

3.3.2 Hip range of motion

As shown in **Figure 3.2**, the hip flexion/extension angle was significantly different among the cohorts, with the highest value for the normal healthy cohort and the lowest value for the LLI patients. The hip abduction/adduction angle of the LLI and THR patients was similar but significantly lower than the healthy cohort. The LLI patients displayed a significantly greater degree of hip internal/external rotation than the healthy people. Additionally, the variation in the hip range of motion for the THR / LLI patients was higher than the normal cohort.

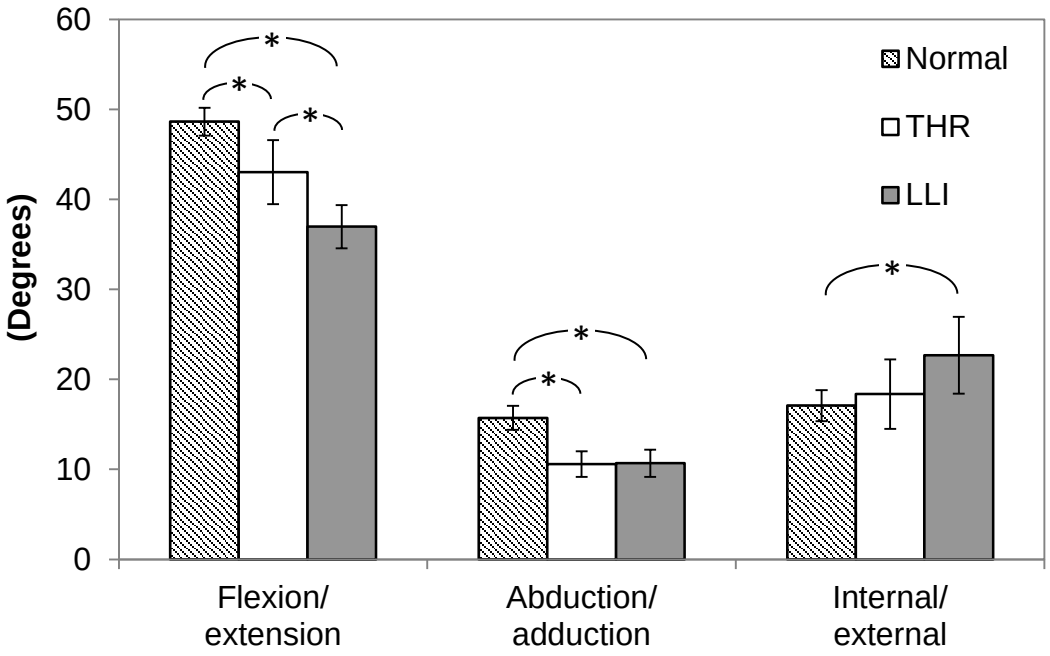

Figure 3.2 Mean ± 95% CI of range of motion for the normal cohort, THR and LLI patients. Statistically significant differences are marked with a star.

For both the THR and LLI patients, the hip flexion/extension angle on the operated limb was significantly lower than that of the non-operated limb (**Figure 3.3**). In addition, the LLI patients exhibited a higher level of asymmetry in the flexion/extension angle, as compared with the THR patients. For the abduction/adduction and internal/external rotation angles, no significant difference was observed between the operated limb and non-operated limb for the THR / LLI cohort.

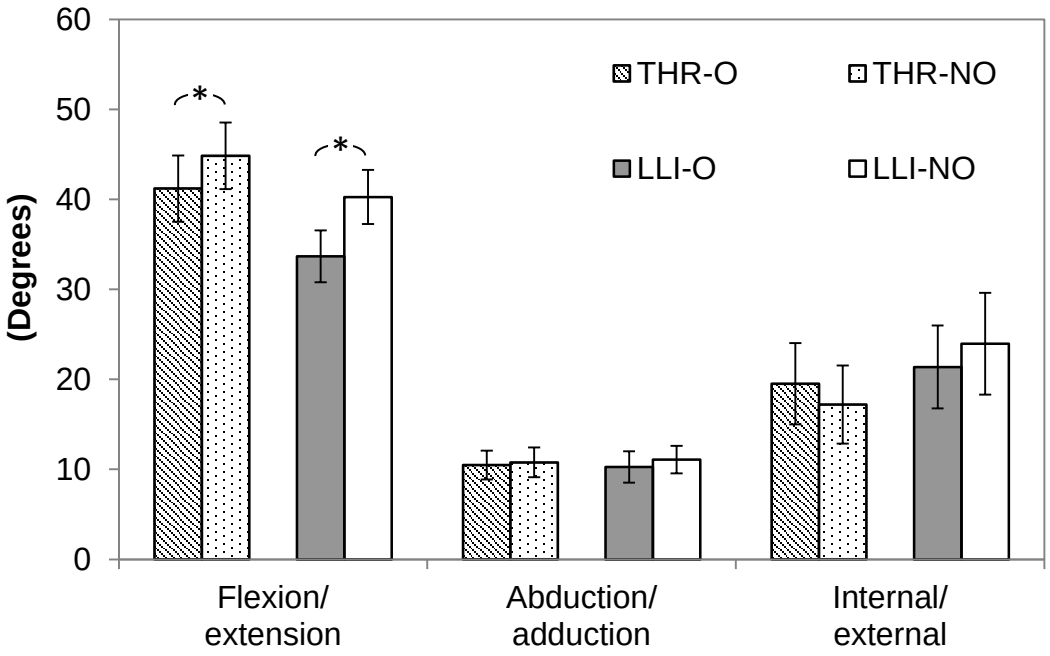

Figure 3.3 Comparison in hip range of motion between the operated and non-operated limbs of the THR / LLI patients. Data were presented by mean ± 95% CI. Statistically significant differences are marked with a star.

3.3.3 Ground reaction force

The magnitude of the ground reaction force in the asymptomatic THR patients was significantly lower than seen in the normal controls (**Figure 3.4**). Such decrease was more evident for the LLI patients. In addition, the peak ground reaction force was significantly different between the operated and non-operated limb of the LLI patients. For the THR cohort, no significant difference in the peak ground reaction force was observed between the operated and non-operated limbs.

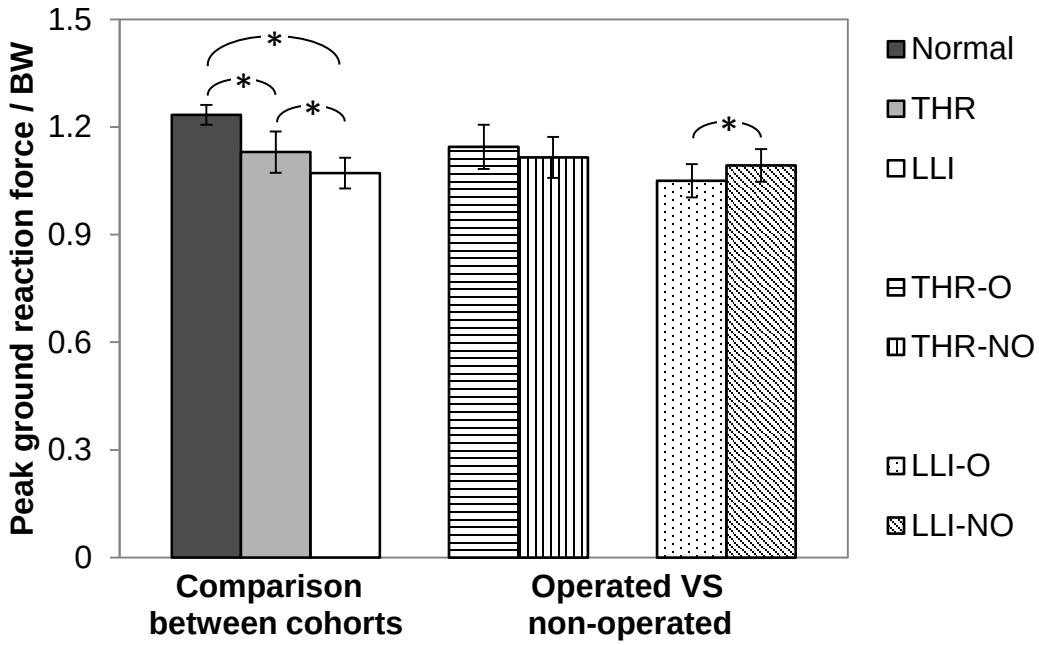

Figure 3.4 Comparison of the peak ground reaction force for the three cohorts of subjects as well as for the operated and non-operated limbs of the THR / LLI patients. Statistically significant differences are marked with a star.

3.3.4 Hip contact force

The mean hip contact force for the three cohorts is shown in **Figure 3.5**. The characteristic dynamic pattern from the 1st peak at heel-strike (~15% cycle) by the trough during mid-stance (~32% cycle), and then the 2nd peak at toe-off (~50% cycle) followed in the hip contact force, was observed in the normal people and the THR patients, but not obvious in the LLI cohort. Compared with the normal people, the THR and LLI patients exhibited a significantly lower 1st peak, higher trough and reduced 2nd peak in the hip contact force. In addition, the 1st peak and trough force of the LLI patients was significantly different from the asymptomatic THR cohort. No significant difference was observed for the 2nd peak force between the THR and LLI patients. According to the 95% CI, the variation in hip contact force of the LLI patients was similar to the asymptomatic THR patients and higher than the normal individuals.

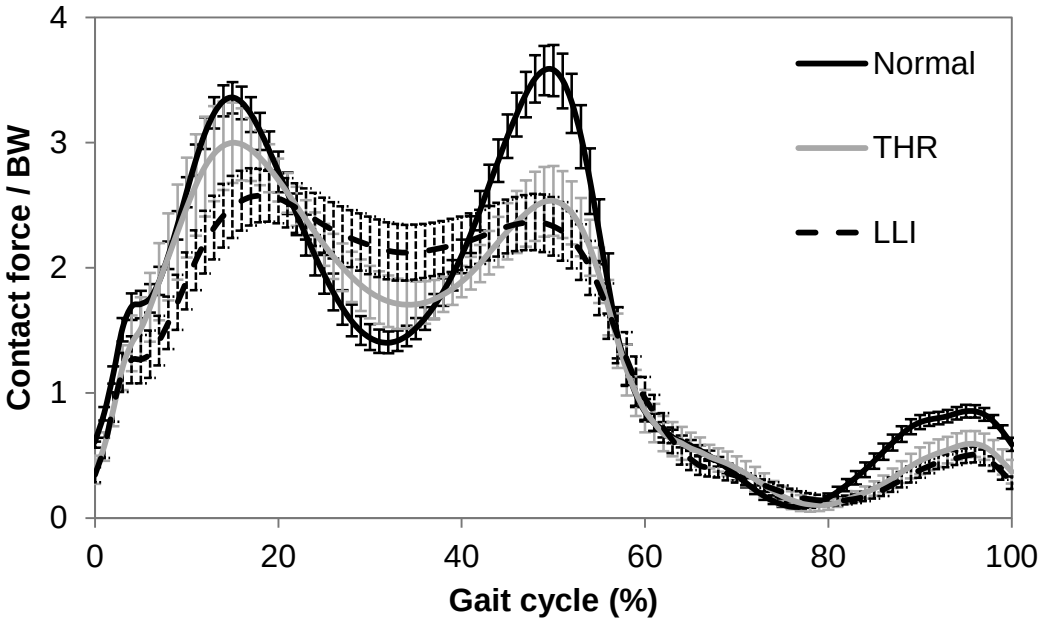

Figure 3.5 Mean contact force ± 95% CI for the normal individuals, THR and LLI patients. The three cohorts exhibited significantly different results on the 1st peak and trough force. The 2nd peak force of the THR / LLI patients was significantly lower than the normal cohort.

For the THR patients, the hip contact force was similar for the operated and non-operated limb during the majority of the cycle. However, the operated limb exhibited a decreased hip contact force around the 2nd peak during toe-off (~50% cycle), although the difference did not reach statistical significance (**Figure 3.6**).

For the LLI cohort, however, the hip contact force of the operated limb was generally lower than that of the non-operated limb (**Figure 3.7**). Such decrease was significant around the 2nd peak during toe-off.

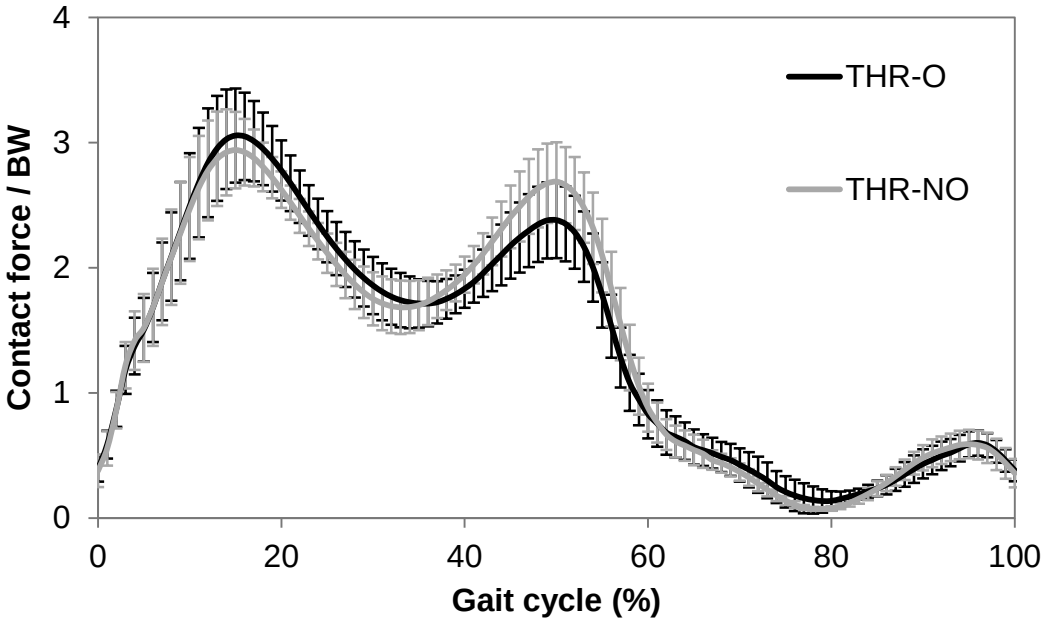

Figure 3.6 Mean contact force ± 95% CI for the THR patients on operated and non-operated limbs. No significant difference was observed in the comparison.

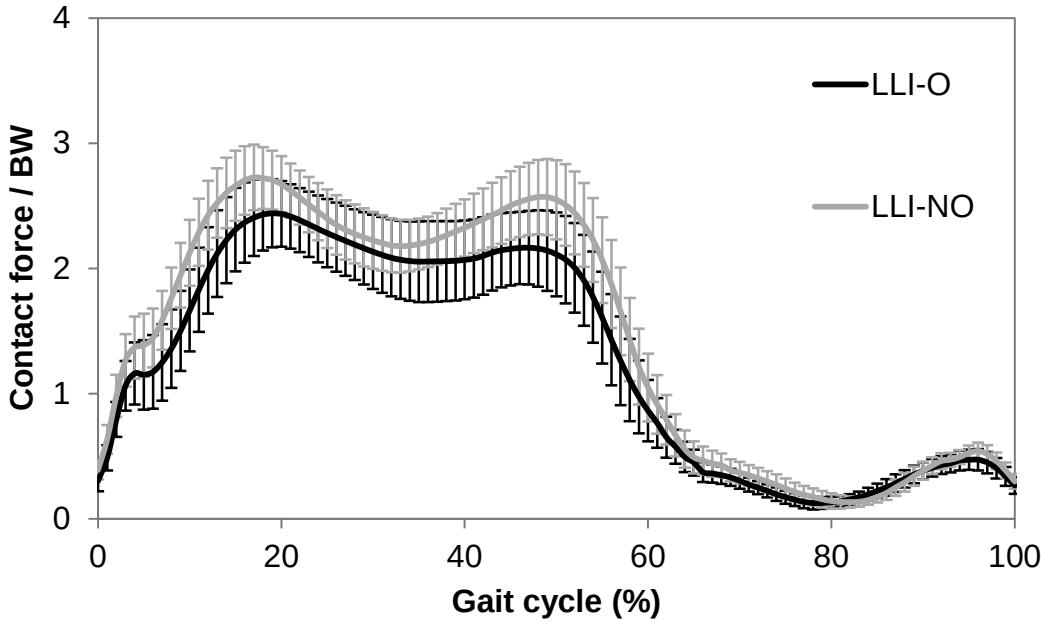

Figure 3.7 Mean contact force ± 95% CI for the LLI patients on operated and non-operated limbs. The hip contact force for the operated side was generally slightly lower than the non-operated side. Such reduction was significant around 50% cycle.

The averaged peak value of the contact force for the groups compared is displayed in **Figure 3.8**. The peak hip contact force of the THR and LLI patients were not significantly different to each other, but significantly reduced in comparison with the normal cohort. In addition, no significant difference was found between the operated and non-operated limbs of the THR cohort. However, the LLI patients displayed a significantly decreased hip contact force on their operated limb.

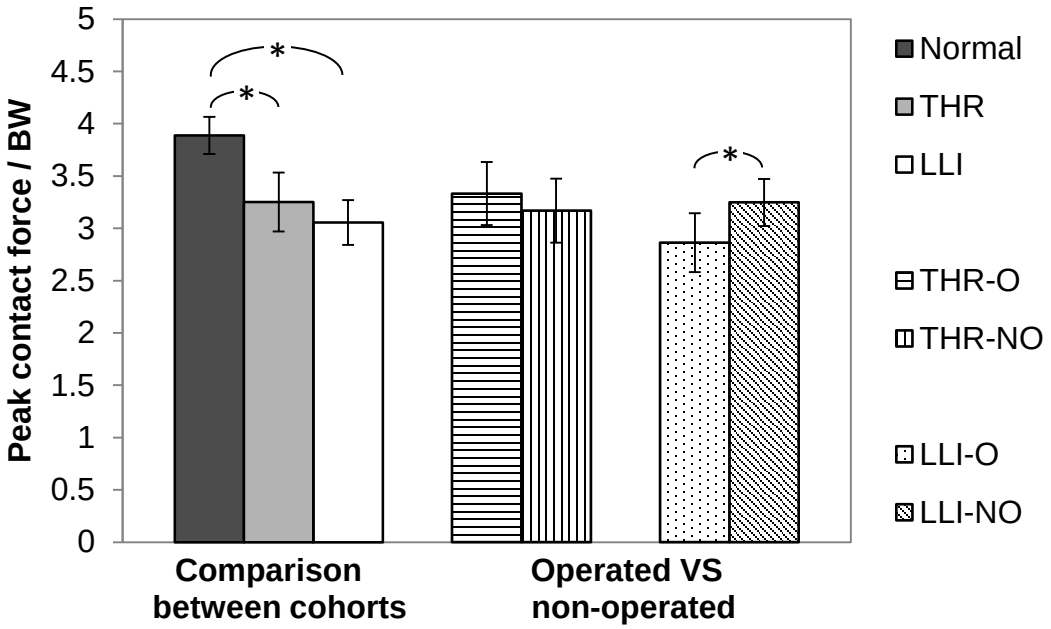

Figure 3.8 Comparison of the averaged value of the peak ground hip contact force for the three cohorts of subjects as well as for the operated and non-operated limbs of the THR / LLI patients. Statistically significant differences are marked with a star.

3.3.5 Comparison with previous studies

The comparison for the hip contact force of the THR and LLI patients on their operated limb, to the patients measured by Bergmann et al. (2001) are shown in **Figure 3.9**. The calculated hip contact force of the asymptomatic THR patients corresponded well to patient HS and KW in the Bergmann dataset, exhibiting a characteristic dynamic pattern with two distinct peaks (F_1 and F_3). However, the symptomatic LLI cohort displayed trends more

similar to the other two Bergmann patients (PF, IB) in which the dynamic loading pattern and especially the F_3 peak was diminished.

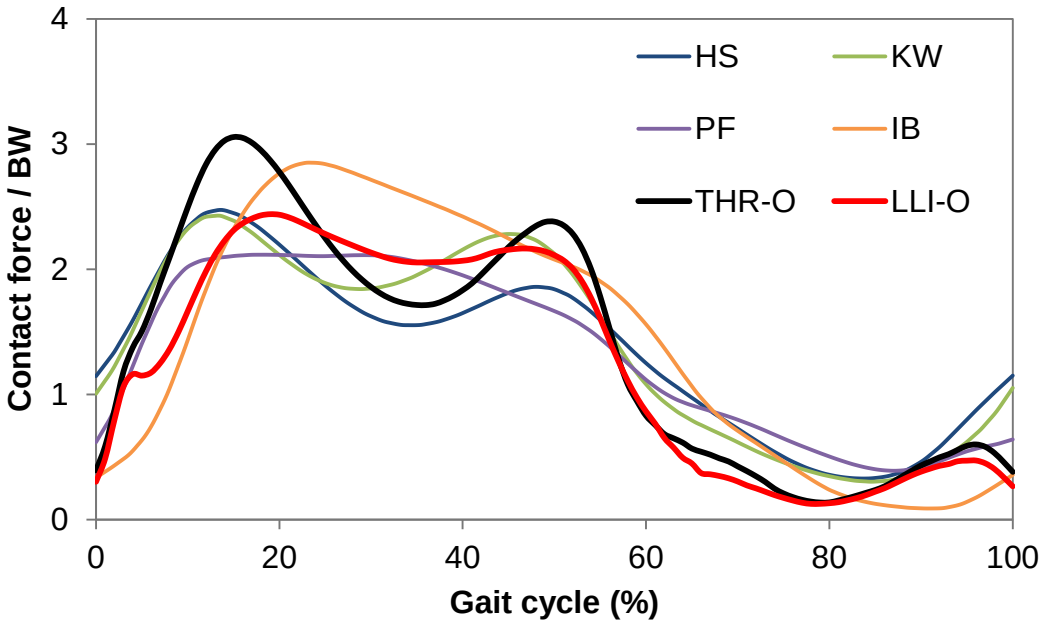

Figure 3.9 Comparison for the contact force of the operated limb of the THR / LLI patients to the Bergmann patients. Hip force pattern of the THR cohort exhibited similar trend to patient HS and KW, while hip force pattern of the LLI cohort was more similar to patient PF and IB.

The comparison of hip contact force for the normal cohort and the operated limb of the THR / LLI patients with the ISO data is presented in **Figure 3.10**. Good consistency was observed between the ISO data and the normal healthy cohort. The THR and LLI cohorts exhibited lower hip contact force for the F_1 and F_3 peaks however, with a less dynamic pattern than seen with the ISO data.

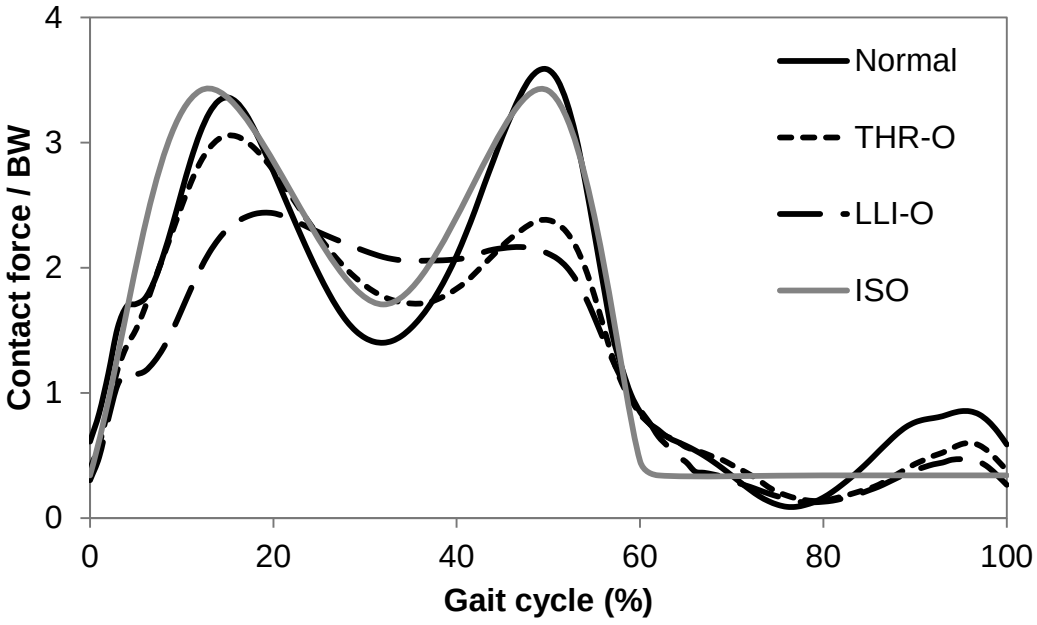

Figure 3.10 Comparison of the mean contact force for the normal cohort and the operated limb of the THR / LLI patients with the ISO data. The normal healthy cohort exhibited good consistency with the ISO data, whilst the THR and LLI cohorts had a lower peak hip contact force with a less dynamic pattern.

3.3.6 Correlation between contact force and model inputs

Results of the correlation tests between the hip contact force and the model inputs are shown alongside the scatterplots in **Figure 3.11**, **Figure 3.12**, **Figure 3.13** and **Figure 3.14**. For both the normal cohort and the THR cohort, the trough and two peaks of the hip contact force were significantly correlated to the ground reaction force. Significant correlations were also observed between the two peaks of the hip contact force and the hip flexion/extension angle, whilst the trough of the hip contact force was significantly correlated to the abduction/adduction angle. There was no significance in correlations for the other sets. In addition, little correlation between the hip contact force and the anthropometric parameters (age, height, weight and BMI) was detected.

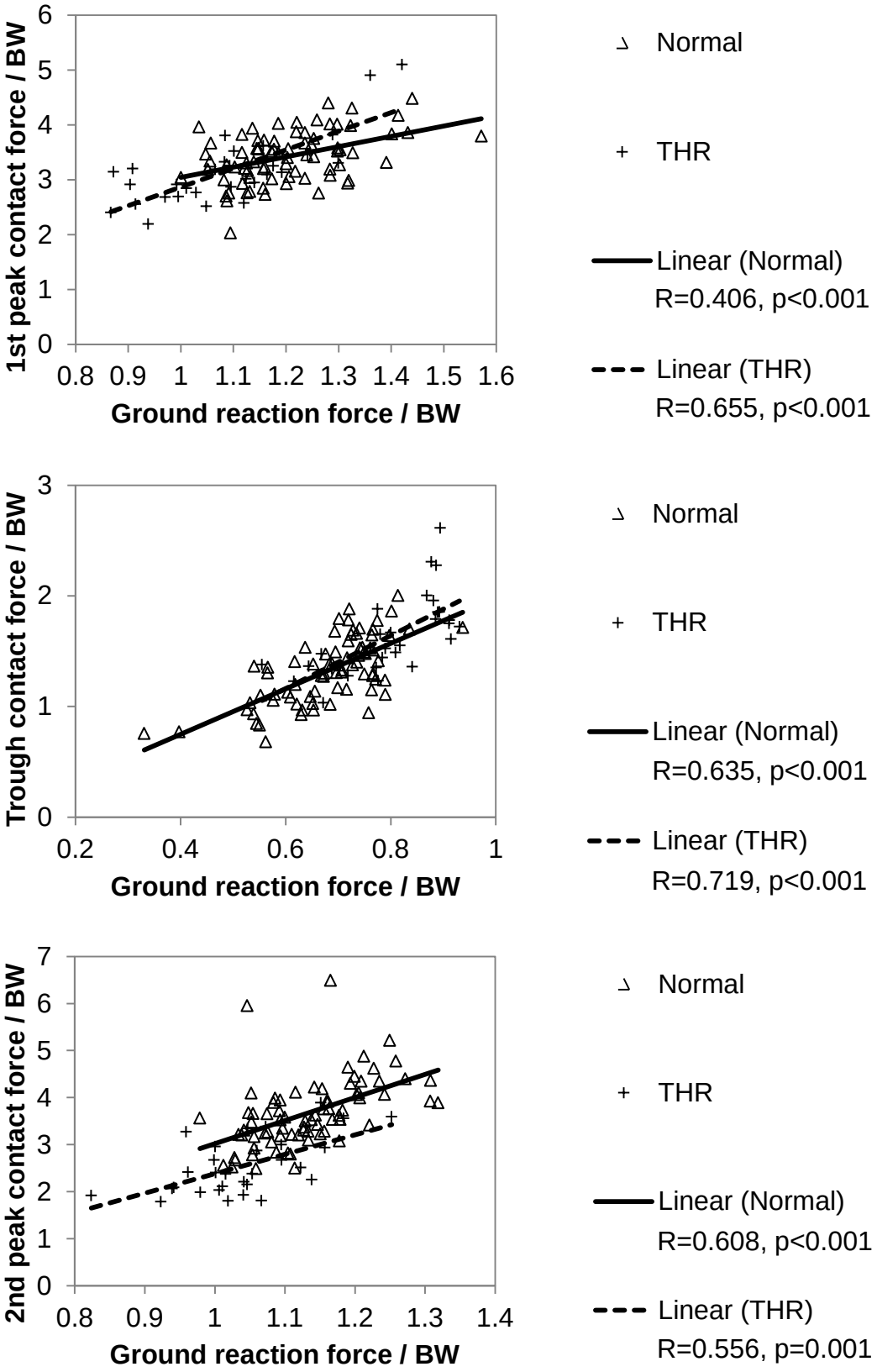

Figure 3.11 Significant correlations existed between the ground reaction force and the trough and two peaks of the contact force for the normal cohort and the THR patients.

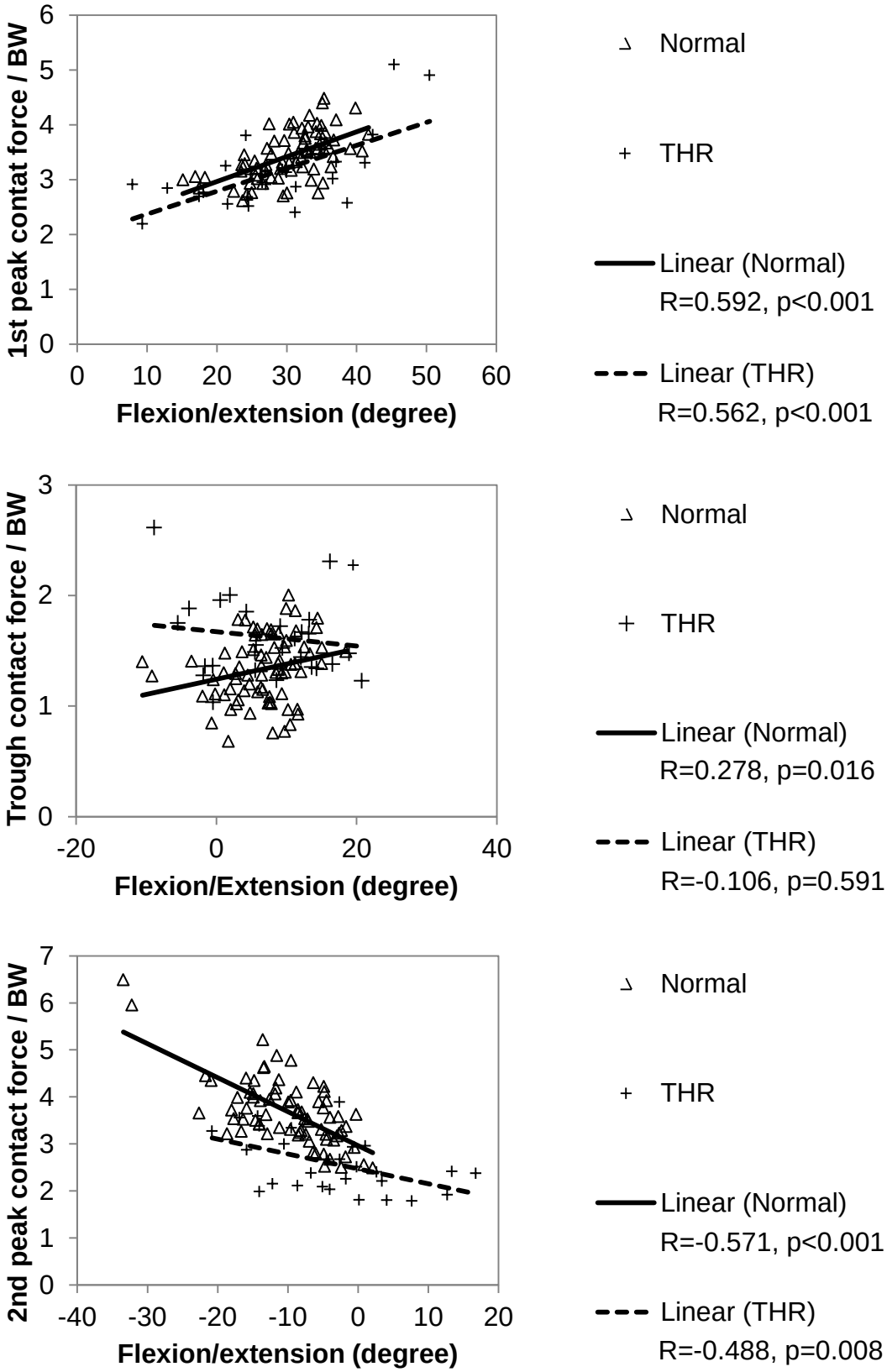

Figure 3.12 The flexion/extension angle and the two peaks of the contact force were significantly correlated for the health people and the THR patients. No significant correlations were found between the flexion/extension angle and the trough force for these two cohorts.

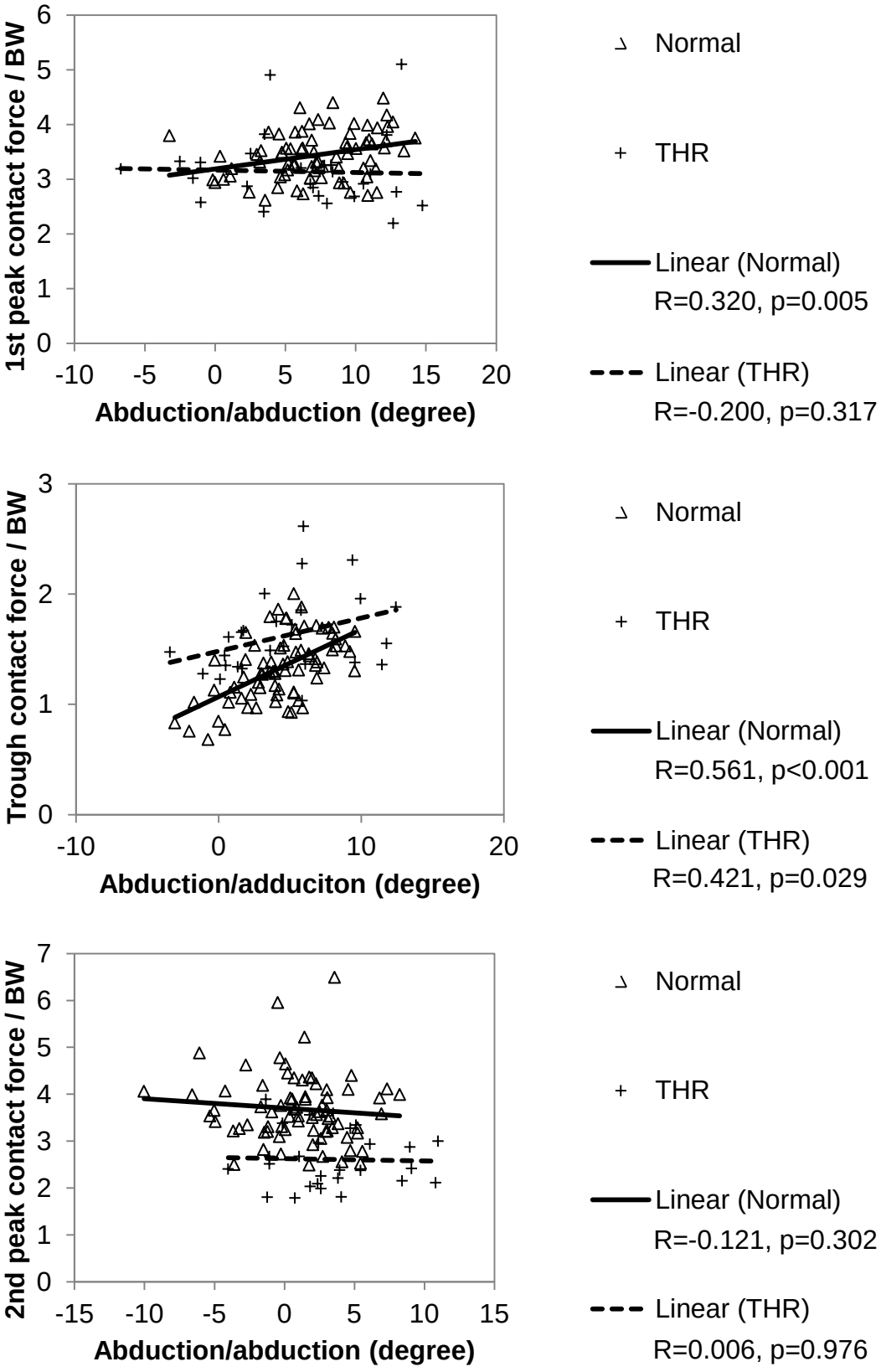

Figure 3.13 No significant correlations were observed between the abduction/adduction angle and the two peaks of the contact force for the normal cohort and the THR patients. The abduction/adduction angle and the trough force were significantly correlated.

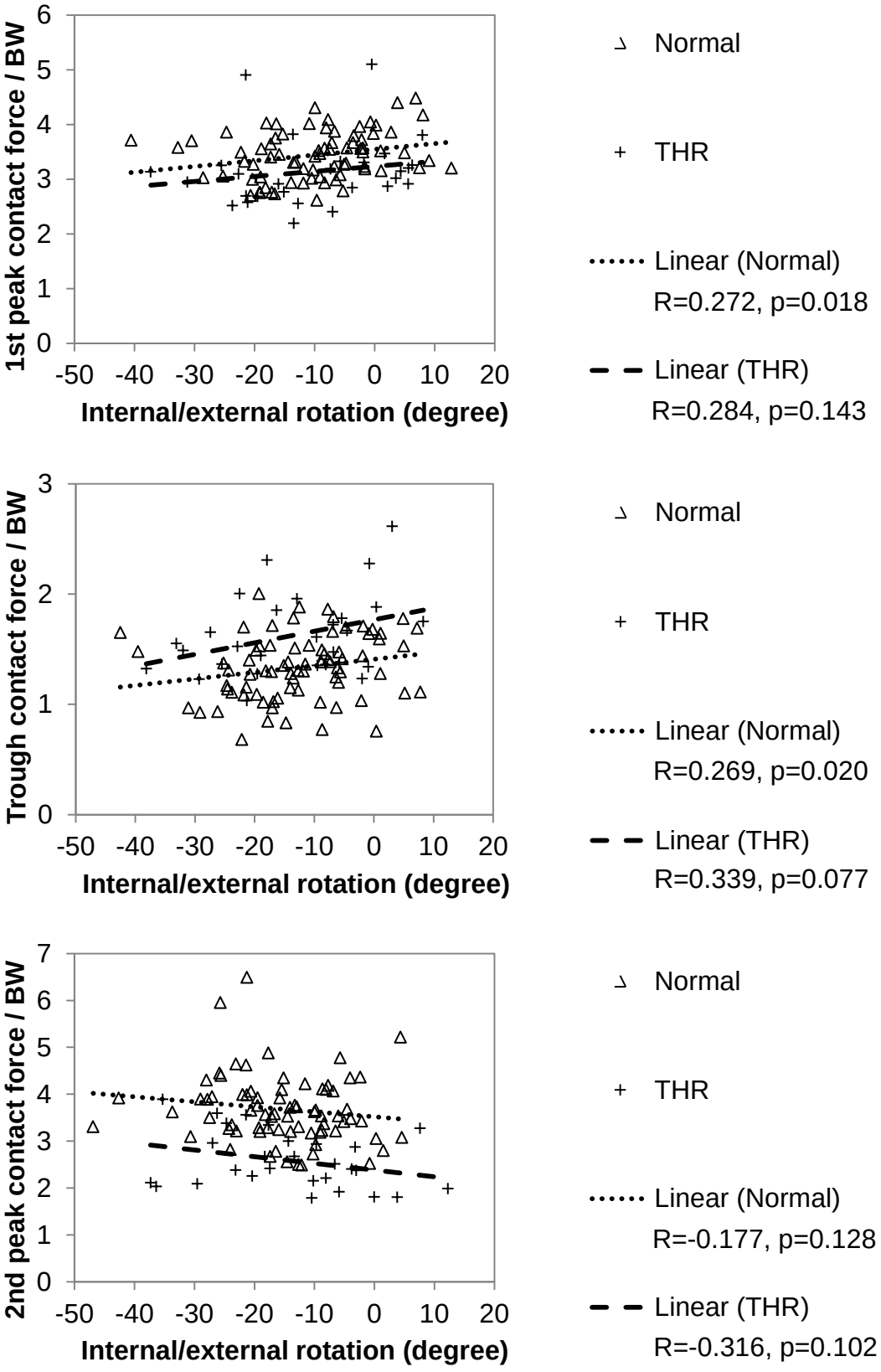

Figure 3.14 No significant correlations were observed between the internal/external rotation angle and the trough and two peaks of contact force for the normal cohort and the THR patients.

3.4 Discussion

In this chapter, the hip kinematics and kinetics of the unilateral asymptomatic THR patients, unilateral symptomatic LLI patients and normal healthy individuals were determined and compared across groups. The novelty of this study is that the patients were clearly categorized, i.e. the asymptomatic THR cohort was carefully screened to have no other history of musculoskeletal disorders, and the LLI cohort were symptomatic enough to require consideration for revision surgery. Both cohorts represented typical outcomes of THR surgeries. Another advantage of the cohorts used in this chapter is that the relatively large number of subjects allowed inferential statistical analyses to be completed. This is different from previous kinematic studies which involved either a small number of subjects or unreported histories, thus leaving a level of ambiguity (e.g. (Stansfield and Nicol, 2002)).

Compared with the normal healthy controls, the asymptomatic THR patients exhibited a less dynamic pattern in the hip contact force during walking at a self-determined normal speed, with a significantly lower magnitude of maximum force during heel-strike and toe-off, but a higher magnitude during stance phase, indicating a loss of dynamic function following THR. Such variations were more evident for the symptomatic LLI patients than for the asymptomatic THR patients. In addition, the hip mobility and ground reaction force of the THR / LLI patients during gait were reduced compared with the normal cohort, which is in agreement with the findings by a multitude of previous kinematic studies on THR patients (Loizeau et al., 1995, Bennett et al., 2008, Beaulieu et al., 2010, Madsen et al., 2004). Although the normal cohort and the THR / LLI cohort did not match closely for age, height, weight and BMI, additional correlation test showed that there is little correlation between the hip contact force and the anthropometric parameters, which excludes the hypothesis that the predictions may be influenced by the anthropometric variations among the cohorts.

For the asymptomatic THR patients and the symptomatic LLI patients, the degree of asymmetry between the two limbs was also different. The contact forces for the operated and non-operated hip of the asymptomatic THR patients were similar, suggesting that the patients were well recovered and

potentially had “forgotten” their replaced joint as described recently by Behrend et al. (2012). For the LLI patients however, the hip contact force was reduced on the operated limb, which is suggestive of a higher degree of limp and a poorer function.

The severity of abnormality in the pattern of the hip contact force for the THR / LLI patients was significantly correlated to their alterations in the hip kinematics, suggesting that it is important to achieve normal hip kinematics in order to have any chance of restoring hip kinetics. These correlations can be theoretically explained. In the human musculoskeletal system, the hip contact force is contributed by the force transferred from the ground as well as by the forces generated by the muscles which act around the joint to balance the hip moment. As synovial joints are nearly frictionless (Mow and Lai, 1980, Jin et al., 1997), the hip moment is mainly determined by the ground reaction force, hip angle and the inertia effect of the moving body segments which is also determined by the angular acceleration of the joint. Therefore, the hip contact force is directly linked with the hip angle and the ground reaction force. During heel-strike and toe-off, the hip flexion/extension angle is substantially higher than the abduction/adduction and internal/external rotation angle, thus contributing more to the joint force. However, the abduction/adduction becomes dominant during the stance phase for the time at which the flexion/extension angle becomes minimal. These theoretical evaluations well supported the model predictions in which the hip contact force was significantly correlated to the ground reaction force, the hip flexion/extension angle during heel-strike and toe-off and the abduction/adduction angle during stance phase.

Derived from the loading conditions of a healthy person by Paul (1967), the ISO standard recommends a maximum load of 3000 N, and is based on a 75 kg patient which equates to a force of 4 times BW. The hip contact force of the normal cohort displayed similar shape to the ISO data, with a comparable magnitude of 3.89 times BW (mean BW = 72 kg). This similarity suggests that the modelling technique utilised provided comparable results to traditional inverse dynamics. However, the ISO data, which have been widely adopted in the pre-clinical testing, does not appear to represent the realistic loading situation for a THR patient, with the ISO standard requiring

substantially greater loads during heel-strike and toe-off than observed in our patients. Such alterations may affect the accuracy of prediction of the wear and durability of prosthesis by the pre-clinical testing relying on ISO data for simulator inputs. Given the recent emphasis on stratified approaches to heath care interventions, these findings support the argument for refinements to the ISO data to better represent the systematic variability of *in vivo* conditions, and a loading pattern of the operated limbs of the asymptomatic THR patients is recommended for the ISO refinement.

The data published by Bergmann et al. (2001) include more additional patient details that may be used for further comparison. The age and BMI of the asymptomatic THR patients (64.27 yrs., 30.74) and the symptomatic LLI patients (58.70 yrs., 27.86) were comparable to the patients measured by Bergmann et al. (2001) (62.17 yrs., 29.05). In the Bergmann dataset, two patients (HS, KW) had a dynamic pattern of gait kinetics with two distinct peaks of loading, similar to our asymptomatic THR cohort, whilst the other two patients (PF, IB) had only a single peak suggesting poorer function which as observed in our symptomatic LLI patients. In comparison with the two patients with better function in the Bergmann data, the hip contact force of the asymptomatic THR patients was comparable during the majority of the gait cycle, but ~20% greater at heel-strike. On the other hand, the joint force of the symptomatic LLI patients lay in the middle of that of the other two patients of with poorer function in the Bergmann data. Besides the good agreement of our predictions to the traditional inverse dynamics (Paul, 1967) and the measured dataset with details of several subjects (Bergmann et al., 2001), the findings in this chapter are consistent with other previous experimental measurements (**Table 3-3**). It should be noted, however, that direct comparison to the existing studies is difficult without the additional consideration of clinical data such as the involvement of multiple joints, bilateral THR or other functional compromises.

Table 3-3 Comparison of the calculated peak hip contact force to the previous *in vivo* measured gait data.

Reference	Peak Hip Joint Force (/ BW)
Current study (THR-O)	3.33
Current study (LLI-O)	2.86
Davy et al. (1988)	2.8
Kotzar et al. (1991)	2.7
Bergmann et al. (1993)	4.1
Brand et al. (1994)	3.3
Bergmann et al. (2001)	2.4

There are some limitations worth mentioning. Computational studies are generally known to overestimate the joint reaction forces by ~10%, due to the lack of a realistic muscle wrapping path around the hip joint within the model (Brand et al., 1994). The non-realistic path generally results in smaller muscle moment arms, leading to higher associated muscle forces to achieve the same hip stabilising moment and a higher resultant joint force. In addition, the ligament was not included in the model, because the detailed anatomical information of the hip ligaments has yet to be reported. In spite of these assumptions, the computational approach is able to predict similar trends and patterns to instrumented prosthesis studies and allow parametric studies to be conducted.

During the acquisition of the kinematic measurements, the movement of peripheral soft tissues may cause inaccuracy in the trajectories of the markers attached to the skin. However, such skin artefacts were proved to have little influence on the hip flexion/extension angle which, compared with the other kinematic parameters, contributed the most to the hip contact force

(Lu and O'Connor, 1999). As a result, the predicted hip contact force may be relatively robust to such measurement errors.

In this study, the model was scaled by a default human model, without accounting for the subject-specific parameters such as individual anatomical landmarks, joint centre and muscle path. This is justifiable because it is difficult to determine such detailed parameters for a cohort study involving a large number of subjects. Furthermore, previous studies demonstrated that the joint contact force was not greatly affected by these localised parameters (Carbone et al., 2012, Besier et al., 2003).

Another limitation is that a uniform muscle recruitment pattern was adopted, and the potential alteration in the muscle recruitment pattern between individuals or cohorts was not considered. For example, the muscle recruitment pattern of THR patients may be altered by postoperative stimuli such as muscle weakness (Long et al., 1993, Bhave et al., 2005, Shih et al., 1994). However, as demonstrated in **Chapter 2**, different muscle recruitment types do not have a great influence on the hip contact force, particularly in terms of the loading trend and pattern which are of most interest for the parametric nature in this chapter.

In conclusion, RBD musculoskeletal modelling is efficient in the prediction of hip contact forces for the current cohort study. The approach taken appears to provide reliable results and is sufficient for the comparative study. The alteration in gait kinematics of the asymptomatic THR patients led to an abnormal hip contact force represented by a less dynamic pattern, a reduced magnitude during heel-strike and toe-off and a greater magnitude during stance phase. Such loss in function was more evident for the symptomatic LLI patients. In addition, the high degree of symmetry in hip kinetics between the operated and non-operated limbs indicates a well post-operative recovery for the asymptomatic THR patients, whilst the obvious hip kinetic asymmetry for the LLI patients reflects a poorer function. The findings will help assist in providing better patient care, pre-operative planning and rehabilitation strategies. Loading conditions for future modelling and testing on a subject-specific or cohort-specific level are also recommended.

Chapter 4
Finite Element Modelling: Methodology Development

4.1 Introduction

As mentioned **Chapter 2** and **Chapter 3**, the kinetic performance of the hip joint can be obtained through the body kinematics. However, it is necessary to account for the local mechanical environment within the hip in order to allow further investigation in more detail. The following chapters will use the FE method to evaluate the biphasic performance of the natural hip joint.

Due to the importance of the interstitial fluid in the functional and tribological behaviour of articular cartilage, it is necessary to incorporate biphasic cartilage layers into the whole joint model in order to better understand the hip function and pathology of hip degeneration. There have been several studies on biphasic modelling for the natural hip (Pawaskar, 2010) or knee joint (Gu and Li, 2011) using FE commercial software ABAQUS (DassaultSystemes, SuresnesCedex, France). However, none of these models have successfully simulated high physiological dynamic or static loads for a prolonged period. To solve this problem, an open-source non-linear FE solver FEBio (mrl.sci.utah.edu/software/febio), which is particularly designed for the simulation of bio-materials, was adopted in this study.

The aim of this chapter was to verify the biphasic simulation capability of FEBio by comparing its predictions to those in ABAQUS and to the results in a previous study (Pawaskar, 2010). Additionally, the contact-dependent fluid flow feature in FEBio was evaluated.

4.2 Methods

4.2.1 Comparison of FEBio and ABAQUS for biphasic simulation

Both linearly elastic and neo-Hookean materials were tested to represent the solid phase in FEBio and ABAQUS. The inputs for a neo-Hookean material in FEBio and ABAQUS are different. In ABAQUS, the input parameters for a neo-Hookean material are C_{10} and D_1. These two parameters can be converted to Young's modulus (E) and Poisson's ratio (υ) which are the input parameters in FEBio by the following equations:

$$G = 2C_{10} = \frac{E}{2(1+\upsilon)} \quad \textbf{(4.1)}$$

$$K = \frac{2}{D_1} = \frac{E}{3(1-2\upsilon)} \quad \textbf{(4.2)}$$

Where G is the shear modulus; K bulk modulus.

Besides, the constitutive equation of neo-Hookean in FEBio (**Equation (4.3)** (Maas and Weiss, 2007)) and ABAQUS (**Equation (4.4)** (ABAQUS Theory Manual, 2011)) are different, with the following strain energy (W) relationships:

$$W = \frac{\mu}{2}(I_1 - 3) - \mu \ln J + \frac{\lambda}{2}(\ln J)^2 \quad \textbf{(4.3)}$$

$$W = \frac{\mu}{2}(I_1 - 3) + (\frac{\lambda}{2} + \frac{\mu}{3})(J-1)^2 \quad \textbf{(4.4)}$$

Where, μ and λ are the Lamé parameters; J volume ratio; I_1 first strain invariant of the deviatoric Cauchy-Green tensor C. For small strains and rotations ($J \approx 1$), **Equation (4.3)** reduces to isotropic linear elastic relationship (Bonet, 1997).

For computational efficiency, an initial comparison between FEBio (version 1.5.0; mrl.sci.utah.edu/software/febio) and ABAQUS (version 6.11-1; Dassault Systemes, Suresnes Cedex, France) was conducted in an

axisymmetric situation represented by a three dimensional model with only one element through the thickness (**Figure 4.1**), because two dimensional or axisymmetric models are not supported in FEBio. The Young's modulus and Poisson's ratio of the aggregate were 0.5 MPa and 0 respectively. The permeability was 0.01 $mm^4/(Ns)$.

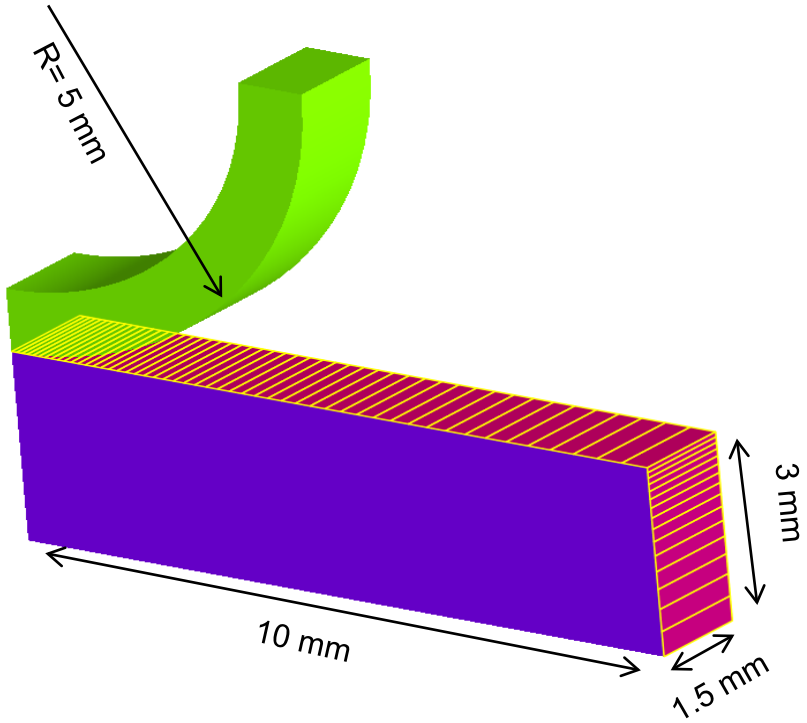

Figure 4.1 Two dimensional indentation model representative of an axisymmetric situation. The indenter (green) is permeable and rigid.

The bottom surface of the cartilage was fixed in all degrees of freedom. The surfaces highlighted in red in **Figure 4.1** were free-draining where fluid flows out freely. The other three surfaces of the cartilage were symmetric to their normal vectors. The indenter was rigid and permeable, and only allowed to move vertically.

A relaxation test and creep test were simulated respectively using the model. In the relaxation test, the indenter was moved 0.2 mm downward in 2 s and then immobilized for 2000 s. In the creep test, the indenter was loaded with a force of 1 N ramped over 2 s downward and held for 2000 s. The models were simulated using both FEBio and ABAQUS. The models analysed in

FEBio were pre-processed using PreView (version 1.7; mrl.sci.utah.edu/software.php) and post-processed using PostView (version 1.4; mrl.sci.utah.edu/software.php).

Contact was defined as facet-to-facet sliding in FEBio and as node to surface finite sliding in ABAQUS. The contact pressure contour displayed in PostView is not smooth, and hence represented by the third principle stress of the element layer on the articulating surface. Fluid pressure and contact stress were recorded. Additionally, reaction force and indenter displacement were tracked for the relaxation test and creep test respectively.

The mesh densities were checked to be high enough to predict nearly identical results (<3%) when doubled (**Figure 4.2**). Parametric studies with varying model parameters (**Table 4-1**) were also carried out to analyse the prediction by the two FE solvers under more circumstances.

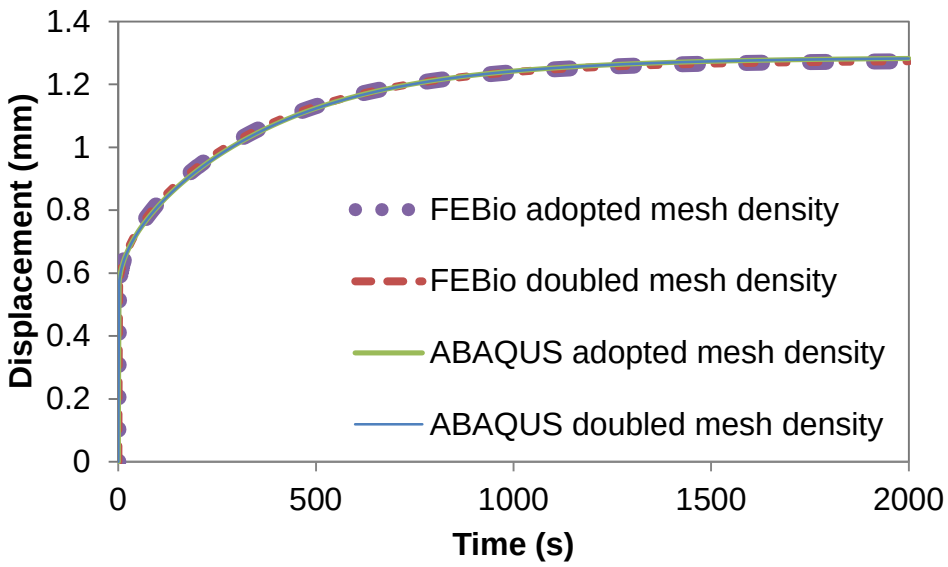

Figure 4.2 Results of the model with different mesh densities under creep tests. The indenter displacement of the model with the adopted mesh density remained nearly constant when its mesh density was doubled in both FEBio and ABAQUS (the four traces nearly overlapped).

Table 4-1 The values of the parameters used in the parametric study. Only one parameter was altered from the original model in each test case. E: Young's modulus of cartilage aggregate; ν: Poisson's ratio; K: cartilage permeability; F: applied force to the indenter.

	E (MPa)	ν	K ($mm^4/(Ns)$)	F (N)
Values used in the parametric study	1, 1.5	0.1, 0.2	0.001, 0.1	0.05, 0.2

4.2.2 Effect of contact-dependent fluid flow and methodology validation

For the indentation test, if the indenter is impermeable, there should be no fluid flow out from surfaces of the acetabular cartilage that are in contact with the indenter. To better present the influence of contact-dependent fluid flow on the result, a three dimensional indentation model of a porcine cartilage pin was developed. For computational efficiency, the indentation model was represented by a quarter geometry (**Figure 4.3**), in which the surfaces of both the cartilage and the underlying bone perpendicular to x and z axes were constrained as symmetric to their normal vectors. The material properties ($\mathrm{E} = 0.455\ \mathrm{MPa}$, $\nu = 0$, $\mathrm{K} = 0.00107\ \mathrm{mm}^4/(\mathrm{Ns})$), geometric parameters and boundary conditions were taken from a previous study (Pawaskar, 2010) to enable validation. The indentor was only allowed to move vertically and loaded with a force of 0.2 N ramped within 2 s downward and held for 15000 s. The pin was immoblized by fixing the bottom surface of the bone in all degrees of freedom. The outer surface of the cartilage, shown in **Figure 4.3**, was free-draining. To evaluate the influence of contact-dependent fluid flow on the results, three different boundary conditions were considered for the upper cartilage surface: free-draining, sealed and contact-dependent fluid flow. All simulations were conducted in FEBio.

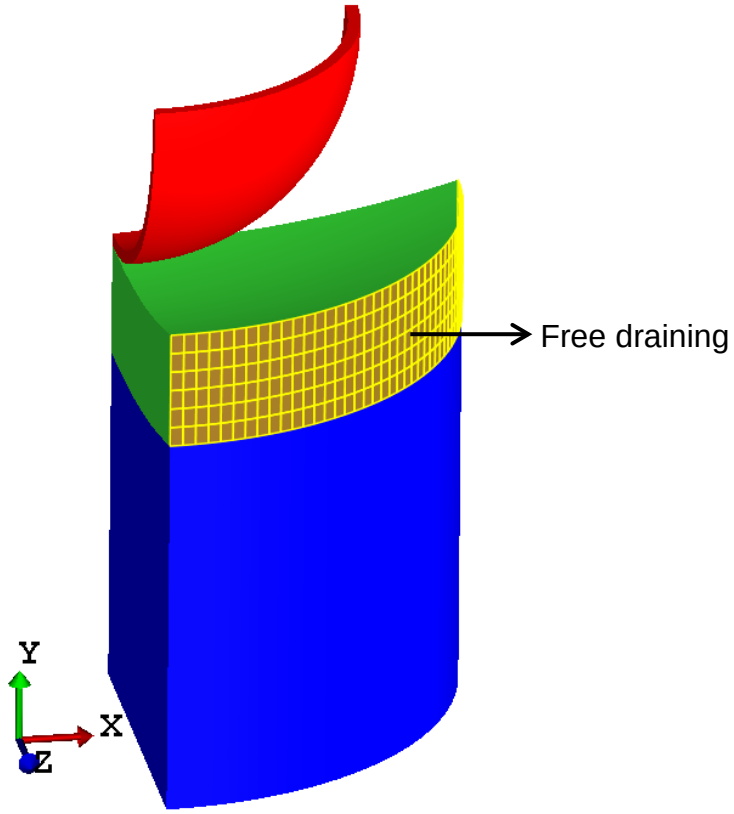

Figure 4.3 Indentation model of a creep test represented by a quater (indenter – red. cartilage – green. underlying bone – blue). The outer surfce of the cartilage is highlighted in yellow. Material properties and geometric parameters were taken from a previous study (Pawaskar, 2010).

To validate the predictions, the results of the model with contact-dependent fluid flow in FEBio was compared against the indenter used in the previous experiment (Pawaskar, 2010). Again, mesh densities were checked to be appropriate (**Figure 4.4**). The fluid flux vectors and indenter displacement were recorded.

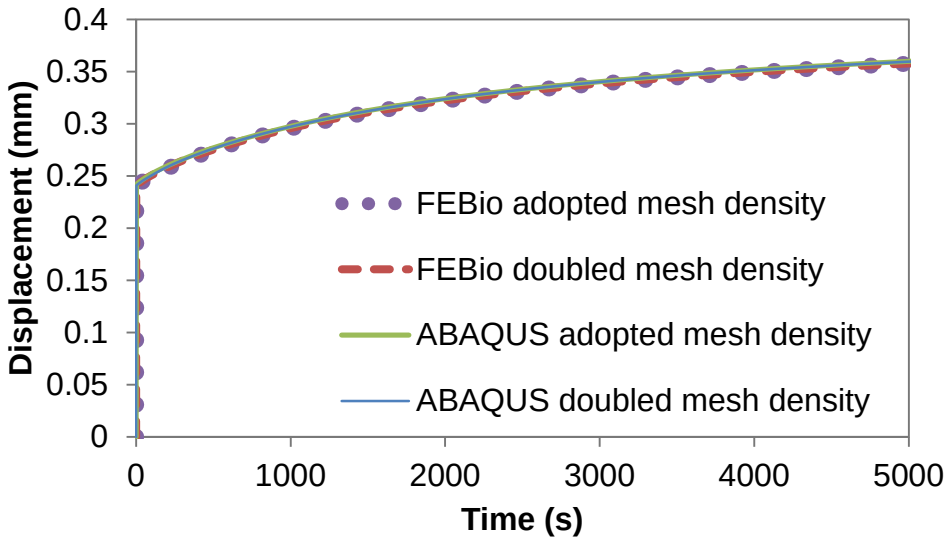

Figure 4.4 Results of the model with different mesh densities under creep tests. The contact-dependent fluid flow was defined on the articulating surfaces. The indenter displacement of the model with the adopted mesh density remained nearly constant when its mesh density was doubled in both FEBio and ABAQUS (the four traces nearly overlapped). Results were presented for only 5000 s, because the model with a doubled mesh density could not achieve convergence for a longer period in ABAQUS.

4.3 Results

4.3.1 Comparison of FEBio and ABAQUS for biphasic simulation

Fluid pressure distribution of the relaxation and creep test in FEBio are shown in **Figure 4.5** and **Figure 4.6** respectively. There was a significant variation in results at different stages, and obvious cartilage consolidation due to the interstitial fluid flow was detected in both tests.

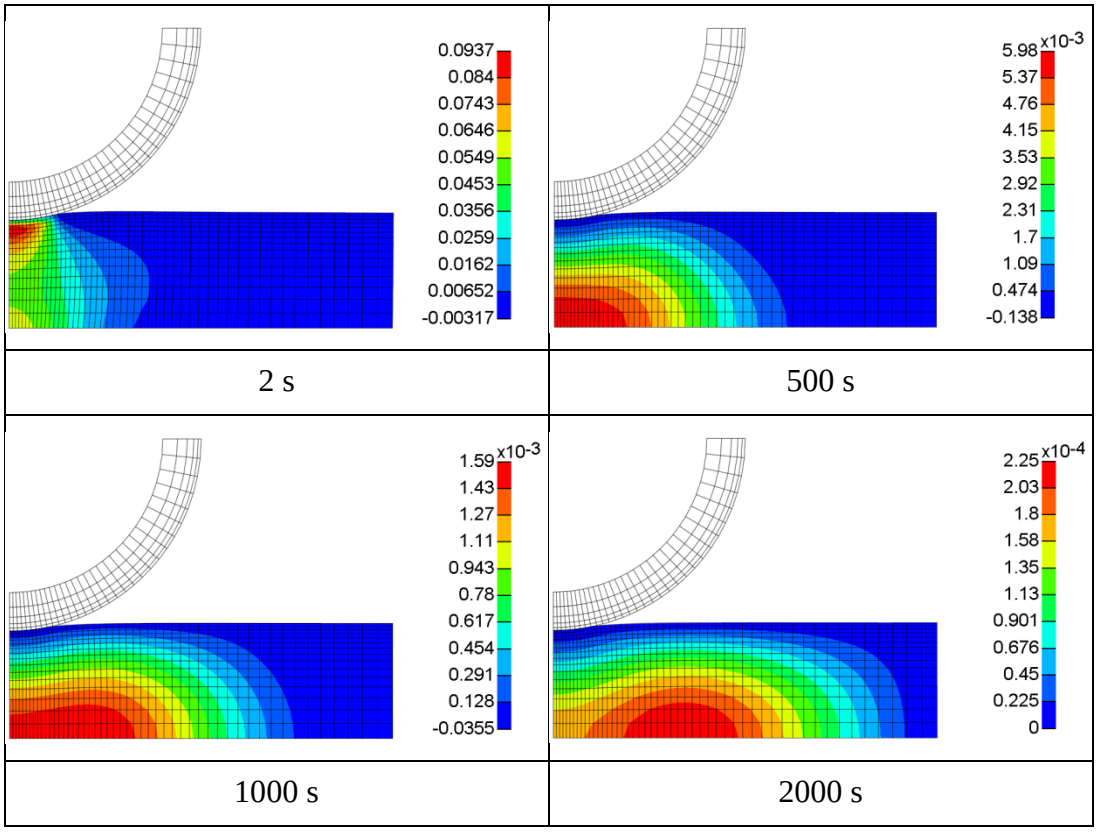

Figure 4.5 Contours of fluid pressure (MPa) at different stages for the relaxation test in FEBio. Cartilage consolidation was obviously detected by the great variation in fluid pressure distribution over 2000 s.

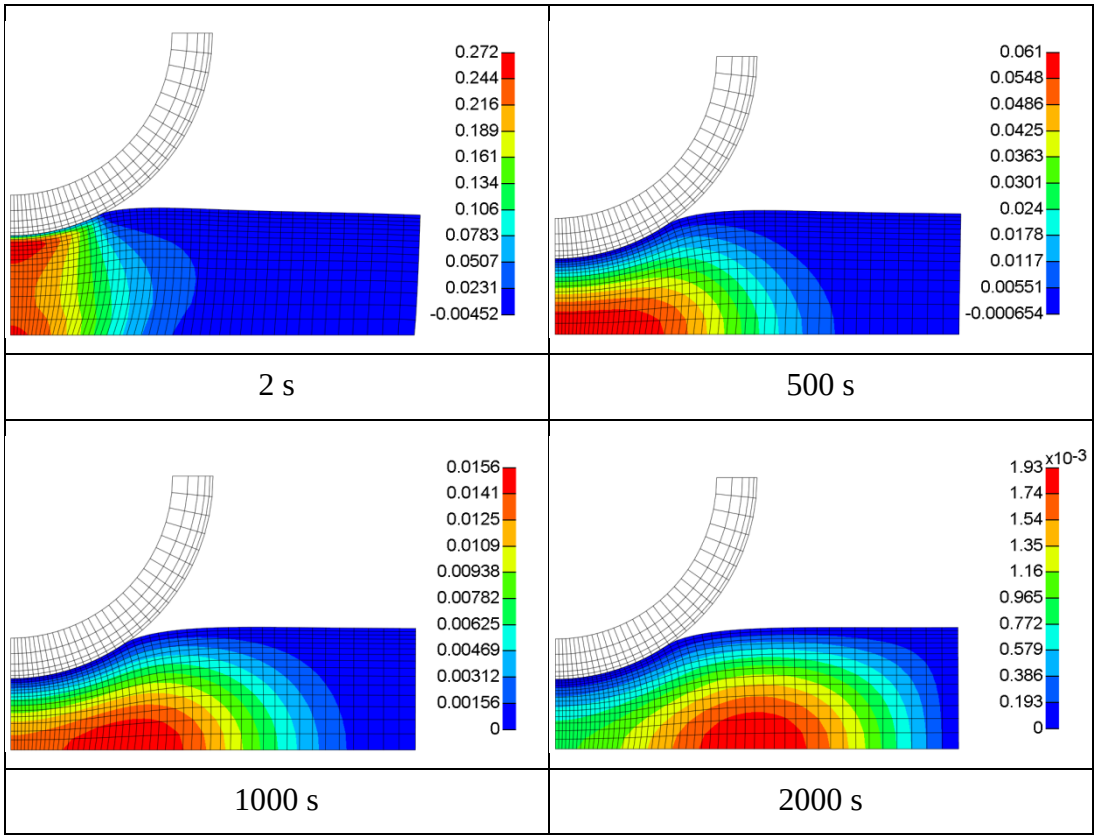

Figure 4.6 Contours of fluid pressure (MPa) at different stages for the creep test in FEBio. Cartilage consolidation was obviously detected by the great variation in fluid pressure distribution over 2000 s.

For the comparison of FEBio and ABAQUS, the results of the relaxation and creep test are shown in **Figure 4.7** and **Figure 4.8** respectively. In both tests, the neo-Hookean model in FEBio showed very similar results to the linearly elastic model in ABAQUS. The linearly elastic model in FEBio had different results as compared with the other models in the relaxation test and exhibited poor convergence ability in the creep test, possibly due to the difficulty of the non-linear solver in dealing with linear constitutive relationship. In ABAQUS, the neo-Hookean model behaved differently from the linearly elastic model in the creep test.

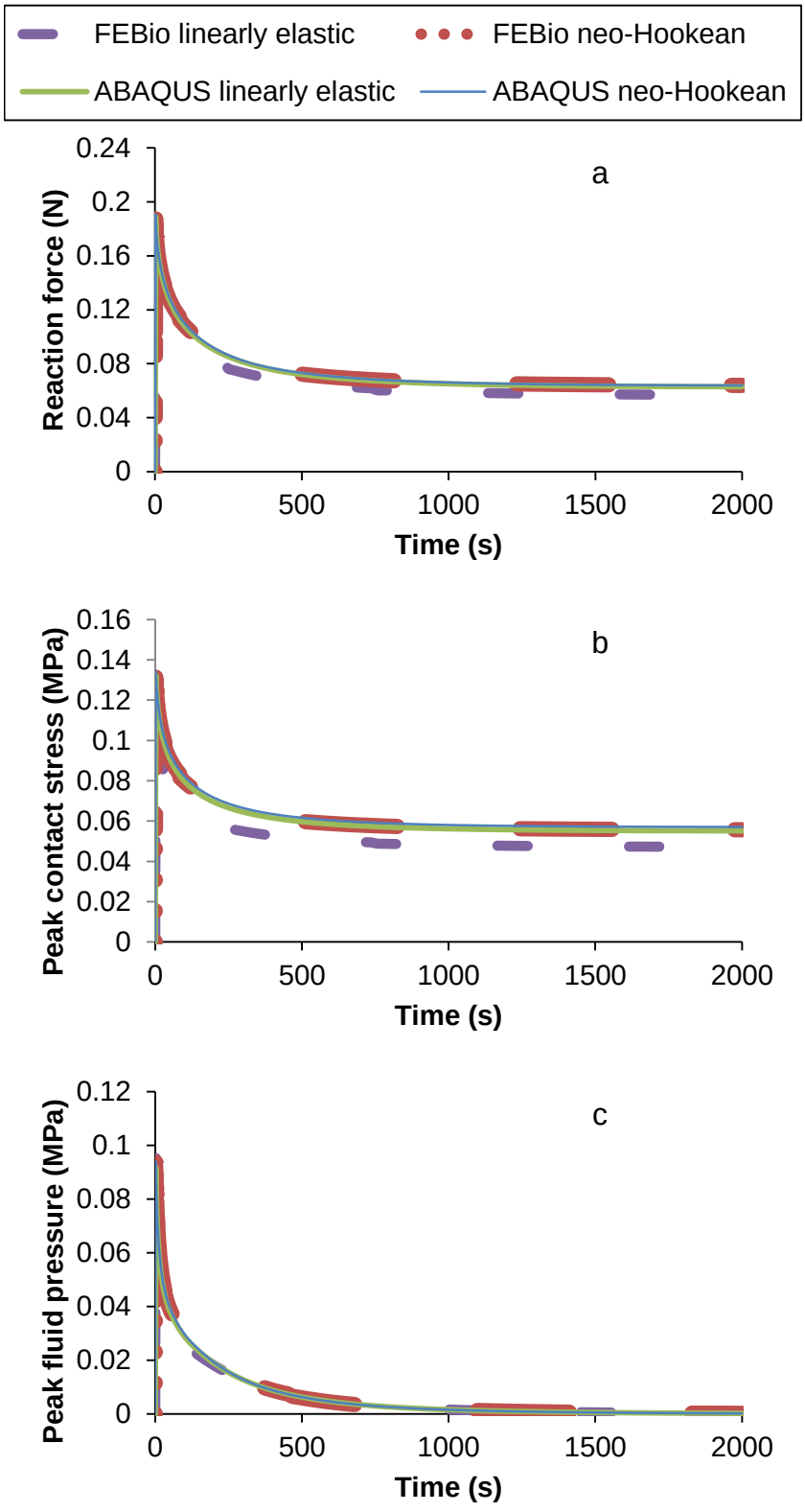

Figure 4.7 Predicted (a) reaction force, (b) peak contact stress and (c) peak fluid pressure against time under relaxation. All the four models converged over 2000 s. Very similar results were found for the neo-Hookean model in FEBio, linearly elastic and neo-Hookean models in ABAQUS (these three traces nearly overlapped). The linearly elastic model in FEBio behaved differently from the other three models.

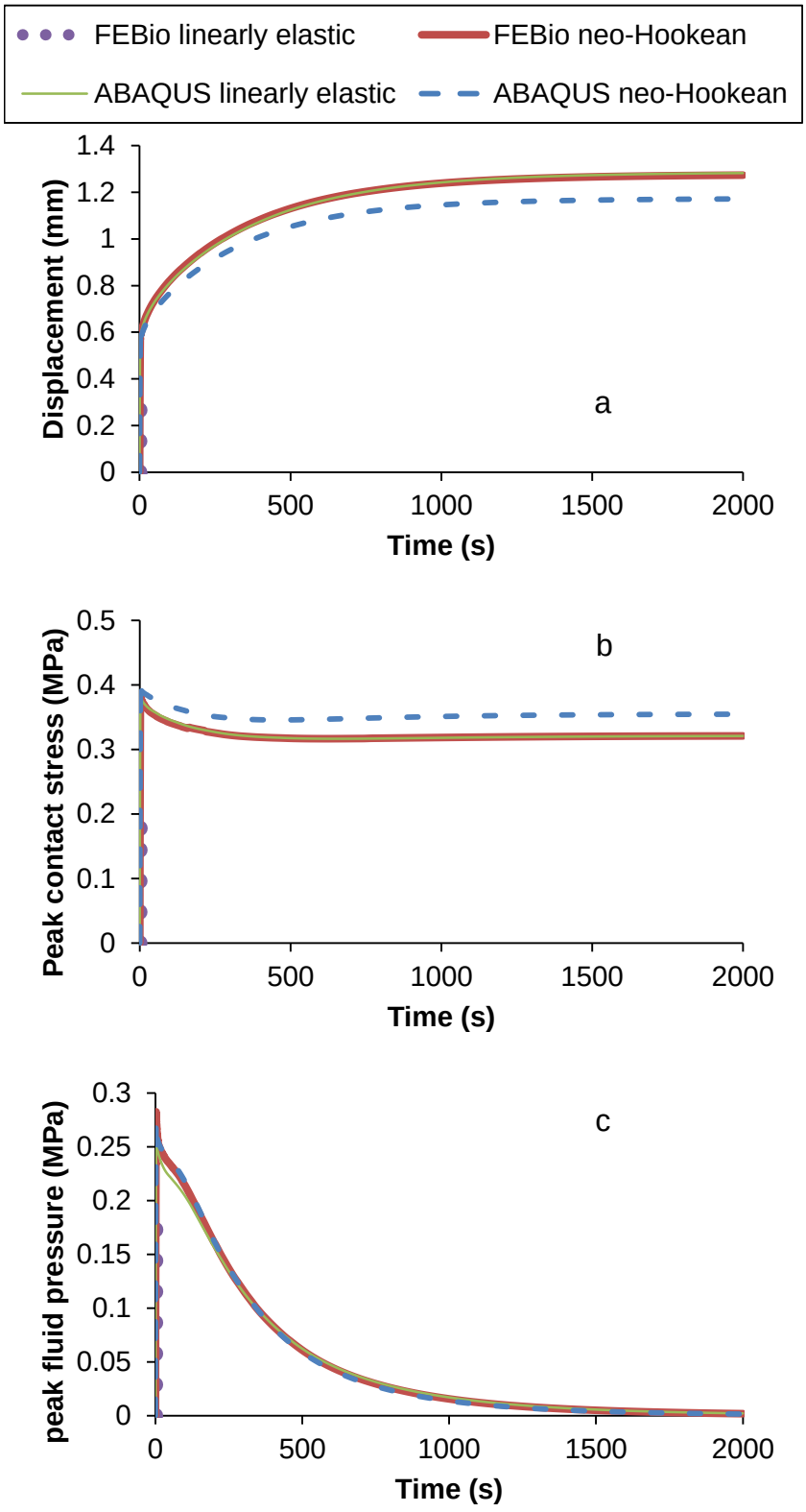

Figure 4.8 Predicted (a) displacement, (b) peak contact stress and (c) peak fluid pressure against time under creep. The model of linearly elastic cartilage could not get converged over 0.8 s. The neo-Hookean model in FEBio and the linearly elastic model in ABAQUS predicted very similar results (these two traces nearly overlapped) which were evidently different from the neo-Hookean model in ABAQUS.

As shown in **Figure 4.8**, the processing of the linearly elastic model in FEBio did not achieve convergence for 2000 s and stopped at only 0.8 s when there were overly distorted elements near the contact surface (**Figure 4.9**), suggesting that in terms of biphasic cartilage modelling, the linearly elastic solid phase does not perform well in the non-linear FEBio solver.

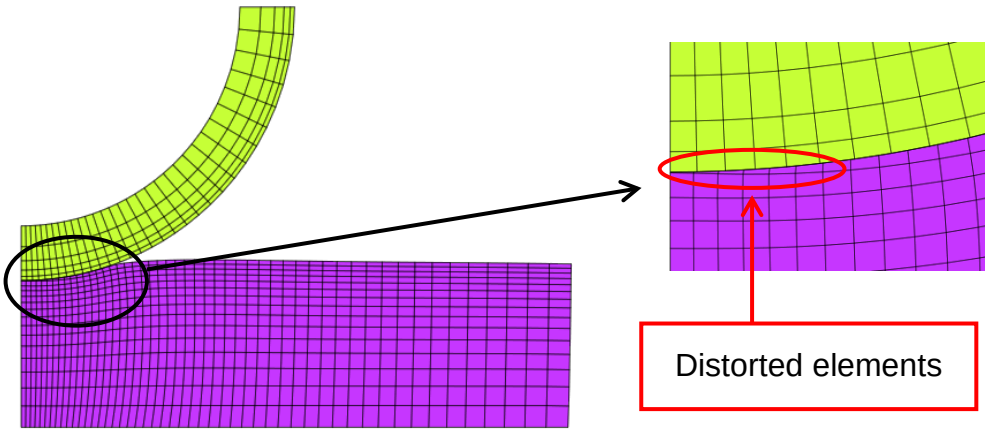

Figure 4.9 In the model with linearly elastic cartilage in FEBio, the cartilage elements on the contact surface were over-distorted.

For the strain levels in the parametric studies with varying model parameters, the neo-Hookean models in FEBio had very similar results to the linearly elastic models in ABAQUS.

4.3.2 Effect of contact-dependent fluid flow and methodology validation

As shown in **Figure 4.10** and **Figure 4.11**, the boundary conditions for fluid flow on the contact surface had a great effect on the magnitude and direction of the fluid flux, as well as on the cartilage consolidation process. Therefore, for biphasic modelling of contact problems, it is necessary to accurately represent the fluid flow conditions on the contact surface.

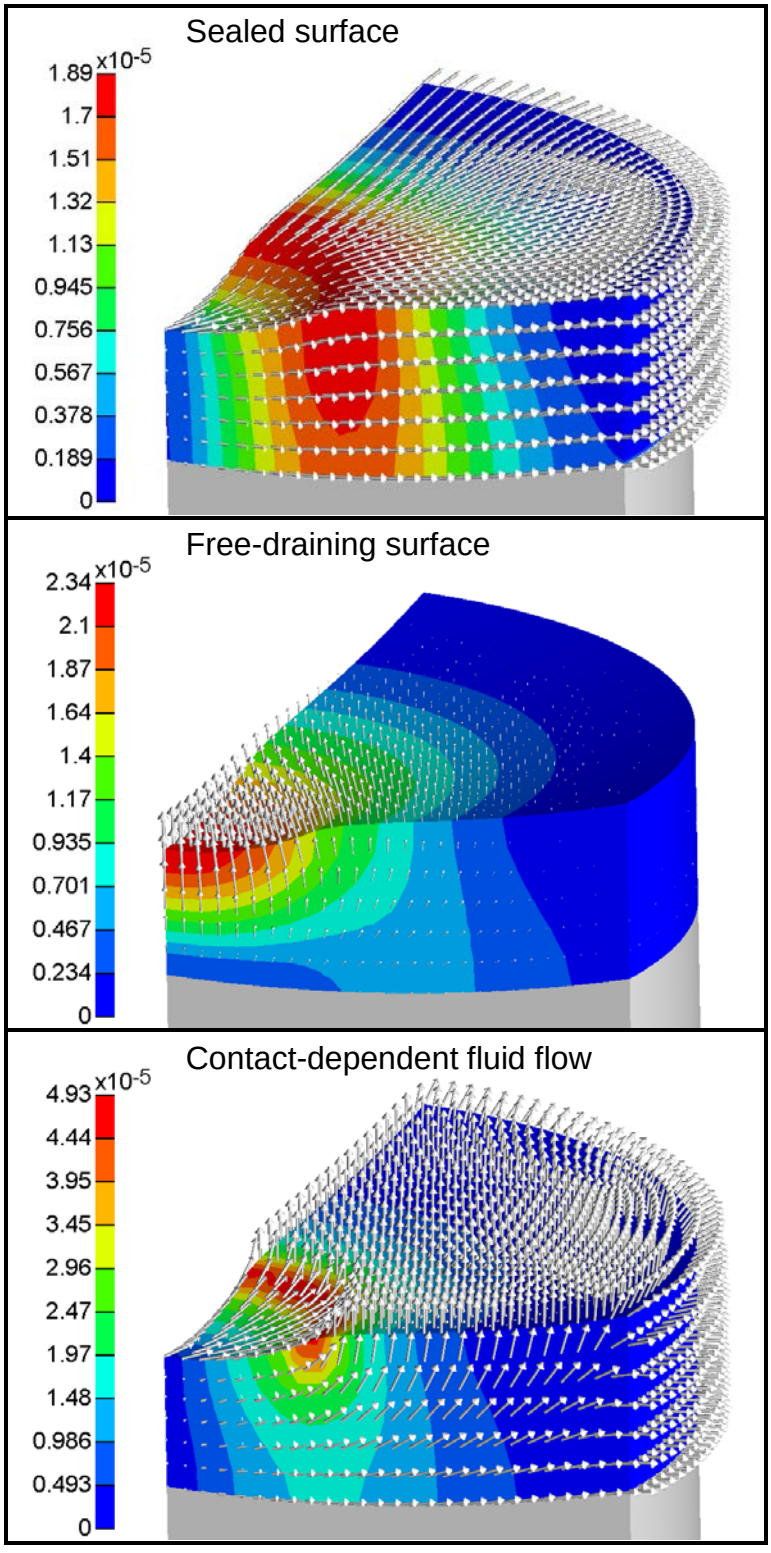

Figure 4.10 Contour of fluid flux (mm/s) for the model with sealed (no draining) surface, free-draining surface and surface of contact-dependent fluid flow at 2000 s. Grey vectors show the direction of fluid flux. The pattern of fluid flux differed markedly for the three cases.

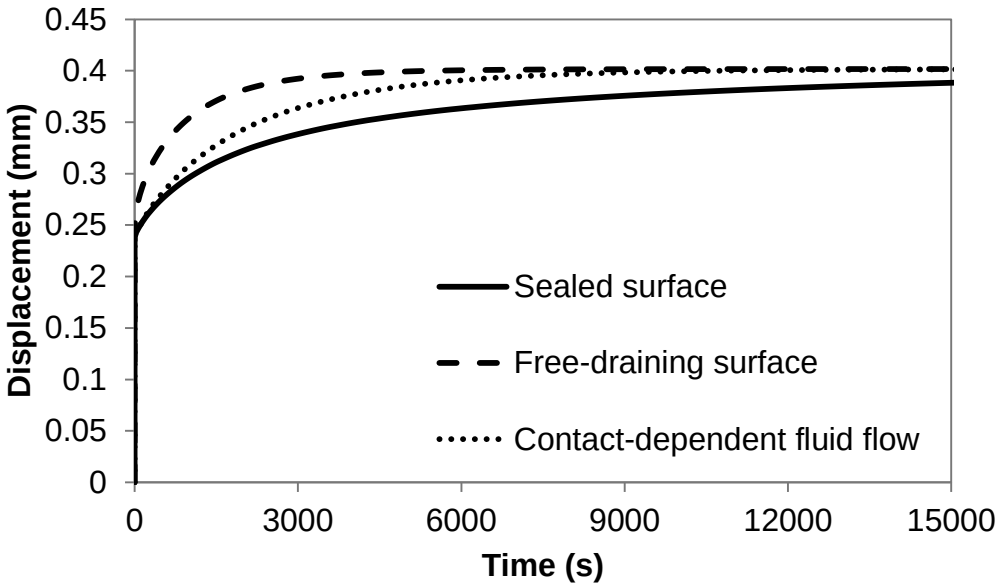

Figure 4.11 Predicted displacement of indenter for the model with sealed (no draining), free-draining and contact-dependent fluid flow assigned to the contact surface of the cartilage. The results were markedly dependent on this boundary condition. The model with free-draining surface had the fastest consolidation process and the model with sealed surface had the slowest consolidation process.

The predicted results of indenter displacement by FEBio are shown in **Figure 4.12**, in comparison with previous experimental results and computational predictions which adopted a linearly elastic solid phase in ABAQUS (version 6.7-1; Dassault Systemes, Suresnes Cedex, France). Again, it was found that the constitutive behaviour of the neo-Hookean solid phase in FEBio predicted identical results to the linearly elastic constitutive behaviour, which is in agreement with the predictions from the axisymmetric model. The predicted results exhibited good similarity to the experimental data, further confirming the reliability of biphasic modelling in FEBio.

However, within the first 1200 s, the calculated results deviated from the experimental data, because the solid phase was assumed to be isotropic in this study, which neglects the fact that the tensile modulus of the cartilage is substantially higher that its aggregate modulus (Soltz and Ateshian, 2000, Cohen et al., 1998). In the indentation test, the cartilage expanded horizontally when compressed vertically. Such expansion / tension was evident during the initial period when the fluid was mostly confined within the

tissue and the Poisson's ratio of the cartilage as a whole is high. The underestimated tensile modulus by the isotropic assumption may increase such expansion / tension, and thus the displacement of the indenter may be overestimated. However, for the latter period, the predicted results corresponded well to the experimental data, because the Poisson's ratio of the cartilage as a whole dropped towards zero when the cartilage consolidated and the tension effect of the cartilage in the indentation test became increasingly less obvious.

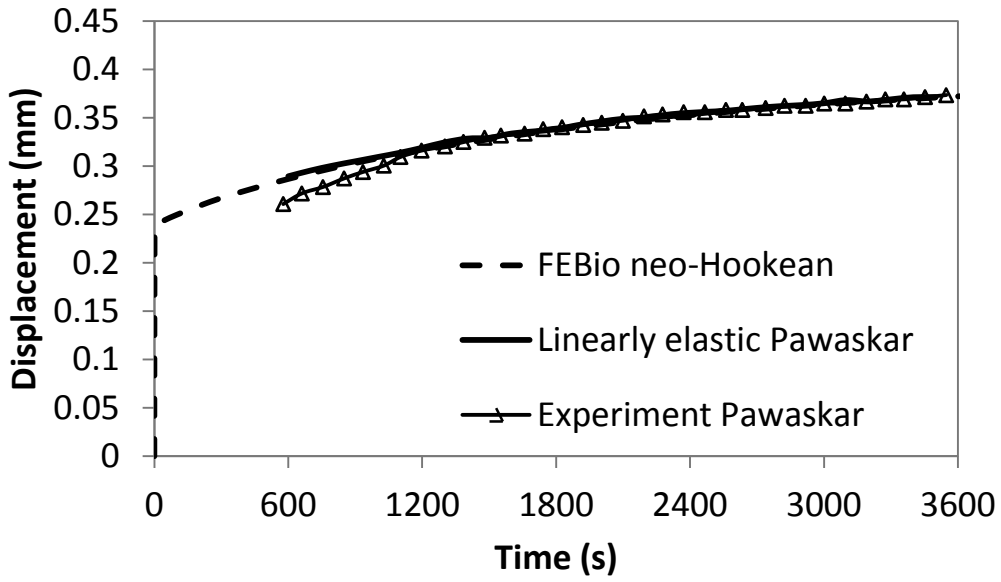

Figure 4.12 Displacement of indenter predicted using neo-Hookean solid phase in FEBio, in comparison with the computational results using linearly elastic solid phase in ABAQUS and experimentally measured data by Pawaskar (2010). Results from 0 to 600 s were not listed in (Pawaskar, 2010).

4.4 Discussion and conclusion

In addition to the indentation model listed in this chapter, models of simple configurations involving biphasic-biphasic cartilage contact (e.g. 3D ball-on-socket, ball-on-cubic contact models) were tested in FEBio and ABAQUS. However, such models were found to be substantially more difficult to achieve convergence in ABAQUS than in FEBio, for both linearly elastic and

neo-Hookean solid phase. Therefore the results of these studies are not presented here.

After careful evaluation, it was found that the linearly elastic solid phase does not perform well in the non-linear FE solver FEBio. Although in theory, as mentioned in **Section 4.2.2**, the neo-Hookean material in FEBio predicts identical results to the linear elastic model only in the circumstance of small strains, the findings in this chapter shows that for all the strain levels tested (max deformation ~40%), the neo-Hookean material is still appropriate to approximate the response of a linear relationship. Larger strains were not investigated here due to the convergence difficulty but also because that the strain level in this chapter is already high enough for the joint models under physiological loads which will be mentioned in the following chapters.

The boundary conditions of fluid flow on the articulating surfaces of the cartilage have a great influence on the model predictions, and thus need to be accurately presented in models involving contact of biphasic materials.

The methodology was verified and validated against the computed results and experimental data in a previous study (Pawaskar, 2010), and was found to show good agreement. There were some differences in the initial period after loading when compared to the experimental data, most likely due to the simplified isotropic behaviour used for the cartilage. Based on the results of this chapter, the following methodology was adopted for the FE models used in **Chapters 5**, **6**, **7** and **8**:

1) FEBio was used for all simulations.
2) The cartilage was simulated using a neo-Hookean model.
3) The contact-dependent fluid flow on the articulating cartilage surfaces was incorporated.

Chapter 5
Natural Human Hip Joint: The Influence of Size, Clearance, Cartilage Properties, Thickness and Hemiarthroplasty on the Contact Mechanics

5.1 Introduction

As mentioned in **Chapter 1**, due to the important role that the pressurisation of interstitial fluid plays in the cartilage function and degradation, it is necessary to consider the biphasic nature of the cartilage within the joint system.

According to the discussion in **Chapter 4**, experimental approaches have been greatly limited in the biphasic investigation of the hip joint, mainly due to their invasive techniques, inaccuracy caused by measurement artefacts and limited parameters that can be measured. Numerical analysis serves as an alternative approach. However, in the existing numerical studies, the biphasic material has not been successfully investigated to a three dimensional whole joint model that involves biphasic cartilage-on-cartilage contact, mainly due to convergence issues (Ferguson et al., 2000a, Ferguson et al., 2000b, Haemer et al., 2012, Pawaskar, 2010, Gu and Li, 2011). As yet, there seems to have been no studies to incorporate the biphasic approach into a three dimensional natural hip joint to examine the contact mechanics over a prolonged period of a physiological load.

It is widely realized that the congruence and size of the human hip joint and the material properties of the hip cartilage vary between individuals (Athanasiou et al., 1994, von Eisenhart et al., 1999, Shepherd and Seedhom, 1999, Xi et al., 2003). However, to what extent and how these parameters influence the contact mechanics of the natural hip joint is not fully understood. Besides, the influence of hemiarthroplasty (e.g. femoral head replaced with metallic prosthesis if only the femoral head cartilage

breaks down) on the hip function under prolonged periods of loads is unclear. Quantifying these influences can serve to better understand the hip function as well as to identify the conditions needed for the development of subject-specific computational models of the hip.

The aim of this study was therefore to develop a FE model for a standard hip anatomy incorporating the biphasic cartilage layers and to use the model to investigate the influence of hip size, clearance, cartilage properties, thickness and hemiarthroplasty on the contact mechanics and the associated fluid pressurisation in the joint over a prolonged period if a physiological load.

5.2 Methods

The general methods determined to be most appropriate from the initial studies in **Chapter 4** were adopted here.

5.2.1 Model geometry

The model utilized in the study was based on a standardized solid model of pelvis and femur from a corpse of a healthy human male (38 years old, 180 mm height and 90 kg at the time of death (Spitzer et al., 1996)), available from the Internet through the BEL repository (Author: Vicceconti, from: www.tecno.ior.it/VRLAB/). The acetabulum and the femoral head surfaces were carefully trimmed spherically (Hammond and Charnley, 1967, Rushfeldt et al., 1981), and a layer of cartilage with uniform thickness was created over the spherical area. The resultant model approximated the native horseshoe shaped acetabular cartilage and the femoral head cartilage coverage (**Figure 5.1**). The geometric model and corresponding FE model were generated using NX I-DEAS (Version 6.1, Siemens PLM Software Inc., Plano, USA).

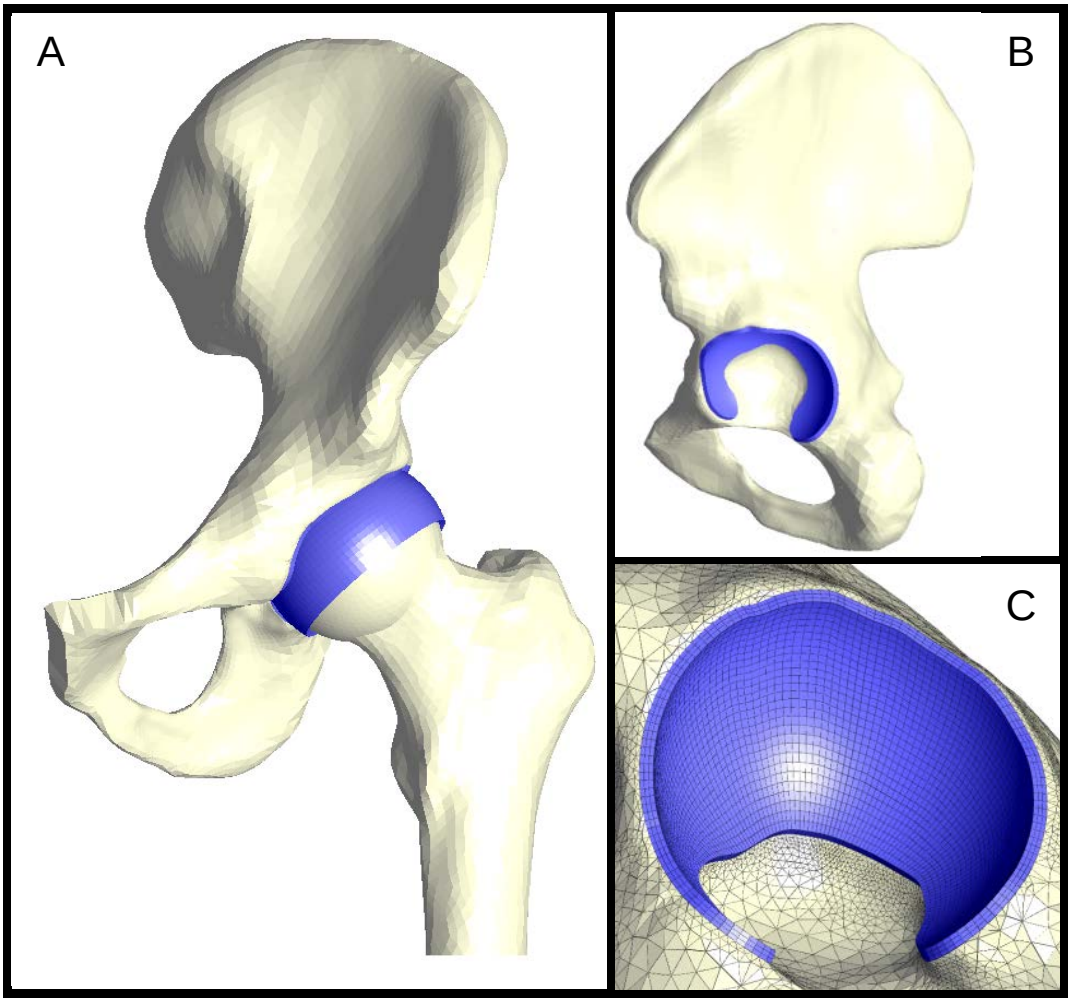

Figure 5.1 FE model creation. A – Entire model of hip joint. B – Lateral view of acetabulum. C – Oblique view of acetabular cartilage with hexahedral elements (3 elements of uniform distribution through thickness).

Additional models with varied geometric parameters (i.e. size, clearance or cartilage thickness) were achieved by scaling the spherically trimmed femur and pelvis and subsequently recreating the cartilage layers. A hemiarthroplasty model was also generated which had identical geometric parameters to the original model, with the femoral head replaced by an impermeable sphere representing a metal femoral head prosthesis.

5.2.2 Finite element mesh

The bone components of the femur and pelvis were meshed with four-noded tetrahedral elements, and the cartilage layers were made up of eight-noded

hexahedral elements. The bone was meshed based on the elements of the acetabular cartilage so that the surface of the subchondral bone shared the same nodes as the inner surface of the cartilage layer. Mesh sensitivity studies were conducted separately for the cartilage and bone by comparing the predictions of the models represented by varying number of elements. A combination of 128458 elements for the bone, 5676 elements for the femoral head cartilage and 8427 elements for the acetabular cartilage was found to be appropriate to generate similar results (<5%) when the numbers of elements were doubled (**Figure 5.2** and **Figure 5.3**). With these element numbers, it was found that the models were able to solve and the solutions converge using the methods described in **Chapter 4**.

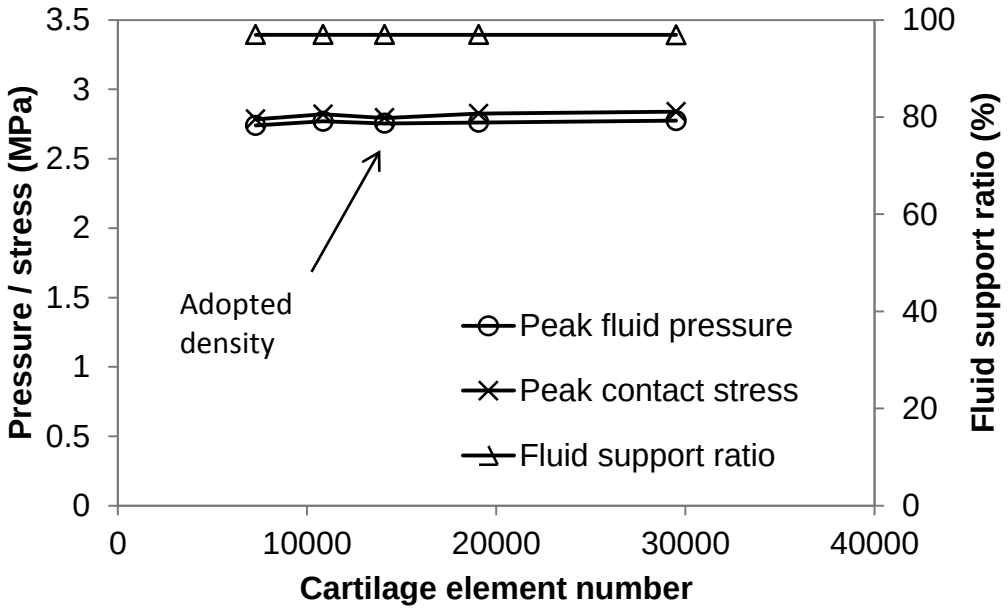

Figure 5.2 Predictions of the cartilage in the original model represented by different numbers of elements. The bone was assumed to be rigid and thus not included. An instantaneous displacement of 0.5 mm, instead of force, was applied to the model, to achieve convergence and computational efficiency. In the parametric studies, 5676 and 8427 elements were adopted for the femoral head cartilage and the acetabular cartilage respectively. Due to worse convergence abilities, models with coarser mesh densities were not adopted.

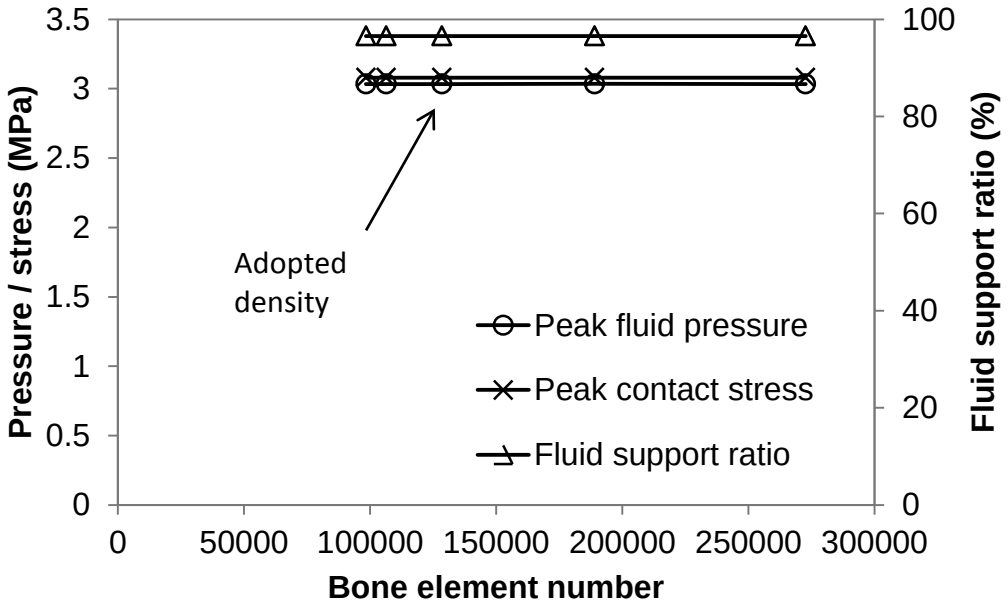

Figure 5.3 Predictions of the bone in the original model represented by different numbers of elements. The loading conditions of the parametric studies were adopted. Results were recorded at the end of 1 s. In the parametric studies, 128458 elements were adopted for the bone. Due to worse convergence abilities, models with coarser mesh densities were not adopted.

5.2.3 Material properties

Values of the material properties and geometric parameters were mentioned in **Section 5.2.5**. The cartilage was modelled as a biphasic solid and the solid phase was represented as neo-Hookean which approximates the linearly elastic constitutive relationship, as demonstrated in **Chapter 4**. The Poisson's ratio of the aggregate was 0.045; this value has been shown to have little influence on the results when varied from 0 to 0.1 (Athanasiou et al., 1994).

The bone was modelled as impermeable and linearly elastic with a Young's modulus of 17000 MPa and Poisson's ratio of 0.3 (Dalstra and Huiskes, 1995). The cortical bone and trabecular bone were not modelled separately because it was found that the results of interest were within 5% if the Young's modulus of the whole region was reduced from that representing all cortical bone (17000 MPa) to that representing all trabecular bone (800 MPa).

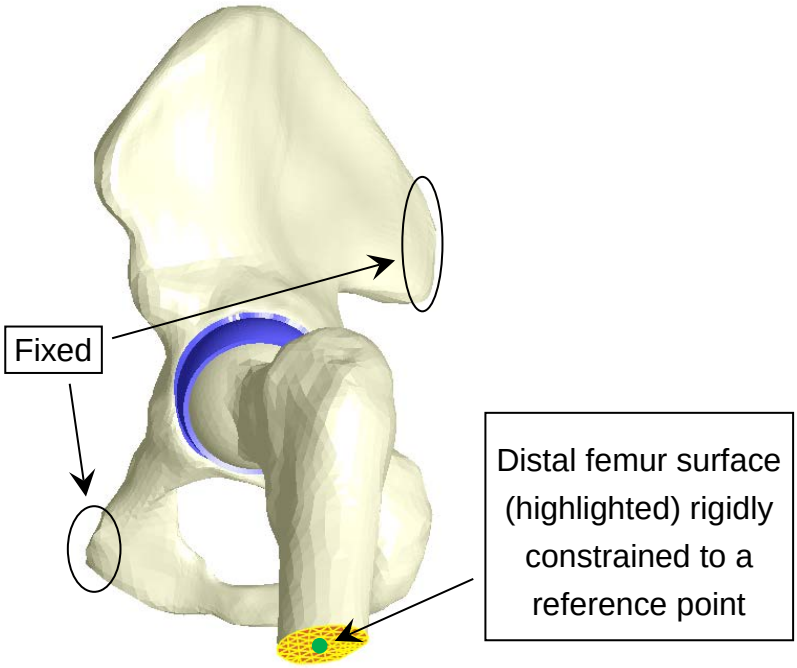

Figure 5.4 Boundary conditions of the model. Nodes at the sacroiliac and pubis symphysis joints were fixed in all degrees of freedom. The femur was constrained by the surface of the distal femur which was rigidly confined to a reference point to which the boundary conditions of the femur were applied.

5.2.4 Boundary conditions and loads

Nodes at the sacroiliac and pubis symphysis joints of the pelvis were fixed in all degrees of freedom (**Figure 5.4**). The distal surface of the femur, to which the load was applied, was rigidly constrained to a reference point, which was fixed in its rotational degrees of freedom. The contact between articulating surfaces was assumed to be frictionless. For the models of natural joints, the contact formulation allowed fluid to flow between contacting surfaces (pressure dependent) as well as from open surfaces of the cartilage. No fluid flow was allowed through the contact-against-rigid surfaces of the acetabular cartilage in the hemiarthroplasty model. A static load of approximately 2130 N, based on the average joint reaction force for one leg stance (Bergmann et al., 2001), was applied to the reference point of the distal femur, which was also constrained in rotational degrees of freedom. The load was ramped over 0.6 s and then held constant for 3000 s. Both the constrains and load of the femur were applied to its distal cut-off surface because (1) the boundary conditions of the distal femur could be equivalently transferred to the femoral

head centre, (2) the bone mechanics was not of interest and the bone had little influence on the contact mechanics and (3) concentrated load to a single node can be avoided.

5.2.5 Parametric studies

Parametric studies were conducted to evaluate the influence of model parameters on the predictions. The material properties and geometric parameters associated with the cartilage were initially taken from the literature and were then sequentially varied (**Table 5-1**).

Table 5-1: The values of the parameters used in the original model and parametric tests. Only one parameter was altered from the original in each test case. E: Young's modulus of cartilage aggregate; K: cartilage permeability; Cl: radial clearance; Size: acetabulum radius; Thick: cartilage thickness.

	Original model	Values used in parametric studies	References
E (MPa)	1.2	0.6, 1.8	(Athanasiou et al., 1994)
K ($mm^4/(Ns)$)	0.0009	0.00036, 0.00143	
Cl (mm)	0.5	0, 1	(von Eisenhart et al., 1999)
Size (mm)	30	26, 28	(Xi et al., 2003)
Thick (mm)	2	1, 3	(Shepherd and Seedhom, 1999)

5.2.6 Simulation method

All analyses were conducted using the open-source nonlinear FE solver FEBio, as determined in **Chapter 4**. The models were pre-processed using PreView (version 1.7; mrl.sci.utah.edu/software.php), and post-processed using PostView (version 1.4; mrl.sci.utah.edu/software.php). The FE simulations were solved on a Linux server with 8 GB of RAM and 8 Intel X5560 cores at 2.8 GHz.

5.2.7 Output measurements

The contact area was calculated as a ratio with respect to the total surface area (3000 mm^2 for the original model) of the acetabular cartilage available for articulation. The fluid support ratio was determined by calculating the load supported by the fluid pressure as a ratio of the total load. The contact stress, contact area, fluid pressure and fluid support ratio were recorded over the time period from 0 to 3000 s to evaluate the load transmission and tribological performance.

5.3 Results

5.3.1 Fluid pressure and contact stress

The fluid pressure distribution and contact stress are presented in **Figure 5.5** and **Figure 5.6** respectively. Over the acetabular cartilage surface, the contact stress and fluid pressure peaked around the centre of the cartilage and decreased gradually towards the edges. The contact stress and fluid pressure contours on both the femoral head and the acetabular cartilage surfaces were very similar. The peak fluid pressure was slightly lower than the peak contact stress over 3000 s for all the models. There was no marked difference in the fluid pressure across the thickness of the cartilage (**Figure 5.7**).

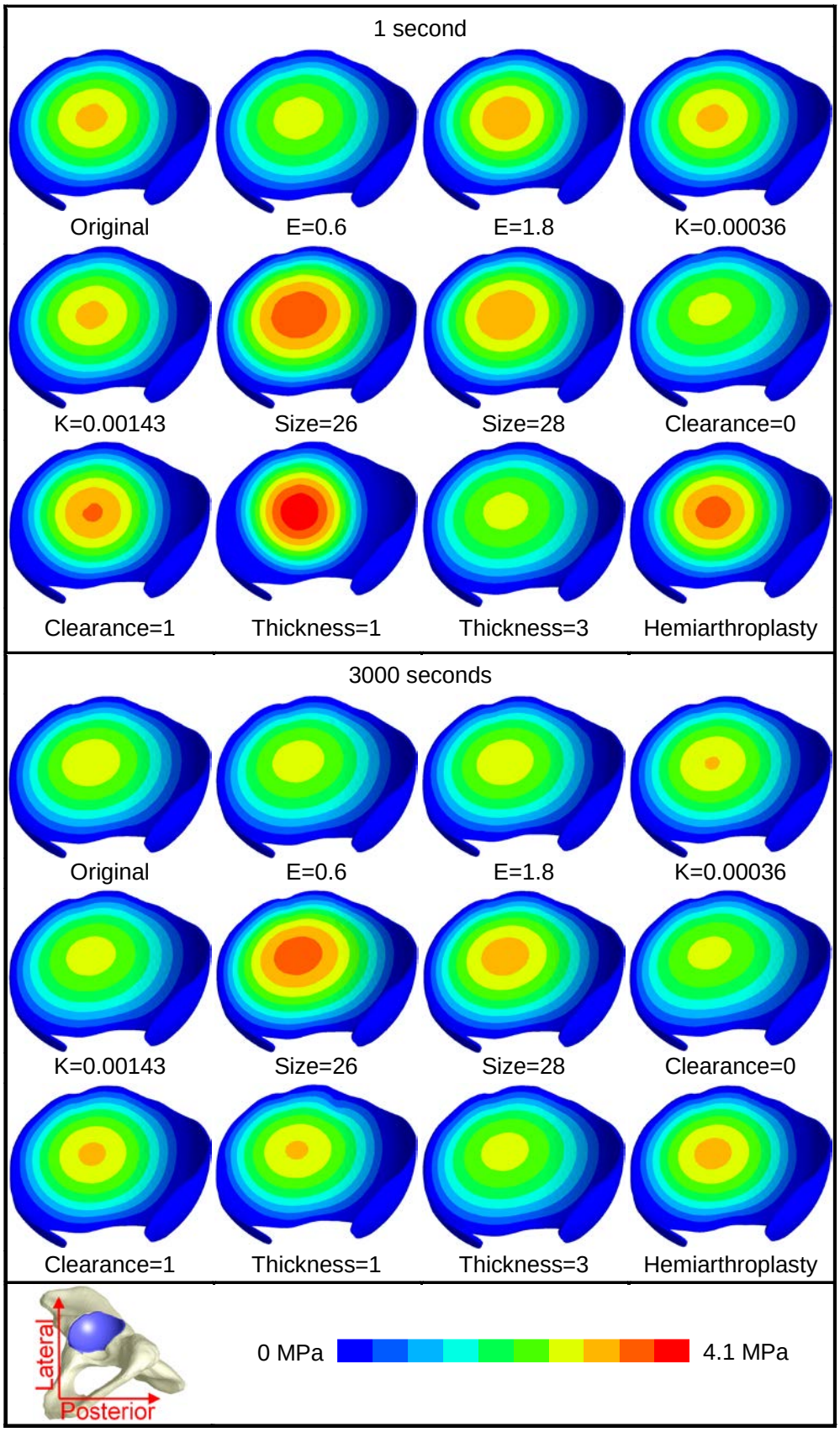

Figure 5.5 Contours of fluid pressure (MPa) of the acetabular cartilage for all the models at 1 s and 3000 s. Obvious cartilage consolidation can be detected.

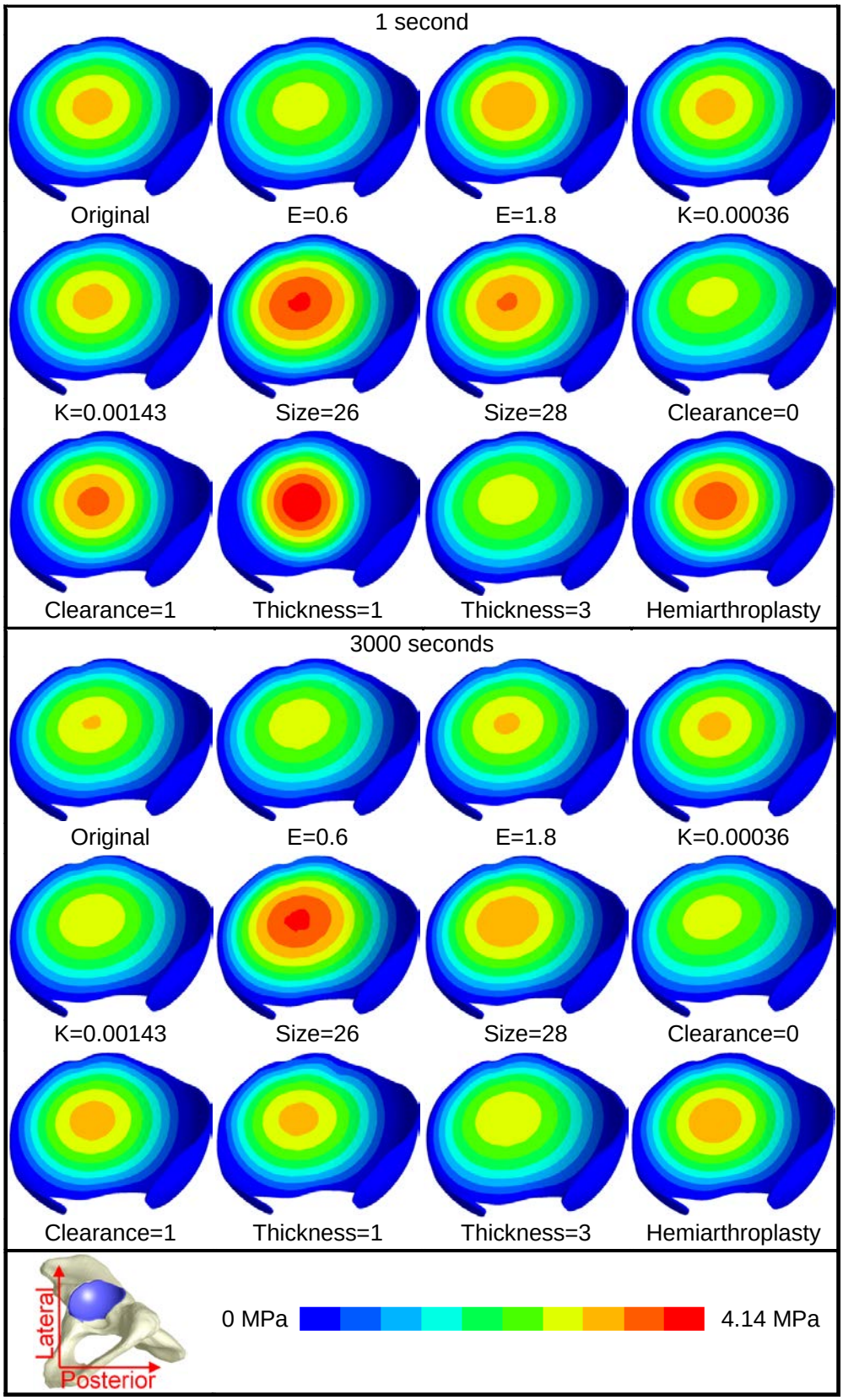

Figure 5.6 Contours of contact stress (MPa) of the acetabular cartilage for all the models at 1 s and 3000 s. Obvious cartilage consolidation can be detected. On the acetabular cartilage, the magnitudes and distributions of the contact stress was similar to those of the fluid pressure.

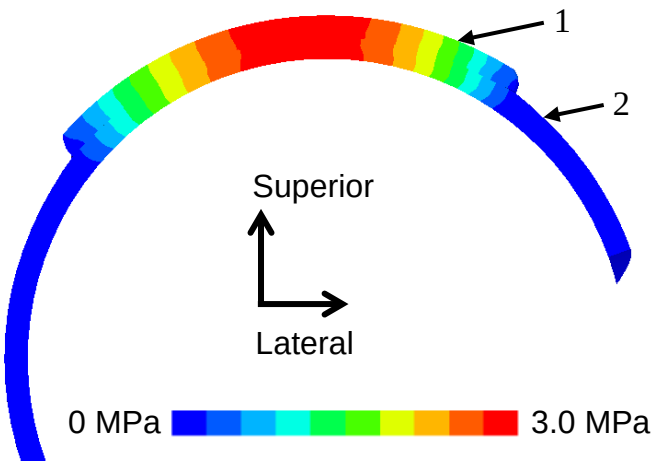

Figure 5.7 Cross-sectional view of fluid pressure (MPa) in the cartilage of the acetabulum (1) and femoral head (2) of the original model at 1 s. Fluid pressure distribution was similar for the femoral head cartilage and acetabular cartilage. There was no marked difference in the fluid pressure across the thickness of the cartilage.

5.3.2 Effect of cartilage properties

The results of models with different cartilage aggregate stiffness are shown in **Figure 5.8**. The models with stiffer cartilage aggregate had higher peak contact stress, higher peak fluid pressure and greater variations in the results over 3000 s. At the end of 1 s, the peak contact stress for the model with 1.8 MPa cartilage Young's modulus was 18% higher than the model with 0.6 MPa cartilage Young's modulus. Over 3000 s, the decrease in the peak contact stress and peak fluid pressure were 9% and 15% respectively for the model with 1.8 MPa cartilage Young's modulus, while the peak contact stress and peak fluid pressure kept almost constant (<1%) for the model with 0.6 MPa cartilage Young's modulus.

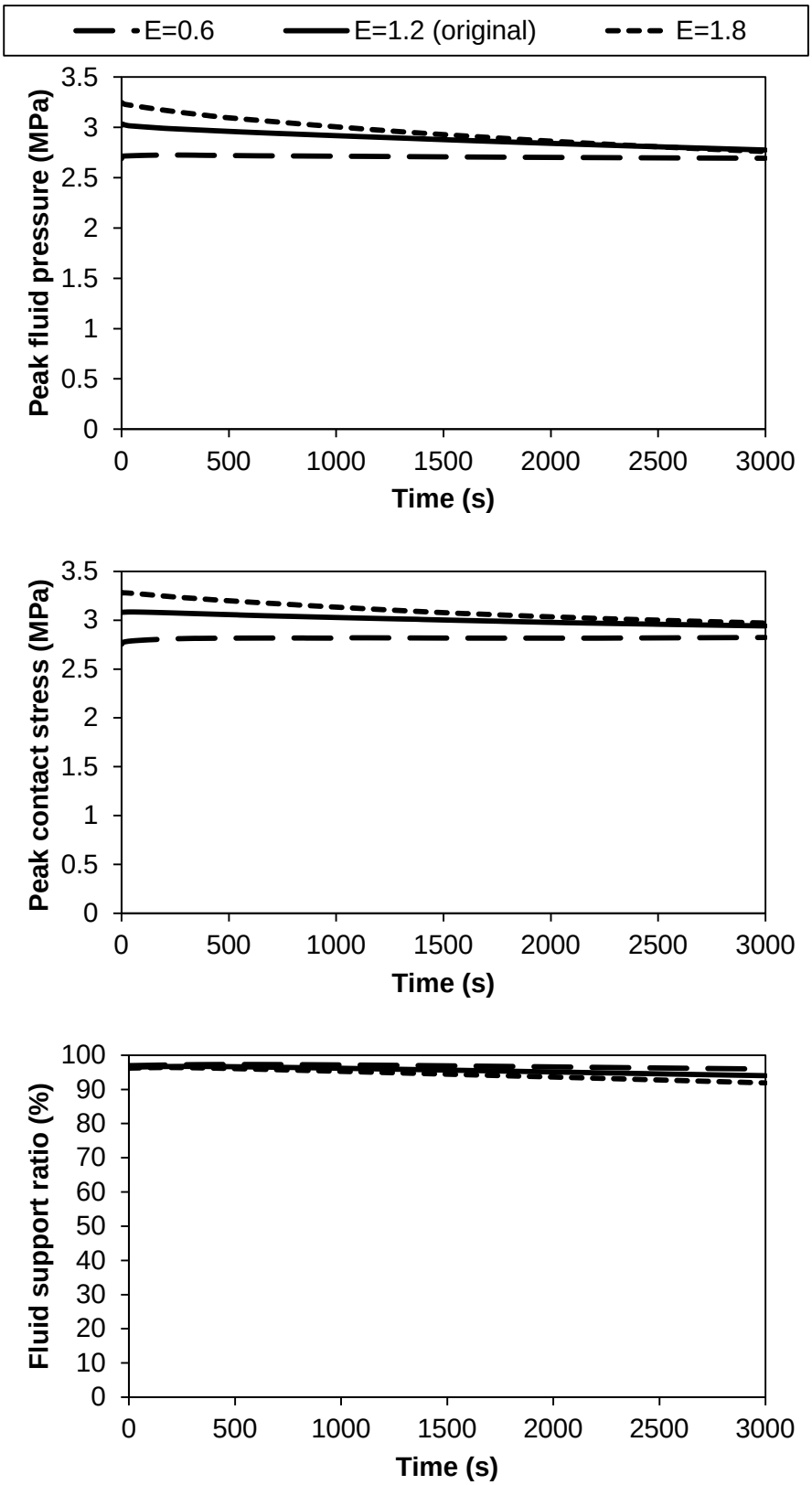

Figure 5.8 Results of models with different aggregate Young's moduli (MPa). The models with stiffer cartilage aggregate had higher peak contact stress, higher peak fluid pressure and greater variations in the results over 3000 s.

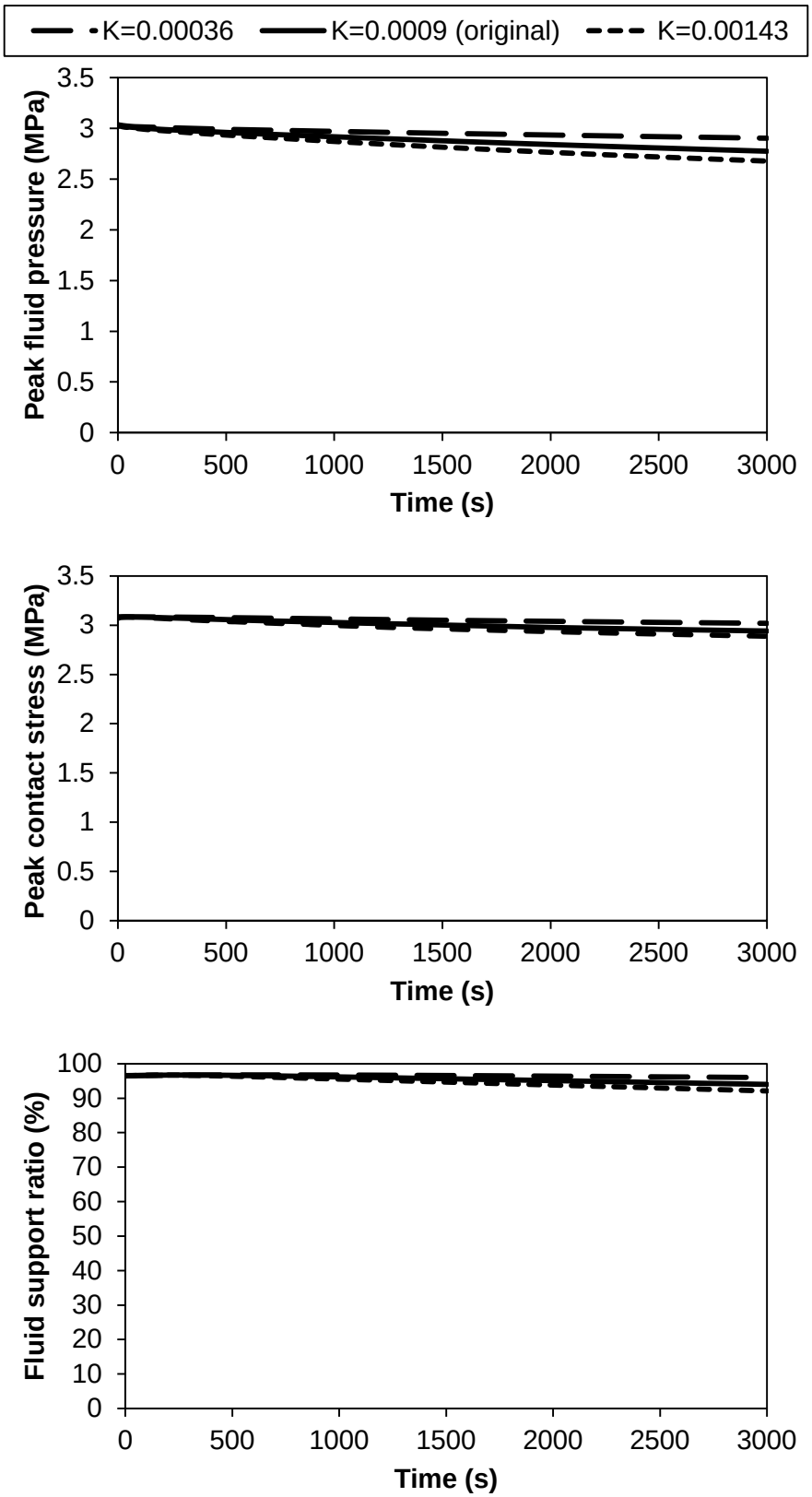

Figure 5.9 Results of models with different permeabilities ($mm^4/(Ns)$). The results of the models with different cartilage permeabilities were very similar for the period soon after loading but evidently different over 3000 s. The models with higher cartilage permeability had greater variations in the results over 3000 s.

The results of models with different cartilage permeabilities are shown in **Figure 5.9**. The models with different permeabilities had similar results for the period soon after loading. The effect of permeability on the results only became evident over a prolonged loading period. Greater variations in the peak contact stress, peak fluid pressure and fluid support ratio were found for the models with higher cartilage permeability over 3000 s. For the model with cartilage permeability of 0.00036 $mm^4/(Ns)$, the variations in these results were less than 5%, whilst for the model with cartilage permeability of 0.00143 $mm^4/(Ns)$, the variations in the peak contact stress, peak fluid pressure and fluid support ratio were 6%, 12% and 5% respectively.

The influence of cartilage thickness on the model predictions is shown in **Figure 5.10**. The models with thinner cartilage had markedly higher peak contact stress, higher peak fluid pressure, higher fluid support ratio and greater variations in the results over 3000 s. At the end of 1 s, the model with 1 mm and 3 mm cartilage had a peak contact stress of 4.1 MPa and 2.7 MPa respectively. Over 3000 s, the results for the model with 3 mm cartilage kept almost constant (<3%), while the peak fluid pressure and contact stress of the model with 1 mm cartilage decreased by 29% and 27% respectively.

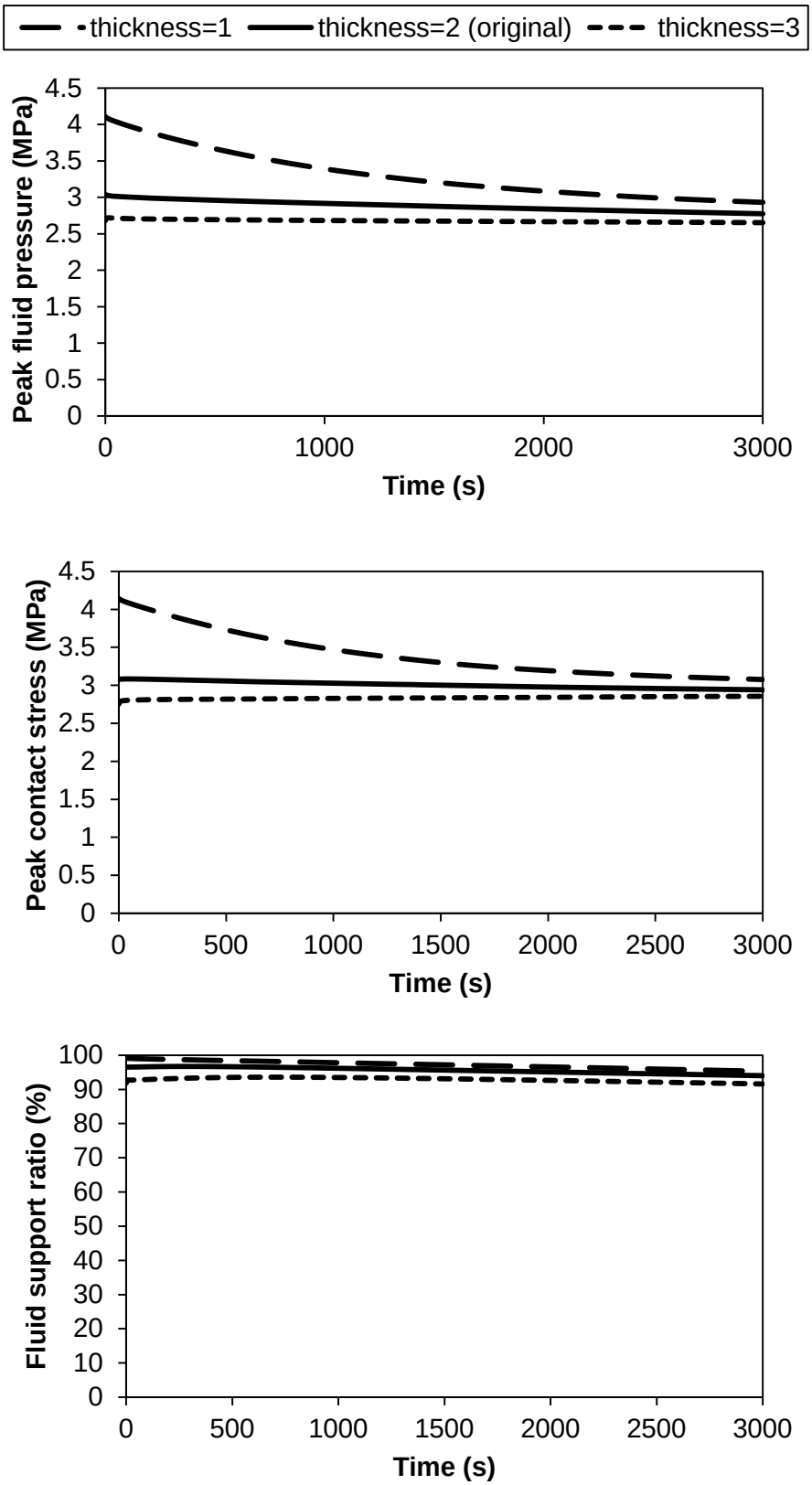

Figure 5.10 Results of models with different cartilage thickness (mm). The models with thinner cartilage had higher peak contact stress, higher peak fluid pressure, higher fluid support ratio and greater variations in the results over 3000 s.

5.3.3 Effect of radial clearance and joint size

The results of models with varied radial clearance are shown in **Figure 5.11**. The models with larger radial clearance had higher peak contact stress, higher peak fluid pressure and greater variations in the results over 3000 s. The fluid support ratio for models with different clearance was similar. Less than 3% variation in the results of interest was found for the model with no clearance over 3000 s. For the model with 1 mm clearance, however, the peak fluid pressure and peak contact stress decreased by 13% and 9% respectively.

As shown in **Figure 5.12**, the models with smaller size had higher peak contact stress and higher peak fluid pressure. At the end of 1 s, the peak fluid pressure and peak contact stress for the model with 26 mm acetabular radius were respectively 22% and 24% higher than the original model which had an acetabular radius of 30 mm. The fluid support ratio for models of different size was 96% at the end of 1 s and decreased to 92% – 94% over 3000 s.

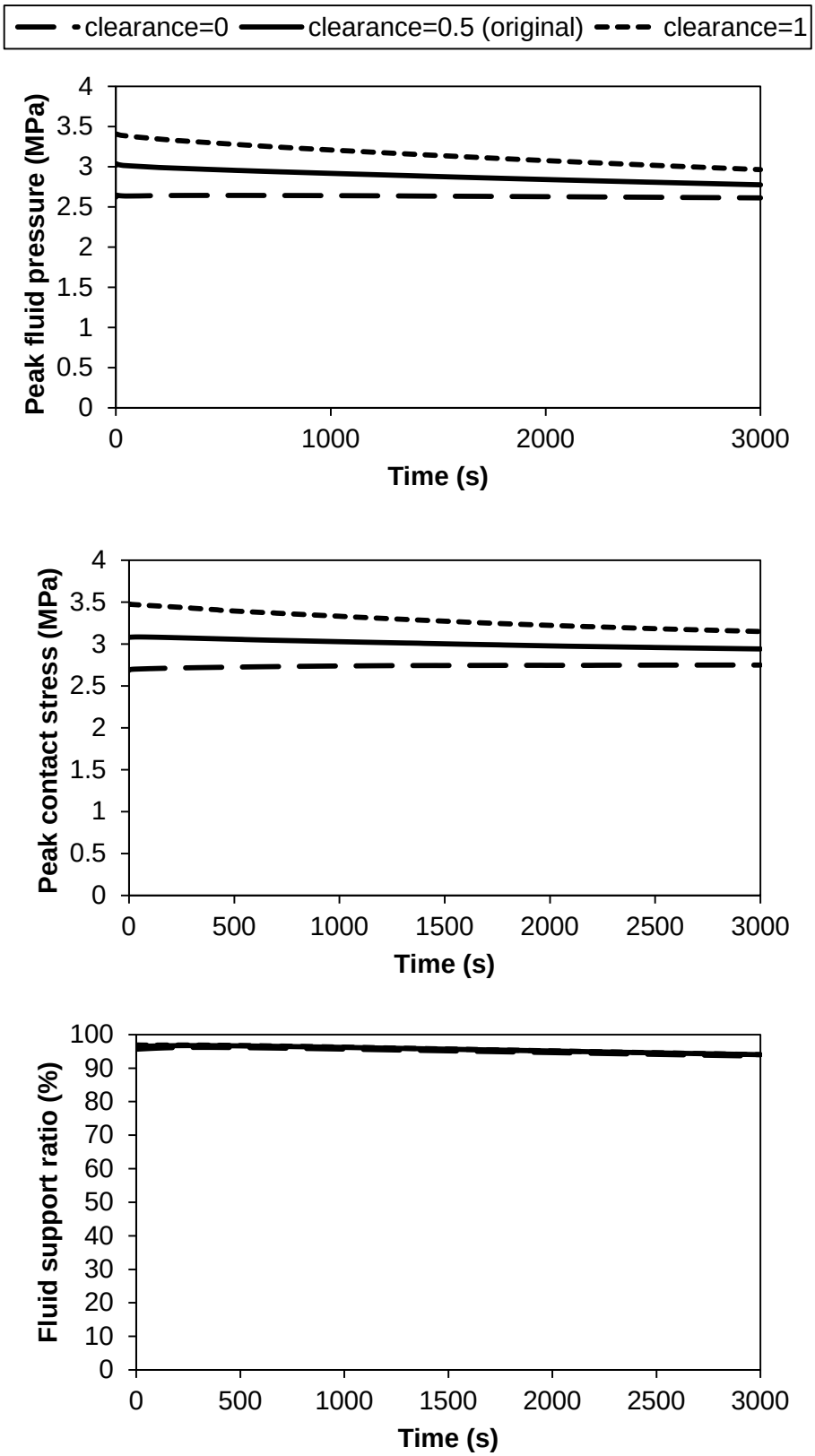

Figure 5.11 Results of models with different radial clearance (mm). The models with larger radial clearance had higher peak contact stress, higher peak fluid pressure and greater variations in the results over 3000 s. The fluid support ratio for models with different clearance was similar.

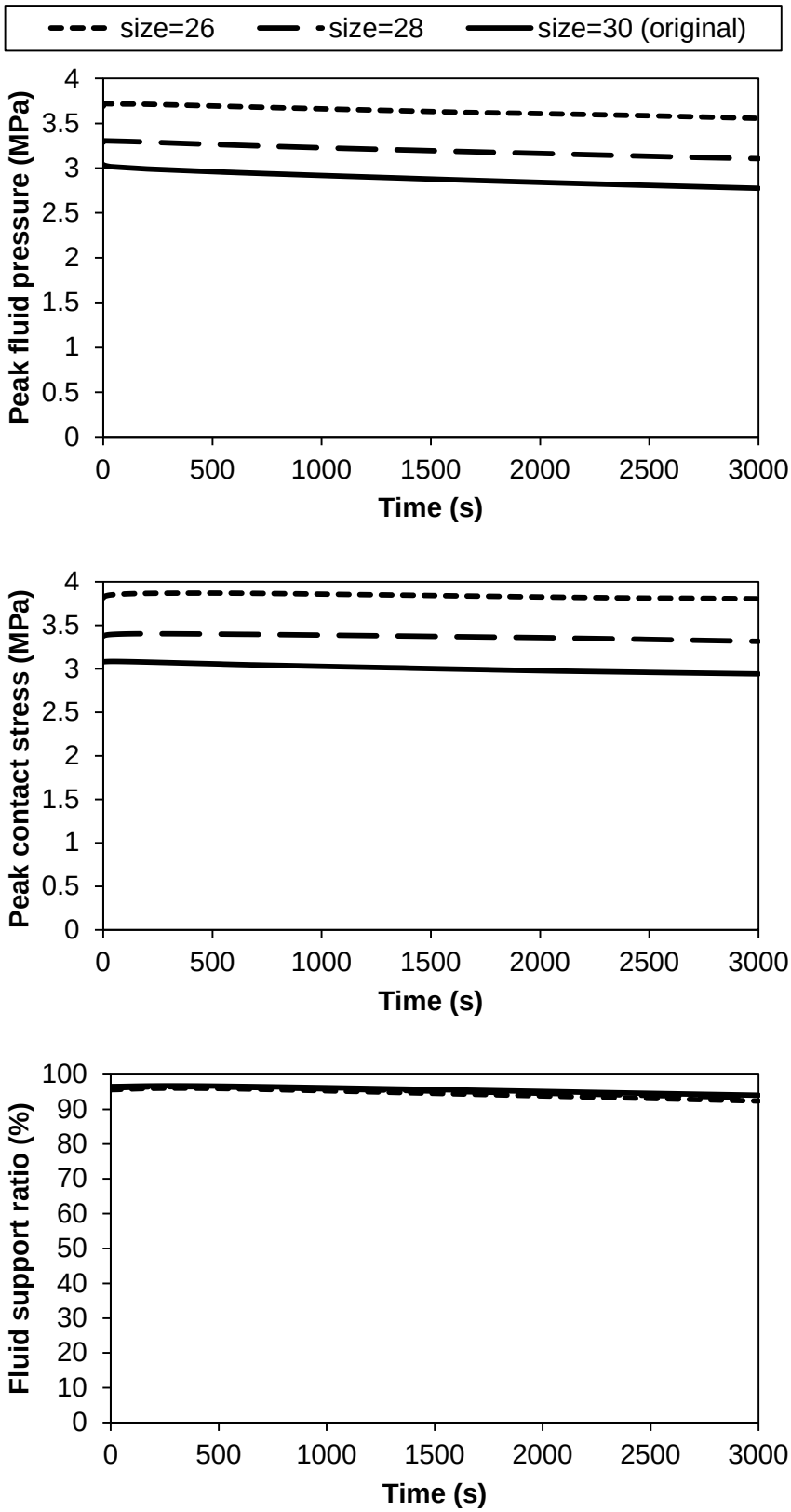

Figure 5.12 Results of models with different acetabulum radius (mm). The models with smaller size had higher peak contact stress and higher peak fluid pressure. The fluid support ratio for models with different sizes was similar.

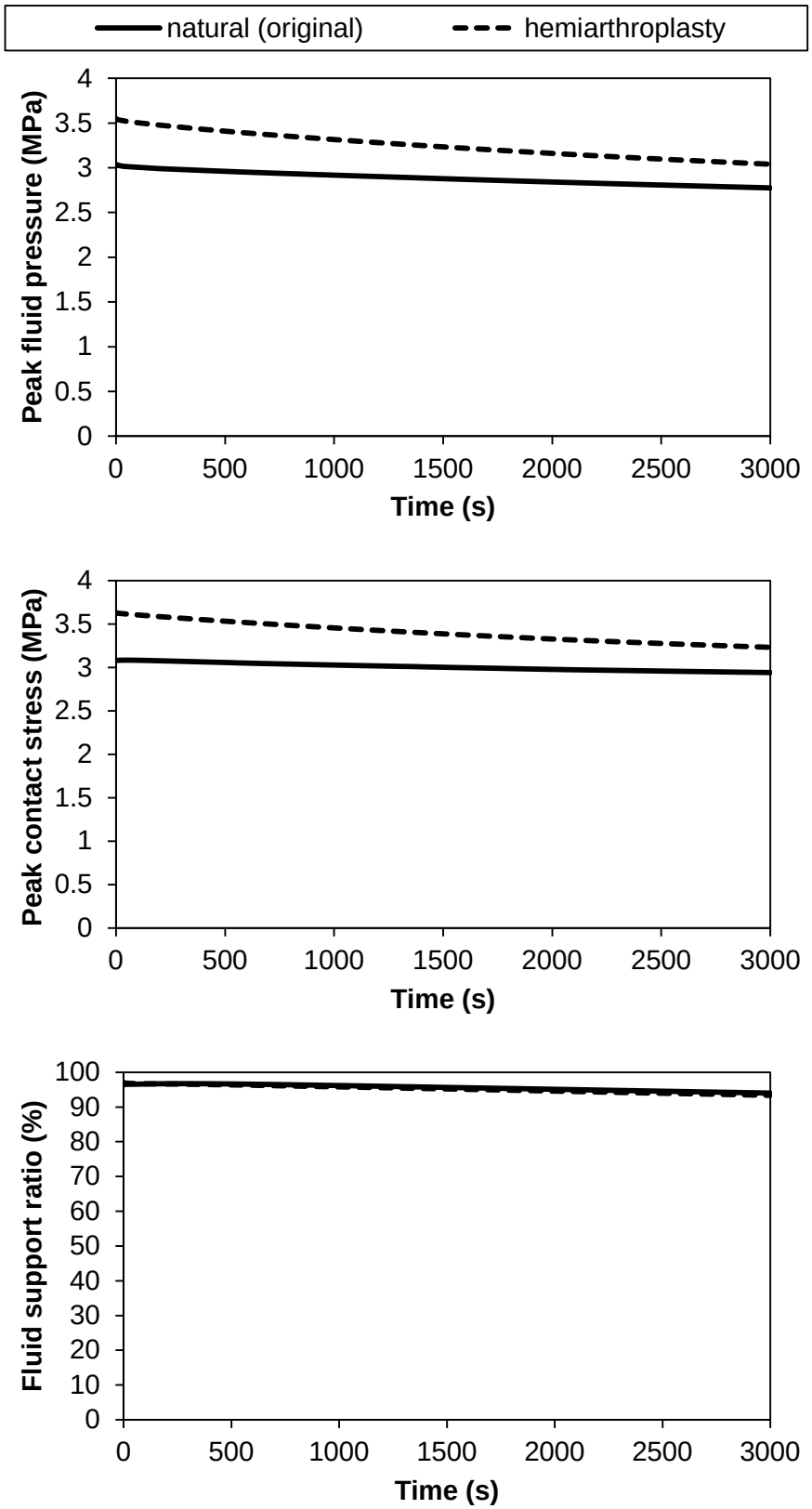

Figure 5.13 Results of natural joint and hemiarthroplasty. The hemiarthroplasty model had higher peak contact stress, higher peak fluid pressure and greater variations in the results over 3000 s. The fluid support ratio was similar for the natural hip model and hemiarthroplasty model.

5.3.4 Comparison of the natural cartilage and hemiarthroplasty models

The comparison between the predictions by the natural hip model and by the hemiarthroplasty model was shown in **Figure 5.13**. The hemiarthroplasty model had markedly higher peak contact stress, higher peak fluid pressure and greater variations in the results over 3000 s. At the end of 1 s, the peak contact stress and peak fluid pressure of the hemiarthropasty model were 17% higher than the original model of natural joint. The fluid support ratio was similar for the natural hip model and hemiarthroplasty model over 3000 s.

5.3.5 Summary of parametric studies

The overall results of the parametric studies are summarized in **Figure 5.14**. Generally, the predictions of the model during both short and long periods were more sensitive to the variation in geometric parameters (i.e. hemiarthroplasty, clearance and cartilage thickness) than material properties of the cartilage (i.e. Young's modulus and permeability). As compared to the other parameters, changes in the fluid support ratio were most sensitive to the variation in cartilage permeability. The fluid support ratio for all the models was more than 90% and changed less than 5% over 3000 s.

	Hemiarthroplasty / HA	E (MPa)	K (mm^4/Ns)	Cl (mm)	Thick (mm)	Size (mm)
×	Yes	0.6	0.00036	0	1	26
Original	No	1.2	0.0009	0.5	2	30
□		1.8	0.00143	1	3	28

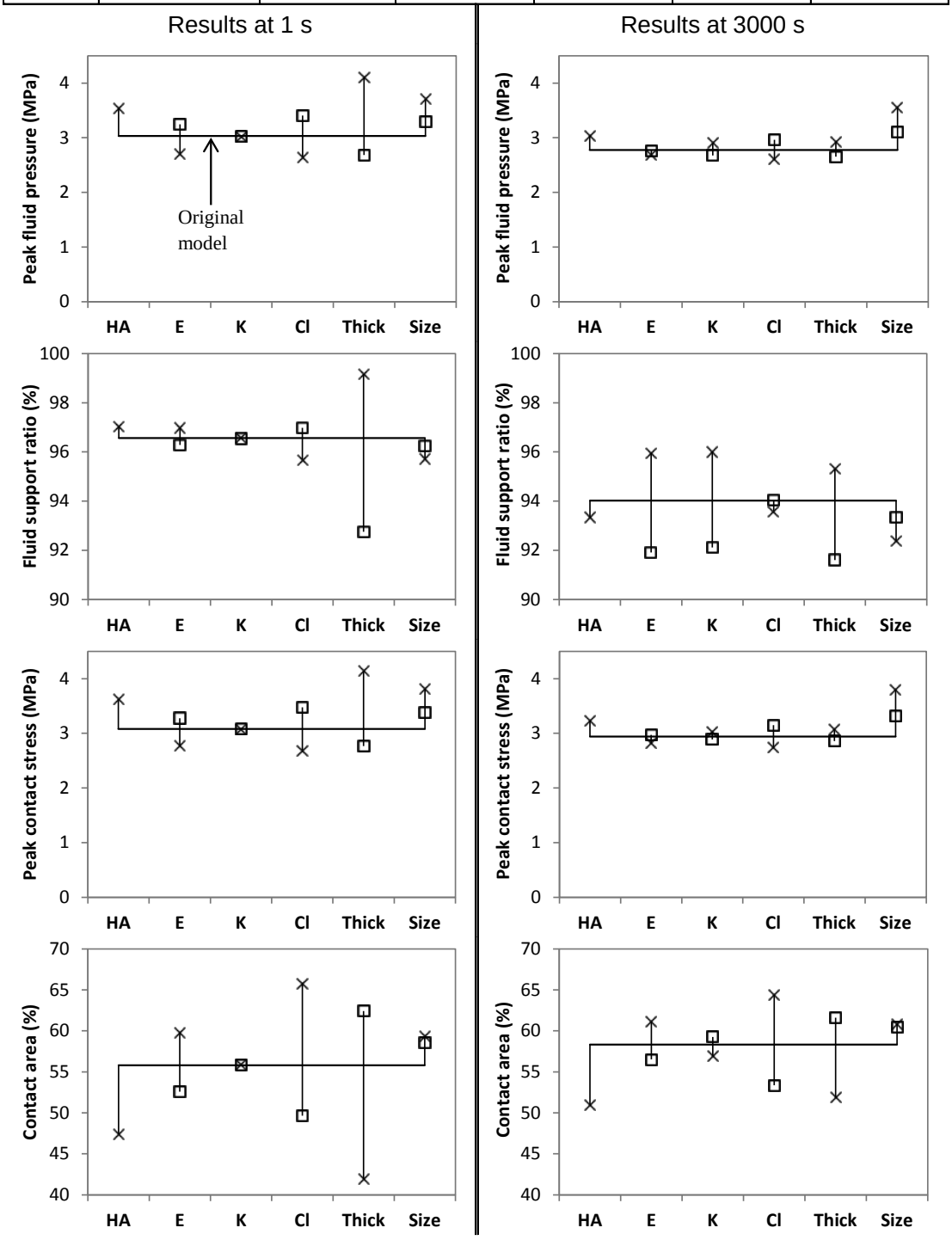

Figure 5.14 Overall results of the parametric tests for all models at 1 s and 3000 s. The model is more sensitive to the variation in geometric parameters than material properties.

5.4 Discussion

The primary aim of this chapter was to develop the biphasic modelling methodology for simulating the natural hip over prolonged physiological periods. Whilst this was achieved, there were some limitations. In reality, as well as being biphasic, the cartilage layer is an inhomogeneous fiber-reinforced structure (Mow et al., 1980, Soulhat et al., 1999, Ateshian et al., 2009), and the homogeneous isotropic elastic model used here as a first approximation does not fully represent its behaviour. Although the 3000 s adopted in this study represents a relatively long physiological loading period, the cartilage behaviour is still relatively early in the transient phase and the results against time had not yet reached the equilibrium state that can be observed eventually in creep tests (Mow et al., 1980, Athanasiou et al., 1994). As mentioned in **Chapter 4**, in terms of capturing the early stage response of creep tests, a tension-compression non-linear model may be more appropriate than the linear isotropic biphasic model which neglects the fact that the tensile modulus of the cartilage is substantially higher than its aggregate modulus (Soltz and Ateshian, 2000, Cohen et al., 1993, Cohen et al., 1998). Consequently, the confinement effect due to the tensile stiffness may be reduced, and the peak fluid pressure, peak contact stress and fluid support ratio may be underestimated. The influence of cartilage thickness may also be amplified since here the confinement is provided more by the underlying bone geometry.

The congruence, size and material properties of the hip joint vary between individuals. The parametric study was therefore undertaken as a precursor to subject-specific modelling to identify the sensitivity of the model to these parameters. The findings of this study show that the contact mechanics of the hip joint are dependent on its congruence, size, cartilage thickness and properties as well as the contact type (i.e. cartilage-on-cartilage and cartilage-on-solid). Over the ranges studied here, the thickness and clearance were found to have the greatest effect on the contact mechanics. This is in agreement with the sensitivity study of Anderson et al. (2010) in an elastic model, where it was found that the cartilage thickness and local surface morphology had a major effect on the contact stress and distribution.

For subject-specific investigations, it is clear that the individual variations in the morphology of the cartilage are important. Whilst the effect of the thickness may be overestimated by the simplified material model used, it is a parameter that needs to be taken into consideration in future sensitivity studies.

The influence of the cartilage material properties was generally less than that of the morphology. In particular, the effect of the cartilage permeability on the contact mechanics of the hip joint was minimal during the early stages, but became evident after a period of load. The fluid support ratio was more sensitive to the cartilage thickness than other parameters at an early period because, as shown by the contact area in **Figure 5.14**, the hip congruence at this stage is highly related to the cartilage thickness as well as the clearance. For the model with thicker cartilage, the contact stress was spread more towards the area near the edge of the cartilage which is less confined than around the central region, leading to a lower fluid support ratio. This is because the fluid support ratio of the cartilage under unconfined compression is substantially lower than that under confined compression (Park et al., 2003, Ateshian and Hung, 2006). However, in reality, such differences may be reduced by the tension-compression nonlinearity of the cartilage. The hemiarthroplasty case showed higher peak stresses and a greater reduction in the fluid-load support over time than the cartilage-on-cartilage case. This illustrates that it is necessary to model both layers of cartilage to represent the natural joint since their interaction plays an important role in the contact mechanics.

For models with different parameters presented in this study, the predicted peak contact stress was found to range from 2.7MPa to 4.1 MPa. For similar loading conditions, the peak contact stress has been reported to lie between 4 MPa and 7 MPa in a study using embedded transducers (Brown and Shaw, 1983, Hodge et al., 1989)) and between 5 MPa and 10 MPa in studies using pressure-sensitive films (Afoke et al., 1987, Anderson et al., 2008). Besides the linear isotropic assumption of the cartilage, the higher values of such measurements could be because the film thickness and stiffness introduce measurement artefacts, but also because of the smooth surfaces and regular morphology assumptions in this study, which have

been shown to reduce the peak contact stress in an elastic FE model (Anderson et al., 2010). The peak stress predictions in this study are consistent with previous numerical studies where similar spherical assumptions have been made (i.e. 3 MPa to 4 MPa) (Mavčič et al., 2002, Yoshida et al., 2006, Pawaskar et al., 2010). For the purpose of the current study, the spherical assumption was necessary in order to undertake the initial parametric study and gain an understanding of the order of importance of the model input conditions.

The labrum was excluded in this study due to the lack of extensive literature on its geometric parameters and material properties (Anderson et al., 2008), which is another potential limitation. Although the labrum plays a minimal role in load supporting for the normal hip (1-2% of total load) (Henak et al., 2011), it is believed to help impede the fluid exudation, owing to its lower permeability compared with the cartilage (Ferguson et al., 2000a, Ferguson et al., 2000b, Ferguson et al., 2003, Haemer et al., 2012). After labrum removal, the edge surface of the acetabular cartilage remains free-draining, potentially leading to a faster process of fluid exudation compared with a hip with the labrum. The findings in this study illustrate that even under the extreme situation where the labrum is removed, the fluid supports most of the load over prolonged physiological loading periods, further demonstrating the excellent function of the hip joint.

The primary advantage of the methodology in this study lies in its ability to investigate the solid phase and fluid phase separately, predict the joint tribological behaviour under both short-term and long-term loading periods, and interpret the influence of model parameters on the fluid-solid phases over prolonged physiological loading periods.

In conclusion, in this chapter a new method for simulating the contact mechanics and associated fluid pressurisation for a biphasic natural hip joint under prolonged physiological loading was presented. The predicted behaviour of the natural hip joint model was found to be subject to hip size, clearance, cartilage aggregate modulus, thickness and hemiarthroplasty for the period soon after loading. The fluid in the cartilage supports over 90% of the load transmitted between the articulating surfaces of the hip joint for a

prolonged physiological loading period. The model with higher congruence or lower cartilage permeability has slower changes over this period. The methodology developed in this chapter can now be used to explore the behaviour of the joint over more realistic daily activities, as will be presented in **Chapter 6**.

Chapter 6
Natural Human Hip Joint: Application to the Study of Different Activities

6.1 Introduction

The hip joint is subject to a range of loading directions and magnitudes during daily activities, which affect both its biphasic performance and the potential for degeneration. In **Chapter 5**, a whole hip model with biphasic cartilage layers under physiological static loads was successfully simulated for a prolonged period, and it was demonstrated that the interstitial fluid supports over 90% of the load transmitted between the articulating surfaces of the hip joint under a physiological static load. Such high ratio of load support by the fluid phase also contributes to the lubrication of articular cartilage (Ateshian et al., 1994, Mow et al., 1980, Mow et al., 1984), and is closed linked with cartilage function and degradation (e.g. osteoarthritis) (Forster and Fisher, 1996, McCann et al., 2009). However, biphasic materials have yet to be successfully applied to a three dimensional whole joint under high physiological dynamic loads which involve consecutively sudden spatial and temporal variations, although such an investigation has the potential to provide valuable information about hip function and the potential for damage associated with daily activities.

The aim of this study was to investigate the cartilage contact mechanics and the associated fluid pressurisation in the hip joint during different daily activities.

6.2 Methods

The model used in this study was similar to the one described in **Chapter 5**. The geometric parameters and material properties of the natural hip model were based on the original model in **Chapter 5**.

The boundary conditions of the models were also as described in **Chapter 5**. In this study, previously measured *in vivo* hip contact forces for eight activities (Bergmann et al., 2001) were adopted and applied to the reference point on the distal femur. It was assumed that the rotation of the femur would not cause a difference in the contact mechanics of the model, because (1) the bone had little influence on the predictions, (2) the joint was assumed to be spherical and frictionless, and (3) the long term cartilage consolidation was not investigated in this study due to the lengthy simulation time required. Consequently, the femur was fixed along rotational degrees of freedom through the reference point.

FE simulations were conducted for eight activities of daily living as shown in **Table 6-1**. The average dataset of the patient KW (Bergmann et al., 2001) was selected because the gait pattern of this patient exhibited good postoperative rehabilitation. The load was based on the coordinate system of the pelvis. The magnitude of vectors for all the activity loads is represented in **Figure 6.1**.

Table 6-1 List of activities and their cycle time (s).

Activity	Fast walk	Normal walk	Slow walk	Stand up	Sit down	Ascend stair	Descend stair	Knee bend
Time	1.0	1.1	1.2	2.5	3.7	1.7	1.5	3.6

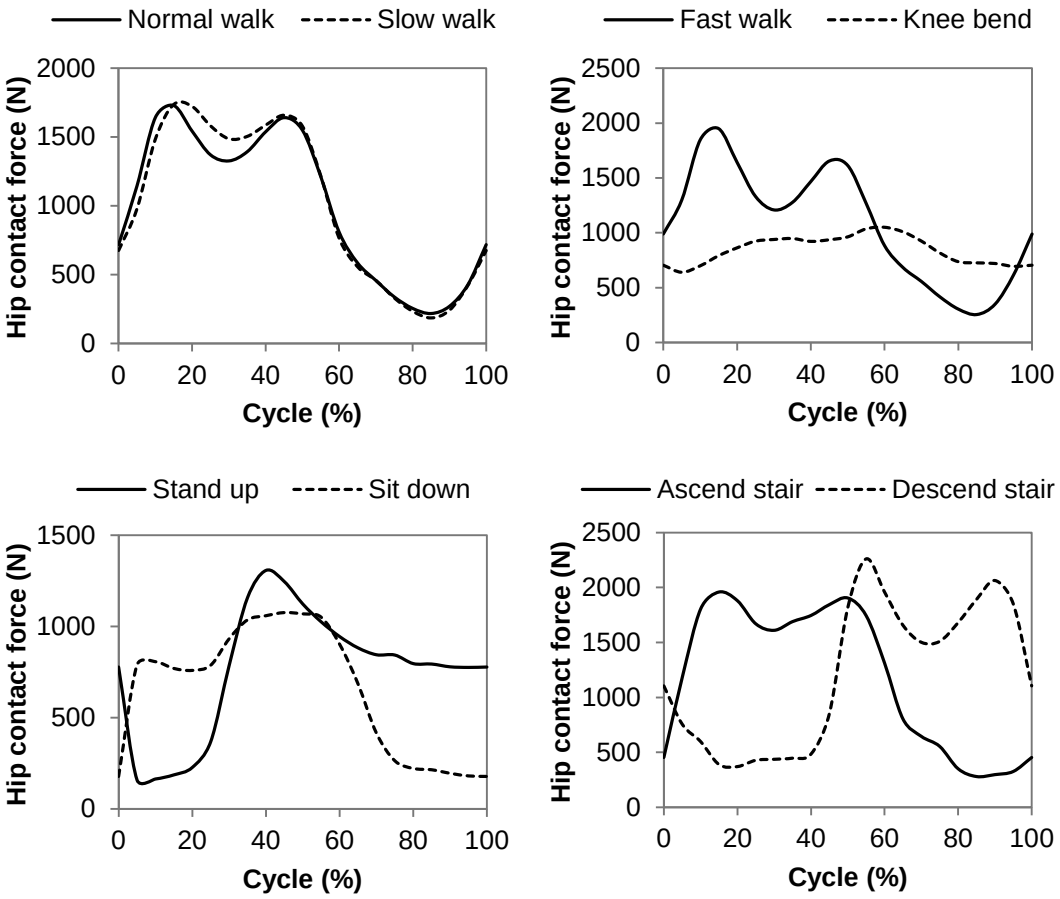

Figure 6.1 Hip contact forces during 8 different activities as model inputs (Bergmann et al., 2001). The magnitude of vectors is presented.

Each cycle of activities was represented by 40 time steps. The directions and magnitudes of the loads were varied to represent time steps through the loading cycle. The lengths of time steps were checked to ensure that the results were insensitive to shorter steps. The load was ramped over 0.2 s for all the activities. For the walking activities, 10 cycles were simulated to investigate the time dependent behaviour of the hip cartilage under dynamic loads, whilst for the other activities, only the 1st cycle was simulated due to the lengthy computational time required. All analyses were conducted using FEBio (version 1.5.0; Musculoskeletal Research Laboratories, Salt Lake City, UT, USA; URL: mrl.sci.utah.edu/software/febio). Fluid pressure, contact stress and fluid support ratio were recorded.

6.3 Results

The fluid pressure and contact stress distributions for all the eight activities for the time at which the peak value occurred are presented in in **Figure 6.2** and **Figure 6.3** respectively. In all the loading cases, the magnitudes and distributions of fluid pressure and contact stress on the acetabular cartilage surface were very similar. At the occurrence of peak contact stress, the location of contact on the acetabular cartilage varied among activities, ranging from the central region for walking, ascending and descending stairs to the posterior region for standing up, sitting down and knee bending.

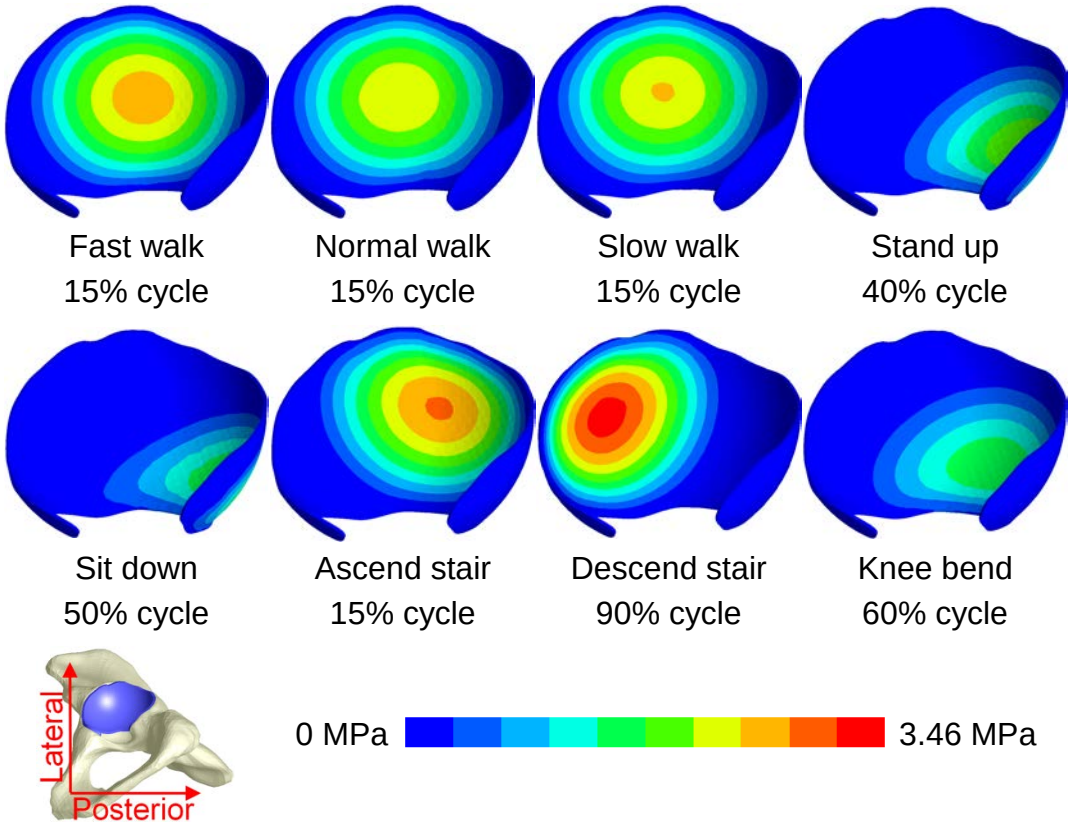

Figure 6.2 Contours of fluid pressure at % cycle when peak value occurred. For different activities, the locations of contact were different, ranging from the central region to the posterior region of the acetabular cartilage.

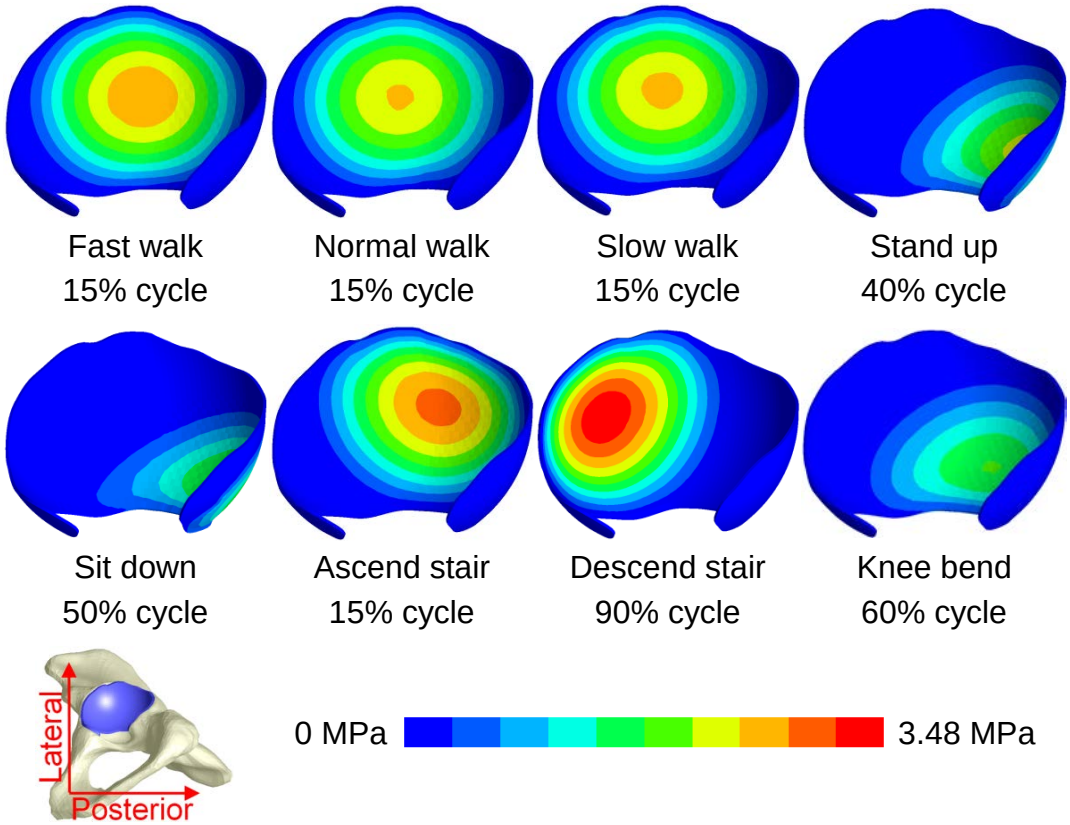

Figure 6.3 Contours of contact stress at % cycle when peak value occurred. The magnitudes and distributions of contact stress for different activities were similar to those of the fluid pressure on the acetabular cartilage surface.

The peak contact stress and fluid support ratio for each activity are presented in **Figure 6.4**. For all the activities, the peak contact stresses displayed similar trends to the load inputs (**Figure 6.1**), with the highest value of 3.5 MPa occurring during stair descend and the lowest value of 1.8 MPa during knee bending. The fluid support ratio was maintained at above 90% for the majority of the cycle for all the activities, but dropped below 90% at certain phases of the walking, standing up and sitting down cycles. During these periods of lower fluid load support ratio, the peak contact stresses were no more than 1 MPa.

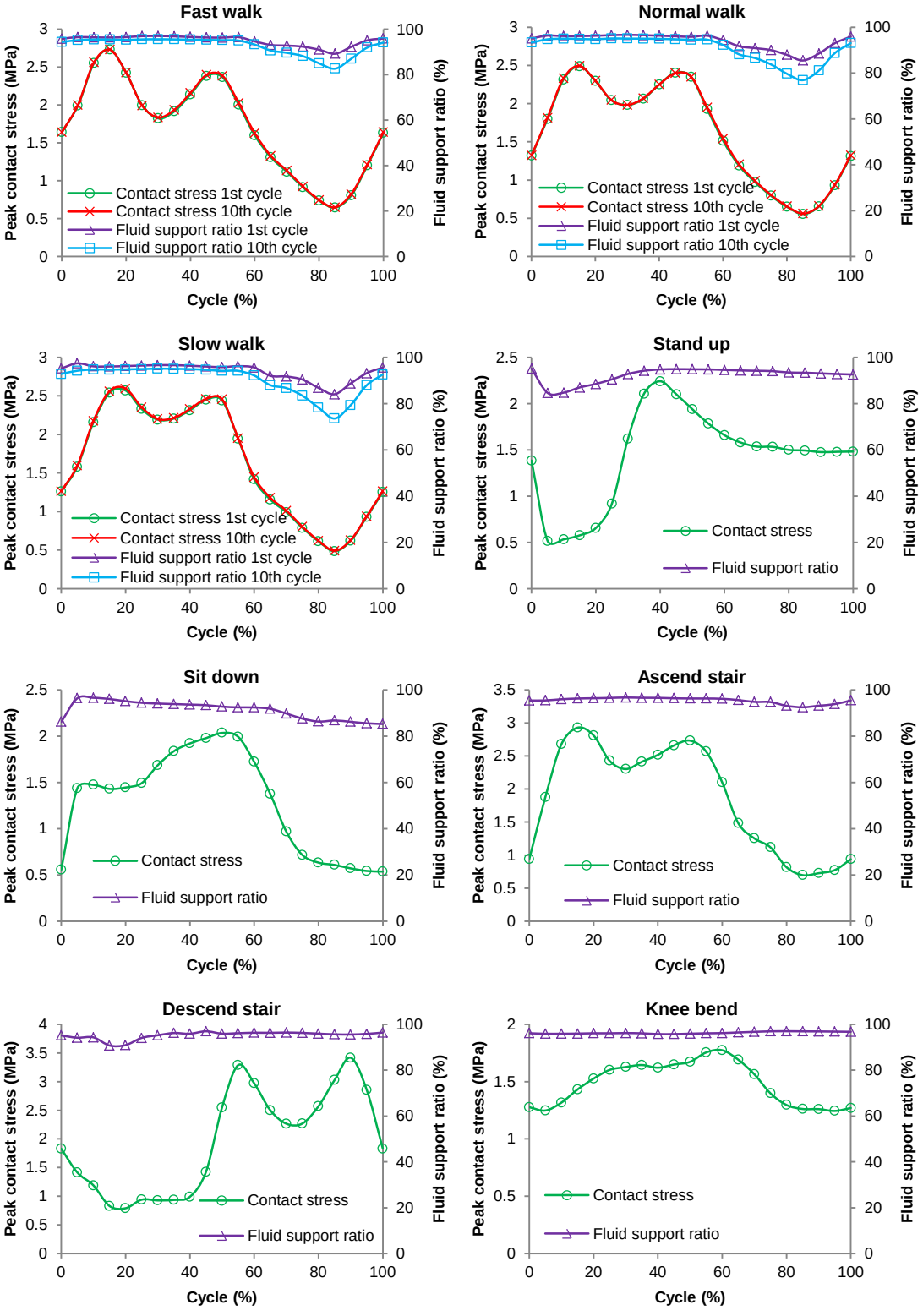

Figure 6.4 Peak contact stress and fluid support ratio of each cycle for all the activities. Results of 1st and 10th cycle of the walking activities were compared. For all the activities, the peak contact stress ranged from 1.8 MPa to 3.5 MPa. The fluid support ratio was over 90% for the majority of a cycle of each activity but decreased below 90% at certain phases for some activities. The time dependent behaviour of the joint cartilage over 10 cycles of gait was minimal.

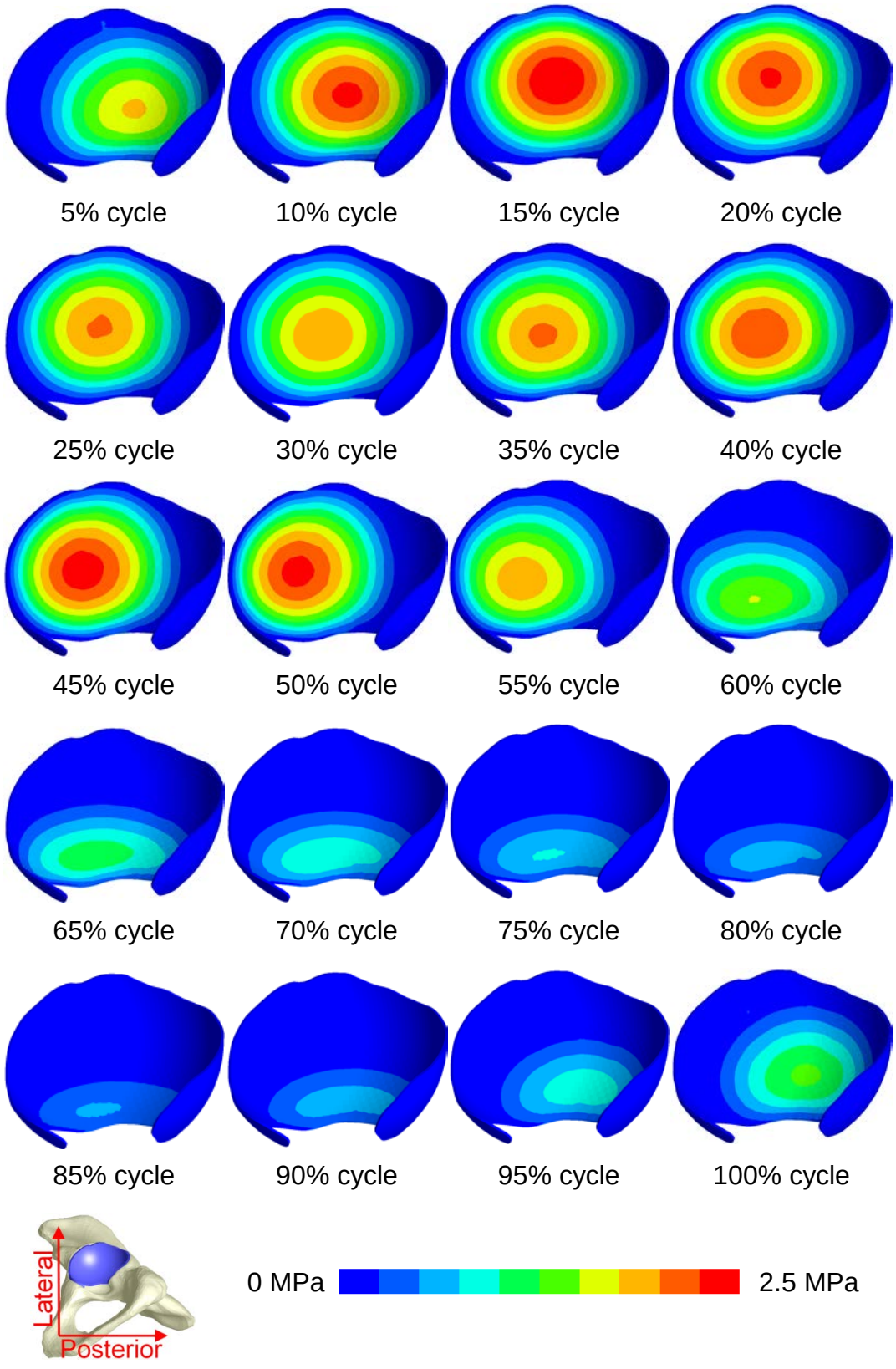

Figure 6.5 Contours of contact stress on the acetabular cartilage at different cycle phases of normal walk. Contact occurred around the central region during the majority of a cycle, and slid toward the interior edge area from around 70% to 90% cycle.

As an example to illustrate the relationship between the fluid support ratio and location of contact, the contact stress distribution at different phases of a cycle for normal walking is shown in **Figure 6.5**. The fluid support ratio was above 90% for the majority of a gait cycle when the contact region remained around the central area of the acetabular cartilage. However, it decreased markedly at around 85% of the cycle, when the minimum peak contact stress occurred and the contact region slid toward the interior edge of the acetabular cartilage. Similar patterns were found for other activities where the fluid support ratio decreased below 90% in that the contact occurred near the interior edge of the acetabular cartilage (**Figure 6.6**).

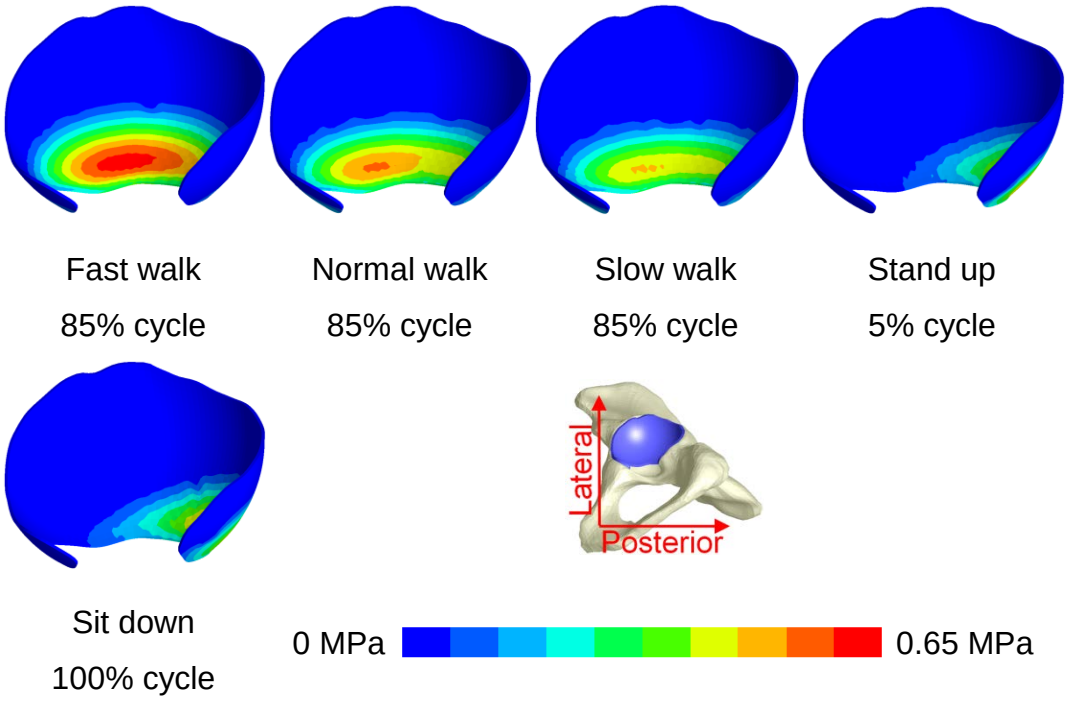

Figure 6.6 Contours of contact stress for activities when fluid support decreased below 90%. In all of such circumstances, the contact region was around the interior edge of the acetabular cartilage, and the stress level was low.

6.4 Discussion

This study is the first successful biphasic investigation of the whole hip joint under dynamic loads for different activities. The application of the biphasic cartilage properties enabled the investigation of the role that the interstitial fluid plays in the contact mechanic of the hip joint during daily activities. The predictions demonstrated that through pressurisation, fluid generally supported over 90% of the load transferred between the articulating surfaces of the hip joint for the daily activities investigated. Such high fluid support ratio would leave only a small portion load to the solid phase, warranting a low level of solid phase stress and friction coefficient that are essential for natural joint function (Forster and Fisher, 1996, McCann et al., 2009). However, at certain stages for several activities, the fluid support ratio decreased below 90% when the contact region slid toward the interior edge of the acetabular cartilage which is less confined than around the central region. This corresponds to previous studies which found that the fluid support ratio of the cartilage under unconfined compression is substantially lower than under confined compression (Park et al., 2003, Ateshian and Hung, 2006). It can be concluded that the stress level of the solid matrix in the hip cartilage is linked with not only the magnitude but also location the contact stress. For the activities investigated in this study, the decrease of fluid support ratio led to an increased proportion of stress for the solid phase around the interior edge region of the acetabular cartilage, but the absolute magnitudes of the contact stress were very low (< 1 MPa) at these stages, therefore potentially not harmful.

Due to the high computational expense involved in the simulation of biphasic materials, only 10 cycles of gait were investigated to present an initial insight into the time dependent behaviour of the hip joint under dynamic loads. Over these 10 cycles, both the peak fluid pressure and contact stress remained nearly constant, suggesting that there was almost no variation in the fluid support ratio around the central region where peak fluid pressure / contact stress occurred. The fluid support ratio across the whole articulating surface decreased slightly, particularly when contact occurred around the interior edge of the acetabular cartilage. This is because the edge surface of the

acetabular cartilage was free-draining, facilitating a substantially faster process of fluid exudation for the region nearby as compared with the central region of the acetabular cartilage. The faster fluid exudation process of the edge region may also contribute to the variation in the fluid support ratio across the whole articulating surface. This is supported by the findings in this chapter where the variation in the fluid support ratio of the model was faster under the gait loads investigated here than under the static load in **Chapter 5**, which confined the contact stress within the central region of the acetabular cartilage.

Besides the challenge of applying high static loads over a prolonged period to the biphasic whole joint as mentioned in **Chapter 5**, it is also difficult to apply dynamic loads (e.g. daily activities) which involve consecutively sudden spatial and temporal variations to such models (Pawaskar, 2010). Although the natural joint model simulated in FEBio shows good convergence ability, as compared with elastic or hyperelastic whole joint models, greater effort on meshing is needed to ensure good element quality in order to enable the biphasic model to converge to a solution.

Although the modelling technique presented here represents an important step forward for whole joint investigations, there are several limitations. Similar to **Chapter 5**, the solid matrix was assumed to be homogeneous isotropic elastic which may not fully represent the inhomogeneous fiber-reinforced structure of the cartilage (Mow et al., 1980, Soulhat et al., 1999, Ateshian et al., 2009). Due to such assumption, the peak fluid pressure, peak contact stress and fluid support ratio may be potentially underestimated. In particular, the level of reduction in fluid support ratio for the edge region of the acetabular cartilage may be overestimated.

As proposed in **Chapter 5**, another potential limitation is the idealized generic geometry of the model, which has been shown to reduce the peak contact stress in an elastic FE model (Anderson et al., 2010). In this study, the peak contact stress was 2.5 MPa to 3.5 MPa for a load of approximate 2000 N, which is lower than previous experimental studies (Afoke et al., 1987, Anderson et al., 2008, Brown and Shaw, 1983, von Eisenhart et al., 1999). As discussed in **Chapter 5**, the higher values of such measurements

may be caused by the measurement artefacts that arise from the highly conforming surfaces, but also by the idealized morphology and isotropic material assumptions used in this study. For the purpose of this study, such assumptions were appropriate in order to compare hip performance among different activities and gain insight into the role of fluid pressurisation on the function of a generic hip joint.

As mentioned in **Chapter 5**, labrum exclusion was assumed in the present model. The labrum is believed to have little assistance in load supporting (Henak et al., 2011), but help impede fluid exudation through its lower permeability than the cartilage (Ferguson et al., 2000a, Ferguson et al., 2000b, Ferguson et al., 2003, Haemer et al., 2012). However, the lack of labrum may not significantly affect the predictions in this study, because a very short loading period was simulated and the time dependent behaviour of the hip cartilage was dominated by the interior edge region.

The load applied to the model is based on the measured hip forces of patients who had THR surgeries and may exhibit different pattern from healthy people during daily activities according to the findings in **Chapter 3**. To the authors' knowledge, there appear no studies on hip contact forces of different activities for a healthy person as yet. To alleviate this limitation, a THR patient was selected who had a more dynamic gait pattern which behaves more similar to that of healthy people, as compared with other THR patients in the database provided by Bergmann et al. (2001). In the following chapter, this aspect was further investigated by incorporating subject-specific gait loadings.

In conclusion, a generic human hip joint model was investigated in terms of its contact mechanics and associated fluid pressurisation during daily activities. The model exhibits good convergence ability dealing with high dynamic loads which involve consecutively sudden spatial and temporal variations. Although several assumptions were made, the predictions provide insight into how the fluid pressurisation assists in hip function during daily activities. For all the daily activities, the fluid supports most of the load transmitted between articulating surfaces of the hip joint, thus playing an essential role in the lifetime survival of natural hip joints. A decreased level in

fluid support ratio and a faster process of fluid exudation were observed for the interior edge region of the acetabular cartilage.

The model developed in this chapter can be used to study a range of activities. In the following chapter, it will be employed to investigate subject-specific gait.

Chapter 7
Combination of Hip Biomechanics and Biotribology for Evaluation of Different Patient Cohorts

7.1 Introduction

The purpose of THR is to relieve pain of patients with hip trauma or disease and to restore normal postoperative activity patterns, the latter of which is difficult in practice. For example, the cohort studies in **Chapter 3** have demonstrated that gait patterns of THR patients, even years after THR surgery, generally cannot return to a level equivalent to normal healthy individuals, and exhibit a decreased range of motion and contact forces in the hip. These alterations are more evident for THR patients with symptoms of LLI. In addition, gait adaptions were also noticeable for the non-operated joint of the unilateral THR / LLI patients. However, to what extent these adaptions alter the contact mechanics of the non-operated hip and whether the non-operated hip functions in a mechanically adverse environment remain, as yet, unknown. Solving these questions is important in providing better patient care, pre-operative planning and rehabilitation strategies to prevent the healthy hip of unilateral THR patients from degeneration.

The aim of this study was to investigate the differences in contact mechanics, particularly focusing on the fluid pressurisation, for different patient groups. The cases studied were the non-operated hips of asymptomatic unilateral THR patients and symptomatic unilateral LLI patients, as well as the hip joints of their normal healthy counterparts, in order to evaluate whether the these differences have a mechanically adverse influence on the non-operated hip of THR / LLI patients.

7.2 Methods

The FE model used in this study was similar to the one described in **Chapter 5**. The geometric parameters and material properties of the natural hip model were based on the original model in **Chapter 5**. The mean hip contact forces calculated in **Chapter 3** for the normal healthy cohort ('Normal'), the non-operated limb of the asymptomatic unilateral THR patients ('THR-NO') and the non-operated limb of unilateral THR patients with symptoms of LLI ('LLI-NO') were normalized to a person of 75 kg by normalizing to BW and then scaling to an average human weight of 75 kg to offset the weight differences between the three cohorts. This data was then used as inputs for the generic human hip model (**Figure 7.1**). The coordinate system for the hip contact forces was based on the pelvis.

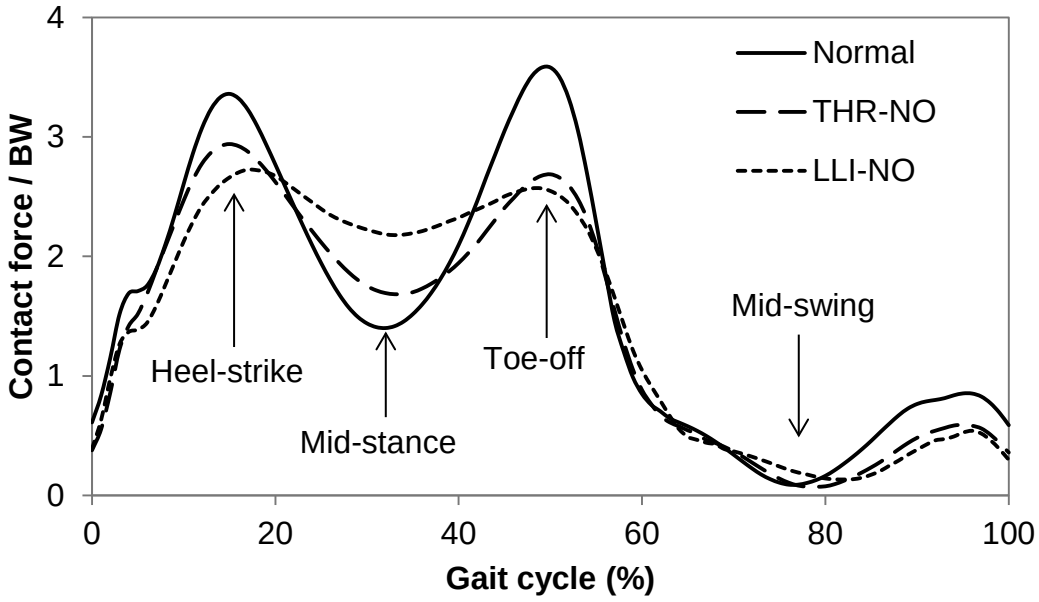

Figure 7.1 Mean hip contact forces for the normal healthy people, asymptomatic THR patients and symptomatic LLI patients on their non-operated limbs, as model inputs. The magnitude of vectors is presented.

The boundary conditions of the joint model and the way the dynamic loads were applied were described in **Chapter 6.** FE analyses were conducted for 10 gait cycles of each cohort using FEBio (version 1.5.0; Musculoskeletal Research Laboratories, Salt Lake City, UT, USA; URL: mrl.sci.utah.edu/software/febio). Contact stress, fluid pressure and fluid support ratio were recorded and cross-compared to evaluate the differences in load transmission and tribological performance between the three cohorts.

7.3 Results

For all the cohorts, the fluid pressure and contact stress had a similar magnitude and distribution on the acetabular cartilage surface. The contact stress distribution at different stages of gait is shown in **Figure 7.2**. During most of a gait cycle from heel-strike to toe-off, the contact generally occurred within the central region of the acetabular cartilage surface for all the cohorts. The contact at the mid-swing of the gait cycle was minimal. The location of contact at each phase of the gait cycle was generally similar for all the three cohorts.

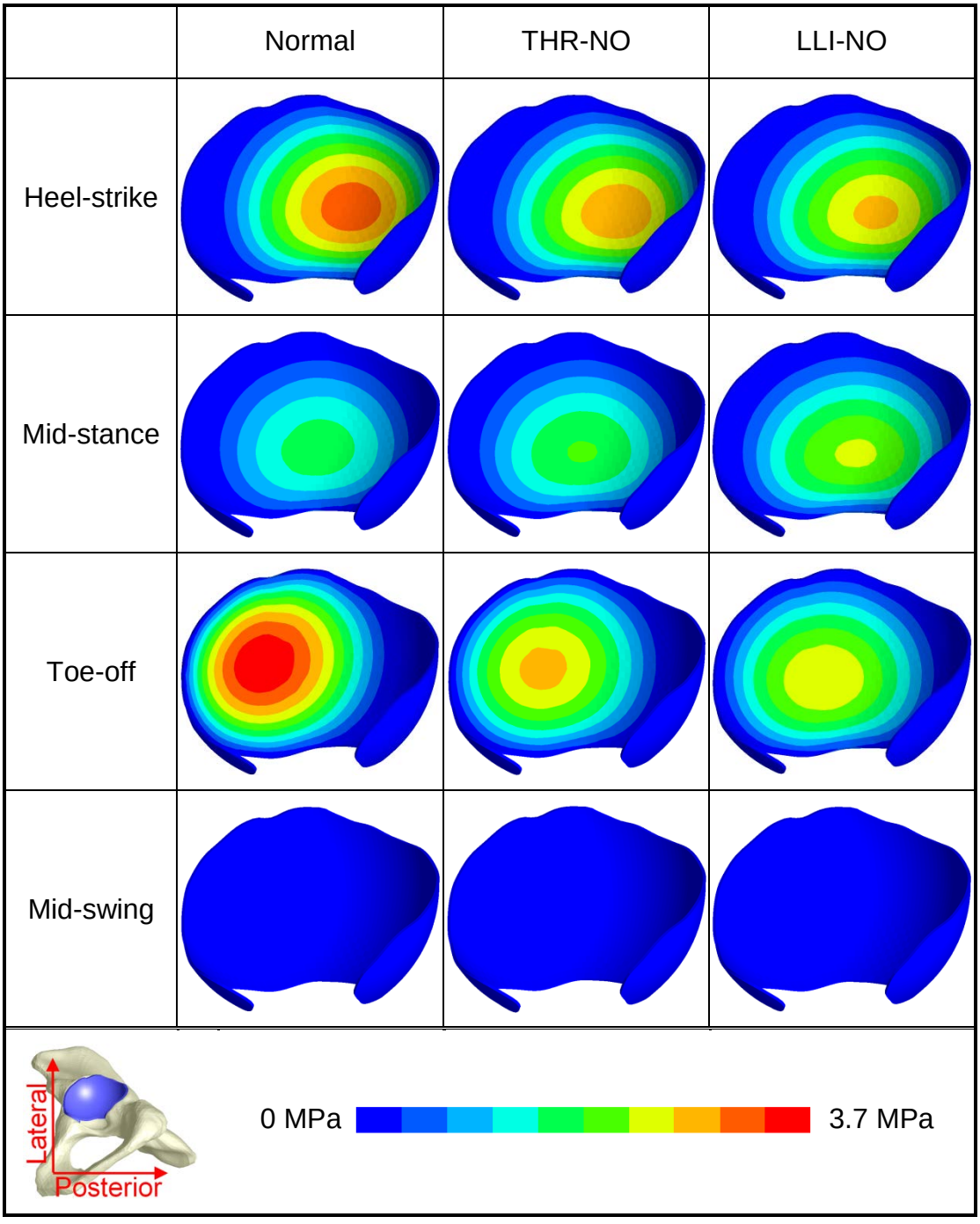

Figure 7.2 Contours of contact stress (MPa) at different phases of gait for the normal healthy cohort, the THR and LLI cohorts in terms of their non-operated hips.

The peak fluid pressure, peak contact stress and fluid support ratio for the three cohorts during the 1st gait cycle are displayed in **Figure 7.3**. The peak contact stress and peak fluid pressure were nearly identical with a similar pattern to the hip contact forces (**Figure 7.1**). Characteristic twin peaks of the maximum contact stress / fluid pressure were found for the healthy cohort and the non-operated limbs of the asymptomatic THR cohort. In terms of the peak contact stress of the three cohorts, the healthy group had the most dynamic pattern (from the 1st peak to the trough to the 2nd peak), while the least dynamic pattern was found for the non-operated limbs of the LLI patients.

During most of the gait cycle, the fluid support ratio was similar for the three cohorts and was over 90%. However, during the swing phase at 75%-85% of a cycle, the fluid support ratio decreased below 90%. At this time, the peak contact stress was minimal (< 0.5 MPa) and slid toward the interior edge region of the acetabular cartilage (**Figure 7.4**). As compared with the other two cohorts, the fluid support ratio of the non-operated limbs of the asymptomatic THR patients decreased more markedly during swing phase.

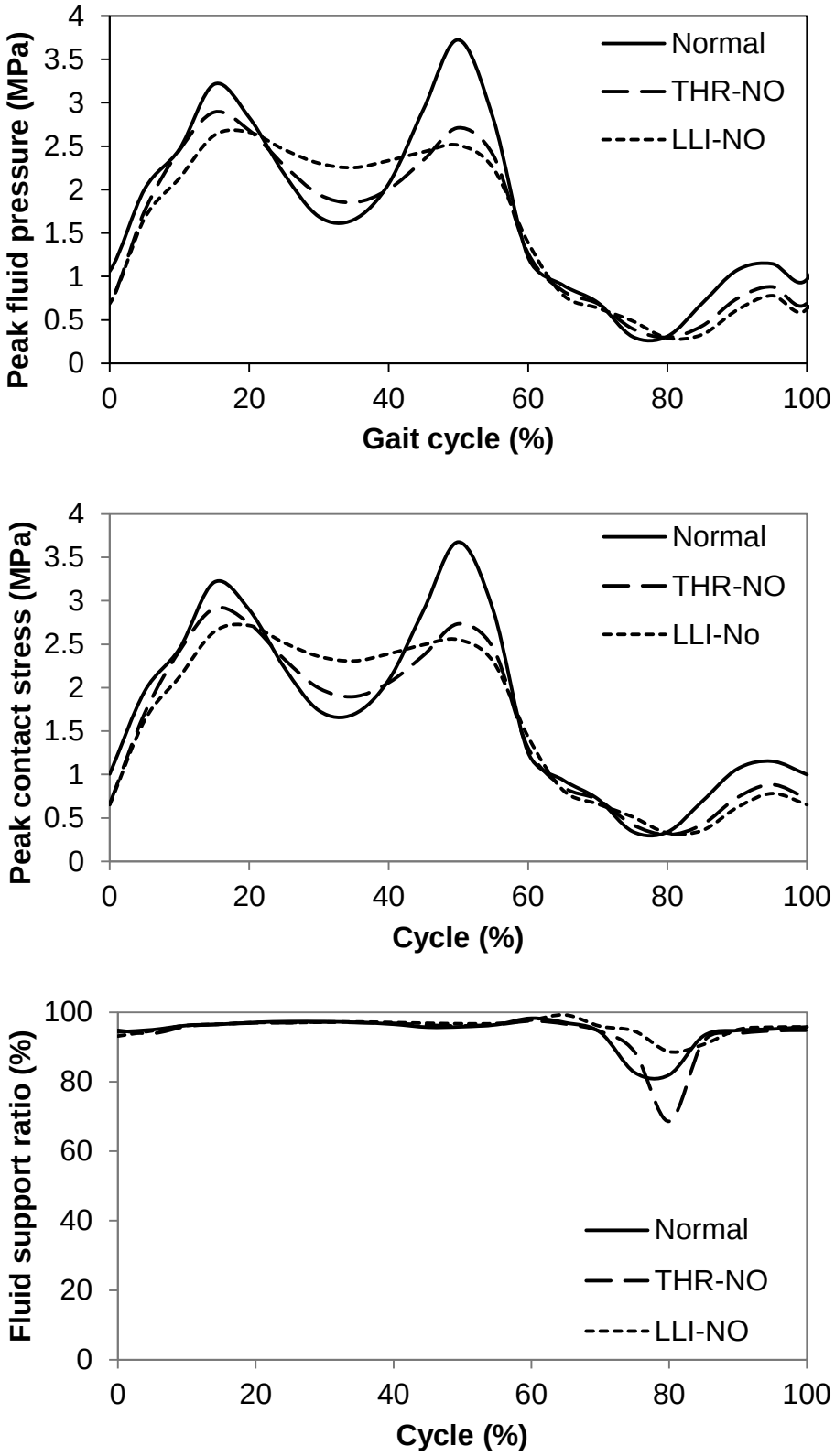

Figure 7.3 Peak contact stress for the normal healthy cohort, non-operated side of the THR and LLI cohorts. The peak contact stress for the THR and LLI cohorts was lower and less dynamic than the normal healthy people.

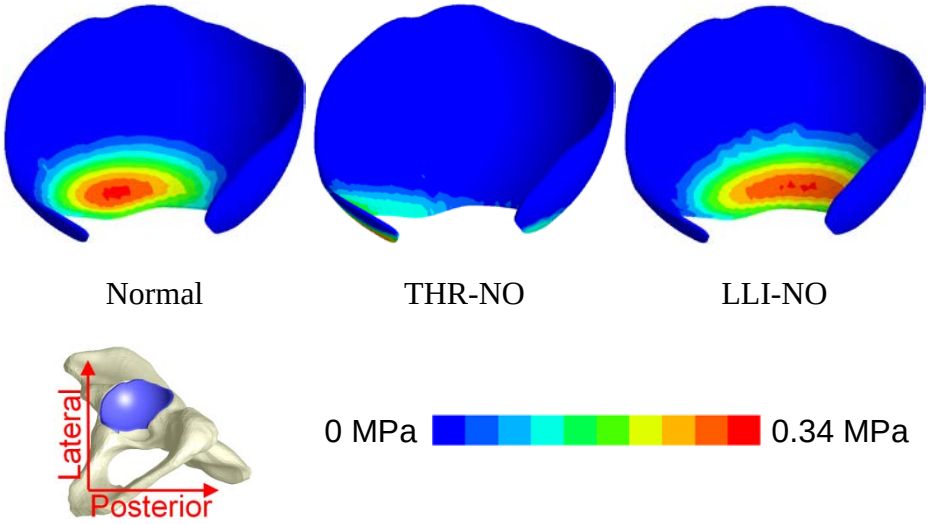

Figure 7.4 Contours of contact stress at mid-swing phase of a gait cycle for the three cohorts when fluid support decreased below 90%. The contact occurred around the interior edge of the acetabular cartilage, and the level of stress was minimal.

Over 10 cycles of gait, the variations in the peak fluid pressure, peak contact stress, and fluid support ratio for the three cohorts are shown in **Figure 7.5**, **Figure 7.6** and **Figure 7.7**. For all the cohorts, there were almost no variations in the peak fluid pressure and peak contact stress. However, an obvious decrease in fluid support ratio was detected, particularly during swing phase for the latter 40% of each cycle. This decrease in the fluid support ratio during swing phase was most marked for the non-operated limbs of the asymptomatic THR patients, as compared with the other two cohorts.

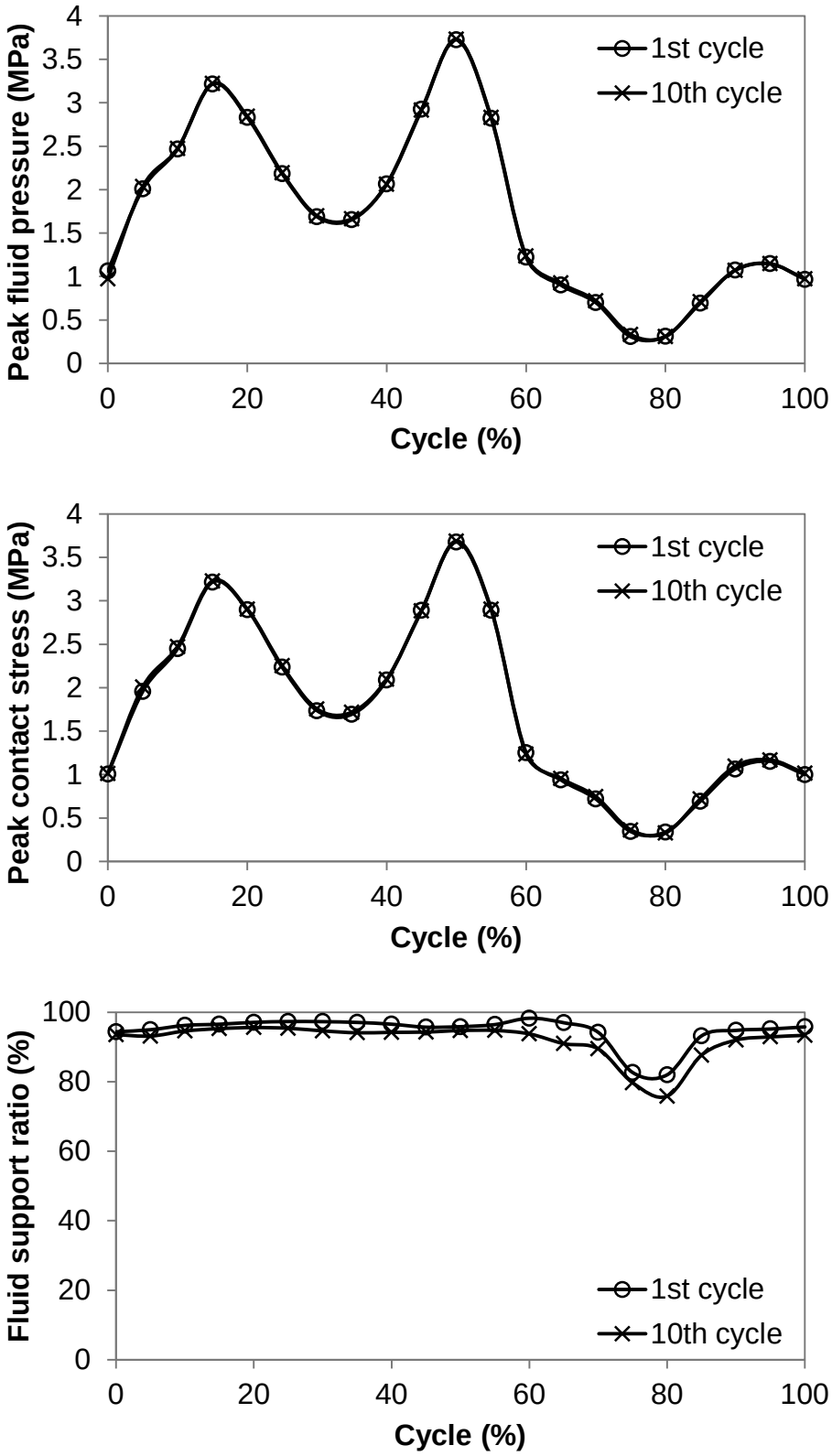

Figure 7.5 Variations in the peak fluid pressure, peak contact stress and fluid support ratio over 10 cycles of gait for the normal healthy people.

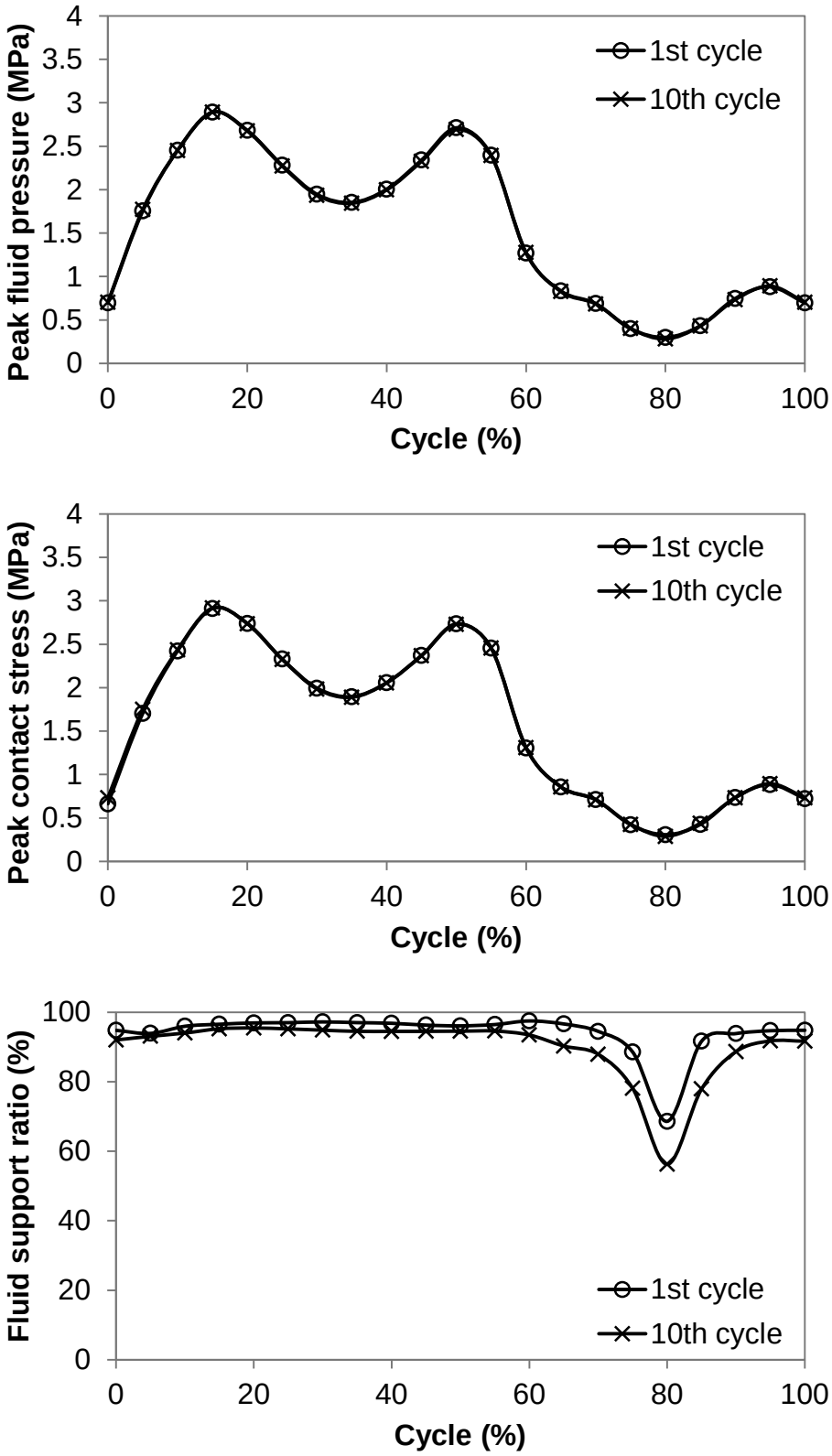

Figure 7.6 Variations in the peak fluid pressure, peak contact stress and fluid support ratio over 10 cycles of gait for the non-operated hip of the asymptomatic THR patients.

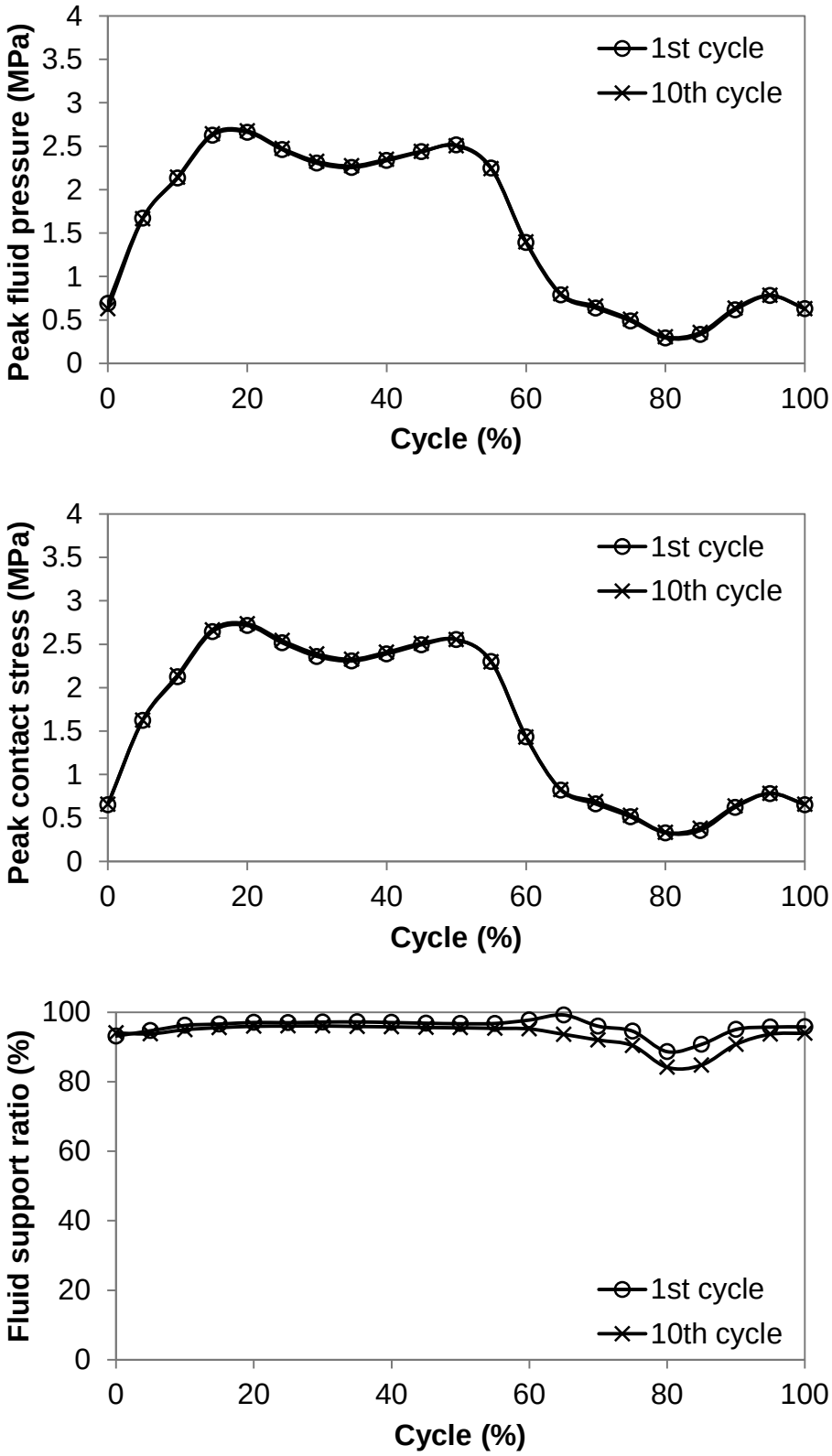

Figure 7.7 Variations in the peak fluid pressure, peak contact stress and fluid support ratio over 10 cycles for the non-operated hip of the symptomatic LLI patients.

7.4 Discussion

In **Chapter 3**, it was demonstrated that hip kinematics and kinetics of the asymptomatic THR patients and the THR patients with symptoms of LLI do not return to those of their normal healthy counterparts even years after THR surgery, and these alterations can also been found in their non-operated hips. To further evaluate whether these abnormalities in the hip contact forces lead to abnormal contact patterns within the non-operated hip joint of the THR / LLI patients, a combination of RBD musculoskeletal modelling and biphasic FE modelling were used in this study. Such a combination enables a systematic and non-invasive investigation of joint contact mechanics directly from gait kinematic measurement, and thus can be applied to evaluate a wide range of clinical issues. Furthermore, the incorporation of biphasic cartilage layers in the FE model allows the consideration of fluid pressurisation in the cartilage, providing more information that is closely linked with joint function and degeneration.

Compared with the normal healthy individuals, the asymptomatic THR patients were found to have a markedly reduced and less dynamic peak contact stress and peak fluid pressure on their non-operated hips. These alterations were more evident for the LLI patients. For the three cohorts, the fluid support ratio within the hip was similar and above 90% when major contact occurred, which, along with the decreased peak contact stress for the THR / LLI patients, suggests that the level of stress transmitted to the solid matrix in the cartilage was reduced on the non-operated hips for the THR / LLI patients. Additionally, the lower levels of stress shared by the solid phase may potentially lead to a lower friction coefficient and shear stress between articulating surfaces in the non-operated hip for the THR / LLI patients during gait. Consequently, it can be inferred from these findings that the abnormal contact mechanics may not lead to a mechanically adverse environment for the non-operated hip of the asymptomatic THR patients and symptomatic LLI patients during gait.

Similar to the findings for the walking activities in **Chapter 6**, the contact region slid toward the interior edge of the acetabular cartilage during swing phase for the three cohorts, and at this time, the fluid support ratio was

obviously reduced. Over 10 cycles of gait, the peak contact stress and peak fluid support ratio remained nearly constant, suggesting that there was also no variation in the fluid support ratio around the central region where the major contact occurred. Yet, the fluid support ratio decreased noticeably, particularly during swing phase. However, the decreased magnitude and faster reduction in the fluid support ratio around the interior edge of the acetabular cartilage during swing phase may not have an adverse influence on the cartilage function within the hip, due to the minimal peak contact stress at this period for all the three cohorts. This further demonstrates that the non-operated hips of the asymptomatic THR patients and symptomatic LLI patients may not function in a mechanically adverse environment during the whole cycle of gait.

However, it should be emphasised that the findings of this study demonstrated a mechanically safe circumstance for the non-operated joint of unilateral THR / LLI patients only in the case of walking. For other activities, high levels of stresses may still exist for the non-operated joint of THR patients. It was not possible to investigate these activities here because only walking data was collected for the THR and LLI patients. Many studies argued that the properties and strength of cartilage tend to adapt to the regular level of stresses (Arokoski et al., 1999, Eggli et al., 1988, Kiviranta et al., 1987, Arokoski et al., 2000), and the cartilage degeneration usually occurs in areas of infrequent but excessive stresses (Swann and Seedhom, 1993). In the light of these theories, the cartilage of the non-operated joint of THR / LLI patients may be adapted to their reduced stress level during gait which is the most common activity, and thus may be more vulnerable to high levels of stress possibly existing during other activities (e.g. stumbling). To better evaluate such risks, further investigations involving a comprehensive range of activities are necessary.

Previous investigations on the contact mechanics of the healthy hip joint under activity loadings generally adopted *in vivo* measured kinetics of THR patients as the loading inputs (Yoshida et al., 2006, Pawaskar et al., 2010, Anderson et al., 2008, Harris et al., 2012). However, as demonstrated in this study, the contact mechanics varied markedly among different cohorts of people due to the alterations in their hip contact forces, suggesting that it is

necessary to adopt the loading conditions of the model on a subject-specific or cohort-specific level.

Comparison between the results predicted by this study and previous studies is difficult because it appears that no previous studies have measured the *in vivo* contact mechanics for natural healthy hips or numerically adopted hip contact forces of natural healthy hips as model inputs. As evaluated in **Chapter 3** and **Chapter 6**, although the predictions of both the musculoskeletal model and hip model were reliable**,** the accuracy of the predictions for each cohort investigated may be influenced by the model simplifications such as the muscle recruitment assumption, adoption of isotropic solid phase for the cartilage and simplified joint model geometry. However, for the purpose of this study, such simplifications were appropriate in order to compare hip performance among different cohorts and gain an understanding of the differences in contact mechanics and the associated fluid pressurisation in the non-operated hips of the THR / LLI patients as compared with their healthy counterparts. Again, for subject-specific studies, it is necessary to develop FE models with anatomical geometric parameters.

In this study, the RBD musculoskeletal model and the FE model were combined in an uncoupled way without accounting for their interactions in which the time dependent deformation of the FE model may both alter and be affected by the kinetics predictions of the musculoskeletal model. However, due to the high stiffness of human bones and the thin layer of articular cartilage, the deformations of these two models should be too minimal in the scale of the whole length of human lower extremity to cause a marked difference in the results. More importantly, the computational cost for a FE simulation involving biphasic materials are too high to allow the numerical iterations that are required to account for the interactions between these two domains. Although it would be possible to realize the whole simulation that includes both the joint force predictions and cartilage contact mechanics solely through a FE model, the lack of a FE based musculoskeletal model with anatomical information, as well as the high computational costs for musculoskeletal model optimizations (e.g. muscle parameters and kinematics) still remain as major challenges.

To conclude, the combination of a RBD musculoskeletal model and a FE hip model with biphasic cartilage layers enabled the prediction of contact mechanics and the associated fluid pressurisation within the hip joints of the normal healthy people and the non-operated limb of the asymptomatic THR patients and symptomatic LLI patients. The abnormal gait kinetics of the THR / LLI patients was found to lead to a resultant reduction and less dynamic pattern in the peak contact stress and fluid pressure on their non-operated hips. The fluid support ratio was similar and decreased very slowly for the three cohorts when the major contact occurred between the articulating surfaces of the hip. These findings demonstrated that the non-operated limb of the THR / LLI patients may not function in a mechanically adverse environment during gait. The findings are important to assist and improve patient care and rehabilitation strategies.

Chapter 8
Validation of a Porcine Hip of Hemiarthroplasty

8.1 Introduction

In **Chapters 4**, **5**, **6**, and **7**, a new method of biphasic cartilage modelling was developed using FEBio (Musculoskeletal Research Laboratories, Salt Lake City, UT, USA; URL: mrl.sci.utah.edu/software/febio) in order to overcome convergence issues that are commonly reported in previous studies (Pawaskar et al., 2010, Pawaskar et al., 2011, Gu and Li, 2011). Using this method, the biphasic cartilage layer was successfully applied to a three dimensional generic human hip joint under both physiological dynamic loads and over a prolonged loading period.

In **Chapter 4**, this methodology of biphasic cartilage simulation was verified and initially validated against the results in a previous study (Pawaskar, 2010) using indentation models. Similar results were achieved, which demonstrated the accuracy of the methodology developed. However, for the application of such a biphasic modelling approach to the hip joint, which has a more complicated configuration than the indentation models, direct validation against experimental measurements is still needed to evaluate the accuracy of the biphasic joint modelling strategy.

As found in **Chapter 5**, the cartilage thickness and hip congruence had a great influence on the predictions of the hip model, and therefore, it is necessary to take into account these geometric parameters on a subject-specific level to direct validate the FE model against experiments. Besides, the role of the tension-compression nonlinear solid phase that plays in the model predictions was not quantified in the previous chapters, although the importance of such constitutive relationship was believed by several previous studies to be able to capture the mechanical performance of the tissue more realistically, as compared with the isotropic one (Soltz and Ateshian, 2000, Cohen et al., 1993, Cohen et al., 1998).

The primary aim of this study was therefore to develop a subject-specific biphasic FE model of a porcine hip with hemiarthroplasty and validate the predictions of the model against experimental measurements. The importance of the tension-compression nonlinear solid phase within the model was also evaluated.

8.2 Methods

8.2.1 Experimental measurement of CT images and contact area

The experimental work of contact area measurement described in this section was undertaken by Dr Qianqian Wang as part of a parallel laboratory investigation.

The acetabulum from a 3 year old pig was used in this study. All soft tissues except for the labrum and cartilage were removed. The acetabulum was hydrated and volumetrically scanned using a micro computed tomography (μCT) scanner (μCT 80, SCANCO Medical AG, Brüttisellen, Switzerland) at a cubic voxel size of 73.6 μm and energy of 70 kV, 114 μA.

After the scanning, the contact area of the cartilage was measured. Briefly, the acetabulum was fixed in a cup holder with cement. The cup holder was constrained on an X-Y table so that it was fixed along vertical translation without rotation (**Figure 8.1**). The acetabulum was then compressed sequentially with two spherical impermeable prosthetic metal heads of diameters 37 mm and 40 mm. The metal head was only allowed to move along vertical translation. In both cases, a set of compressive loads of 50 N, 100 N, 200 N and 400 N ramped up in 10 s were applied to the femoral head. Before each load, the metal head was painted using a fluid gel that would stain the cartilage on contact (101RF, Microset Products Ltd, UK). Two marks were made on both the cup holder and cement to ensure the same orientation for each measurement. After each measurement, the image was captured by a digital camera (**Figure 8.2**).

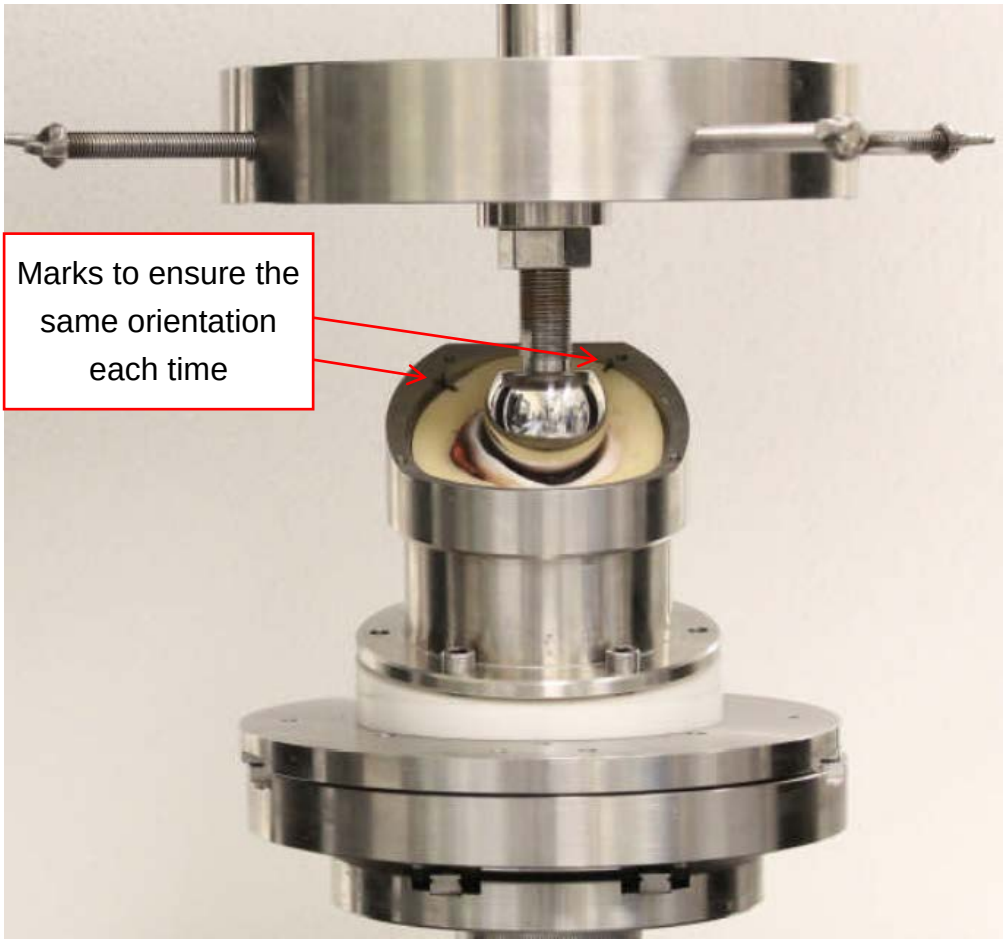

Figure 8.1 Experimental setups. The acetabulum was held in a cup holder which can move horizontally. The load was applied vertically to the head.

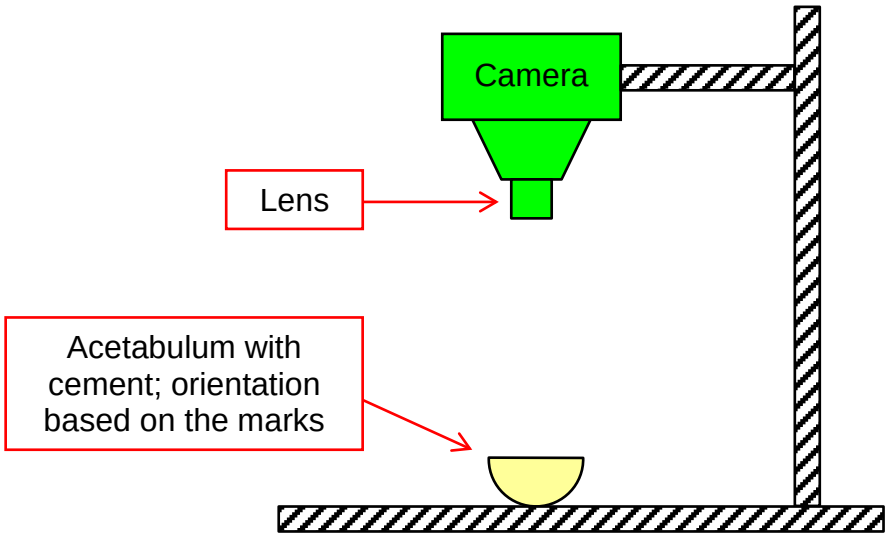

Figure 8.2 Imaging after each measurement. The acetabulum with cement was positioned based on the marks to achieve the same orientation each time.

8.2.2 Solid model construction

The FE model was constructed from the µCT scan using the steps outlined in **Figure 8.3**.

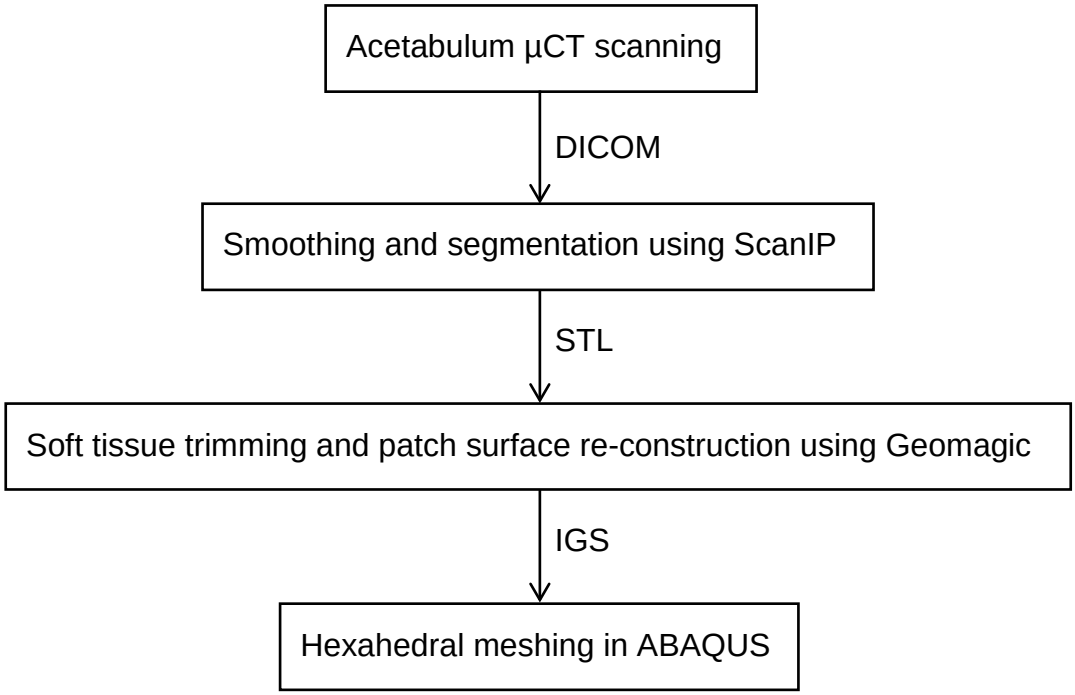

Figure 8.3 Flowchart for constructing the FE model from the µCT scan.

The volumetric CT data in DICOM format derived from the scanning were imported into an image processing and meshing software package (ScanIP version 5.1; Simpleware Ltd., Exeter UK) for segmentation and smoothing. The bone and the whole acetabulum including both the bone and soft tissues were identified sequentially by greyscale thresholding. The surface of the bone model and the whole acetabular model were meshed with 3-noded triangular elements, exported in STL format, and then loaded into another surface-generation software package (Geomagic Studio 11, Geomagic Inc., Research Triangle Park, NC, USA). Boolean algorithms were performed to exclude the bone model from the whole acetabular model that included both the bone and soft tissues in order to obtain a model representing just the soft tissue. Because regions of different soft tissues could not be distinguished automatically from the scanned image (**Figure 8.4**), all soft tissues with the

exception of the cartilage were excluded manually based on the margin of the bone cavity of the acetabulum (**Figure 8.5**).

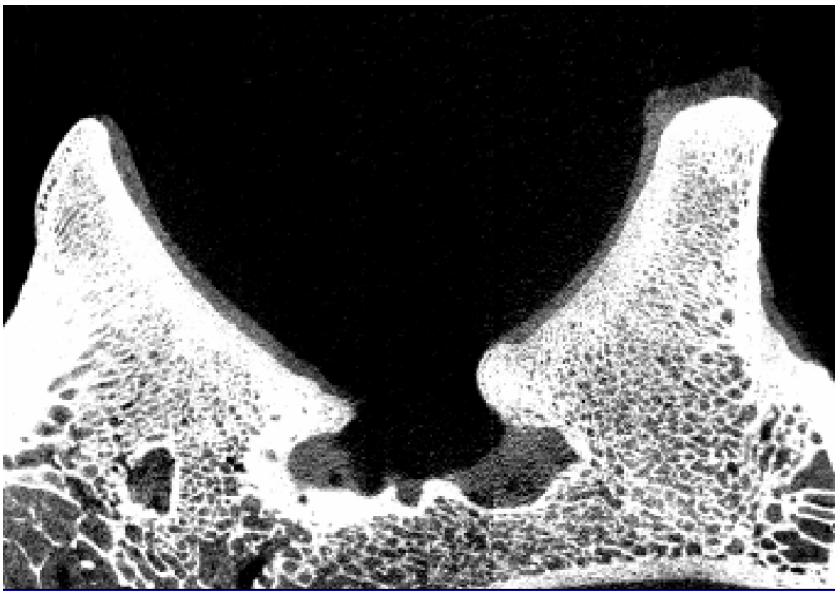

Figure 8.4 A typical CT slice. The junction of the soft tissue and bone was obvious. The boundaries of the cartilage, labrum and other soft tissues had similar brightness and thus cannot be distinguished automatically.

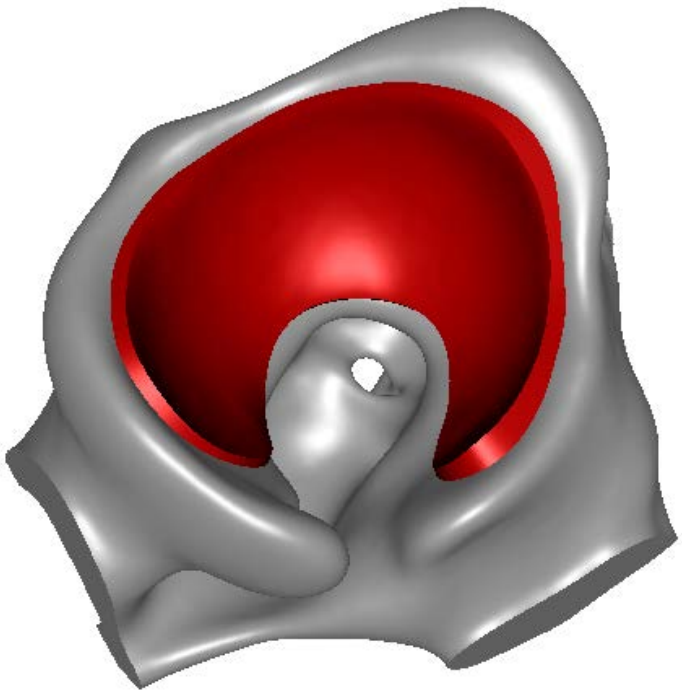

Figure 8.5 The three dimensional solid model constructed in Geomagic. Soft tissues with the exception of the cartilage were excluded.

8.2.3 Finite element mesh

The cartilage surfaces were reconstructed from tens of thousands of triangles into several patches to form a solid model which was then imported into ABAQUS (version 6.11-1, Dassault Systemes, Suresnes Cedex, France) for meshing. The FE model of the cartilage was composed of 9906 eight-noded hexahedral elements. The prosthesis heads used in the experiment were represented by two spheres with a diameter of 37 mm and 40 mm respectively (**Figure 8.6**). The spherical head was composed of 7800 eight-noded hexahedral elements. The bone was assumed to be rigid and therefore was not included in the FE model. Mesh sensitivity studies were performed to ensure that the predictions were insensitive to a higher mesh density (**Figure 8.7**).

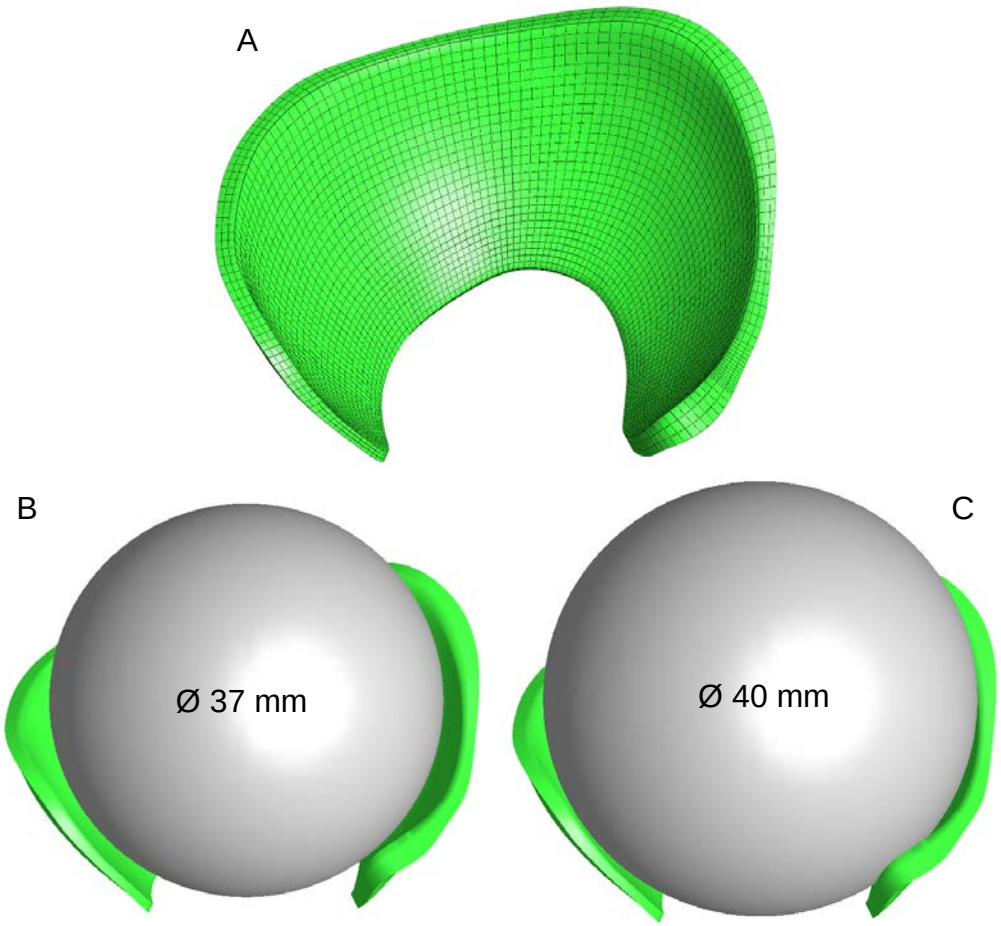

Figure 8.6 FE model creation. A – The cartilage represented by hexahedral elements. B and C – FE models of hemiarthroplasty with heads of two different dimensions.

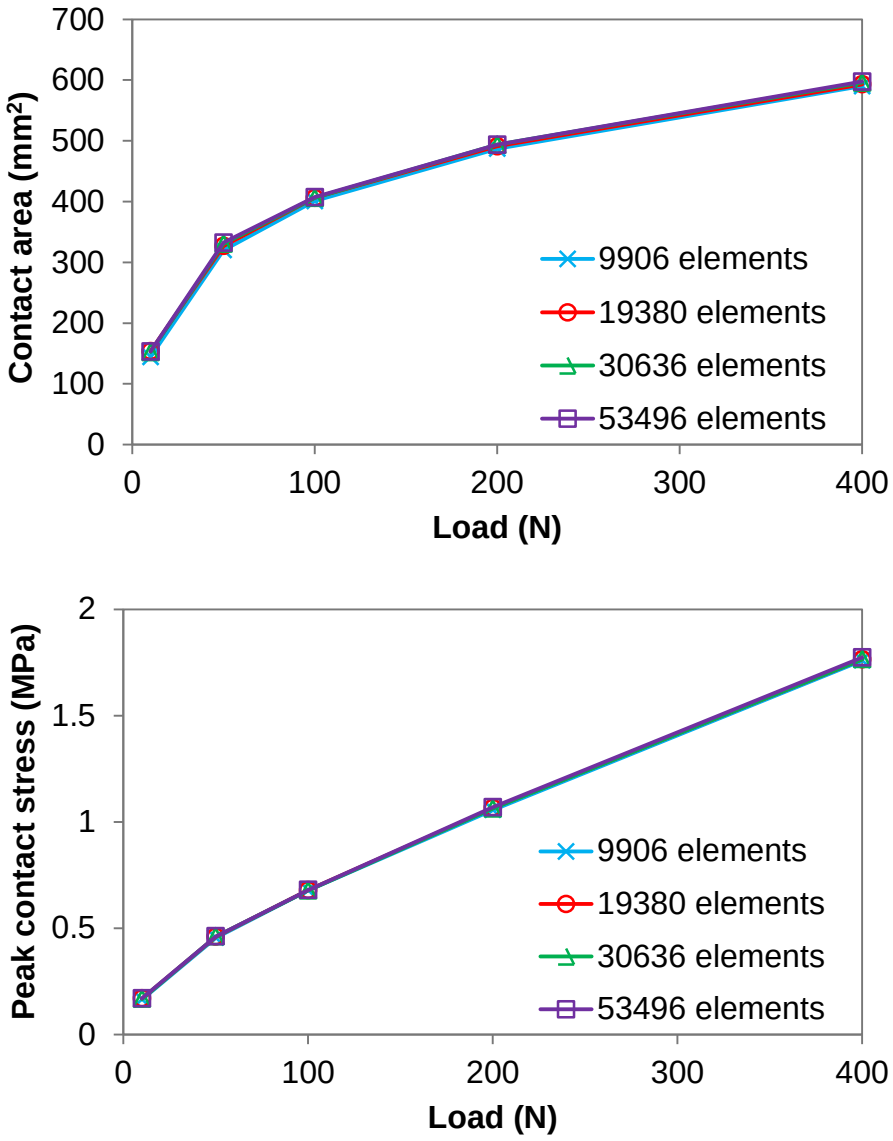

Figure 8.7 Predictions of models with different mesh densities in the case of 40 mm head diameter under different magnitudes of loads (the four traces nearly overlapped). The isotropic solid phase was adopted for the mesh sensitivity tests. The predictions of the cartilage model with 9906 elements were found to be insensitive to higher mesh densities.

8.2.4 Boundary conditions and loads

The meshed model was then imported into PreView (version 1.7; mrl.sci.utah.edu/software.php) for pre-procession. The acetabular cartilage was oriented and positioned according to the setup of the experimental measurement. The surface of the cartilage that was connected to the subcondral bone was rigidly constrained to a reference point which was fixed in all the degrees of freedom in order to represent the rigid bone. The spherical head was assumed to be impermeable. The contact was assumed to be frictionless, and the fluid flow on the articulating surface of the cartilage was considered as contact-dependent so that fluid could only flow out from the area of the articulating surface that was not in contact with the impermeable head. To replicate the constraints of the head relative to the acetabular cartilage, four sets of load were applied within 3 s to the rigid head which was fixed along rotational degrees of freedom. The shorter loading period of the FE models than the experiment was to enhance the computational efficiency but would not affect the model prediction, because as demonstrated in **Chapter 4**, the model predictions were insensitive to instantaneous loads.

8.2.5 Material properties

The metal head was assumed to be rigid, and the cartilage was treated as a biphasic solid. Both an isotropic solid phase and a tension-compression nonlinear solid phase were tested respectively to evaluate the effect of different constitutive relationships on model predictions. The solid phase of the isotropic models were represented by the neo-Hookean constitutive relationship with the properties adopted from a previous study (**Table 8-1**) (Pawaskar et al., 2011). Additionally, the isotropic model was run with twice the aggregate stiffness to investigate the sensitivity to this value. For the tension-compression nonlinear model, the aggregate modulus was the same to the isotropic model and the tensile modulus was set to 10 times higher (Soltz and Ateshian, 2000, Cohen et al., 1993).

Table 8-1 Material properties for the models with different solid phase properties. Isotropic: the model with isotropic solid phase; 2E: the isotropic model with doubled aggregate stiffness; T-C: the model with tension-compression nonlinear solid phase.

	Isotropic	2E	T-C
Aggregate modulus (MPa)	0.562	1.124	0.562
Tensile modulus (MPa)	N/A	N/A	5.62
Poisson's ratio	0	0	0
Permeability ($mm^4/(Ns)$)	0.00157	0.00157	0.00157

8.2.6 Simulation method and output measurements

The FE simulations were conducted using FEBio (version 1.6.0; Musculoskeletal Research Laboratories, Salt Lake City, UT, USA; URL: mrl.sci.utah.edu/software/febio) on a Linux server with 8 GB of RAM and 8 Intel X5560 cores at 2.8 GHz. Contact stress was recorded. Contact area was calculated by adding up the area of the articulating surface elements in which the contact stress was non-zero. The experimentally-measured and computed contact areas were compared.

8.3 Results

The contour of contact stress of the FE models and the measured contact area in the case of the 37 mm head diameter is shown in **Figure 8.8**. Generally, the location and shape of the contact area for the models with different solid phase properties were similar. The model with isotropic solid phase had larger contact area and lower peak contact stress, as compared with the one with tension-compression nonlinear solid phase. However, comparable magnitude of contact stress and contact area was found between the tension-compression nonlinear model and the isotropic model with doubled stiffness.

Good agreement in the location, shape and area of the contact was found between the FE models and the experimental measurement over the loads of different magnitudes. As compared with the isotropic solid phase model, the model with tension-compression nonlinear solid phase had a more comparable shape and area of contact to the experiment.

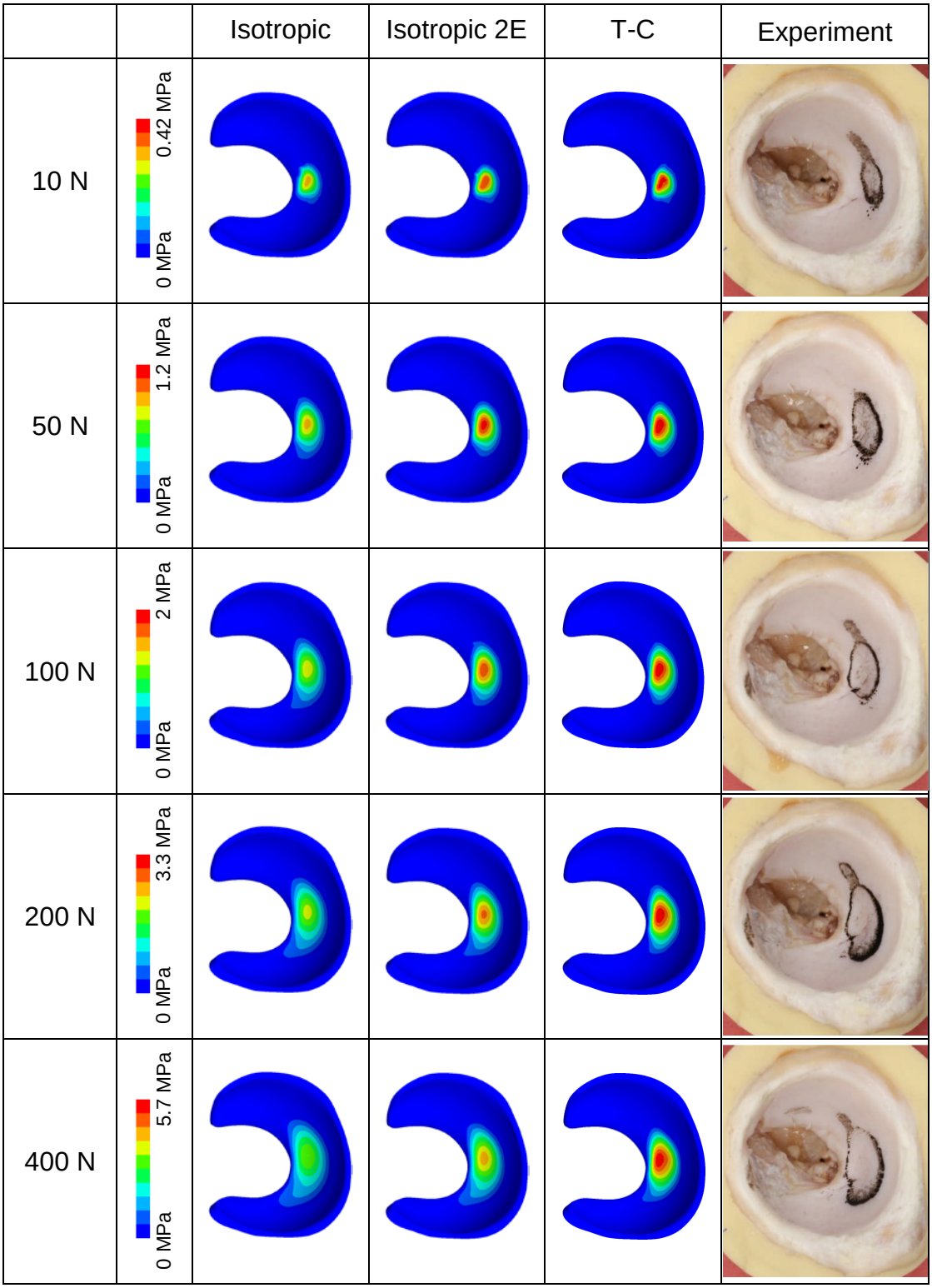

Figure 8.8 Contours of contact stress of the FE models (head diameter = 37 mm) with different solid phase properties in comparison to the experimentally-measured contact area (gel mark in black colour).

The results of the models with the head of 40 mm diameter are shown in **Figure 8.9**. Again, the location and shape of the contact area for the models with different solid phase properties were similar. The model with the isotropic solid phase had a larger area and lower magnitude of contact stress than the one with tension-compression nonlinear solid phase. However, when the aggregate modulus of the isotropic model was doubled, the magnitude of contact stress and contact area were similar to the tension-compression nonlinear model.

The contact areas of the model with the 40 mm diameter heads were substantially larger than those with the 37 mm diameter heads. The location, shape and area of the contact predicted by the FE models corresponded well to the experimental measurement over the loads with different magnitudes. According to the experimental measurement, the contact occurred in two separate locations under loads from 10 N to 100 N, and merged into one region for the loads of 200 N and 400 N. This pattern was observed for the FE model with tension-compression nonlinear model and the isotropic model with doubled aggregate stiffness. However, in the isotropic model, the two separate contact locations joined together at loads of 100 N or greater. In terms of the shape and area of the contact, the tension-compression nonlinear model was more comparable to the experimental measurement than the isotropic model.

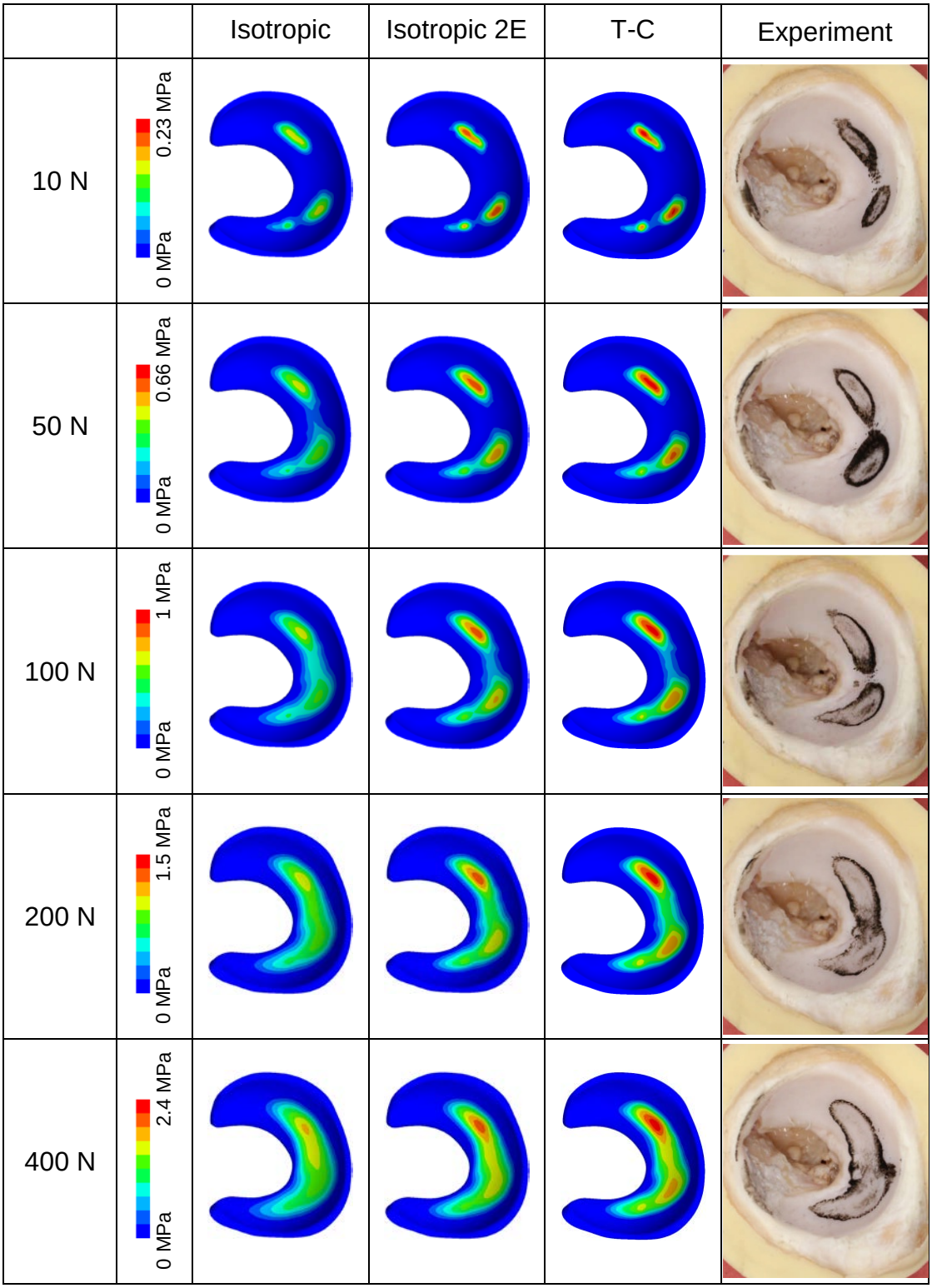

Figure 8.9 Contours of contact stress of the FE models (head diameter = 40 mm) with different solid phase properties in comparison to the experimentally-measured contact area (gel mark in black colour).

The magnitudes of contact area for the heads of diameters 37 mm and 40 mm are shown in **Figure 8.10** and **Figure 8.11** respectively. Under different magnitudes of loads, the contact area of the tension-compression nonlinear model was substantially lower than that of the isotropic model. Generally, the FE models with different solid phase properties provided higher magnitude but similar trend for the contact area versus load to the experimental measurement. This similarity in trend was greater for the tension-compression nonlinear model, as compared with the isotropic model. However, when the aggregate modulus of the isotropic model was doubled, its magnitude and trend for the contact area versus load were more comparable to the tension-compression nonlinear model as well as the experimental measurement. It is unclear why the experiment measurement of contact area did not increase for load increase of 200 N to 400 N for the 37 mm head (**Figure 8.10**). It should be noted that in the stress contours of the FE models in **Figure 8.8** and **Figure 8.9**, the region with contact stress less than 10% of the peak value is represented by dark blue, and thus the area displayed by other colours (>10% of the peak value) is smaller than the area of non-zero stress of the FE models in **Figure 8.10** and **Figure 8.11** under each circumstance.

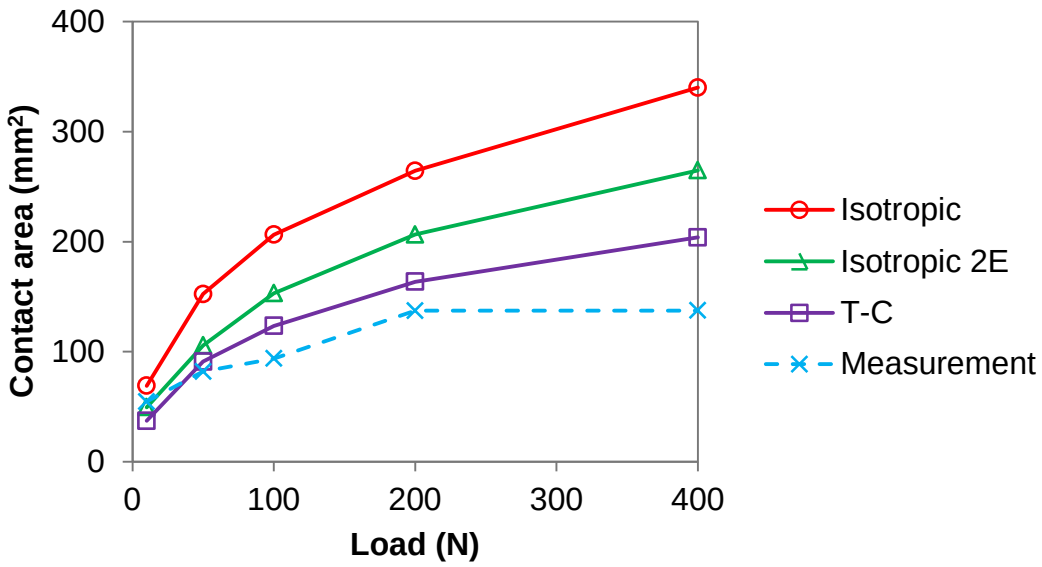

Figure 8.10 Contact area of the FE models (head diameter = 37 mm) with different solid phase properties in comparison with the experimental measurements.

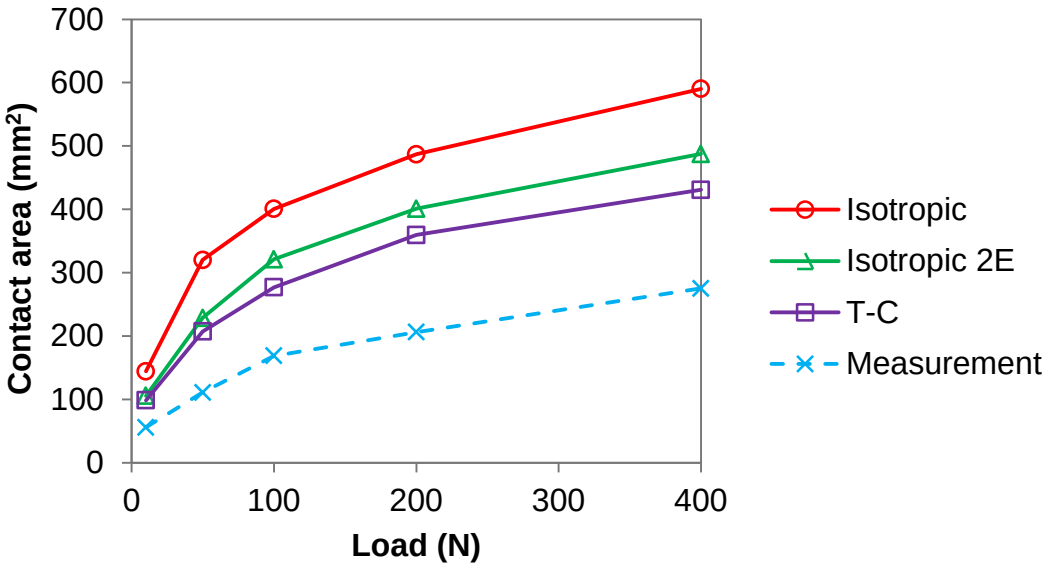

Figure 8.11 Contact area of the FE models (head diameter = 40 mm) with different solid phase properties in comparison with the experimental measurements.

8.4 Discussion

The aim of this study was to validate the FE hip model of a hemiarthroplasty which incorporated the biphasic modelling methodology by comparison with experimental measurements. As yet, there seem to have been only two studies that have reported direct validation of FE models of the hip contact conditions against experiments (Anderson et al., 2008, Pawaskar et al., 2011). In these studies, contact pressure and contact area were measured using pressure-sensitive films. However, such measurement techniques are open to question, because the thickness (approximately 0.2 mm) and stiffness of such films may markedly alter the contact behaviour of the hip joint due to its highly congruent surfaces. To alleviate such artefacts, a staining fluid gel was used in this study to measure the contact area. However, other parameters such as contact pressure and fluid pressure cannot be predicted using this method.

In this study, the hemiarthroplasty model was composed of porcine acetabular cartilage and a spherical prosthetic head. This was used as it was a technique developed in a separate study by Dr. Qianqian Wang. At

the time of writing the thesis, the experimental technique for the natural joint with two cartilage surfaces had not been developed. In order to validate the contact area as well as its trend under different circumstances, two types of head with diameters of 37 mm and 40 mm were tested and loads of different magnitudes were applied. In addition, different properties for the solid phase of the cartilage were considered to evaluate the importance of the tension-compression nonlinear constitutive relationship within the model. Generally, the contact area predicted by both the isotropic and tension-compression nonlinear FE models corresponded well to the experimental measurement. Both the shape and the location of the contact contour for the FE models were comparable to the experiment. As compared with the experiment, the higher magnitude of contact area in the FE predictions was most likely due to the fact that the sensitivity of the experiment to the contact stress might not be as high as that of the FE models in which the contact area was calculated based on the area of the articulating surface with non-zero contact stress. For both the isotropic and tension-compression nonlinear models, similar trends in the magnitude of contact area to the experiment were observed over the loads investigated.

In comparison to the measured area, a higher similarity in the shape and area of the contact contour was detected for the model with tension-compression nonlinear solid phase than the isotropic model. However, better agreement was also found between the tension-compression nonlinear model and the isotropic model with doubled aggregate stiffness. This demonstrates the hypothesis in the discussion of **Chapter 4**, **5** and **6** that the stiffness of the cartilage was potentially underestimated by the isotropic assumption during the early loading period.

Although good agreement between the FE predictions and the experimental data was achieved, there are some limitations that should be mentioned. Only one set of experiment was conducted and thus a certain level of measurement errors may exist. Besides, only the instantaneous contact areas were evaluated without accounting for the time dependent behaviour of the cartilage, because the variation in the contact area during the cartilage consolidation process within the hip is difficult to be accurately measured using the staining fluid gel. However, the high similarity in the instantaneous

results for a range of different input conditions provides some confidence in the model predictions.

For the experiment and the modelling, ideally identical boundary conditions would have been applied, but this was difficult to achieve. In this study, the acetabular component in the FE model was oriented manually based on the bony landmarks. However, the great similarity in the location of contact between the FE models and the experimental measurement that was obtained using this technique suggests it was adequate to locate the component. Besides, in the experiment, the cartilage was attached to the underlying bone which was supported by the cement. Whilst in the FE model, the bone was assumed to be rigid. However, as found in **Chapter 5**, such assumption may have little influence on the model predictions.

In the current study, the material properties of the cartilage were based on a previous curve fitted test for another porcine hip (Pawaskar et al., 2011), and the tensile modulus in the tension-compression nonlinear model was assumed to be 10 times higher than the aggregate modulus. Due to the potential variations in cartilage properties between different subjects, this simplification may potentially decrease the accuracy in the model predictions.

Owing to the high resolution of the scanned images (**Figure 8.4**), the realistic geometric parameters of the tissue can be obtained to a great extent. However, minimal errors in model geometry may still exist due to the semi-automatic segmentation and smoothing techniques. According to the findings of the parametric studies in **Chapter 5**, the minimal variations in geometry may not greatly affect the accuracy of the models, yet the potential error should be evaluated more systematically. Another limitation is that the labrum was excluded in the FE models, given that its material properties were unknown in the literature and it is difficult to distinguish the labrum from other soft tissues (e.g. capsule). However, such assumption is appropriate in this study, because as shown in the measurement (**Figure 8.8** and **Figure 8.9**), no contact occurred around the region near the labrum. Although the labrum may affect the cartilage consolidation process (Ferguson et al., 2000a, Ferguson et al., 2000b, Haemer et al., 2012, Ferguson et al., 2003),

the loading period in this study was too short to allow an obvious time dependent response of the tissue.

In conclusion, in the comparison of the FE predictions and the experimental measurement, good agreement in the location and shape of contact was achieved, and a similar trend in the relationship between contact area and load was observed. As compared with the isotropic solid phase, a higher similarity in these results was obtained with the tension-compression nonlinear solid phase which, in terms of calculating the contact area, had similar effect to a stiffer isotropic model. The findings provide some confidence that the new biphasic methodology for modelling the cartilage is able to predict the contact mechanics of the hip joint.

Chapter 9
Overall Discussion and Conclusions

9.1 Overall discussion

9.1.1 Musculoskeletal modelling in gait analysis

The investigation on the hip kinematics and kinetics of THR patients is promising, because it assists in providing better patient care, pre-operative planning and rehabilitation strategies. As a result, such investigations have been conducted by a multitude of previous studies. However, gait kinematics and kinetics of patients with different levels of THR outcomes have been poorly reported, particularly in terms of hip contact force which is directly linked with joint damage (Wearing et al., 2006, Arokoski et al., 2000). For the prediction of joint contact force, RBD musculoskeletal modelling has been widely adopted, mainly due to its non-invasive nature and computational efficiency as well as the development of musculoskeletal analysis software that incorporates detailed anatomical information of human body and provides reasonable results. For the above reasons, a musculoskeletal model was constructed and applied to the gait kinetic analysis for different cohorts.

A musculoskeletal model composed of the bones and muscles of the human lower extremity was developed in **Chapter 2**. The model enables the calculation of joint contact forces directly from the body kinematics that can be measured easily and non-invasively. Due to the large number of subjects investigated, measurement and simulation efficiency is of necessity and thus simplifications were made. The sensitivity of the model to the model and measurement simplifications was therefore evaluated, and the adoption of simple muscle model, ground reaction measurement for one foot and quadratic muscle recruitment along with the scaling approach were verified.

In **Chapter 3**, the method was then applied to quantify the differences in gait kinematics and kinetics for normal healthy individuals, asymptomatic THR patients and symptomatic LLI patients. Compared with the normal healthy people, the asymptomatic THR patients exhibited a less dynamic pattern in hip contact force with a significantly lower magnitude, reduced range of motion and decreased peak ground reaction force. These abnormalities were more evident for the symptomatic LLI patients. In addition, a higher degree of asymmetry in these gait parameters was found between the operated and non-operated limbs of the symptomatic LLI patients, as compared with the asymptomatic THR patients. Since the hip contact force was greatly correlated with hip flexion/extension angle as well as ground reaction force, improving these parameters during post-operative rehabilitation is important to restore a normal hip load. Besides, due to the large variations between the normal healthy people and THR patients in hip kinetics during gait, refinement to the hip loading of the ISO standard that was derived from joint forces of a healthy person is recommended in order to provide more realistic loading criteria for artificial joint tests.

Apart from the verified parameters in **Chapter 2**, there were, however, several other simplifications in the model that need to be investigated to evaluate the accuracy of the predictions, which have been discussed in **Section 3.4**. For computational efficiency, the modelling was based on RBD, and the joint models were greatly simplified. These assumptions are justifiable to investigate the hip joint because the deformation of bones and the locomotion involved in joint contact are minimal in the scale of the whole lower extremity and may therefore have little influence on the hip contact force. Generally, in most of the current musculoskeletal studies, the computed peak joint contact force was overestimated by approximately 10% due to the lack of a realistic muscle wrapping path around the hip joint within the model (Brand et al., 1994). Although this weakness is difficult to overcome until more detailed anatomical information is provided, it is suitable for a comparative study focusing on the deviations among different cohorts. Another major limitation is that the model is not fully subject-specific, as some parameters were generalized. For example, the muscle recruitment pattern of THR patients may differ from normal people, due to

pre-operative or post-operative stimuli such as the weakness of certain muscles. Future studies need to be undertaken to investigate the influence of the subject-specific parameters on model predictions and measurement efficiencies to determine whether it is necessary to incorporate these more subject-specific features.

Due to the highly invasive techniques, direct validation of musculoskeletal models against *in vivo* measurements in terms of predicting joint contact forces is difficult to be conducted. Although the model can be alternatively validated by adopting the body kinematic information of previous studies on hip contact force measurements as model inputs, there seem to be no studies that provide both the hip contact force as well as the corresponding kinematic data detailed enough to drive the whole lower extremity model stably. As compared with previous experimental and numerical studies, our predictions were in similar patterns and magnitudes, which along with the model verification, demonstrates the reliability of the results to some extent. Additionally, the accuracy of the lower extremity musculoskeletal model in AnyBody (AnyBody Technology, Denmark) has been previously confirmed in the literature (Forster, 2004, Manders et al., 2008).

In spite of these limitations, RBD musculoskeletal modelling is a non-invasive, efficient and reliable tool to predict joint contact forces and suitable for cohort studies that involve large numbers of subjects. The findings may assist in providing better patient care, pre-operative planning and rehabilitation strategies. For example, the higher degree of gait abnormality observed for the LLI patients indicates that efforts should be attempted for surgeons to decrease LLI. Because the hip contact force is significantly correlated with the flexion/extension and abduction/adduction angle, it is important to ensure a wide range of mobility for the implanted prosthesis during surgery as a premise to retrieve a normal loading pattern after THR. Also, for the post-operative rehabilitation of THR patients, the level of dynamics in gait pattern should be emphasised. To improve the acceptance of the predictions in clinical community, direct validation with the consideration of more subject-specific parameters of the model should be incorporated in future studies.

9.1.2 FE modelling of hip joint with biphasic cartilage layers

Due to the important role that the interstitial fluid plays in the cartilage function and degradation, it is necessary to consider the biphasic nature of the cartilage within the joint system. Whilst biphasic cartilage have been employed previously for simple geometry with two dimensions (Wu et al., 1997, Ferguson et al., 2000a, Ferguson et al., 2000b, Haemer et al., 2012), it has yet to be successfully applied to a three dimensional whole joint either under high physiological dynamic loads which involve consecutively sudden spatial and temporal variations or over a prolonged period of loading, because the convergence is difficult to be achieved in the FE solvers adopted by previous studies. For example, Pawaskar (2010) employed Abaqus (DassaultSystemes, SuresnesCedex, France) to simulate both the natural hip joint and the hip joint with hemiarthroplasty incorporating biphasic cartilage properties. Whilst the hemiarthroplasty model, which involved a rigid body on biphasic cartilage contact, could be simulated for 600 s under a static load, the natural joint model, also with spherical articulating surfaces, could only be solved for 1 s under a ramped load, due to convergence difficulties. To address this problem, a recently developed FE solver FEBio (mrl.sci.utah.edu/software/febio) was adopted in this thesis.

In **Chapter** 4, the results calculated in FEBio were compared to those solved in ABAQUS as well as to previous experimental data (Pawaskar, 2010), in order to test the convergence ability and the reliability of the predictions in FEBio for biphasic simulation. It was found that the linearly elastic solid phase does not perform well in the non-linear FE solver FEBio. However, neo-Hookean solid phase in FEBio can be used to approximate the linearly elastic constitutive property. In addition, good agreement was achieved between the calculated results in FEBio and the data in the previous study (Pawaskar, 2010). Based on the methods determined in **Chapter 4**, biphasic material was applied to the hip joint modelling in **Chapters 5**, **6**, **7,** and **8**.

In **Chapter 5** and **Chapter 6**, a whole hip model with biphasic cartilage layers under both physiological static loads was successfully simulated both for high physiological dynamic loads and over a prolonged period of loading. The results illustrated how the cartilage geometry and structure aid in the

function of the natural hip joint. The soft and conforming contact surfaces ensured a large contact area and low peak contact stress, despite a high load being applied. Owing to the good congruence of the hip joint and the very low cartilage permeability, fluid exudation occurred slowly and the fluid supported most of the load even under extreme situations (e.g. 3000 s and high dynamic loads), leaving a small portion of load transferred to the solid phase of the cartilage and the solid-solid contact which would reduce the frictional coefficient and shear stress in reality (Krishnan et al., 2004). This would explain the survival potential of the hip joint for the life time of human. Due to the importance of interstitial fluid in cartilage function both over long-term loading periods and during different daily activities, this modelling approach could allow further investigation of the functional and tribological behaviour of the joint and the pathology of joint degeneration.

For the eight different daily activities investigated in **Chapters 6**, a decreased level in fluid support ratio and a faster process of fluid exudation was observed for the interior edge region of the acetabular cartilage, but when these occurred, the absolute level of the peak contact stress was minimal, therefore potentially not harmful. Further studies involving more comprehensive and larger number of cycles of activities, and potentially abnormal activities and anatomies are needed to better characterize the potential vulnerability of the interior edge region of the acetabular cartilage caused by its decreased fluid support ratio and faster fluid exudation process observed in this study.

For the purpose of determining the order of importance of the model input conditions and gaining insight into the role of fluid pressurisation on the function of a generic hip joint, an idealized generic geometry was assumed for the human hip model with spherical articulating surfaces and uniform cartilage thickness. However, such assumption has been shown to reduce the peak contact stress in an elastic FE model (Anderson et al., 2010). Additionally, in **Chapter 5**, it was demonstrated that the predicted behaviour of the natural hip joint model was subject to hip size and clearance as well as cartilage thickness. For subject-specific investigations, it is clear the individual variations in the hip morphology are important.

Besides the idealized model configuration, the isotropic solid phase was assumed in the human hip models in this thesis which may not fully represent the tension-compression non-linear behaviour caused by the fiber-reinforced structure of the cartilage. As demonstrated in **Chapter 8**, due to the isotropic assumption, the stiffness of the tissue may be potentially underestimated, leading to a lower peak contact stress and a larger contact area, particularly during the early loading period. Besides, the fluid pressure and fluid support ratio may be depreciated. In addition, the confinement effect due to the tensile stiffness may be reduced, which may result in an amplified influence of cartilage thickness as discussed in **Chapter 5** and an overestimated reduction in fluid support ratio for the edge region of the acetabular cartilage observed in **Chapter 6**.

Whilst there were some simplifications to the material model and geometry used in this human hip model, the methods presented provide a basic platform and initial understanding of the sensitivity of the model onto which more sophisticated material models and geometric parameters could be added, as well as insight into the role of fluid pressurisation on the function of a generic hip joint during daily activities. This computational approach has the potential to aid in understanding the mechanisms of hip function and the pathology of hip degeneration.

In **Chapter 8**, the methodology was validated against experiment using a porcine hip for a hemiarthroplasty. Given the importance of the cartilage thickness to the model prediction as found in **Chapter 5**, subject-specific geometric parameters were taken into account. In addition, the tension-compression solid phase was considered to evaluate its importance to the model predictions. The contact area was compared between the FE model and the measurement, and good agreement was achieved in terms of the shape and location of contact as well as the trend in contact area versus load. Using the tension-compression nonlinear solid phase, a higher degree of similarity to the experiment was obtained. Additionally, the shape of contact area was not as smooth as the spherical model in **Chapter 5**, **6** and **7**. These indicate that it is necessary to incorporate these more sophisticated constitutive relationship and individual geometric parameters in future subject-specific studies and clinical applications, as well as in future

validation studies. For the validation to be truly independent, the material properties also need to be defined more clearly.

9.1.3 Combination of biomechanics and biotribology

This thesis mainly focuses on two domains of hip modelling: biomechanics in terms of joint contact force and biotribology in terms of contact mechanics. These two aspects have been separately conducted in the previous studies. Previous predictions on joint contact force have not been further applied to evaluate the biphasic joint contact mechanics. On the other hand, highly standardised joint loading was adopted in the current studies on the hip contact mechanics as the inputs of their FE models or *in vitro* tests, which may not represent the realistic loading conditions for the subject investigated. The combination of biomechanics and biotribology opens the opportunities to investigate the hip performance more systematically and comprehensively.

In **Chapter 7**, the hip contact mechanics and the associated fluid pressurisation were investigated for three different patient groups: normal healthy people, the non-operated hips of asymptomatic unilateral THR patients and symptomatic unilateral LLI patients. The calculated hip contact forces in **Chapter 3** for these three cohorts were adopted as the loading inputs for the FE model of human hip developed in **Chapter 5** and **Chapter 6**. The abnormal gait kinetics of the THR / LLI patients was found to lead to a resultant reduction and less dynamic pattern in the peak contact stress and fluid pressure on their non-operated hips. However, the fluid support ratio was generally similar for the three cohorts, with a high (>90%) magnitude and slow decrease. Similar to the findings in **Chapter 6**, a decreased level in fluid support ratio and a faster process of fluid exudation was observed for the interior edge region of the acetabular cartilage, but this may not be harmful due to the minimal peak contact stress that occurred at this period for all the three cohorts. The reduced stress level and similar fluid support ratio demonstrated that the non-operated hips of the asymptomatic THR patients and symptomatic LLI patients may not function in a mechanically adverse environment during the whole cycle of gait. Further investigations

involving a comprehensive range of activities are necessary to better evaluate the risk of joint damage for the non-operated joint of THR / LLI patients.

The magnitude and distribution of the contact stress and fluid pressure predicted in **Chapter 7** were markedly different (~40% higher in magnitude) from those of the walking activities in **Chapter 6**, due to the variations in the hip contact force that was used as the loading inputs for the model. This, along with the findings of the differences in contact mechanics between different cohorts, demonstrates the importance of adopting the loading conditions of the model on a subject-specific or cohort-specific level.

Although there are several limitations for both the musculoskeletal model and the FE model as have mentioned in **Chapters 3**, **5**, and **6**, they are justified for the comparative purpose of this study. Additionally, as discussed in **Chapter 7**, the uncoupled combination of the RBD musculoskeletal model and the FE model is necessary and appropriate when accounting for the substantially higher computational expenses and the potential minimally enhanced model accuracy for the coupled approach.

Through the combination of the RBD musculoskeletal modelling for joint loading and FE modelling for contact mechanics, a high level of subject-specific predictions can be achieved along with a wide range of parameters that can be calculated. As a result, this method can be applied appropriately to the clinic. For example, the performance of the joint after special interventions (e.g. tissue substitution) can be evaluated pre-operatively using this method to provide better surgical strategies in order to decrease the risk of post-operative failure.

9.2 Conclusion and Future work

9.2.1 Musculoskeletal modelling in gait analysis

Major conclusions:

1) A musculoskeletal modelling technique that can predict joint contact force directly from measured kinematic data was developed. The model shows good computational efficiency and therefore is suitable for cohort studies.
2) Compared with normal healthy people, significant differences in hip kinematics and kinetics during gait existed in asymptomatic THR patients and were substantially more evident in symptomatic LLI patients. The gait abnormalities of THR / LLI patients were reflected by the decreased magnitude and dynamic pattern in hip contact force, reduced range of motion, lower peak ground reaction force and greater asymmetry in these parameters.
3) Due to such large variations, refinement of ISO standard is recommended to provide more realistic *in vitro* loading conditions.
4) The pattern of hip contact force was greatly correlated with flexion/extension angle and ground reaction force, suggesting that improving these parameters is important in post-operative rehabilitation in order to restore a normal loading condition for the hip.

Suggestions to future work:

1) Evaluation of the influence of the following subject-specific parameters on model predictions to determine the necessities to incorporate these features:
    - Muscle recruitment pattern
    - Muscle wrapping path
    - Bony landmarks
    - Other soft tissues i.e. ligaments
2) Application of the kinetic and kinematic predictions to wear models to investigate the influence of THR / LLI on wear.

3) Consideration of different activities in order to evaluate the potential outcome of THR and post-operative rehabilitation more comprehensively.

9.2.2 FE modelling of hip joint with biphasic cartilage layers

Major conclusions:

1) FEBio exhibited substantially better convergence capability in dealing with biphasic cartilage-on-cartilage contact than ABAQUS.
2) Neo-Hookean solid phase in FEBio can be used to approximate the linearly elastic constitutive property.
3) Successful methodologies were developed for three dimensional biphasic hip joint modelling under physiological loads and for prolonged loading periods.
4) The fluid supported most of the load (>90%) transferred between the articulating surfaces of the hip joint both under high dynamic physiological load and over a prolonged loading period.
5) The model predictions for the period soon after loading were sensitive to the hip size, clearance, cartilage aggregate modulus, thickness and hemiarthroplasty, while the time dependent behaviour over a prolonged loading period was influenced by the hip congruence and cartilage permeability.
6) It is necessary to model both layers of cartilage to represent the natural joint.
7) The methodology of modelling the hip cartilage as biphasic was validated against experiment and good agreement was achieved.
8) Tension-compression nonlinear solid phase and subject-specific geometric parameters were important to the model predictions, and therefore needs to be incorporated in future subject-specific studies and clinical applications.
9) The developed methodology of biphasic hip modelling has the potential to aid in understanding the mechanisms of hip function and the pathology of hip degeneration.

Suggestions to future work:

1) Investigation of a wider range of parameters, particularly the higher values of permeability.
2) Validation of more parameters for the whole joint model with larger number of specimens, including validation of human specimen.
3) Determination of subject-specific tension-compression constitutive relationship for cartilage (of different ages, species and locations).
4) Application of the findings to investigate unique interventions in the hip joint.
5) Implementation of the fiber-reinforced solid phase into the joint model in order to evaluate inhomogeneous nature of the tissue.
6) Consideration of the role that the labrum plays in cartilage consolidation within the joint.
7) Application of the method to clinical problems such as hips of dysplasia and femoroacetabular Impingement, and the treatment of such clinical situations.

9.2.3 Combination of biomechanics and biotribology

Major conclusions and suggestions to future work:

1) The combination of a musculoskeletal model and a FE model with biphasic cartilage layers enables the prediction of contact mechanics and the associated fluid pressurisation within the hip joints of different cohorts.
2) The abnormal gait kinetics of the THR / LLI patients was found to lead to a resultant reduction and less dynamic pattern in the peak contact stress and fluid pressure on their non-operated hips.
3) The fluid support ratio within the hip cartilage of the non-operated limbs of the THR / LLI patients was found to be normal.
4) The reduced stress level and similar fluid support ratio demonstrated that the non-operated hips of the asymptomatic THR patients and symptomatic LLI patients may not function in a mechanically adverse environment during the whole cycle of gait.
5) Future subject-specific investigations on a more comprehensive range of activities to better evaluate the risks the THR / LLI patients had on their non-operated hips.
6) Combination of the musculoskeletal model and the FE model with subject-specific geometries and material properties in the future.

This thesis has advanced a significant step forward in biphasic modelling capability in the hip. It provides a new simulation platform for an extensive range of future studies, beyond these described above, to advance our knowledge of disease progression and surgical interventions.

List of References

ABAQUS THEORY MANUAL, V. 2011. Dassault Systemes. Suresnes Cedex, France.

ABRAHAM, C. L., MAAS, S. A., WEISS, J. A., ELLIS, B. J., PETERS, C. L. & ANDERSON, A. E. 2013. A new discrete element analysis method for predicting hip joint contact stresses. *Journal of Biomechanics,* 46**,** 1121-1127.

ACCARDI, M. A., DINI, D. & CANN, P. M. 2011. Experimental and numerical investigation of the behaviour of articular cartilage under shear loading—Interstitial fluid pressurisation and lubrication mechanisms. *Tribology International,* 44**,** 565-578.

ADAM, C., ECKSTEIN, F., MILZ, S. & PUTZ, R. 1998. The distribution of cartilage thickness within the joints of the lower limb of elderly individuals. *Journal of Anatomy,* 193**,** 203-214.

AFOKE, N. Y., BYERS, P. D. & HUTTON, W. C. 1987. Contact pressures in the human hip joint. *Journal of Bone and Joint Surgery (British),* 69**,** 536-41.

AKIZUKI, S., MOW, V. C., MÜLLER, F., PITA, J. C., HOWELL, D. S. & MANICOURT, D. H. 1986. Tensile properties of human knee joint cartilage: I. Influence of ionic conditions, weight bearing, and fibrillation on the tensile modulus. *Journal of Orthopaedic Research,* 4**,** 379-392.

AL NAZER, R., RANTALAINEN, T., HEINONEN, A., SIEVÄNEN, H. & MIKKOLA, A. 2008. Flexible multibody simulation approach in the analysis of tibial strain during walking. *Journal of Biomechanics,* 41**,** 1036-1043.

ALEXOPOULOS, L. G., WILLIAMS, G. M., UPTON, M. L., SETTON, L. A. & GUILAK, F. 2005. Osteoarthritic changes in the biphasic mechanical properties of the chondrocyte pericellular matrix in articular cartilage. *Journal of Biomechanics,* 38**,** 509-517.

AMARANTINI, D. & MARTIN, L. 2004. A method to combine numerical optimization and EMG data for the estimation of joint moments under dynamic conditions. *Journal of Biomechanics,* 37**,** 1393-1404.

ANDERSON, A. E., ELLIS, B. J., MAAS, S. A., PETERS, C. L. & WEISS, J. A. 2008. Validation of finite element predictions of cartilage contact pressure in the human hip joint. *Journal of Biomechanical Engineering,* 130**,** 051008.

ANDERSON, A. E., ELLIS, B. J., MAAS, S. A. & WEISS, J. A. 2010. Effects of idealized joint geometry on finite element predictions of cartilage contact stresses in the hip. *Journal of Biomechanics,* 43**,** 1351-1357.

ANDERSON, F. C. & PANDY, M. G. 2001. Static and dynamic optimization solutions for gait are practically equivalent. *Journal of Biomechanics,* 34**,** 153-161.

ARMSTRONG, C. G. & MOW, V. C. 1982. Variations in the intrinsic mechanical properties of human articular cartilage with age, degeneration, and water content. *Journal of Bone and Joint Surgery (American),* 64**,** 88-94.

AROKOSKI, J. P. A., HYTTINEN, M. M., HELMINEN, H. J. & JURVELIN, J. S. 1999. Biomechanical and structural characteristics of canine femoral and tibial cartilage. *Journal of Biomedical Materials Research,* 48**,** 99-107.

AROKOSKI, J. P. A., JURVELIN, J. S., VÄÄTÄINEN, U. & HELMINEN, H. J. 2000. Normal and pathological adaptations of articular cartilage to joint loading. *Scandinavian Journal of Medicine and Science in Sports,* 10**,** 186-198.

ASAKAWA, D. S., PAPPAS, G. P., BLEMKER, S. S., DRACE, J. E. & DELP, S. L. 2003. Cine phase-contrast magnetic resonance imaging as a tool for quantification of skeletal muscle motion. *Semin Musculoskelet Radiol,* 7**,** 287-95.

ATESHIAN, G. A. 2009. The role of interstitial fluid pressurization in articular cartilage lubrication. *Journal of Biomechanics,* 42**,** 1163-1176.

ATESHIAN, G. A., A., G., WANG, H., LAI & M., W. 1998. *The role of interstitial fluid pressurization and surface porosities on the boundary friction of articular cartilage. Discussion,* New York, NY, ETATS-UNIS, American Society of Mechanical Engineers.

ATESHIAN, G. A. & HUNG, C. T. 2006. The natural synovial joint: Properties of cartilage. *Proceedings of the Institution of Mechanical Engineers, Part J: Journal of Engineering Tribology,* 220**,** 657-670.

ATESHIAN, G. A., LAI, W. M., ZHU, W. B. & MOW, V. C. 1994. An asymptotic solution for the contact of two biphasic cartilage layers. *Journal of Biomechanics,* 27**,** 1347-1360.

ATESHIAN, G. A. & MOW, V. C. 2005. Friction, lubrication, and wear of articular cartilage and diarthrodial joints. *In Basic orthopaedic biomechanics and mechano-biology.* Third ed.: Lippincott Williams & Wilkins: Philadelphia.

ATESHIAN, G. A., RAJAN, V., CHAHINE, N. O., CANAL, C. E. & HUNG, C. T. 2009. Modeling the matrix of articular cartilage using a continuous fiber angular distribution predicts many observed phenomena. *Journal of Biomechanical Engineering,* 131**,** 061003.

ATESHIAN, G. A. & WANG, H. 1995. A theoretical solution for the frictionless rolling contact of cylindrical biphasic articular cartilage layers. *Journal of Biomechanics,* 28**,** 1341-1355.

ATHANASIOU, K. A., AGARWAL, A. & DZIDA, F. J. 1994. Comparative study of the intrinsic mechanical properties of the human acetabular and femoral head cartilage. *Journal of Orthopaedic Research,* 12**,** 340-349.

BACHTAR, F., CHEN, X. & HISADA, T. 2006. Finite element contact analysis of the hip joint. *Medical and Biological Engineering and Computing* 44**,** 643-51.

BAKER, R. 2006. Gait analysis methods in rehabilitation. *Journal of NeuroEngineering and Rehabilitation,* 3**,** 4.

BARBOUR, P. S. M., STONE, M. H. & FISHER, J. 1999. A hip joint simulator study using simplified loading and motion cycles generating physiological wear paths and rates. *Proceedings of the Institution of Mechanical Engineers, Part H: Journal of Engineering in Medicine,* 213**,** 455-467.

BARRANCE, P. J., WILLIAMS, G. N., NOVOTNY, J. E. & BUCHANAN, T. S. 2005. A method for measurement of joint kinematics in vivo by

registration of 3-D geometric models with cine phase contrast magnetic resonance imaging data. *Journal of Biomechanical Engineering,* 127**,** 829-37.

BAURA, G. D. 2012. Chapter 18 - Total Hip Prostheses. *Medical Device Technologies.* Oxford: Academic Press.

BEAULIEU, M. L., LAMONTAGNE, M. & BEAULÉ, P. E. 2010. Lower limb biomechanics during gait do not return to normal following total hip arthroplasty. *Gait and Posture,* 32**,** 269-273.

BEHREND, H., GIESINGER, K., GIESINGER, J. M. & KUSTER, M. S. 2012. The "Forgotten Joint" as the Ultimate Goal in Joint Arthroplasty: Validation of a New Patient-Reported Outcome Measure. *The Journal of Arthroplasty,* 27**,** 430-436.e1.

BENNETT, D., HUMPHREYS, L., O'BRIEN, S., KELLY, C., ORR, J. F. & BEVERLAND, D. E. 2008. Gait kinematics of age-stratified hip replacement patients—A large scale, long-term follow-up study. *Gait and Posture,* 28**,** 194-200.

BERGMANN, G., DEURETZBACHER, G., HELLER, M., GRAICHEN, F., ROHLMANN, A., STRAUSS, J. & DUDA, G. N. 2001. Hip contact forces and gait patterns from routine activities. *Journal of Biomechanics,* 34**,** 859-871.

BERGMANN, G., GRAICHEN, F. & ROHLMANN, A. 1993. Hip joint loading during walking and running, measured in two patients. *Journal of Biomechanics,* 26**,** 969-990.

BESIER, T. F., STURNIEKS, D. L., ALDERSON, J. A. & LLOYD, D. G. 2003. Repeatability of gait data using a functional hip joint centre and a mean helical knee axis. *Journal of Biomechanics,* 36**,** 1159-1168.

BHAVE, A., MONT, M., TENNIS, S., NICKEY, M., STARR, R. & ETIENNE, G. 2005. Functional Problems and Treatment Solutions After Total Hip and Knee Joint Arthroplasty. *Journal of Bone and Joint Surgery (American),* 87**,** 9-21.

BHAVE, A., PALEY, D. & HERZENBERG, J. E. 1999. Improvement in Gait Parameters After Lengthening for the Treatment of Limb-Length Discrepancy. *Journal of Bone and Joint Surgery (American),* 81**,** 529-34.

BONET, J. 1997. *Nonlinear continuum mechanics for finite element analysis*, Cambridge university press.

BRAND, R. A., PEDERSEN, D. R., DAVY, D. T., KOTZAR, G. M., HEIPLE, K. G. & GOLDBERG, V. M. 1994. Comparison of hip force calculations and measurements in the same patient. *The Journal of Arthroplasty,* 9**,** 45-51.

BRAND, R. A., PEDERSEN, D. R. & FRIEDERICH, J. A. 1986. The sensitivity of muscle force predictions to changes in physiologic cross-sectional area. *Journal of Biomechanics,* 19**,** 589-596.

BRINCKMANN, P., FROBIN, W. & HIERHOLZER, E. 1981. Stress on the articular surface of the hip joint in healthy adults and persons with idiopathic osteoarthrosis of the hip joint. *Journal of Biomechanics,* 14**,** 149-156.

BROCKLEHURST, R., BAYLISS, M. T., MAROUDAS, A., COYSH, H. L., FREEMAN, M. A., REVELL, P. A. & ALI, S. Y. 1984. The composition of normal and osteoarthritic articular cartilage from human knee joints. With special reference to unicompartmental replacement and

osteotomy of the knee. *Journal of Bone and Joint Surgery (American),* 66**,** 95-106.

BROWN, T. D. & DIGIOIA, A. M. 1984. A contact-coupled finite element analysis of the natural adult hip. *Journal of Biomechanics,* 17**,** 437-448.

BROWN, T. D. & SHAW, D. T. 1983. In vitro contact stress distributions in the natural human hip. *Journal of Biomechanics,* 16**,** 373-384.

BUCHANAN, T. S. & SHREEVE, D. A. 1996. An evaluation of optimization techniques for the prediction of muscle activation patterns during isometric tasks. *Journal of Biomechanical Engineering,* 118**,** 565-74.

BUDENBERG, S., REDMOND, A., WHITE, D., GRAINGER, A., O'CONNOR, P., STONE, M. H. & STEWART, T. D. 2012. Contact surface motion paths associated with leg length inequality following unilateral total hip replacement. *Proceedings of the Institution of Mechanical Engineers, Part H: Journal of Engineering in Medicine*.

CARBONE, V., VAN DER KROGT, M. M., KOOPMAN, H. F. J. M. & VERDONSCHOT, N. 2012. Sensitivity of subject-specific models to errors in musculo-skeletal geometry. *Journal of Biomechanics,* 45**,** 2476-2480.

CHARNLEY, J. 1964. The bonding of prostheses to bone by cement. *Journal of Bone and Joint Surgery (British),* 46**,** 518-529.

CHARNLEY, J. 1972. The long-term results of low-friction arthroplasty of the hip performed as a primary intervention. *Journal of Bone and Joint Surgery (British),* 54-B**,** 61-76.

COHEN, B., GARDNER, T. R. & ATESHIAN, G. A. 1993. The influence of transverse isotropy on cartilage indentation behavior - A study of the human humeral head. *Transactions on Orthopaedic Research Society,* 18**,** 185.

COHEN, B., LAI, W. M. & MOW, V. C. 1998. A transversely isotropic biphasic model for unconfined compression of growth plate and chondroepiphysis. *Journal of Biomechanical Engineering,* 120**,** 491-496.

COLE, G. K., NIGG, B. M., VAN DEN BOGERT, A. J. & GERRITSEN, K. G. M. 1996. Lower extremity joint loading during impact in running. *Clinical Biomechanics,* 11**,** 181-193.

COLLINS, J. J. 1995. The redundant nature of locomotor optimization laws. *Journal of Biomechanics,* 28**,** 251-267.

CROWNINSHIELD, R. D. & BRAND, R. A. 1981. A physiologically based criterion of muscle force prediction in locomotion. *Journal of Biomechanics,* 14**,** 793-801.

CROWNINSHIELD, R. D., JOHNSTON, R. C., ANDREWS, J. G. & BRAND, R. A. 1978. A biomechanical investigation of the human hip. *Journal of Biomechanics,* 11**,** 75-77, 79-85.

DAGENAIS, S., GARBEDIAN, S. & WAI, E. 2009. Systematic Review of the Prevalence of Radiographic Primary Hip Osteoarthritis. *Clinical Orthopaedics and Related Research,* 467**,** 623-637.

DALSTRA, M. & HUISKES, R. 1995. Load transfer across the pelvic bone. *Journal of Biomechanics,* 28**,** 715-724.

DAMSGAARD, M., RASMUSSEN, J., CHRISTENSEN, S. T., SURMA, E. & DE ZEE, M. 2006. Analysis of musculoskeletal systems in the

AnyBody Modeling System. *Simulation Modelling Practice and Theory,* 14**,** 1100-1111.

DANIEL, M., IGLIC, A. & KRALJ-IGLIC, V. 2008. Hip contact stress during normal and staircase walking: The influence of acetabular anteversion angle and lateral coverage of the acetabulum. *Journal of Applied Biomechanics,* 24**,** 88-93.

DAVIS, M. A. 1988. Epidemiology of osteoarthritis. *Clinics in Geriatric Medicine,* 4**,** 241-255.

DAVY, D. T., KOTZAR, G. M., BROWN, R. H., HEIPLE, K. G., GOLDBERG, V. M., HEIPLE, K. G., JR., BERILLA, J. & BURSTEIN, A. H. 1988. Telemetric force measurements across the hip after total arthroplasty. *Journal of Bone and Joint Surgery (American),* 70**,** 45-50.

DELP, S. L., ANDERSON, F. C., ARNOLD, A. S., LOAN, P., HABIB, A., JOHN, C. T., GUENDELMAN, E. & THELEN, D. G. 2007. OpenSim: Open-Source Software to Create and Analyze Dynamic Simulations of Movement. *Biomedical Engineering, IEEE Transactions on,* 54**,** 1940-1950.

DELP, S. L. & LOAN, J. P. 1995. A graphics-based software system to develop and analyze models of musculoskeletal structures. *Computers in Biology and Medicine,* 25**,** 21-34.

DENNERLEIN, J. T., DIAO, E., MOTE, C. D., JR. & REMPEL, D. M. 1998. Tensions of the flexor digitorum superficialis are higher than a current model predicts. *Journal of Biomechanics,* 31**,** 295-301.

DEVAS, M. & HINVES, B. 1983. Prevention of acetabular erosion after hemiarthroplasty for fractured neck of femur. *Journal of Bone and Joint Surgery (British),* 65-B**,** 548-551.

DOUGADOS, M., GUEGUEN, A., NGUYEN, M., BERDAH, L., LEQUESNE, M., MAZIERES, B. & VIGNON, E. 1996. Radiological progression of hip osteoarthritis: definition, risk factors and correlations with clinical status. *Annals of the Rheumatic Diseases,* 55**,** 356-362.

EBERHARDT, A. W., KEER, L. M., LEWIS, J. L. & VITHOONTIEN, V. 1990. An analytical model of joint contact. *Journal of Biomechanical Engineering,* 112**,** 407-13.

ECKSTEIN, F., TIESCHKY, M., FABER, S., ENGLMEIER, K. H. & REISER, M. 1999. Functional analysis of articular cartilage deformation, recovery, and fluid flow following dynamic exercise in vivo. *Anatomy and Embryology,* 200**,** 419-424.

EGGLI, P. S., HUNZINKER, E. B. & SCHENK, R. K. 1988. Quantitation of structural features characterizing weight- and less-weight-bearing regions in articular cartilage: A stereological analysis of medical femoral condyles in young adult rabbits. *The Anatomical Record,* 222**,** 217-227.

ERDEMIR, A., MCLEAN, S., HERZOG, W. & VAN DEN BOGERT, A. J. 2007. Model-based estimation of muscle forces exerted during movements. *Clinical Biomechanics,* 22**,** 131-154.

FELSON, D. T. 1988. Epidemiology of hip and knee osteoarthritis. *Epidemiologic Reviews,* 10**,** 1-28.

FENLIN, J. M., JR. & FRIEMAN, B. G. 1998. Indications, technique, and results of total shoulder arthroplasty in osteoarthritis. *Orthopedic Clinics of North America,* 29**,** 423-34.

FERGUSON, S. J., BRYANT, J. T., GANZ, R. & ITO, K. 2000a. The acetabular labrum seal: a poroelastic finite element model. *Clinical Biomechanics,* 15**,** 463-468.

FERGUSON, S. J., BRYANT, J. T., GANZ, R. & ITO, K. 2000b. The influence of the acetabular labrum on hip joint cartilage consolidation: a poroelastic finite element model. *Journal of Biomechanics,* 33**,** 953-960.

FERGUSON, S. J., BRYANT, J. T., GANZ, R. & ITO, K. 2003. An in vitro investigation of the acetabular labral seal in hip joint mechanics. *Journal of Biomechanics,* 36**,** 171-178.

FERNANDEZ, J. W. & PANDY, M. G. 2006. Integrating modelling and experiments to assess dynamic musculoskeletal function in humans. *Experimental Physiology,* 91**,** 371-382.

FISHER, J. 2011. Bioengineering reasons for the failure of metal-on-metal hip prostheses: an engineer's prespective. *Journal of Bone and Joint Surgery (British),* 93-B**,** 1001-1004.

FORSTER, E. 2004. *Predicting Muscle Forces in The Human Lower Limb During Locomotion.* Ph.D. Thesis, Germany: University of Ulm.

FORSTER, H. & FISHER, J. 1996. The influence of loading time and lubricant on the friction of articular cartilage. *Proceedings of the Institution of Mechanical Engineers, Part H: Journal of Engineering in Medicine,* 210**,** 109-119.

FORSTER, H. & FISHER, J. 1999. The influence of continuous sliding and subsequent surface wear on the friction of articular cartilage. *Proceedings of the Institution of Mechanical Engineers, Part H: Journal of Engineering in Medicine,* 213**,** 329-345.

FOUCHER, K. C., HURWITZ, D. E. & WIMMER, M. A. 2007. Preoperative gait adaptations persist one year after surgery in clinically well-functioning total hip replacement patients. *Journal of Biomechanics,* 40**,** 3432-3437.

FOUCHER, K. C., HURWITZ, D. E. & WIMMER, M. A. 2008. Do gait adaptations during stair climbing result in changes in implant forces in subjects with total hip replacements compared to normal subjects? *Clinical Biomechanics,* 23**,** 754-761.

GEBHARD, J. S., AMSTUTZ, H. C., ZINAR, D. M. & DOREY, F. J. 1992. A Comparison of Total Hip Arthroplasty and Hemiarthroplasty for Treatment of Acute Fracture of the Femoral Neck. *Clinical Orthopaedics and Related Research,* 282**,** 123-131.

GENDA, E., IWASAKI, N., LI, G., MACWILLIAMS, B. A., BARRANCE, P. J. & CHAO, E. Y. S. 2001. Normal hip joint contact pressure distribution in single-leg standing--effect of gender and anatomic parameters. *Journal of Biomechanics,* 34**,** 895-905.

GLITSCH, U. & BAUMANN, W. 1997. The three-dimensional determination of internal loads in the lower extremity. *Journal of Biomechanics,* 30**,** 1123-1131.

GU, K. B. & LI, L. P. 2011. A human knee joint model considering fluid pressure and fiber orientation in cartilages and menisci. *Medical Engineering and Physics,* 33**,** 497-503.

HAEMER, J. M., CARTER, D. R. & GIORI, N. J. 2012. The low permeability of healthy meniscus and labrum limit articular cartilage consolidation

and maintain fluid load support in the knee and hip. *Journal of Biomechanics,* 45**,** 1450-1456.

HALONEN, K. S., MONONEN, M. E., JURVELIN, J. S., TÖYRÄS, J. & KORHONEN, R. K. 2013. Importance of depth-wise distribution of collagen and proteoglycans in articular cartilage—A 3D finite element study of stresses and strains in human knee joint. *Journal of Biomechanics,* 46**,** 1184-1192.

HAMMOND, B. & CHARNLEY, J. 1967. The sphericity of the femoral head. *Medical and Biological Engineering and Computing,* 5**,** 445-453.

HARRIS, M. D., ANDERSON, A. E., HENAK, C. R., ELLIS, B. J., PETERS, C. L. & WEISS, J. A. 2012. Finite element prediction of cartilage contact stresses in normal human hips. *Journal of Orthopaedic Research,* 30**,** 1133-1139.

HAYES, W. C. & MOCKROS, L. F. 1971. Viscoelastic properties of human articular cartilage. *Journal of Applied Physiology,* 31**,** 562-568.

HEINTZ, S. & GUTIERREZ-FAREWIK, E. M. 2007. Static optimization of muscle forces during gait in comparison to EMG-to-force processing approach. *Gait and Posture,* 26**,** 279-288.

HENAK, C. R., ELLIS, B. J., HARRIS, M. D., ANDERSON, A. E., PETERS, C. L. & WEISS, J. A. 2011. Role of the acetabular labrum in load support across the hip joint. *Journal of Biomechanics,* 44**,** 2201-2206.

HEWITT, J., GUILAK, F., GLISSON, R. & VAIL, T. P. 2001. Regional material properties of the human hip joint capsule ligaments. *Journal of Orthopaedic Research,* 19**,** 359-364.

HOAGLUND, F. T. & LOW, W. D. 1980. ANATOMY OF THE FEMORAL-NECK AND HEAD, WITH COMPARATIVE DATA FROM CAUCASIANS AND HONG-KONG CHINESE. *Clinical Orthopaedics and Related Research***,** 10-16.

HODGE, W. A., CARLSON, K. L., FIJAN, R. S., BURGESS, R. G., RILEY, P. O., HARRIS, W. H. & MANN, R. W. 1989. Contact pressures from an instrumented hip endoprosthesis. *Journal of Bone and Joint Surgery (American),* 71**,** 1378-86.

HODGE, W. A., FIJAN, R. S., CARLSON, K. L., BURGESS, R. G., HARRIS, W. H. & MANN, R. W. Year. Contact pressures in the human hip joint measured in vivo. *In*, 1986 Washington, DC, ETATS-UNIS. National Academy of Sciences.

HOLMES, M. H. 1985. A theoretical analysis for determining the nonlinear hydraulic permeability of a soft tissue from a permeation experiment. *Bulletin of Mathematical Biology,* 47**,** 669-683.

HORSMAN, K. & DIRK, M. 2007. *The Twente lower extremity model : consistent dynamic simulation of the human locomotor apparatus.*

HUDELMAIER, M., GLASER, C., HOHE, J., ENGLMEIER, K. H., REISER, M., PUTZ, R. & ECKSTEIN, F. 2001. Age-related changes in the morphology and deformational behavior of knee joint cartilage. *Arthritis and Rheumatism,* 44**,** 2556-2561.

HUNTER, D. J., NIU, J. B., ZHANG, Y., LAVALLEY, M., MCLENNAN, C. E., HUDELMAIER, M., ECKSTEIN, F. & FELSON, D. T. 2008. Premorbid knee osteoarthritis is not characterised by diffuse thinness: the Framingham Osteoarthritis Study. *Annals of the Rheumatic Diseases,* 67**,** 1545-9.

HUYGHE, J. M. & JANSSEN, J. D. 1997. Quadriphasic mechanics of swelling incompressible porous media. *International Journal of Engineering Science,* 35**,** 793-802.

IPAVEC, M., BRAND, R. A., PEDERSEN, D. R., MAVCIC, B., KRALJ-IGLIC, V. & IGLIC, A. 1999. Mathematical modelling of stress in the hip during gait. *Journal of Biomechanics,* 32**,** 1229-1235.

ISO-14242-1 2002. Implants for surgery -- Wear of total hip-joint prostheses -- Part 1: Loading and displacement parameters for wear-testing machines and corresponding environmental conditions for test.

ITO, H., SONG, Y., LINDSEY, D. P., SAFRAN, M. R. & GIORI, N. J. 2009. The Proximal Hip Joint Capsule and the Zona Orbicularis Contribute to Hip Joint Stability in Distraction. *Journal of Orthopaedic Research,* 27**,** 989-995.

JIN, Z., DOWSON, D. & FISHER, J. 1997. Analysis of fluid film lubrication in artificial hip joint replacements with surfaces of high elastic modulus. *Proceedings of the Institution of Mechanical Engineers, Part H: Journal of Engineering in Medicine,* 211**,** 247-256.

KARVONEN, R. L., NEGENDANK, W. G., TEITGE, R. A., REED, A. H., MILLER, P. R. & FERNANDEZ-MADRID, F. 1994. Factors affecting articular cartilage thickness in osteoarthritis and aging. *The Journal of Rheumatology,* 21**,** 1310-8.

KELLGREN, J. H., JEFFREY, M. & BALL, J. 1963. *Atlas of standard radiographs,* Oxford, Blackwell Scientific.

KELLY, B. T., WILLIAMS, R. J. & PHILIPPON, M. J. 2003. Hip arthroscopy: Current indications, treatment options, and managment issues. *American Journal of Sports Medicine,* 31**,** 1020-1037.

KEMPSON, G. E., FREEMAN, M. A. R. & SWANSON, S. A. V. 1971. The determination of a creep modulus for articular cartilage from indentation tests on the human femoral head. *Journal of Biomechanics,* 4**,** 239-250.

KIVIRANTA, I., JURVELIN, J., TAMMI, M., SÄÄMÄUNEN, A.-M. & HELMINEN, H. J. 1987. Weight bearing controls glycosaminoglycan concentration and articualr cartilage thickness in the knee joints of young beagle dogs. *Arthritis and Rheumatism,* 30**,** 801-809.

KOO, T. K. K. & MAK, A. F. T. 2005. Feasibility of using EMG driven neuromusculoskeletal model for prediction of dynamic movement of the elbow. *Journal of Electromyography and Kinesiology,* 15**,** 12-26.

KOTZAR, G. M., DAVY, D. T., GOLDBERG, V. M., HEIPLE, K. G., BERILLA, J., BROWN, R. H. & BURSTEIN, A. H. 1991. Telemeterized in vivo hip joint force data: A report on two patients after total hip surgery. *Journal of Orthopaedic Research,* 9**,** 621-633.

KREBS, D. E., ELBAUM, L., ORILEY, P., HODGE, W. A. & MANN, R. W. 1991. Exercise and Gait Effects on In Vivo Hip Contact Pressures. *Physical Therapy,* 71**,** 301-309.

KRISHNAN, R., KOPACZ, M. & ATESHIAN, G. A. 2004. Experimental verification of the role of interstitial fluid pressurization in cartilage lubrication. *Journal of Orthopaedic Research,* 22**,** 565-570.

LAI, W. M., HOU, J. S. & MOW, V. C. 1991. A triphasic theory for the swelling and deformation behaviors of articular cartilage. *Journal of Biomechanical Engineering,* 113**,** 245-58.

LAI, W. M. & MOW, V. C. 1980. Drag-induced compression of articular cartilage during a permeation experiment. *Biorheology,* 17**,** 111-123.

LANE, J. M., CHISENA, E. & BLACK, J. 1979. Experimental knee instability: early mechanical property changes in articular cartilage in a rabbit model. *Clinical Orthopaedics and Related Research* 262-5.

LI, L. P., BUSCHMANN, M. D. & SHIRAZI-ADL, A. 2000. A fibril reinforced nonhomogeneous poroelastic model for articular cartilage: inhomogeneous response in unconfined compression. *Journal of Biomechanics,* 33**,** 1533-1541.

LIU, F., LESLIE, I., WILLIAMS, S., FISHER, J. & JIN, Z. 2008. Development of computational wear simulation of metal-on-metal hip resurfacing replacements. *Journal of Biomechanics,* 41**,** 686-694.

LLOYD, D. G. & BESIER, T. F. 2003. An EMG-driven musculoskeletal model to estimate muscle forces and knee joint moments in vivo. *Journal of Biomechanics,* 36**,** 765-776.

LOIZEAU, J., ALLARD, P., DUHAIME, M. & LANDJERIT, B. 1995. Bilateral gait patterns in subjects fitted with a total hip prosthesis. *Archives of Physical Medicine and Rehabilitation,* 76**,** 552-557.

LONG, W. T., DORR, L. D., HEALY, B. & PERRY, J. 1993. Functional Recovery of Noncemented Total Hip Arthroplasty. *Clinical Orthopaedics and Related Research,* 288**,** 73-77.

LU, T. W. & O'CONNOR, J. J. 1999. Bone position estimation from skin marker co-ordinates using global optimisation with joint constraints. *Journal of Biomechanics,* 32**,** 129-134.

MAAS, S. A. & WEISS, J. A. 2007. *FEBio Theory Manual*, http://mrl.sci.utah.edu/software/febio.

MADSEN, M. S., RITTER, M. A., MORRIS, H. H., MEDING, J. B., BEREND, M. E., FARIS, P. M. & VARDAXIS, V. G. 2004. The effect of total hip arthroplasty surgical approach on gait. *Journal of Orthopaedic Research,* 22**,** 44-50.

MAK, A. F. 1986. The apparent viscoelastic behavior of articular cartilage--the contributions from the intrinsic matrix viscoelasticity and interstitial fluid flows. *Journal of Biomechanical Engineering,* 108**,** 123-130.

MANDERS, C., NEW, A. & RASMUSSEN, J. 2008. Validation of Musculoskeletal Gait Simulation For Use In Investigation Of Total Hip Replacement. *16th Congress of the European Society of Biomechanics.* J Biomech.

MANNING, M., BARRON, D., LEWIS, T. & SLOAN, J. 2008. Soft tissue injuries: 4 Hip and thigh. *Emergency Medicine Journal* 25**,** 679-85.

MARTIN, J. A. & BUCKWALTER, J. A. 2001. Roles of articular cartilage aging and chondrocyte senescence in the pathogenesis of osteoarthritis. *Iowa Orthopaedic Journal,* 21**,** 1-7.

MARTIN, J. A. & BUCKWALTER, J. A. 2002. Aging, articular cartilage chondrocyte senescence and osteoarthritis. *Biogerontology,* 3**,** 257-64.

MATTEI, L., CAMPIONI, E., ACCARDI, M. A. & DINI, D. 2013. Finite element analysis of the meniscectomised tibio-femoral joint: implementation of advanced articular cartilage models. *Computer Methods in Biomechanics and Biomedical Engineering***,** 1-19.

MAVČIČ, B., POMPE, B., ANTOLIČ, V., DANIEL, M., IGLIČ, A. & KRALJ-IGLIČ, V. 2002. Mathematical estimation of stress distribution in

normal and dysplastic human hips. *Journal of Orthopaedic Research,* 20**,** 1025-1030.

MCCANN, L., INGHAM, E., JIN, Z. & FISHER, J. 2009. Influence of the meniscus on friction and degradation of cartilage in the natural knee joint. *Osteoarthritis and Cartilage,* 17**,** 995-1000.

MCCRORY, J. L., WHITE, S. C. & LIFESO, R. M. 2001. Vertical ground reaction forces: objective measures of gait following hip arthroplasty. *Gait and Posture,* 14**,** 104-109.

MCWILLIAMS, A., STEWART, T. D., GRAINGER, A. J., O'CONNOR, P. J., WHITE, D., REDMOND, A. & STONE, M. H. 2011. Leg length inequality following total hip replacement. *Orthopaedics and Trauma,* 25**,** 37-42.

MONONEN, M. E., MIKKOLA, M. T., JULKUNEN, P., OJALA, R., NIEMINEN, M. T., JURVELIN, J. S. & KORHONEN, R. K. 2012. Effect of superficial collagen patterns and fibrillation of femoral articular cartilage on knee joint mechanics—A 3D finite element analysis. *Journal of Biomechanics,* 45**,** 579-587.

MOW, V. C. & GUO, X. E. 2002. Mechano-electrochemical properties of articular cartilage: Their inhomogeneities and anisotropies. *Annual Review of Biomedical Engineering,* 4**,** 175-209.

MOW, V. C., HOLMES, M. H. & MICHAEL LAI, W. 1984. Fluid transport and mechanical properties of articular cartilage: A review. *Journal of Biomechanics,* 17**,** 377-394.

MOW, V. C., KUEI, S. C., LAI, W. M. & ARMSTRONG, C. G. 1980. Biphasic creep and stress relaxation of articular cartilage in compression: Theory and experiments. *Journal of Biomechanical Engineering,* 102**,** 73-84.

MOW, V. C. & LAI, W. M. 1980. Recent Developments in Synovial Joint Biomechanics. *SIAM Review,* 22**,** 275-317.

MOW, V. C., RATCLIFFE, A. & ROBIN POOLE, A. 1992. Cartilage and diarthrodial joints as paradigms for hierarchical materials and structures. *Biomaterials,* 13**,** 67-97.

NAISH, J. H., XANTHOPOULOS, E., HUTCHINSON, C. E., WATERTON, J. C. & TAYLOR, C. J. 2006. MR measurement of articular cartilage thickness distribution in the hip. *Osteoarthritis and Cartilage,* 14**,** 967-973.

NEVITT, M. C., LANE, N. E., SCOTT, J. C., HOCHBERG, M. C., PRESSMAN, A. R., GENANT, H. K. & CUMMINGS, S. R. 1995. Radiographic osteoarthritis of the hip and bone mineral density. *Arthritis and Rheumatism,* 38**,** 907-916.

NILSDOTTER, A.-K., PETERSSON, I. F., ROOS, E. M. & LOHMANDER, L. S. 2003. Predictors of patient relevant outcome after total hip replacement for osteoarthritis: a prospective study. *Annals of the Rheumatic Diseases,* 62**,** 923-930.

PANDY, M. G. 2001. Computer modeling and simulation of human movement. *Annual Review of Biomedical Engineering,* 3**,** 245-73.

PARK, S., KRISHNAN, R., NICOLL, S. B. & ATESHIAN, G. A. 2003. Cartilage interstitial fluid load support in unconfined compression. *Journal of Biomechanics,* 36**,** 1785-1796.

PARSONS, J. R. & BLACK, J. 1977. The viscoelastic shear behavior of normal rabbit articular cartilage. *Journal of Biomechanics,* 10**,** 21-29.

PATRIARCO, A. G., MANN, R. W., SIMON, S. R. & MANSOUR, J. M. 1981. An evaluation of the approaches of optimization models in the prediction of muscle forces during human gait. *Journal of Biomechanics,* 14**,** 513-525.

PAUL, J. P. 1967. Forces transmitted by joints in the human body. *ARCHIVE: Proceedings of the Institution of Mechanical Engineers, Conference Proceedings 1964-1970 (vols 178-184), Various titles labelled Volumes A to S,* 181**,** 8-15.

PAWASKAR, S. S. 2010. *Joint contact modelling of articular cartilage in synovial joints.* Ph.D. Thesis, University of Leeds.

PAWASKAR, S. S., GROSLAND, N. M., INGHAM, E., FISHER, J. & JIN, Z. 2011. Hemiarthroplasty of hip joint: An experimental validation using porcine acetabulum. *Journal of Biomechanics,* 44**,** 1536-1542.

PAWASKAR, S. S., INGHAM, E., FISHER, J. & JIN, Z. 2010. Fluid load support and contact mechanics of hemiarthroplasty in the natural hip joint. *Medical Engineering and Physics,* 33**,** 96-105.

PEACH, C. A., CARR, A. J. & LOUGHLIN, J. 2005. Recent advances in the genetic investigation of osteoarthritis. *Trends in Molecular Medicine,* 11**,** 186-191.

PEAT, G., MCCARNEY, R. & CROFT, P. 2001. Knee pain and osteoarthritis in older adults: a review of community burden and current use of primary health care. *Annals of the Rheumatic Diseases,* 60**,** 91-97.

PEDERSEN, D. R., BRAND, R. A. & DAVY, D. T. 1997. Pelvic muscle and acetabular contact forces during gait. *Journal of Biomechanics,* 30**,** 959-965.

PERRON, M., MALOUIN, F., MOFFET, H. & MCFADYEN, B. J. 2000. Three-dimensional gait analysis in women with a total hip arthroplasty. *Clinical Biomechanics,* 15**,** 504-515.

PHILLIPS, A. T. M., PANKAJ, P., HOWIE, C. R., USMANI, A. S. & SIMPSON, A. 2007. Finite element modelling of the pelvis: Inclusion of muscular and ligamentous boundary conditions. *Medical Engineering and Physics,* 29**,** 739-748.

PIAZZA, S. J. & DELP, S. L. 1996. The influence of muscles on knee flexion during the swing phase of gait. *Journal of Biomechanics,* 29**,** 723-733.

PRAAGMAN, M., CHADWICK, E. K. J., VAN DER HELM, F. C. T. & VEEGER, H. E. J. 2006. The relationship between two different mechanical cost functions and muscle oxygen consumption. *Journal of Biomechanics,* 39**,** 758-765.

RADIN, E., PAUL, I. & ROSE, R. 1972. Role of mechanical factors in pathogenesis of primary osteoarthritis. *The Lancet,* 299**,** 519-522.

RALPHS, J. R. & BENJAMIN, M. 1994. The joint capsule - structure, composition, aging and disease. *Journal of Anatomy,* 184**,** 503-509.

RASMUSSEN, J., DAMSGAARD, M. & VOIGT, M. 2001. Muscle recruitment by the min/max criterion — a comparative numerical study. *Journal of Biomechanics,* 34**,** 409-415.

REBMANN, A. J. & SHEEHAN, F. T. 2003. Precise 3D skeletal kinematics using fast phase contrast magnetic resonance imaging. *Journal of Magnetic Resonance Imaging,* 17**,** 206-13.

REIKERAS, O., HOISETH, A., REIGSTAD, A. & FONSTELIEN, E. 1982. Femoral-neck angles - a specimen study with special regard to bilateral differences. *Acta Orthopaedica Scandinavica,* 53**,** 775-779.

ROTH, V. & MOW, V. C. 1980. The intrinsic tensile behavior of the matrix of bovine articular cartilage and its variation with age. *Journal of Bone and Joint Surgery (American),* 62**,** 1102-17.

RUSHFELDT, P. D., MANN, R. W. & HARRIS, W. H. 1981. Improved techniques for measuring in vitro the geometry and pressure distribution in the human acetabulum—I. Ultrasonic measurement of acetabular surfaces, sphericity and cartilage thickness. *Journal of Biomechanics,* 14**,** 253-260.

RYDELL, N. W. 1966. Forces acting on the femoral head-prosthesis. A study on strain gauge supplied prostheses in living persons. *Acta Orthopaedica Scandinavica,* 37**,** Suppl 88:1-132.

SCHUIND, F., GARCIA-ELIAS, M., COONEY III, W. P. & AN, K.-N. 1992. Flexor tendon forces: In vivo measurements. *The Journal of Hand Surgery,* 17**,** 291-298.

SCHWARTZ, M. H., LEO, P. H. & LEWIS, J. L. 1994. A microstructural model for the elastic response of articular cartilage. *Journal of Biomechanics,* 27**,** 865-873.

SELINGER, A. 2007. Chapter 4 - Posture. *Physical Rehabilitation.* Saint Louis: W.B. Saunders.

SHARMA, L., CAHUE, S., SONG, J., HAYES, K., PAI, Y.-C. & DUNLOP, D. 2003. Physical functioning over three years in knee osteoarthritis: Role of psychosocial, local mechanical, and neuromuscular factors. *Arthritis and Rheumatism,* 48**,** 3359-3370.

SHEPHERD, D. E. & SEEDHOM, B. B. 1999. Thickness of human articular cartilage in joints of the lower limb. *Annals of the Rheumatic Diseases,* 58**,** 27-34.

SHIH, C. H., DU, Y. K., LIN, Y. H. & WU, C. C. 1994. Muscular recovery around the hip joint after total hip arthroplasty. *Clinical Orthopaedics and Related Research***,** 115-120.

SICARD-ROSENBAUM, L., LIGHT, K. E. & BEHRMAN, A. L. 2002. Gait, Lower Extremity Strength, and Self-Assessed Mobility After Hip Arthroplasty. *The Journals of Gerontology Series A: Biological Sciences and Medical Sciences,* 57**,** M47-M51.

SOKOLOFF, L. 1966. Elasticity of aging cartilage. *Federation Proceedings,* 25**,** 1089-95.

SOLTZ, M. A. & ATESHIAN, G. A. 1998. Experimental verification and theoretical prediction of cartilage interstitial fluid pressurization at an impermeable contact interface in confined compression. *Journal of Biomechanics,* 31**,** 927-934.

SOLTZ, M. A. & ATESHIAN, G. A. 2000. A Conewise Linear Elasticity mixture model for the analysis of tension-compression nonlinearity in articular cartilage. *Journal of Biomechanical Engineering,* 122**,** 576-86.

SOULHAT, J., BUSCHMANN, M. D. & SHIRAZI-ADL, A. 1999. A fibril-network-reinforced biphasic model of cartilage in unconfined compression. *Journal of Biomechanical Engineering,* 121**,** 340-347.

SPITZER, V., ACKERMAN, M. J., SCHERZINGER, A. L. & WHITLOCK, D. 1996. The visible Human Male: A Technical Report. *Journal of the American Medical Informatics Association,* 3**,** 118-130.

STAGNI, R., FANTOZZI, S., CAPPELLO, A. & LEARDINI, A. 2005. Quantification of soft tissue artefact in motion analysis by combining

3D fluoroscopy and stereophotogrammetry: a study on two subjects. *Clinical Biomechanics,* 20**,** 320-329.

STANSFIELD, B. W. & NICOL, A. C. 2002. Hip joint contact forces in normal subjects and subjects with total hip prostheses: walking and stair and ramp negotiation. *Clinical Biomechanics,* 17**,** 130-139.

SWANN, A. C. & SEEDHOM, B. B. 1993. The stiffness of normal articular cartilage and the predominant acting stress levels: implications for the aetiology of osteoarthrosis. *British journal of rheumatology,* 32**,** 16-25.

TANK, P. W., GEST, T. R. & BURKEL, W. E. 2009. *Lippincott Williams & Wilkins atlas of anatomy*, Wolters Kluwer Health/Lippincott Williams & Wilkins.

VALLIAPPAN, S., SVENSSON, N. L. & WOOD, R. D. 1977. Three dimensional stress analysis of the human femur. *Computers in Biology and Medicine,* 7**,** 253-264.

VAN DER MEULEN, M. C. H., BEAUPRÉ, G. S., SMITH, R. L., GIDDINGS, V. L., ALLEN, W. A., ATHANASIOU, K. A., ZHU, C. F., SONG, Y., MANDELL, J. A., POSER, R. D. & GOODMAN, S. B. 2002. Factors influencing changes in articular cartilage following hemiarthroplasty in sheep. *Journal of Orthopaedic Research,* 20**,** 669-675.

VIGNON, É., VALAT, J.-P., ROSSIGNOL, M., AVOUAC, B., ROZENBERG, S., THOUMIE, P., AVOUAC, J., NORDIN, M. & HILLIQUIN, P. 2006. Osteoarthritis of the knee and hip and activity: a systematic international review and synthesis (OASIS). *Joint Bone Spine,* 73**,** 442-455.

VON EISENHART, R., ADAM, C., STEINLECHNER, M., MULLER-GERBL, M. & ECKSTEIN, F. 1999. Quantitative determination of joint incongruity and pressure distribution during simulated gait and cartilage thickness in the human hip joint. *Journal of Orthopaedic Research,* 17**,** 532-539.

WANG, C. C. B., HUNG, C. T. & MOW, V. C. 2001. An analysis of the effects of depth-dependent aggregate modulus on articular cartilage stress-relaxation behavior in compression. *Journal of Biomechanics,* 34**,** 75-84.

WEARING, S. C., HENNIG, E. M., BYRNE, N. M., STEELE, J. R. & HILLS, A. P. 2006. Musculoskeletal disorders associated with obesity: a biomechanical perspective. *Obesity Reviews,* 7**,** 239-250.

WEHNER, T., CLAES, L. & SIMON, U. 2009. Internal loads in the human tibia during gait. *Clinical Biomechanics,* 24**,** 299-302.

WEI, H.-W., SUN, S.-S., JAO, S.-H. E., YEH, C.-R. & CHENG, C.-K. 2005. The influence of mechanical properties of subchondral plate, femoral head and neck on dynamic stress distribution of the articular cartilage. *Medical Engineering and Physics,* 27**,** 295-304.

WILLIAMS, S., JALALI-VAHID, D., BROCKETT, C., JIN, Z., STONE, M. H., INGHAM, E. & FISHER, J. 2006. Effect of swing phase load on metal-on-metal hip lubrication, friction and wear. *Journal of Biomechanics,* 39**,** 2274-2281.

WINTERS, J. M. & STARK, L. 1985. Analysis of fundamental human movement patterns through the use of in-depth antagonistic muscle models. *Biomedical Engineering, IEEE Transactions on,* BME-32**,** 826-839.

WU, J. Z., HERZOG, W. & EPSTEIN, M. 1997. Evaluation of the finite element software ABAQUS for biomechanical modelling of biphasic tissues. *Journal of Biomechanics,* 31**,** 165-169.

XI, J., HU, X. & JIN, Y. 2003. Shape analysis and parameterized modeling of hip joint. *Journal of Computing and Information Science in Engineering,* 3**,** 260-265.

YOSHIDA, H., FAUST, A., WILCKENS, J., KITAGAWA, M., FETTO, J. & CHAO, E. Y. S. 2006. Three-dimensional dynamic hip contact area and pressure distribution during activities of daily living. *Journal of Biomechanics,* 39**,** 1996-2004.

ZAJAC, F. E. 1989. Muscle and tendon: properties, models, scaling, and application to biomechanics and motor control. *Critical Reviews in Biomedical Engineering* 17**,** 359-411.

Appendix A Publications

Journals

[1] LI, J., STEWART, T. D., JIN, Z., WILCOX, R. K. & FISHER, J. The influence of size, clearance, cartilage properties, thickness and hemiarthroplasty on the contact mechanics of the hip joint with biphasic layers. Journal of Biomechanics. 2013. 46, 1641-1647.

[2] LI, J., JIN, Z., FISHER, J & WILCOX, R. K. Biphasic investigation of contact mechanics in natural human hips during activities. Under review.

[3] LI, J., Redmond, A., JIN, Z., FISHER, J., Stone, H. S., STEWART, T. D. Hip kinematics and contact forces in asymptomatic total hip replacement patients differ from normal healthy individuals. Under review.

[4] LI, J., McWilliams, A. B., JIN, Z., FISHER, J., Stone, H. S., Redmond, A. & STEWART, T. D. Influence of leg length inequality on hip reaction forces. 2013. Under review.

[5] LI, J., JIN, Z., FISHER, J & WILCOX, R. K. Experimental validation of a new biphasic model of the contact mechanics of the porcine hip. Under review.

[6] LI, J., STEWART, T. D., JIN, Z., WILCOX, R. K. & FISHER, J. The influence of unilateral total hip replacement on contact mechanics and fluid pressurisation of non-operated hip. 2013. To be written and submitted.

[7] LI, J., JIN, Z., FISHER, J & WILCOX, R. K. Influence of clearance on time-dependent performance of hip in hemiarthroplasty with biphasic acetabular cartilage. 2013. Under reivew.

Conferences

[1] LI, J., STEWART, T. D., JIN, Z., FISHER, J., WILCOX, R. K The influence of unilateral total hip arthroplasty on contact mechanics of non-operated limbs. Podium. 5th International Conference on Computational Bioengineering. Leuven, Belgium. Sept 2013.

[2] LI, J., REDMOND, A., JIN, Z., FISHER, J., STONE, M. H. & STEWART, T. D. Effect of leg length inequality on hip kinetics after total hip replacement. Podium. 19th Congress of the European Society of Biomechanics, Patras, Greece. Aug 2013.

[3] LI, J., JIN, Z., FISHER, J., WILCOX, R. K. Application of biphasic cartilage to a three dimensional natural hip under static and dynamic loads. Podium. 11th International Symposium on Computer Methods in Biomechanics and Biomedical Engineering, Salt Lake City, Utah, USA. April 2013.

[4] LI, J., Wilkins, R., JIN, Z., FISHER, J., STONE, M. H., REDMOND, A. & STEWART, T. D. Kinematics and joint reaction forces for asymptomatic total hip replacement patients differ from normal healthy individuals. Poster No. 1002. 56th Annual Meeting of the Orthopaedic Research Society, San Antonio, TX, USA. January 2013.

[5] LI, J., JIN, Z., STEWART, T. D., WILCOX, R. K., FISHER, J. The influence of hip size, clearance, cartilage properties and cartilage thickness on the contact mechanics of natural hip joint with biphasic layers. Poster No. 0970. 56th Annual Meeting of the Orthopaedic Research Society, San Antonio, TX, USA. January 2013.